

Development of a Biomimetic Phosphoserine Modified Calcium Phosphate Adhesive for the Regeneration of Bone Defects



Antzela Tzagiollari, MSc

Submitted for the Award of Doctor of Philosophy (PhD)

School of Mechanical & Manufacturing Engineering
Dublin City University

Supervised by:

Professor Nicholas Dunne

Dr. Tanya Levingstone

Dr. Owen Clarkin

July 2024

I hereby certify that this material, which I now submit for assessment on the programme of study leading to the award of Doctor of Philosophy is entirely my own work, and that I have exercised reasonable care to ensure that the work is original, and does not to the best of my knowledge breach any law of copyright, and has not been taken from the work of others save and to the extent that such work has been cited and acknowledged within the text of my work.

Signed: 

ID No.: 19211196

Date: 07/12/2023

Acknowledgements

Looking back on the past four years of my PhD journey, I feel a deep sense of gratitude and accomplishment. These years have been more than just academic research; they've been a time of learning, growing, and overcoming challenges. I've not only gained knowledge in my field but also built relationships and learned a lot about myself.

Here, I would like to acknowledge that this PhD research support is provided by the Irish Research Council Government of Ireland Postgraduate Scholarship Award (GOIPG/2020/371). A PhD journey is special. It's hard work and it pushes you, but it also opens new opportunities to learn and to grow. My journey has been especially meaningful because of the support and guidance of many individuals, each playing a crucial role in my development as a researcher and as a person. As I reach this important milestone, I want to take a moment to say thank you to all those who have been a part of my PhD.

The first big thanks go to my supervisory team – Nicholas, Tanya and Owen, for their thoughtful feedback and consistent support throughout these years, which elevated the methodological approaches in this work. Nicholas as my primary supervisor supported me and believed in me from the first day of the PhD. Also, I thank him for the patient guidance, encouragement and advice he has provided throughout my time as his student. Tanya although my second supervisor, has been equally important. Her valuable comments have greatly improved my understanding and approach to my work. Nicholas, Tanya and Owen were always available, ensuring that I had the support and guidance I needed at every phase of my research. I must also extend my thanks to the technical staff and support team at DCU, including everyone in MME and the NRF. Their assistance has been vital in my research.

My sincere thanks go to PBC Biomed as industrial partners for generously funding the first year of my PhD studies. This support was fundamental in setting the stage for my research. A special acknowledgment is extended to Gerard Insley and his valuable expertise, support and enthusiasm about my PhD project. Gerard and PBC team gave me the opportunity to participate in an industrial placement during my PhD which was not only enlightening but also helpful in improving my practical skills. I'm grateful for their trust in letting me be part of the team for various studies. It was an honour and I learned so much.

In this journey, my heartfelt thanks are extended to my colleagues and friends. Dr. Redmond, my “friend at work” as he calls it, and his commitment to understanding and adhering to all the regulations and policies has been both impressive and inspiring. Moreover, his

appreciation for good quality coffee has been a delightful aspect of our time together, often providing much-needed breaks and moments of light-hearted conversation among our hard work. Ghaydah and Halima, despite their differing personalities, their playful arguments and sense of humour have been a refreshing escape from the stress and hard work of PhD life. They always remind me to step back from my intense focus and to stop speaking like I'm writing a scientific article. I would also like to express my deepest gratitude to Katerina and Despoina, my dearest friends and ex housemates, for their support and advice over the years. Their constant encouragement, well-wishes, and the shared moments of laughter have been a source of great joy and comfort. Emma my friend from Greece, despite her busy life, she always found time to call and remind me to stay focused on finishing my PhD so I can go back. Her willingness to spend time with me during the summers, creating moments of relaxation and joy, have been a huge comfort. Last but certainly not least, I must thank my forever friend, Nikoletta. She has been by my side since the beginning of our career, starting from our bachelor's degree days. She's always been there for me, making sure I never felt alone. Every discussion with her, often lasting for hours, has helped me grow and be a better person. Her trust in me has been boosting my confidence and teaching me the importance of celebrating every small achievement in life. Also, a big thank you to Nikoletta's parents for always sending us cooked food and save us hours of cooking, really appreciated. All of them has been crucial in keeping my spirits high during the challenging journey of completing a PhD.

Finally, I want to express my deepest gratitude to my parents back in Greece. Your daily calls have been a constant reminder of your love and support. You always made sure I knew that I was doing well and that I was never alone in the decisions I made during my PhD journey. A special thank you to my brother Eneas. Despite me being the younger sibling, your pride in my achievements and your trust in seeking my advice have been sources of great encouragement and joy for me. Your belief in me has been a driving force in my success.

Table of Contents

Acknowledgements.....	ii
Table of Contents.....	iv
List of Abbreviations	vii
List of Units	ix
List of Figures.....	xi
List of Tables	xiii
List of Equations.....	xiv
List of Publications and Oral/Poster Presentation	xvi
Abstract	xx
Chapter 1: Introduction and Literature Review.....	22
1.1. Overview	5
1.2. Bone.....	7
1.2.1. Bone Macro- and Microscopic Structure	8
1.2.2. Bone Cells	11
1.2.3. Bone Fractures	13
1.2.4. Natural Bone Healing Mechanism	16
1.3. Current Surgical Approaches – Orthopaedic.....	18
1.3.1. Open Reduction and Internal Fixation (ORIF)	18
1.3.2. External Fixation.....	22
1.4. Dental Prosthetics or Implants	23
1.4.1. Endosteal or Endosseous Dental Implants	24
1.4.2. Subperiosteal Dental Implants	25
1.4.3. Transosteal Implants	26
1.5. Type of Adhesives.....	26
1.5.1. Synthetic and Natural Derived Adhesives	27
1.5.2. Biomimetic-Based Adhesives	32
1.6. Clinical Requirements of Adhesives	41
1.7. Reinforcement of Current Adhesives	43
1.8. Summary	45
1.9. Aim and Objectives	48
Chapter 2: Analysis and Optimisation of the Phosphoserine-modified Calcium Phosphate (PM-CPC) Adhesive Composition.....	49
2.1. Introduction	53
2.2. Chapter Aim	58

2.3.	Material and Methods.....	59
2.3.1.	Synthesis of Micro-sized Ceramic Particles (α -TCP).....	59
2.3.2.	Analytical Assessment of α -TCP Powder.....	60
2.3.3.	Box-Behnken Factorial Design.....	62
2.3.4.	Formulation of PM-CPC Adhesive.....	62
2.3.5.	Analytical Assessment of PM-CPC Adhesive.....	64
2.3.6.	DoE Modelling and Optimisation.....	68
2.4.	Results.....	69
2.4.1.	Analytical Assessment of α -TCP Powder.....	69
2.4.2.	DoE Assessment of Different PM-CPC Composition.....	75
2.4.3.	DoE Optimisation and Validation.....	84
2.5.	Discussion.....	86
2.6.	Conclusions.....	90
Chapter 3: Functional Assessment of Optimal Phosphoserine-modified Calcium Phosphate Adhesive (PM-CPC) for Bone Repair and Implant Augmentation		91
3.1.	Introduction.....	95
3.2.	Chapter Aim.....	96
3.3.	Material and Methods.....	96
3.3.1.	Formulation of Optimal PM-CPC Adhesive.....	96
3.3.2.	Analytical Assessment of Optimal Hand-mixed PM-CPC Adhesive.....	97
3.4.	Statistical Analysis.....	105
3.5.	Results.....	105
3.5.1.	Handling and Mechanical Properties.....	105
3.5.2.	Washout Resistance.....	108
3.5.3.	Degradation and <i>In vitro</i> Degradation Properties.....	108
3.5.4.	Biological Activity.....	110
3.5.5.	Adhesion Strength on Dental Implants.....	113
3.5.6.	Adhesion Strength on Orthopaedic Screws.....	116
3.5.7.	Bone-to-Bone Adhesion using PM-CPC.....	118
3.6.	Discussion.....	120
3.7.	Conclusions.....	123
Chapter 4: Development of an Injectable Phosphoserine-modified Calcium Phosphate (PM-CPC) and a Minimally Invasive Delivery Device.....		125
4.1.	Introduction.....	127
4.2.	Chapter Aim.....	128
4.3.	Material and Methods.....	129

4.3.1.	Formulation of Hand-Mixed PM-CPC Adhesive	129
4.3.2.	Formulation of Dual Syringe-Mixed PM-CPC Adhesive.....	129
4.3.3.	Analytical Assessment of Individual Components	131
4.3.4.	Analytical assessment of dual syringe-mixed PM-CPC Adhesive	133
4.4.	Statistical Analysis	134
4.5.	Results	134
4.5.1.	Analytical Assessment of Individual Components	134
4.5.2.	Analytical Assessment of Dual Syringe-mixed PM-CPC Adhesive	140
4.6.	Discussion	148
4.7.	Conclusion.....	151
Chapter 5: <i>In Vitro</i> and <i>In Vivo</i> Evaluation of PM-CPC Adhesive: Biocompatibility and Efficacy as a Bioadhesive for Implant Stabilisation and Bone Repair		153
5.1.	Introduction	155
5.2.	Chapter Aim	157
5.3.	Material Methods	158
5.3.1.	<i>In Vitro</i> Assessment of the Dual Syringe-mixed and Hand-mixed PM-CPC adhesives.....	158
5.3.2.	<i>In Vivo</i> Assessment of PM-CPC Adhesives	162
5.4.	Results	168
5.4.1.	<i>In Vitro</i> –Cytotoxicity Analysis	168
5.4.2.	<i>In Vitro</i> –Cell Proliferation	171
5.4.3.	<i>In Vivo</i> –Mechanical Characterisation	173
5.4.4.	Histological Analysis	175
5.5.	Discussion	178
5.6.	Conclusion.....	181
Chapter 6: Overall Discussion, Concluding Remarks and Future Perspectives.....		183
6.1.	Overall Discussion	185
6.2.	Concluding Remarks	191
6.3.	Future Perspectives.....	192
Bibliography		195
Appendices.....		231

List of Abbreviations

2θ	Diffraction Angle
ANOVA	Analysis Of Variance
BCP	Biphasic Calcium Phosphate
BMU	Basic Multi-Cellular Unit
Ca	Calcium
Ca/P	Calcium To Phosphate Ratio
Ca^{2+}	Calcium Ions
Ca_2SiO_4	Calcium Silicate
CaCO_3	Calcium Carbonate
CaHPO_4	Calcium Phosphate
CO_2	Dioxide Carbone
CPCs	Calcium Phosphate Cements
D_{10}	Diameter Below 10%
D_{50}	Diameter Below 50%
D_{90}	Diameter Below 90%
DI	Deionised
d_i	Desirability Function
DoE	Design Of Experiment
EDX	Energy-Dispersive X-Ray Spectroscopy
EHT	Extra-High Tension
FTIR	Fourier Transform Infrared
HA	Hydroxyapatite
ICDD	International Centre for Diffraction Data
LD	Laser Diffraction
L-DOPA	Levodopa-3,4-Dihydroxy-L-Phenylalanin
LPR	Liquid To Powder Ratio
MC3T3	Pre-Osteoblast Cells
MSCs	Mesenchymal Stem Cells
MTT	Multi-Transaction Translator
Na_2HPO_4	Sodium Dihydrogen Phosphate
NC	Negative Control

ns	Non-Significant
OCA	2-Octyl Cyanoacrylate
OCP	Octacalcium Phosphate
OPN	Osteopontin
ORIF	Open Reduction and Internal Fixation
PBS	Phosphate Buffered Solution
PC	Primary Contact
PCL	Polycaprolactone
PDL	Periodontal Ligament
PEG	Poly(Ethylene Glycol)
PEGDMA	Photocurable Poly(Ethylene Glycol) Dimethacrylate
PGA	Poly(Glycolic Acid)
PLA	Poly(Lactic Acid)
PLGA	Poly(Lactic-Co-Glycolic Acid)
PM-CPC	Phosphoserine Modified Calcium Phosphate Cements
PM-CPC	Phosphoserine Modified-Calcium Phosphate
PMMA	Poly(Methyl Methacrylate)
PO_4^{3-}	Phosphate
PPL-PBS	Porcine Pancreas Lipase-Phosphate Buffer Solution
PTFE	Polytetrafluoroethylene
RSM	Response Surface Methodology
SBF	Simulated Body Fluid
SC	Secondary Contact
SD	Standard Deviation
SEM	Scanning Electron Microscopy
Si	Silicate
SPI	Soybean Protein Isolate
t_f	Final Setting Time
t_i	Initial Setting Time
U/g	Units Per Gram
U/mL	Units Per Millilitre
XRD	X Ray Diffraction
ZrO ₂	Zirconium Dioxide

α -TCP	Alpha-Tricalcium Phosphate
β -CPP	Beta-Calcium Pyrophosphate
β -TCP	Beta-Tricalcium Phosphate

List of Units

mm	Millimetre
μ m	Micrometre
cm ²	Centimetre Square
cm ⁻¹	Per Centimetre
mm ²	Millimetre Square
mm ³	Millimetre Cube
h	Hour
min	Minutes
s	Second
g	Gram
mg	Milligram
mL	Millilitre
kPa	Kilopascal
MPa	Megapascal
kN	Kilonewton
N	Newton
kGy	Kilogray
kV	Kilovolt
mV	Millivolt
Ncm	Newton Centimetre
M	Molar
°	Angle Degree
wt. %	Weight %
°C	Degree Celsius
RPM	Rotations Per Minutes
°C/min	Degree Celsius Per Minutes
wt./wt.	Weight/Weight
mPa*s	Millipascal Second

mg/mL	Milligram Per Millilitre
cells/cm ²	Cells Per Centimetre Square
% v/v	Percent Volume Per Volume
mL/g	Millilitre Per Gram
mm/min	Millimetre Per Minutes

List of Figures

Figure 1.1: Bone Structure.....	11
Figure 1.2: Cells Found within Bone Tissue	12
Figure 1.3: Types of Bone Fractures	15
Figure 1.4: Natural Bone Healing.....	17
Figure 1.5: Surgical Approaches used for Internal Bone Fixation	21
Figure 1.6: Surgical Approaches used for External Bone Fixation.	23
Figure 1.7:Types of Dental Implants	24
Figure 1.8: Clinical requirements	42
Figure 2.1: Setting Time Analysis	64
Figure 2.2: Compression Test.....	67
Figure 2.3: Adhesive Shear Test.....	67
Figure 2.4: X-ray Diffraction (XRD) Analysis.....	70
Figure 2.5: FT-IR Analysis.....	71
Figure 2.6: SEM Analysis and Particle Size.....	73
Figure 2.7: LPR Influence on Setting Properties.....	77
Figure 2.8: Phosphoserine Influence on Setting Properties.....	78
Figure 2.9: Interactions on Setting Properties	79
Figure 2.10: LPR and Phosphoserine Influence on Compressive Strength.....	81
Figure 2.11: LPR and Phosphoserine Influence on Adhesive Strength.....	83
Figure 3.1: Set-up of Pull-out and Torque Removal Test for Dental Implants	101
Figure 3.2: Set-up of Pull-out Test for Orthopaedic Implants.....	102
Figure 3. 3: Bovine Femur Specimens for Bone-to-Bone Adhesion Test.....	104
Figure 3.4: Setting Times of PM-CPC Adhesive	106

Figure 3.5: Static-Mechanical Properties of PM-CPC Adhesive	107
Figure 3.6: Washout Resistance of PM-CPC Adhesive	109
Figure 3.7: Degradation and Biological Activity of PM-CPC Adhesive	111
Figure 3.8: Torque Removal Forces of Dental Implants	114
Figure 3.9: Pull-out Forces of Dental Implants	115
Figure 3.10: Pull-out Forces of Orthopaedics Implants.....	117
Figure 3.11: Bone-to-Bone Adhesion Properties.....	119
Figure 4.1: Double Syringe Mixing System used for the injectable and on-demand mixed PM-CPC adhesive.....	131
Figure 4.2: Phase Separation of Individual components	135
Figure 4.3: Injectability of Individual Pastes.....	137
Figure 4.4: Variation of Viscosity over Time for the Optimal Components.....	139
Figure 4.5: Handling Properties of the Dual Syringe-mixed and Hand-mixed PM-CPC Adhesive	140
Figure 4.6: Mechanical Properties of the Adhesive as a Consequence of Different Mixing Techniques.....	141
Figure 4.7: Washout Resistance of the Dual Syringe-mixed and Hand-mixed PM-CPC Adhesive	142
Figure 4.8: Degradation of the Dual Syringe-mixed and Hand-mixed PM-CPC Adhesive and Biological Activity of the Dual Syringe-mixed Adhesive.....	144
Figure 4.9: Maximum Pull-out Forces of Augmented Orthopaedics Screws.....	146
Figure 4.10: Bone to Bone Adhesion Properties	147
Figure 5.1: Overall <i>in vivo</i> study design.....	167
Figure 5.2: Cell Viability of Non-Cured Samples	170

Figure 5.3: Cell Viability of Cured Samples	171
Figure 5.4: Cell Proliferation.....	172
Figure 5.5: Mechanical Characterisation of the PM-CPC–Bone and Implant–PM-CPC Interface	176
Figure 5.6: Representative images from the histological sections prepared from specimens of artificial extraction sockets	177

List of Tables

Table 1.1: Comparison of the different properties of all the synthetic-based adhesives.....	34
Table 1.2: Comparison of the different biomimetic-based adhesives.	39
Table 2.1: Numerical and categorical factors and their levels used for the three different DoE studies, changing the levels of grinding cycles.	65
Table 2.2: Characteristic peaks of α -TCP, HA, β -TCP, β -CPP phases as appeared in Rietveld software after analysing XRD data.....	70
Table 2.3: Particle size distribution and zeta potential of α -TCP powder as a function of increasing the particle attrition cycles.	74
Table 2.4: Results of DoE optimisation of the PM-CPC composition showing the acceptable clinical ranges for each factor and validation of the models by comparing the difference between predicted responses for the optimal PM-CPC composition and the actual values from experimental data.....	85
Table 3.1: Percentage of α -TCP and HA phase from XRD data and Ca/P and Ca/O molar ratios after 1-, 3- and 7-days immersion of PM-CPC bone adhesive in Ringer’s solution.	112

List of Equations

Equation 2.1: Conversion of compression force (N) to compressive strength (MPa).....	67
Equation 4.1 – Percentage of Phase Separation between oil and powder phase:	132
Equation 4.2 –Injectability:	133
Equation 5.1– Calculation of cell viability %:.....	160
Equation 5.2– Percentage (%) reduction of alamarBlue reagent:.....	161

List of Publications and Oral/Poster Presentation

Publications

1. N. Dunne, **A. Tzagiollari**, M. Sahebalzamani, and T. J. Dunne, “8 - *Acrylic cements for bone fixation in joint replacement*,” in Woodhead Publishing Series in Biomaterials, P. B. T.-J. R. T. (Third E. Revell, Ed. Woodhead Publishing, 2021, pp. 213–262. <https://doi.org/10.1016/B978-0-12-821082-6.00021-2>
2. **Tzagiollari, A.**; McCarthy, H.O.; Levingstone, T.J.; Dunne, N.J. “*Biodegradable and Biocompatible Adhesives for the Effective Stabilisation, Repair and Regeneration of Bone*”. Bioengineering 2022, 9, 250. <https://doi.org/10.3390/bioengineering9060250>
3. Banche-Niclot, Federica, Ilaria Corvaglia, Caterina Cavalera, Elena Boggio, Casimiro Luca Gigliotti, Umberto Dianzani, **Antzela Tzagiollari**, Nicholas Dunne, Antonio Manca, Sonia Fiorilli, and et al.. “*Optimization of an Injectable, Resorbable, Bioactive Cement Able to Release the Anti-Osteoclastogenic Biomolecule ICOS-Fc for the Treatment of Osteoporotic Vertebral Compression Fractures*” Biomolecules 13, no. 1: 94. <https://doi.org/10.3390/biom13010094>
4. Samuel Black, **Antzela Tzagiollari**, Subrata Mondal, Nicholas Dunne, David B. MacManus. “*Mechanical behaviour of gel-filled additively-manufactured lattice structures under quasi-static compressive loading*”. Materials Today Communications 2023, 35,106164. <https://doi.org/10.1016/j.mtcomm.2023.106164>
5. **Antzela Tzagiollari**, John Redmond, Helen O. McCarthy, Tanya J. Levingstone, and Nicholas J. Dunne, “*Multi-objective property optimisation of a phosphoserine-modified calcium phosphate cement for orthopaedic and dental applications using Design of Experiments methodology*”. Acta Biomaterialia 2023. <https://doi.org/10.1016/j.actbio.2023.11.024>
6. Phillip Chambers, Monika Ziminska, Ahmed Elkashif, Jordan Wilson, John Redmond, **Antzela Tzagiollari**, Cole Ferreira, Auden Balouch, Jasmine Bogle, Seth W Donahue, Nicholas J Dunne, Helen O McCarthy; “*The osteogenic and angiogenic potential of microRNA-26a delivered via a non-viral delivery peptide for bone repair*”. Journal of Ophthalmology Clinics and Research 2023. 362: 489-501. <https://doi.org/10.1016/j.jconrel.2023.09.006>

Oral Presentations

1. Tzagiollari A., Levingstone T. Dunne N. “*Design and development of novel biomaterials for the treatment of the bone related diseases and injuries*”. 25th Annual Conference of the Section of Bioengineering of the Royal Academy of Medicine in Ireland (Limerick, Ireland, 18th-19th January 2019).
2. Tzagiollari, A., Levingstone, T.J., Insley, G., Dunne, N. “*Bioresorbable and biomimetic bone adhesive for defect repair and regeneration of bone*”. 26th Annual Conference of the Section of Bioengineering of the Royal Academy of Medicine in Ireland (Co Carlow, Ireland, 17th-18th January 2020).
3. Tzagiollari A., Levingstone T.J., Insley G.2, Kelly D., Procter P., Dunne N. “*Injectable Bioceramic-based Adhesives for Surgery and Tissue Engineering*”. 11th World Biomaterials Congress (Virtual, 11th-15th December 2020).
4. Tzagiollari A., Insley G., Kelly D., Procter P., McCarthy H.O, Levingstone T.J., Dunne N “*Injectable Bioceramic Adhesives for Bone Repair and Regeneration*”. 31st Congress of the European Society of Biomechanics (Virtual, 5th-9th September 2021).
5. Tzagiollari A., Insley G., Kelly D., Procter P., Levingstone T.J., Dunne N. “*Development of a Bioresorbable and Biomimetic Bone Adhesive (OsStic) for the regeneration of Bone Defects*”. 24th Sir Bernard Crossland Symposium 2021. (Trinity College Dublin, Ireland, 22nd-23rd September 2021).
6. Tzagiollari A., Levingstone T. Dunne N. “*Biomimetic Adhesive for Bone Fracture Repair and Remodelling*”. Research Day 2022. (Dublin City University, Dublin, Ireland, 7th April 2022).
7. Tzagiollari A., Insley G., Kelly D., Procter P., Levingstone T.J., Dunne N. “*Design of Experiment Approach for the Optimisation of an Adhesive for Bone Repair and Regeneration*”. 27th Royal Academy of Medicine in Ireland - Bioengineering in Ireland. (Galway, Ireland, 20th-21st May 2022).
8. Tzagiollari A., Insley G., Kelly D., Procter P., Levingstone T.J., Dunne N. “*Injectable Biomimetic Mussel – Based Adhesive for Bone Repair and Remodelling.*”. 32nd Congress of the European Society of Biomaterials. (Bordeaux, France, 4th-8th September 2022).
9. Tzagiollari A., Insley, G., Procter, P., Pippenger, B., Andersen, O.Z., McCarthy, H.O., Levingstone, T.J., Dunne, N.J. “*Development of a Bioresorbable and Biomimetic Bone Adhesive for the Regeneration of the Bone*”. 28th Royal Academy of Medicine in Ireland - Bioengineering in Ireland. (County Meath, Ireland, 27th-28th January 2023).

Poster Presentations

1. Tzagiollari A., Levingstone T. Dunne N. “*Injectable hydrogels loaded with ceramic particles for enhanced in situ bone regeneration*”. 11th World Biomaterials Congress (Virtual, 11th-15th December 2020).
2. Tzagiollari A., Insley G., Kelly D., Procter P., Levingstone T.J., Dunne N. “*Development of a Bioresorbable and Biomimetic Bone Adhesive (OsStic) for the regeneration of Bone Defects.*” 31st Congress of the European Society of Biomaterials (Virtual, 5th-9th September 2021).
3. Tzagiollari A., Insley, G., Procter, P., Pippenger, B., Andersen, O.Z., McCarthy, H.O., Levingstone, T.J., Dunne, N.J. “*Bioinspired Adhesive for Bone Stabilization and Regeneration*”. Orthopaedic Research Society (Dallas, Texas, 10th-14th February 2023).
4. Tzagiollari A., Insley G., Kelly D., Procter P., Levingstone T.J., Dunne N. “*Development of a Biomimetic-Based Adhesive for Bone Repair and Regeneration*” Congress of the European Society of Biomaterials (Davos, Switzerland, 4th-8th September 2023).

Awards

1. 26th Annual Conference of Bioengineering of the Royal Academy of Medicine in Ireland
Winner - **1st Place in the Biomaterials & Regenerative Medicine Early Stage Researcher Category** (January 2020).
2. Irish Research Council Scholarship – GOIPG/2020/371 - **Three-year funded PhD at the Dublin City University** (September 2020).
3. Postgraduate Accommodation Scholarship award from School of Mechanical and Manufacturing Engineering – **Awarded based on outstanding achievement at undergraduate and postgraduate level** (2020-21)
4. 24th Sir Bernard Crossland Symposium 2021 – **1st Prize Winner of the Engineers Ireland best paper award** (September 2021)
5. DCU Faculty Research Day 2022 – **1st Prize Winner for the project with the highest impact among other 2nd and 3rd year PhD students** (April 2022)

Abstract

Antzela Tzagiollari

Development of a Bioresorbable and Biomimetic Bone Adhesive for the Regeneration of Bone Defects

Phosphoserine is a ubiquitous molecule found in numerous proteins and demonstrates the ability to generate an adhesive biomaterial capable of stabilising and repairing bone fractures. This study aimed to develop phosphoserine-modified calcium phosphates (PM-CPC), which incorporate phosphoserine, with alpha-tricalcium phosphate (α -TCP) and calcium silicate for bone stabilisation and regeneration. The PM-CPC formulation was characterised and optimised using Design of Experiments (DoE) with the following inputs: grinding cycles of α -TCP, liquid to powder ratio (LPR) and the molar ratios of phosphoserine and calcium silicate. Also, a dual syringe-mixed PM-CPC adhesive was developed and assessed. The optimal PM-CPC formulation either hand-mixed or through the mixing system, necessitated a mixing time of 20 s and displayed an initial setting time between 3-4 min, and a bone-to-bone bond strength of 1.05 ± 0.3 MPa under wet environment providing suitable properties for surgeons to apply and stabilise bone fractures. Cell viability $>70\%$ and cell proliferation were obtained after indirect cytotoxicity study in both PM-CPC adhesives. The *in vivo* study in mini pigs clearly demonstrated the ability of PM-CPC to stabilise dental implants with implant stability quotient (ISQ) values of 65–85 after 15 min that indicates the level of stability and osseointegration in dental implants. The PM-CPC-bone-implant interface was sufficiently mature enough to have a measurable mechanical effect (pull-out force=287 N, torque strength=80 Ncm) at 8 weeks post-surgery. Qualitative histological analysis on an *in vivo* study of trabecular bone demonstrated newly formed bone around the implants and in the adhesive bone interface. The design, characterisation and development of the proposed bone adhesive and associated delivery device represent a major step forward in both orthopaedic and dental injuries and has the potential to improve patient outcomes.

**Chapter 1: Introduction and Literature
Review**

Sections of this Chapter have previously been presented (with some modification) in a literature review published in MDPI: *Bioengineering* (2022): ***Tzagiollari A, McCarthy HO, Levingstone TJ, Dunne NJ. Biodegradable and Biocompatible Adhesives for the Effective Stabilisation, Repair and Regeneration of Bone. Bioengineering. 2022; 9(6):250.***

1.1. Overview

Bone fractures are a common orthopaedic injury and a significant health problem that affects millions of people worldwide. According to the Global Burden of Disease Study, annually an estimated 178 million individuals (53% males and 47% females) worldwide suffer bone fractures, an increase of approximately 34% since 1990 [1]. The prevalence of fractures varies depending on age, sex, and underlying medical conditions [2]. Osteoporotic fractures alone account for 1.7 million disability-adjusted life years lost annually and the economic impact of fractures is substantial with estimates suggesting that the direct and indirect costs of osteoporotic fractures will exceed \$25 billion in the US by 2025 [3,4].

Traditional methods of fracture treatment involve immobilisation of the affected limb using casts or braces, and in more severe cases, surgical fixation with plates, screws, or other hardware. While these methods can be effective, they are associated with a range of complications including infection, non-union (failure of the bone to heal), and hardware failure especially in the treatment of complex bone fractures [5,6]. Specifically, in cases where multiple fragments of bone have resulted from multiple breaks, there is currently no convenient way to stabilise the small fragments of the fractured bone and prevent gaps between the bone fragments. Currently developed bone cements are either used in joint replacement surgeries or as bone void fillers, rather than directly binding small bone fragments, filling spaces between bone fragments and implants to create a stable composite structure. Overall they mainly provide stability and support in fracture sites, ensuring the alignment and mechanical strength during the healing process.

In addition to orthopaedic challenges, bone loss and bone defects can also pose challenges in oral implantology or tooth [7]. Teeth and oral implants rely on being anchored in the alveolar bone, however tooth loss or implant weakness/failure can occur due to oral diseases [8]. According to the Global Oral Health Status Report, approximately 50% of the population

suffer from at least one form of oral disease, with a low number of available oral care providers globally. Dental implants represent a widely employed treatment modality for tooth replacement, with titanium being the preferred metal due to its proven superiority in terms of corrosion resistance, biocompatibility, and mechanical strength [9]. While titanium dental implants yield satisfactory results, ongoing research and innovation in the improvement of implant materials has the potential to further enhance treatment outcomes [10].

Advances in materials science and tissue engineering have led to the development of a range of biomaterials that can be used to promote bone healing, including calcium phosphate cements (CPCs), which are biocompatible and can be engineered to have a range of mechanical and biological properties [11]. Such materials are capable of stabilising the fractured bone, creating a bond between the metal implant and bone, or bone to bone [12]. For instance, in biological fluids, alpha-tricalcium phosphate (α -TCP) when used as a cement component, transforms into hydroxyapatite phase, however α -TCP without the use of any additive is not able to promote bone remodelling providing only mechanical support within a void. This class of calcium phosphate offers the advantage of improved biological properties, controlled biodegradation, suitable moulding capabilities, and ease of delivery [13]. However, limitations relating to the use of cements remain, including inflammatory responses, stress shielding and mechanical failure that can lead to premature implant failure [14,15]. Therefore, improving our understanding of the underlying mechanisms of fractures, identifying modifiable risk factors, and developing effective prevention and treatment strategies are critical for reducing the burden of fractures and bone regeneration/remodelling on individuals and society.

Recently, to overcome these drawbacks, research relating to bone fracture healing and fixation has been focused on the development of bone adhesives enhanced with additives found on terrestrial organisms and marine animals to improve properties of current cements

[16]. These bone adhesives incorporate amino acid additives with calcium phosphates enhancing handling and setting properties, templating mineralisation of nanoscale amorphous calcium phosphate, and achieving metastable ceramic phase stabilisation—thereby improving mechanical properties and cell attachment, survival and proliferation [17,18].

The development of such biomaterials could provide solutions to clinical challenges associated with non-degradable and non-adhesive fixation devices used in bone reconstruction procedures. Biocompatible and biodegradable bone adhesives with satisfactory bone adhesive and cohesive strength could introduce new advanced therapies in the fields of orthopaedics and oral implantology.

1.2. Bone

Human bones are a vital part of the musculoskeletal system with remarkable adaptability, dynamic structure, and metabolic activity. The human skeletal system consists of over 200 bones, which are categorised into different groups based on their type (long, short, flat, or irregular), location (axial or appendicular), composition (cortical or trabecular) or predominant tissue support [19]. The extracellular components of skeletal system are mineralised, providing substantial strength and toughness [20–22]. Bone provides internal support through countering the force of gravity, forming specific cavities which serve to protect vital internal organs and provides attachment sites for muscles allowing motion to occur at specialised bone-to-bone linkages. The mechanical integrity and performance of bone under various loading conditions are directly affected by its mechanical properties and geometric characteristics, which are both indicators of bone health and underpin bone strength.

Bone consists of cells, mineralised matrix (i.e., composed primarily of calcium and phosphate), and ground substance [19,23,24]. The bone matrix is composed of both organic and inorganic components. The organic matrix, which makes up approximately 20% of the

wet weight of bone, is primarily comprised of type I collagen, with smaller amounts of other proteins and proteoglycans. Collagen gives bone its flexibility, and non-collagenous proteins and proteoglycans serve several important functions during osteoblast differentiation, tissue mineralisation, cell adhesion, and bone remodelling [25]. The inorganic matrix is predominantly composed of calcium hydroxyapatite crystals, which contribute to bone's stiffness and serve as an ion reservoir storing approximately 99% of total body calcium, approximately 85% of phosphorus, and between 40% and 60% of the body's sodium and magnesium [24].

Bone continuously modifies and regenerates itself in the presence or absence of mechanical loading, involving the careful cellular regulation and coordination of osteoblasts and osteoclasts [26,27]. Osteoblast cells are responsible for building new bone tissue, while osteoclast cells break down old bone tissue to make way for new growth. A further cell group, known as osteocytes, biochemically promote osteogenesis in response to loading demands by regulating and co-ordinating osteoblast and osteoclast activity. To fulfil these mechanical roles bone needs to be stiff to resist deformation, yet flexible to absorb energy. Also, it needs to be able to meet important auxiliary functions such as maintaining calcium homeostasis and haematopoiesis.

1.2.1. Bone Macro- and Microscopic Structure

Important information related to the function and properties of the bone can be obtained through understanding the predominant tissue type in a specific bone or bone region. Cortical and trabecular bone are the two main types of bone tissue (macroscopically), which have the same matrix composition but differ in structure, function, and distribution within bones (Figure 1.1).

Cortical bone forms the outer shell of bones, providing strength and helping with bone metabolism and marrow production [24,28–30]. Cortical bone makes up 80% of skeletal

tissue mass and is characterised by its high matrix mass and low porosity. It is primarily found in the diaphysis (cylindrical shaft) of long bones in the appendicular skeleton, providing strength and rigidity for weight bearing and muscle action. Cortical bone includes concentric layers along the periosteum (a dense fibrous membrane forming the outside layer) and endosteum (a thin membrane forming the inner layer) of the diaphyseal shaft, and contains cells responsible for bone modelling and remodelling [31,32]. The thickness and distribution of cortical bone plays a significant role in fracture risk, particularly at the femoral neck. Despite the dense structure, cortical bone does contain a porosity of approximately 10% of total cortical bone volume for vascular/neural supply and delivery of nutrients [19,23]. The degree of porosity can change with age, disease states, and pharmacological intervention, impacting bone strength and fracture risk. Cortical bone surrounds trabecular bone, but its distribution and composition differ among different bones within the skeleton. The unique structural and compositional characteristics of cortical bone contribute to its mechanical properties and function in the skeletal system.

Trabecular bone (or cancellous bone), in contrast to cortical bone, has high porosity with pores comprising 50-90% of total trabecular bone volume [3,19,20]. Trabecular bone is characterised by an organised network of vertical and horizontal plate- and rod-like structures called trabeculae, giving it a sponge-like appearance. Although trabecular bone has reduced compressive strength compared to cortical bone, due to its lower matrix mass per unit volume and high porosity, it serves important functions such as providing increased surface area for red bone marrow, blood vessels, and connective tissues to be in contact with bone [23]. This facilitates the role of bone in haematopoiesis (formation of blood cells) and mineral homeostasis (maintenance of mineral balance in the body). Furthermore, the trabecular bone can provide internal mechanical support by allowing for even distribution of load and energy absorption, especially near joints. Trabecular bone is also important during aging, as it tends

to be lost earlier and at a faster rate than cortical bone, which contributes to osteoporosis in areas rich in trabecular bone. The strength of trabecular bone depends on various factors such as the number, thickness, spacing, distribution, and connectivity of trabeculae, with connectivity being of particular importance [33]. Studies have shown that loss of trabecular connectivity has a greater negative impact on bone strength than the presence of thin but well-connected trabeculae. This is evident in women with low bone mass and vertebral fractures, who have a higher number of unconnected trabeculae compared to women without fractures, despite having similar bone mineral density [34,35]. This suggests that trabecular connectivity is a critical factor in determining bone strength. Overall, trabecular bone contributes to the mechanical and structural integrity of bone, playing an important role in bone health and function.

Cortical and trabecular bone have two types of tissue structure: woven and lamellar [36,37]. Woven bone is disorganised and primarily found during embryonic development, in pathological conditions or after injury. It is flexible but less stiff than lamellar bone [38]. Lamellar bone is organised into layers or lamellae, similar to plywood. Lamellar bone is stiffer compared to woven bone and is gradually formed during later stages of healing. In cortical bone, lamellae form osteons, while in trabecular bone, they form packets. The arrangement of lamellae differs in cortical and trabecular bone, with outer lamellae forming first in cortical bone, and the first lamellae forming toward the centre of trabeculae in trabecular bone[19]. Each successive lamella is deposited concentrically in cortical bone, and parallel layers away from the centre of trabeculae toward the bone surface in trabecular bone. This organisation of lamellar bone provides strength and stability to the bone tissue [29]. Overall, the presence of both woven and lamellar bone in different stages of bone development and healing allows for flexibility and strength as needed for various functional requirements of bone. It also highlights the dynamic nature of bone tissue remodelling and adaptation.

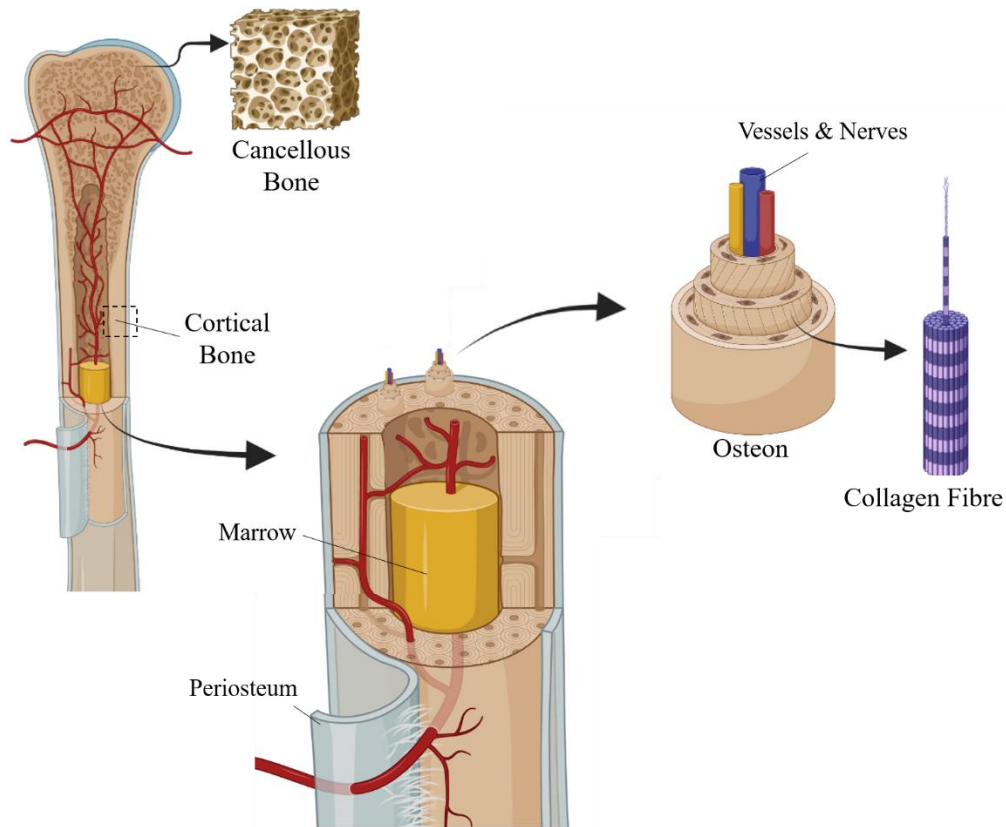


Figure 1.1: Bone Structure - The hierarchical macroscopic and microscopic anatomy and physiology of bone.

1.2.2. Bone Cells

Bone development, regulation, and maintenance is mediated by four key cells: osteoblasts, osteoclasts, osteocytes, and extra-cellular lining cells (Figure 1.2) [31,39,40]. Osteoblasts are responsible for producing new bone material by synthesizing and calcifying newly generated collagen [40]. They can also transform into bone lining cells or osteocytes during the osteogenic process. Osteoclasts, on the other hand, degrade, dissolve, and resorb bone material, often in response to material damage or disuse. Osteoclasts have a limited lifespan, undergoing apoptosis (programmed cell death) within 2 to 4 weeks of osteoclastogenesis [41]. Osteoblasts and osteoclasts work independently during bone creation and formation (modelling), and co-operatively via a basic multi-cellular unit during bone maintenance and homeostasis (remodelling) [39]. Osteocytes are central to bone development and renewal as the most abundant residential cell in bone, accounting for approximately 90% to 95% of all

bone cells. Osteocytes, the most abundant residential cell in bone, are descendants of osteoblasts produced during osteogenesis and are responsible for forming a well-connected network of sensory channels to detect environmental alterations and communicate reactionary processes to other bone cells. The well-connected network, proliferate through canaliculated passages to provide a functional and mechanosensitive platform integral to the detection of mechanical load and associated microdamage [39]. This mechanically sensitive function, known as mechanotransduction, enables bone to physiologically detect and convert mechanical energy into proportionate biochemical signals in order to promote growth and repair processes. The process of mechano-transduction is essential for bone adaptation, which is the ability of bone to modify its structure and composition in response to mechanical loading, and is dependent on the activation of osteocytes and their signalling pathways [31].

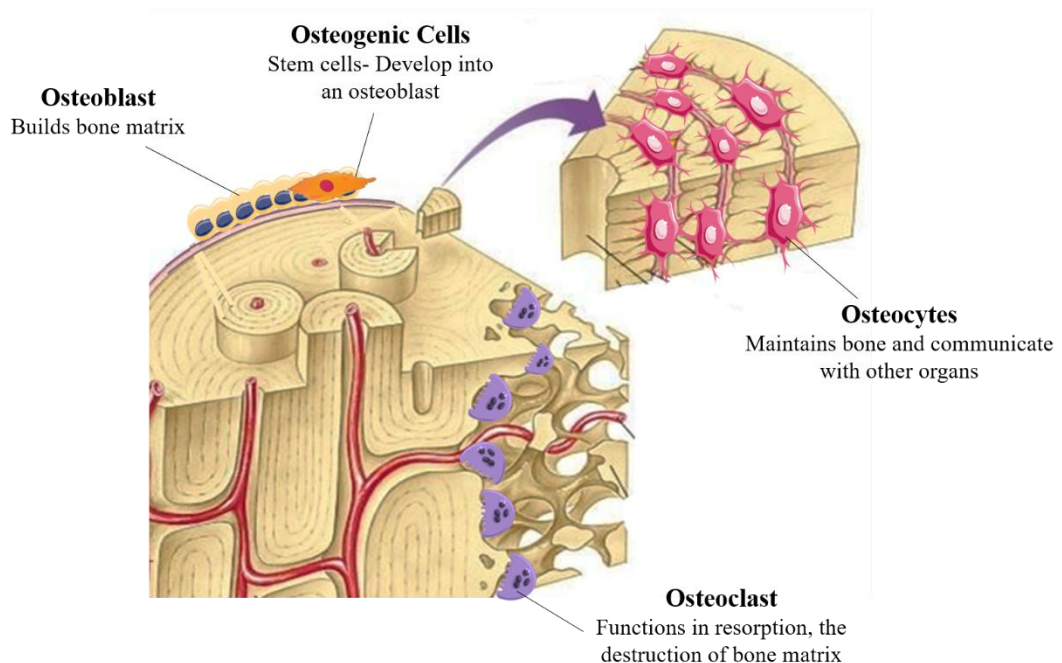


Figure 1.2: Cells Found within Bone Tissue - Osteogenic cells are undifferentiated and develop into osteoblasts which get trapped within the calcified matrix and changes into osteocytes. Osteoclasts develop from monocytes and macrophages and differ in appearance from other bone cells.

1.2.3. Bone Fractures

Complex bone fractures generally consist of multiple fragments and pose several challenges in terms of diagnosis, treatment, and management [42]. Bone fractures range in severity, from hairline cracks to complex fractures which require surgical intervention [43,44]. Due to the association of fractures with various complications such as non-union, mal-union, and infection, prolonged recovery times and increased morbidity can occur. For instance, a recent systematic review and meta-analysis found that hip fractures were associated with a two-fold increase in mortality risk over ten years in older adults. These fractures therefore present significant challenges for orthopaedic surgeons and often lead to poor clinical outcomes [45].

Surgical treatment approaches are aimed at establishing stability to the broken bones, both above and below the fracture site, with internal or external supports [46]. Post-operative management may involve physical therapy and rehabilitation to promote healing and restore function [47]. Furthermore, pain management, nutritional support, and monitoring for potential complications, which may require additional surgical interventions are considered current challenges.

The most common types of challenging bone fractures are distal radius fractures, facial bone fractures and foot/ankle bone fractures (Figure 1.3) [48–50]. Currently, 20% of distal radius fractures and 71% of facial fractures require surgical intervention, with almost 20% of facial fracture requiring secondary surgical procedures [51,52]. The number of fractures that require surgical intervention is reportedly increasing among the younger patient population, with 45% of fractures in those under 25 years old and 37.5% of fractures in the age group of 25-30 years old requiring surgical intervention [52]. Scaphoid fractures are the most common carpal bone fractures (70% of all carpal bone fractures) that cause long-term pain and frequently require surgery [53]. Facial bone fractures also occur frequently with an increased number of fractures being reported annually [52,54–56].

In terms of long bone fractures, it is estimated that there are 9 million incidents worldwide annually caused by medical conditions such as osteoporosis [57]. According to Fisher *et al.* [58], 20% of fractures result in one or more complications such as deep infections (i.e., pain, erythema and pus discharge), fixation or implant failures (i.e., loosening of the screws and re-fracture following mobilisation), delayed union/non-union due to deep infection or failure of implant/fixation and re-fracture through the site of original injury or the screw hole. Treatment of long bone fractures at more than one anatomical site presents many clinical challenges and requirements due to the weakness of the osseous tissue, which ultimately leads to poor clinical outcomes [59,60]. Proximal humeral fractures are also complex and challenging to manage and treat due to the complexity of the bone anatomical site [61]. Conventional surgical treatment for fracture of the proximal humeral bone normally results in a reduction in the range of motion, poor restoration of anatomical congruity, pain and a risk of infection [60]. The cost of treating complex fractures can be substantial, particularly in cases involving prolonged hospitalisation and surgical interventions. A study by Metsemakers *et al.* reported that the mean cost of treating complex tibial fractures was approximately €16,000 per patient between 2009 and 2014 [4]. As complex fractures are very painful and difficult to recover from, the treatment plan must be carefully designed to achieve the best clinical outcomes.

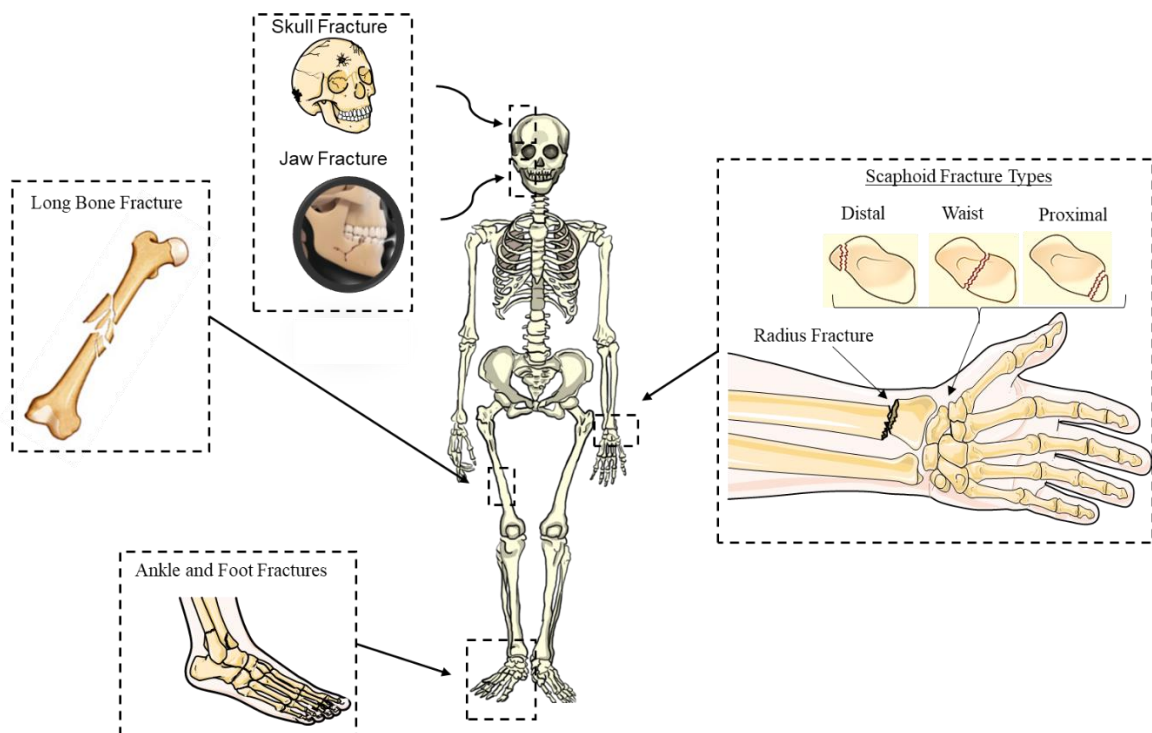


Figure 1.3: Types of Bone Fractures - Complex fractures occur most frequently in the long bones, carpal, facial, ankle and foot bones. The wrist, facial, ankle and foot bones contain several small bones close to each other, leading to complex fractures.

1.2.4. Natural Bone Healing Mechanism

Bone is a biomaterial well-suited for physiological and biomechanical investigation due to its mechanical receptivity, biological adaptability, and metabolic activity. The skeleton has the ability to construct (model) and reconstruct (remodel) itself through cellular processes in response to developmental and mechanical loading demands.

During the normal bone healing process, three overlapping stages occur: (1) inflammation, (2) bone production and (3) bone remodelling (Figure 1.4). Initial bleeding into the fracture area is followed by inflammation and clotting of blood at the fracture site. These processes involve haematopoietic and immune cells within the bone marrow and mesenchymal stem cells (MSCs) from the surrounding tissue and bone marrow [32,62]. Clotted blood is replaced with fibrous tissue and cartilage (soft callus) within 2 to 4 weeks. Callus formation around the fractured bone provides early stabilisation and protects the repair tissue from external forces [63]. Subsequently, the calcium formation that is laid down in the matrix within the next 4 to 12 months results in the callus becoming visible on radiographic images. The successful restoration of the original shape and structure of bone (i.e., bone remodelling) is the final stage in the normal healing process. In some incidences, bone healing does not occur in accordance with the normal bone repair processes. For example, micromotion at the repair site can interrupt the healing process and lead to other possible complications such as bleeding into a joint space that causes the joint to swell (hemarthrosis), and blood clot formation that can cause blockage within a blood vessel locally or elsewhere in the body. Non-union fractures occur when the broken bones are not able to heal due to insufficient nutrition, limited blood supply or inadequate stability (poor immobilisation). In these cases, the healing process can last from months to years. Fractures that contain small bone fragments require careful management in order to achieve fracture repair and bone remodelling [5]. The objective of early fracture management is to control bleeding, prevent ischemic injury (i.e. bone death)

and remove sources of infection such as foreign bodies and dead tissues [64]. Fracture management includes reduction of the fracture followed by maintenance of the fraction reduction using immobilisation techniques.

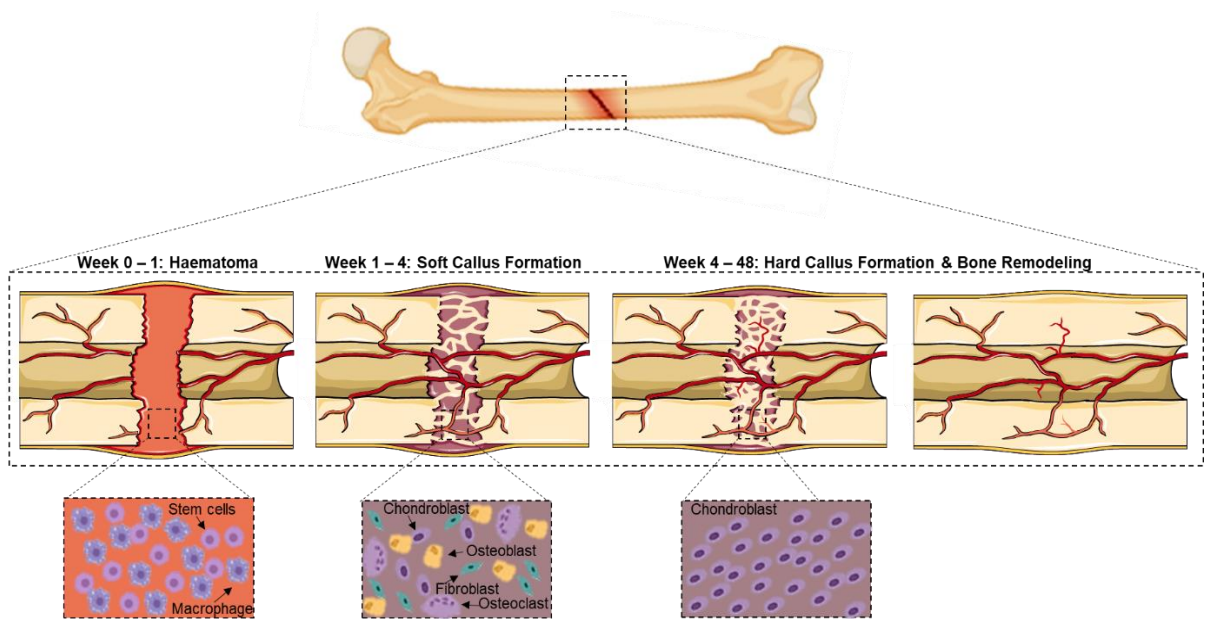


Figure 1.4: Natural Bone Healing - Stages of bone healing: (1) haematoma formation from stem and macrophage cells at the fracture site (week 0-1), (2) soft callus formation at the fracture site, from chondroblast, osteoblast, fibroblast and osteoclast, replaces the hematoma (week 1-4) and (3) hard callus replaces the soft callus, using chondroblast cells and after week 6-8 bone starts to replace the hard callus (week 4-48).

1.3. Current Surgical Approaches – Orthopaedic

Currently used immobilisation techniques range from the use of a cast or wrap (i.e. non-operative therapy) for simple fractures to the use of metal hardware (i.e. operative therapy). Metallic plates and wires have been used to provide compression and stabilisation between the fractured bone fragments in internal fixation procedures for +100 years. Surgical treatment approaches are aimed at establishing stability to the broken bones above and below the fracture site with internal or external support. Another purpose of surgical intervention is to supply of fracture site and surrounding soft tissue with blood and to remove the dead bone and any poorly vascularised or scarred tissue from the fracture site to encourage healing. Sometimes healthy soft tissue along with its underlying blood vessels may be removed from another part of the body and transplanted at the fracture site to promote healing. More complicated fractures require surgical intervention such as open reduction and internal fixation (ORIF) or external fixation.

1.3.1. Open Reduction and Internal Fixation (ORIF)

ORIF is a surgical procedure where the fracture site is adequately exposed, and reduction of fracture is conducted. Several devices have been used for the internal fixation of bone fractures, including plates, interlocking nail devices, intramedullary compression nail devices, bridging devices, and balloons [65]. There are a number of different types of plates with the most common being dynamic compression plates. Dynamic compression plate (Figure 1.5a and 1.5b) are designed to exert dynamic pressure between the bone fragments, which is achieved either by attaching a tension device to a plate or by using a special plate. For the placement of the tension device, a longer surgical incision is required and there is a possibility of re-fracture after the plate is removed. The benefits of dynamic compression plates include low incidence of malunion and stable internal fixation, allowing immediate movement. However, the use of dynamic compression plates for fracture repair have several

disadvantages such as delayed union, existence of microscopic fracture gaps and cortical bone loss after plate removal [6]. For instance, Mardam-Bey *et al.* reported outcomes for tibial eminence fracture repair using screw fixation on dynamic compression plates, reporting that 20% of patients show anterior screw relaxation following treatment and 10% of patients experience rotational instability and loss of motion [66].

Intramedullary compression nails [67] (Figure 1.5c) and interlocking nails [68] (Figure 1.5d) are also widely used in bone fracture repair. The intramedullary compression and interlocking nail are inserted into the medullary cavity of a bone to re-join and reinforce the broken bone parts and permit the functional rehabilitation of the limb within a few days. These nails usually do not demonstrate sufficient mechanical strength to enable full load-bearing capability, therefore functional use of the limb is not possible until the healing process is complete. Consequently, immobilisation of the limb for long periods is required, which can impact the patient's quality-of-life and ability to work during that time and also poses risks of muscle atrophy and other ailments. The interlocking nail method is frequently used for the treatment of complex and unstable fractures of the femoral shaft. Generally, femoral shaft fractures are considered relatively uncommon but serious injuries, often resulting from high-energy trauma like vehicle accidents or falls from height and represent about 3% of all fractures. This is a technically challenging procedure due to the requirement for accurate placement of locking and stabilisation screws that secure the compression nail in place.

A bridging device is an expandable fracture fixating device used for internal fixation by implanting the device within the medullary cavity (marrow conduit) of the bone and positioning it across the fracture (Figure 1.5e) [69]. These expandable and hollow structures are able to "bridge" the bone fracture site, fixate the site upon expansion and allow the maintenance of the majority of the bone marrow volume. Their use has been shown to enhance bone health, healing and the ability of the body to generate red blood cells [70]. This device

can be implanted for the temporary stabilisation and fixation of bone fractures, but after a period, surgical removal is required. These devices are part of a broader category of intramedullary fixation methods and are commonly used for long bone fractures, such as those of the tibia, femur, and humerus. Tibial shaft fractures, represent about 37% of all long bone fractures in adults, with an overall incidence of 17–21 per 100,000 population. A similar method developed by Berger *et al.* involved the use of a balloon catheter fixation device [71]. In this approach, a balloon catheter was placed either proximal or distal to the fracture site, adding compressive force to enable reduction and stabilisation of the fracture (Figure 1.5f). The main objective of these devices is, firstly to stabilise the fracture site and secondly to increase the rate of healing. The elastic property of the catheter that is tightened against the rigid immobile force of the anchoring balloon allows the fractured segments of the bone to align and come in intimate contact.

While these expandable fixation devices are considered to be minimally invasive, they are limited to long bones only, due to their length. Also, complications may occur such as persistent infection (e.g. chronic osteomyelitis) of bone or bone marrow since it requires delivery and penetration into the medullary cavity. For example, a meta-analysis found the incidence of hardware irritation to be approximately 22%, soft tissue problems around 9%, and infection also around 9%. These complications can vary depending on the specific type of fracture and the overall health and circumstances of the patient. Infections, including chronic osteomyelitis, can be as high as 2.4% for deep infections, with other studies indicating infection rates between 5% and 16% depending on the fracture location and patient conditions. Treatment of such infections requires, hospitalisation and treatment with antibiotics or surgical drainage and curettage [65]. Post-surgical infections are one of the major complications associated with the application of all internal fixation devices. Frequently these infections result in bone or tissue necrosis and in severe cases can result in

the death of patient - therefore additional surgical intervention and therapy is required. Although most bone fractures heal without complications, in some cases successful healing is not achieved resulting in delayed unions or non-unions, necessitating a bone graft.

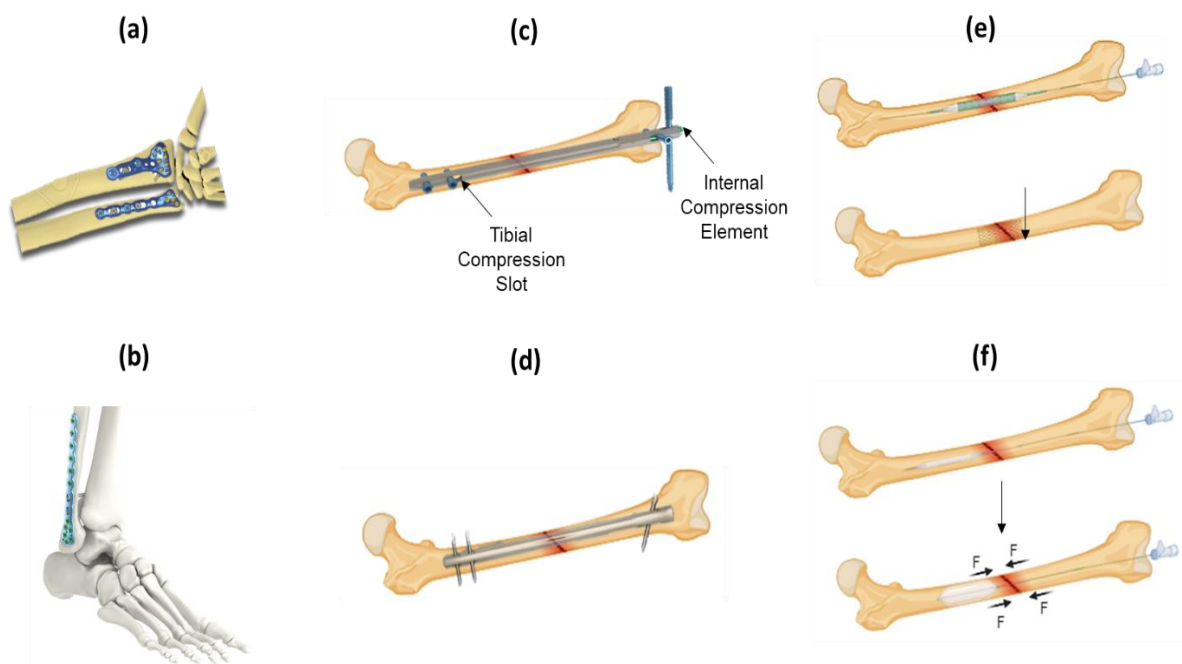


Figure 1.5: Surgical Approaches used for Internal Bone Fixation - (a) dynamic compression plates for ulna and radius and (b) ankle bone fractures, including screws for the bone stabilisation, (c) intramedullary compression nail, (d) interlocking nail, (e) metallic stent to the fracture site “bridge” and (f) balloon application to the fracture site.

1.3.2. External Fixation

External fixation is a procedure in which the fracture stabilisation is achieved at a distance from the site of fracture. It helps to maintain bone length and alignment without casting. Devices used for external fixation are made of metal or carbon fibre and, as with skeleton traction methods, these devices have pins placed into the bone directly through the skin [72]. External fixation has evolved from being used primarily as a last resort fixation method to becoming a mainstream technique used to treat bone and soft tissue pathologies. Percutaneous techniques are used for the treatment of tibia periarticular [73] and femoral shaft [68] complex fractures, leading to the enhancement of biologic fracture healing and a decrease in the complications observed with other open reduction techniques. Development of unilateral frames and circular frames [72] have been reported (Figure 1.6). Unilateral and circular frames are positioned on one side of or around the limb with the use of pins, allowing the limb to remain functional, avoiding the complications associated with immobilisation, and providing bone stability. However, these techniques are characterised by a high risk of wound and pin tract infection and incisional morbidity as well as damage to surrounding tissue, nerves, skin, blood vessels, or nearby organs [65]. Furthermore, these devices require substantial attention and care to prevent inflammation.

Despite the widespread use of metal hardware, they have associated limitations and frequently result in poor healing, such as mal-unions [74]. In particular, the loosening of bone plates, screws and pins often occurs over time post-surgery while external plates and frames require removal, which can lead to cortical bone loss or post-surgery complications [6]. In cases where multiple fragments of bone have resulted from multiple breaks, there is currently no convenient way to stabilise the small fragments of the fractured bone and prevent gaps between the bone fragments. An alternative approach to overcome some of the challenges relating to the use of metal hardware in fracture repair is the use of bone adhesive materials.

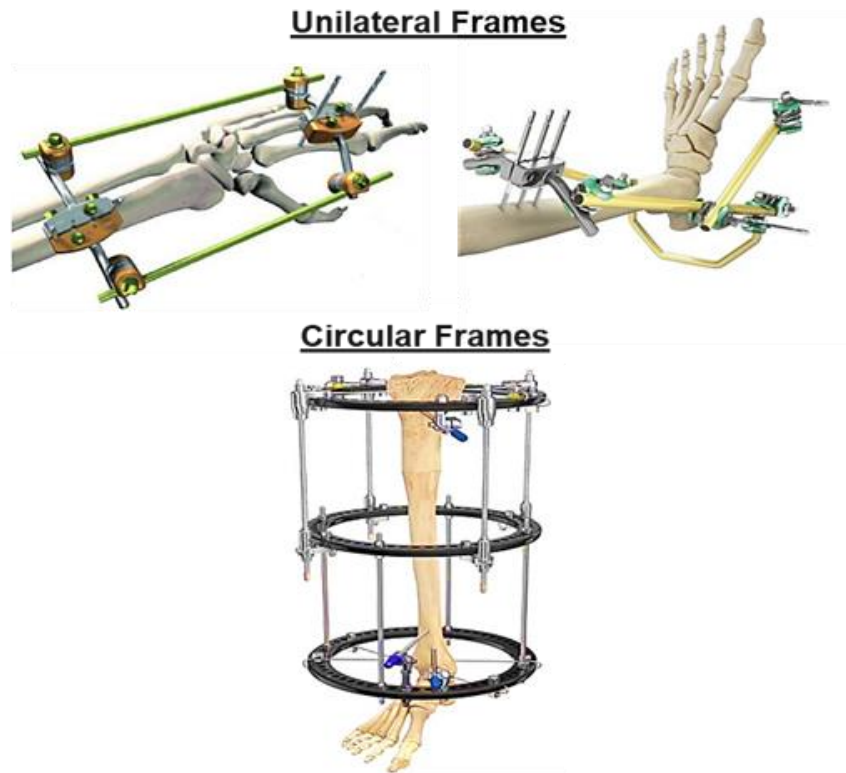


Figure 1.6: Surgical Approaches used for External Bone Fixation - Fixation devices such as unilateral frames [75] placed on one side of the ankle or distal bone and miniplates or screws including pins for molar bones and circular frames [76] placed around the long bone, allowing functionality and bone stability during the bone healing process.

1.4. Dental Prosthetics or Implants

The mouth, also known as the oral or buccal cavity, acts as the entrance to our digestive system, facilitating the intake of food and air into the body [77]. When it comes to materials used in dentistry, certain essential biological qualities are needed, including non-toxicity, biocompatibility, prevention of bacterial microleakage, low plaque formation, and the capacity to facilitate tissue regeneration [78].

Dental implants and prosthetics are used to replace missing or damaged teeth with more than 90% success rate [79]. There are three main types of dental implants, each suited for different

situations and patient needs: endosteal or endosseous, subperiosteal, and transosteal (Figure 1.7).



Figure 1.7:Types of Dental Implants – Endosteal implants placed directly into the jawbone, subperiosteal implants consist of a metal frame that is fitted onto the jawbone just below the gum tissue and transosteal implants inserted through the jawbone from underneath the chin.

1.4.1. Endosteal or Endosseous Dental Implants

Endosseous dental implants serve as substitutes for dental roots and are typically placed within the mandible or maxilla. These implants are commonly constructed using titanium due to their heightened resistance to corrosion, increased strength, and excellent biocompatibility. Endosseous implants can be further categorised into two main types: root implants and blade implants [80]. Root implants are utilised for supporting dentures or replacing damaged tooth roots and can be inserted in either the mandible or maxilla, depending on the location of the damage. The choice of implant type depends on factors such as the patient's root cavity condition, the nature of the damage, and the patient's age. Root implants are available in various designs, including screw-threaded, solid-body press-fit, and porous material-coated designs [81].

Extensive research has been conducted to enhance the success rates of screw-threaded implants. Factors such as implant diameter, length, geometry, and threading have been investigated in depth [82,83]. Typically, the length of root screws ranges from 8 mm to

15 mm, with diameters spanning from 3 mm to 7 mm [80]. Longer screws distribute stress across a larger surface area, promoting effective osseointegration. Wider screws engage with more substantial bone areas and are well-suited for removal torque tests. The addition of threads to the root implant enhances initial stability, increases initial contact, and enlarges the surface area [84]. On the other hand, blade implants are custom-made anchors for dental prosthetics. These implants support abutments using metal plates placed laterally rather than vertically along a dental root. An essential consideration in the design of blade implants is their flexibility, allowing them to align parallel to the curved mandible or maxilla while maintaining abutment alignment [85].

While endosteal dental implants offer a highly effective solution for tooth replacement and denture support, it's important to acknowledge their limitations [86]. One notable limitation is the requirement for a sufficient quantity and quality of bone in the implantation area [87]. In cases where the patient has experienced significant bone loss or has an inadequate bone structure due to various factors, such as long-term tooth loss or periodontal disease, endosteal implants may not be feasible without prior bone augmentation procedures. Additionally, the healing process and osseointegration, which are critical for implant success, can be affected by factors such as patient health, smoking habits, and certain medical conditions [87]. Moreover, the placement of endosteal implants necessitates a surgical procedure, which carries inherent risks and may not be suitable for patients with certain medical conditions or preferences. Finally, the cost of endosteal dental implants and associated procedures can be a limiting factor for some patients, making affordability a consideration in treatment planning [88].

1.4.2. Subperiosteal Dental Implants

Subperiosteal implants are designed to sit between the jawbone and the gum tissue, eventually becoming securely anchored to the jawbone through osseointegration [77]. Within this

category, there are two primary types of implants: dentures and ramus frames [89,90]. Dentures can be further categorised into fixed dental dentures and removable dentures. Based on placement technique and patient requirements, removable dentures can be classified as partial or full. Currently, removable partial dentures are the preferred choice for many patients due to considerations related to anatomy, physiology, and cost-effectiveness however there is need for rehabilitation in either the maxillary or mandibular region. Subperiosteal implants are particularly useful when conventional implant support placements are lacking.

1.4.3. Transosteal Implants

Transosteal implants come into play when patients face severe resorption and jaw damage due to inadequate implant support [77]. This implant type involves affixing a metal plate with screws that penetrate through the jawbone, securing it to the lower mandible. The metal rods from other implants extend from the superior mandible to the inferior border, effectively serving as a horizontal support beam. The procedure requires both intra- and extra-oral incisions to ensure proper stability, often referred to as a mandibular staple. It's important to note that transosteal implants are not commonly employed due to their prohibitive cost, with more cost-effective alternatives typically explored.

1.5. Type of Adhesives

Bone adhesive present a promising approach for bone fracture stabilisation, repair and regeneration applications, with the potential to overcome limitations of existing fracture repair techniques [16,91]. For a bone adhesive to be suitable for use in bone fracture stabilisation and repair applications it must meet several clinical requirements [12,91–94]. Bone adhesives must provide early mechanical stability combining optimal adhesive and cohesive properties. Appropriate adhesion to the bone under clinically relevant situations such as a moist environment, presence of bleeding and uneven surfaces, as well as stability under internal or external forces (e.g., tensile, compression or shear forces) must be achieved

[92,95]. Biocompatibility is also an important requirement in order to avoid cytotoxic responses and facilitate fracture healing through osteogenesis and ultimately bone regeneration [96]. The bone adhesive also needs to be biodegradable and bioresorbable with non-toxic by-products such as gases (e.g., CO₂), water and inorganic salts that can be processed naturally by the body without causing cytotoxic effects [97].

A number of the synthetic naturally derived and biomimetic-based bone adhesives that have been previously discussed have been explored and adapted for use in bone repair applications including fracture fixation, bone defect repair and prosthetic implant bonding to soft/hard tissue [95,98]. These bone adhesives have the potential to overcome the disadvantages of conventional invasive surgical techniques and meet clinical requirements.

1.5.1. Synthetic and Natural Derived Adhesives

Early investigations into the use of bone adhesives in bone repair applications involved the development of epoxy resin-based bone adhesives such as phenol-formaldehyde resins. While these materials offered a high mechanical strength, they have been reported to lack biocompatibility [99]. Cyanoacrylate- (e.g. cyacrin) and polyurethane-based synthetic polymers have also been proposed as bone adhesives due to the high bonding strength and ability to achieve adhesion in a wet environment [100]. Although, these cyanoacrylate- and polyurethane-based bone adhesive demonstrated high tensile and adhesion properties, high infection rates, non-union (e.g., fracture displacement), low biodegradation and severe local reactions have been reported [99,101]. The poor outcomes from these initial materials have resulted in research into alternative bone adhesives with more suitable functional properties and improved clinical outcomes.

One such study investigated the application of a non-elastomeric crosslinked polyurethane-based bone adhesive for the stabilisation and repair of bone fragments from the tibia [102]. The bone adhesive was improved by incorporating calcium and phosphate

compounds. *In vivo* results demonstrated that stabilisation and bonding of the bone fragments as well as *de novo* bone growth were achieved with no evidence of inflammation/infection at the fracture site, as well as some biodegradation and good biocompatibility [102]. A similar polyurethane-based bone adhesive was developed by Schreader *et al.* for bone-to-bone fixation. This material consisted of a foam-like bone adhesive containing 4,4-methylene diphenyl diisocyanate and caprolactone-based diol (polyol) reinforced with hydroxyapatite nanoparticles [103]. The crosslinking occurred via moisture-curing polyurethane chemistry which can influence the physical properties. However, the final physicochemical and functional properties were dependent on the chemistry and structure of polyol. This bone adhesive demonstrated strong bone-to-bone bonding with an adhesion strength of 4.47 MPa after 20 h, which is four-fold greater than conventional poly(methyl methacrylate) (PMMA)-based bone cement.

Several studies have focused on the development of PMMA-based bone adhesives for bone repair applications. These bone adhesives have been predominantly used in dentistry and orthodontics due to their weak adhesion to bone, especially in a wet environment [104]. Another issue is the exothermal reaction that occurs during the polymerisation that can lead to cell death and bone tissue necrosis [105]. Enhancement of the adhesive strength of PMMA-based bone adhesives has been reported by enriching the bone adhesive with hydroxyapatite particles [106]. However, despite the increase in adhesion strength, the lack of biodegradability has limited the clinical application as a bone adhesive for bone repair applications [107]. A bone adhesive that shows improvements in adhesive properties particularly in an environment with high humidity as well as improved biodegradation have been achieved by Wistlich *et al.* [108]. They developed a bone adhesive for bone repair applications using a photocurable poly(ethylene glycol) dimethacrylate (PEGDMA) matrix, adding an isocyanate functional (six-armed) star-shaped prepolymer with ethylene oxide and

propylene oxide copolymerised (NCO-sP(EO-stat-PO)) in a ratio of (4:1). The NCO-sP(EO-stat-PO) enhanced the biodegradation properties and demonstrated a low level of cytotoxicity. Furthermore, improved adhesive properties were achieved by modifying the matrix PEGDMA with biodegradable ceramic adjuvants. In addition to improving the adhesive properties of the bone adhesive, these ceramic-based adjuvants also increased the porosity of the adhesive, leading to ingrowth of new bone via ion release. This bone adhesive has also been shown to be cytocompatible, easy to apply, demonstrate appropriate bone-to-bone adhesion in a wet environment, as well as supporting bone formation during fracture healing.

In 1982, researchers investigated the potential applications of fibrin glue in oral and maxillofacial surgery, primarily as a haemostatic agent for managing soft tissue injuries [109]. However, the true breakthrough came in 1985 when Keller *et al.* introduced fibrin glue as a composite of fibrinogen and thrombin, highlighting its suitability as a scaffold for enhancing bone regeneration in craniofacial bone reconstruction [110,111]. This research was significant due to fibrin glue's remarkable biocompatibility, biodegradability, and its ability to facilitate cell binding. Subsequent investigations have demonstrated the multifaceted benefits of fibrin glue in various aspects of oral and maxillofacial surgery [112–114]. From these studies it was found that that they can lead to reduced operative durations during periodontal surgery, along with accelerated and improved healing of grafts that are isolated from the oral cavity. Moreover, fibrin glue has proven instrumental in enhancing the bone graft healing process and the bone graft incorporation and remodelling, thereby reducing the risk of infection and hospitalization in maxillary surgeries [109].

Results of another study on the use of autogenous bone combined with fibrin glue for maxillary sinus grafting and simultaneous implant placement led to significantly higher volume of bone formation [115]. Additionally, this combination exhibited the potential to

improve the osseointegration of dental implants in sinus floor augmentation procedures with simultaneous implant placement [110]. Autologous bone graft has been considered for reconstructing oral and maxillofacial defects their application is still limited due to its disadvantages [116,117]. These drawbacks include the necessity for an additional surgical site, donor site-related morbidity and infection risks, as well as the potential for bone graft particles to shift during placement [117].

Fibrin-based natural polymers have also been applied clinically as bone adhesives, providing biocompatibility, biodegradability and cost effectiveness [117]. Fibrin glue is a biological adhesive made from fibrinogen and thrombin, which are components of the blood coagulation cascade. These bone adhesives have been extensively used in bone tissue engineering applications, mainly for the acceleration, union and revascularisation of osteochondral fragments [118,119]. Nihouannen *et al.* [120] developed a bone adhesive by incorporating macro- and micro-porous biphasic calcium phosphate (BCP) ceramic granules within a fibrin-based sealant (i.e., Tissucol). 60% hydroxyapatite and 40% beta-tricalcium phosphate (β -TCP) were incorporated into the fibrin-based sealant and the osteoinductive properties evaluated. The formation of a well mineralised ectopic bone was observed between the BCP particles within the dorsal muscles of sheep, proving the ability of the BCP-fibrin-based sealant to promote osteogenesis [120]. Cassaro *et al.* [121] developed a bone adhesive that included a fibrin-based biopolymer, which demonstrated haemostatic, sealant, adhesive, scaffolding and drug-delivery properties. The adhesive further included biphasic calcium phosphate particles and MSCs. Cassaro *et al.* [121] demonstrated the bone adhesive to be cost-effective to manufacture, offering good biocompatibility, as well as effective repair of fractured bone and the formation of new bone in the male Wistar rats.

Polysaccharide-based bone adhesives have also been developed for bone repair applications. For instance, Kumbar *et al.* [122] investigated bone adhesives from cellulose derivatives such

as cellulose acetate and ethyl cellulose, which are linear polysaccharides of D-glucose units linked by $\beta(1\rightarrow4)$ glycosidic bonds. The hydrogen-bonded structure resulting from the $\beta(1\rightarrow4)$ glycosidic bonds led to good biocompatibility and high mechanical properties. This study reported that the polysaccharide-based bone adhesive can form adhesive bonds between cellulose and bone through the carboxylic acid groups, as well as demonstrate a compressive strength (27-33 MPa) close to human trabecular bone. Two component bone adhesives derived from polysaccharides were developed by combining biocompatible chitosan or dextran with degradable starch [123]. Initially, the polysaccharides were oxidised with periodic acid (L-3,4-dihydroxy-L-phenylalanine (L-DOPA)) to generate aldehyde groups, which is the main component found in mussels to help them adhere to the surface of a rock. In this bone adhesive, a covalent bond that is developed enabled a strong adhesion bond at the bone-bone interface as well as a high cohesion strength within the bone adhesive. This bone adhesive demonstrated excellent biocompatibility with higher mechanical properties than fibrin glues.

L-DOPA, a hydroxylated form of tyrosine, has also been incorporated with the functional binder (mussel-derived adhesive protein) to effectively retain deproteinised bovine bone mineral within the bone defect for bone tissue engineering applications [124]. Assessment of the biomechanical properties demonstrated the formation of an aggregate by the binding of the particles. An improvement in osteoconductivity and acquisition of osteoinductivity was observed, which resulted in an acceleration in bone remodelling and regeneration with the density of new bone similar to the normal bone. The different applications sites as well as properties and drawbacks of the synthetic-based bone-adhesive materials described in this section are summarised in Table 1.1.

1.5.2. Biomimetic-Based Adhesives

Some terrestrial organisms as well as marine plants and animals use combinations of proteins and polysaccharides for the formulation of bioadhesives to meet specific requirements to function in the natural environment (e.g. settlement, hunting, and defense) [101]. In many cases, these bioadhesives demonstrate higher mechanical properties compared to the currently developed synthetic or natural polymer-based adhesives and adhesion within a wet environment. Specifically, these types of adhesives are able to create ionic and/or covalent bonds with the bone surface or bone collagen. The ability to cure at physiological temperatures, and to achieve a high bonding strength to biological materials including bone materials has prompted research into its use as a bioadhesive for bone tissue engineering applications.

To date, a number of bioadhesives that mimic these animals and plants have been investigated and/or developed but the bioadhesive produced have not yet been translated for clinical use for bone tissue engineering applications. Different types of biomimetic adhesives discussed, and the properties are summarised in Table 1.2. There are a number of terrestrial organisms that are capable of forming bioadhesives, including the Australian frog (e.g. *Notaden bennetti*) and Caddisfly (e.g. *Trichoptera*). The *Notaden bennetti*, can form a protein-based elastic hydrogel-based adhesive that is able to function in moist environments, bind to biological tissues as well as other surfaces [92]. The bonding is achieved by covalent bonding with amines present in the bone collagen matrix. These frog-derived bioadhesives performed significantly better than fibrin glues in cartilage repair models, providing biocompatibility and resorbability although they did not outperform cyanoacrylates in terms of adhesion strength [125]. Overall, the unique properties of these biomimetic copolymers suggest that they could have great potential for application as bioadhesives for bone tissue engineering applications. However, the research related to this bioadhesive is still at a primary stage and

further investigation is required to evaluate this material as a bioadhesive for bone fragments stabilisation and repair [126].

Stewart *et al.* described a bioadhesive, that mimics caddisfly silk, combining phosphate-functionalised and amino acid-based poly(ester urea) copolymers for the enhancement of the mechanical properties [127]. These bioadhesives demonstrated higher levels of adhesion to bovine bone when crosslinked with Ca^{2+} ions.

Marine animals, such as the blue mussel (e.g. *Mytilus edulis*), barnacle (e.g. *Balanus hameri*) and the sandcastle worm (e.g. *Phragmatopoma californica*) also produce adhesive proteins. *Mytilus edulis* have the ability to strongly attach themselves to both inorganic and organic host surfaces at various levels of salinity and humidity at ambient temperature [137]. The functionality of these mussel-derived bioadhesives is based on an extremely complex interaction between different proteins. These bioadhesive usually consists of four main components: (1) acid mucopolysaccharides acting as a primer, (2) polyphenolic proteins as adhesive proteins rich in both L-DOPA and lysine, (3) fibrous proteins between mussel and the substrate as an attachment thread and (4) polyphenoloxidase to promote intermolecular cross-linking [138]. In the context of bone repair, adhesion is achieved through ionic bonding between catecholic hydroxyl and carboxylic acid groups of the adhesive system with Ca^{2+} present on the surface of bone. The complex interactions between the proteins within mussel-derived bioadhesives causes technical difficulties relating to protein extraction resulting in high production costs that hamper clinical application. Many studies have been conducted to evaluate the properties of mussel-derived bioadhesives [139].

Table 1.1: Comparison of the different properties of all the synthetic-based adhesives.

	Application	Advantages	Disadvantages
Cyanoacrylates [128–131]	Craniofacial, osteochondral and trabecular fractures Bone formation and fragments fixation Enhancement or replacement of screws/plates	Max adhesive strength of 9 MPa Enhanced tensile & shear bond in wet and dry environment. Higher shear strength (1-2 MPa) than screws & plates	Partial bone formation/non-degradable Less efficient than screws with low mechanical properties Chronic inflammatory response and tissue necrosis Cytotoxicity to cells <i>in vitro</i> & dermatitis <i>in vivo</i>
Polyurethane [101–103]	Bone formation and fragments fixation Bone to bone adhesion Closure of fractures	High adhesive of 4.9 MPa or/and cohesive strength of 2.2 MPa Osteogenic, non-toxic and biocompatible Degradation in wet environment	Bond failure between bone and adhesive Low biodegradability Infection Tissue necrosis
Polyester [132–134]	Scaffold in bone regeneration Tissue adhesion	Faster degradation in wet environment than polyurethane-based High mechanical & adhesion strength of 4.1–5.5 MPa	Mechanical stability during degradation Inflammation at the application site- cytotoxicity Low yield strength
PMMA [135,136]	Bone fragment and implant fixation Adhesives in dentistry Bone formation	Increased bonding to wet bone (tensile Strength of 62-83.0 MPa) Easy application Cytocompatibility	Low adhesive strength Thermal necrosis of bone tissue Lack of biodegradability

Initial efforts to mimic these materials have focused on the development of synthetic polymers and cell attachment proteins that mimic the components that provide mussels with strong adhesion. Mussel-derived bioadhesives assessed for bone tissue engineering applications have demonstrated good biodegradability, non-immunogenicity and a greater adhesion on various substrates (e.g. metal, glass, plastic, and biological substances) [140,141] compared to polymer-based adhesives. The mechanical properties of mussel-derived bioadhesives include an adhesion strength of 10 MPa, low Young's modulus of 0.9 GPa and residual resilience of 53% following mechanical assessment under fatigue loading. Initially, pre-modified intestinal bacteria combined with an enzyme capable of inserting in the amino acid named DOPA (a key component in the mussel proteins) was developed, using photochemical crosslinking [142]. Apart from photochemical crosslinking, mussel-derived bioadhesives can be successfully crosslinked using oxidation agents (e.g. iron). Iron-induced networks showed strong adhesion, biodegradability, low cytotoxicity, and a low exothermic reaction suitable for the bonding of sternal bones [143]. Furthermore, positive results were exhibited in terms of the suitability of these mussel-derived bioadhesives for bonding titanium prosthetic implants to bone. Other bioinspired approaches include the use of allyl, methacrylamide, and thiol groups for bone priming using a layer-by-layer coating technique leading to improved shear strength (0.3 MPa) and cellular response [144]. Inspired from the mussel-derived bioadhesives, further research is on-going to investigate the incorporation of DOPA into a range of different synthetic polymers to synthesize new copolymers with adhesive properties. Researchers have demonstrated that the bonding strength increased as a function of DOPA content, copolymer solution concentration, copolymer molecular weight, and curing temperatures or by incorporating a crosslinker (e.g. tyrosinase, hydrogen peroxide, or basic aqueous solution) [142,145]. While the capability of these bioadhesive to bond

various materials has been demonstrated, their suitability as bioadhesives for bone tissue engineering application is still under investigation.

Another marine creature, which has inspired the improvement of bioadhesive properties is the sandcastle worm (i.e. *Phragmatopoma californica*), which produces an adhesive commonly known as ‘sandcastle glue’ comprising of polyphenolic proteins. The sandcastle worm produces an adhesive that can bind seashell fragments, grains, and sand to each other. The maximum adhesion strength of this adhesive is achieved in less than 30 s in water and it fully hardens within 1-2 h [146]. Cost-effective adhesion can be achieved using only small amounts of the secreted adhesive instead of typical amounts of 5 g to 10 g required for other adhesives. The glue includes phosphate and amine side groups, which are well-known bioadhesive groups that can be used for bone tissue engineering applications. The suitability of this bioadhesive for underwater adhesion makes this hybrid naturally-derived model an attractive potential bioadhesive for the stabilisation and repair of hard tissue (e.g. bone). A range of synthetic-based materials, which mimic the adhesive function of the sandcastle glue have been developed. For instance, Ailei Li *et al.* developed a sandcastle glue-derived copolymer using bone block specimens from bovine femur cortical bone, which exhibited an *in vitro* bone-bond strength of 0.1 MPa [147].

Another sandcastle worm-based bioadhesive was developed by combining O-phospho-L-serine, which is a phospho-related amino acid component of many proteins with tetracalcium phosphate [95] or alpha-tricalcium phosphate (α -TCP) [148]. This bioadhesive provided high levels of bone-to-bone bonding with a fast setting in a wet environment. Furthermore, the shear strength observed was 10-fold higher than PMMA-calcium phosphate-based bioadhesives and 40-fold higher than commercial cyanoacrylate-based bioadhesives, with an appropriate biodegradation rate that promoted osteointegration and supported effective bone ingrowth. An alternative approach by Kirillova

et al., comprising of O-phosphoserine and tetracalcium phosphate, led to the development of another bone adhesive, which exhibited a setting time of less than 10 min and the ability to achieve high bone-to-bone adhesive strength [95]. This bone adhesive demonstrated a shear strength ten-fold higher than calcium phosphate cements and PMMA bone cements. In addition to the high adhesive strength achieved, both sandcastle worm-derived bone adhesives also demonstrated osteointegration, bone ingrowth and biodegradability.

A new class of sandcastle worm-derived calcium phosphate-based bone adhesives was reported by Pujari-Palmer *et al.* that have the potential to bond soft/hard tissue together and bond soft/hard tissue to metallic and polymeric prosthetic implants [148]. Pajari-Palmer *et al.* reported that phosphoserine can create an amorphous stable bone adhesive within a wet environment, improving the physicochemical properties since they exhibited atomic-scale and macroscale interactions [148]. Furthermore, they reported that the existence of phosphoserine within the bone adhesive can lead to accelerated bone regeneration without causing any inflammation or adverse responses [149]. The assessment of the biodegradation behaviour of phosphoserine-based bone adhesives in physiological fluid *ex vivo* demonstrated the decrease of degradation increasing the density (lower porosity) and the surface area of the adhesive [118]. For bone tissue engineering applications, an effective bone adhesive requires high mechanical strength, low biodegradation and retention of bond strength within the initial days and weeks post-fracture stabilisation. The phosphoserine-based bone adhesive demonstrated a relatively high bond strength (39-50 MPa) and slow biodegradation (8-14% mass loss after 14 days) until the formation of new hard tissue, while also presenting amorphous calcium phosphate and metastable α -TCP on the surface of the bone adhesive [150]. Hulsart-Billström *et al.* [119] demonstrated the first *in vivo* biological safety assessment of a phosphoserine-based bone adhesive for bone tissue engineering applications. The study demonstrated that the phosphoserine-based bone adhesives investigated supported

a rate of cell proliferation of 45-64% with no evidence of redness, swelling, inflammation, fibrotic tissue, disruption or bleeding. The lack of increased immune response and absence of ectopic bone formation demonstrated in this study confirms the highly desirable characteristics of sandcastle worm adhesives in order to achieve effective gluing of bone fragments while successfully guiding osteogenesis to promote bone repair and regeneration.

Table 1.2: Comparison of the different biomimetic-based adhesives.

	Description	Application	Advantages	Disadvantages
<i>Notaden bennetti</i> frog bioadhesives [125,151]	Protein-based elastic glue	Bone adhesion and fragments fixation (cartilage bone repair) Binding to biological tissues as well as other surfaces	Better biocompatibility and biodegradation than fibrin glues Function in moist environments Adhesion of 16.5 ± 2.2 MPa on metals	Lower adhesion strength than cyanoacrylates
Caddisfly silk bioadhesives [95,152,153]	Phosphate-functionalised and amino acid-based polyester copolymers	Bovine bone adhesion (orthopaedic) / Scaffold materials for spinal cord injury Mesh grafts to treat hernias, ulcers, and burns	Adhesion strength of 1.17 MPa Biodegradable <i>in vitro</i> and <i>in vivo</i> Higher interface compliance	Cohesive failure Low curing kinetics and adhesive properties on translationally relevant substrates
<i>Balanus hameri</i> barnacle bioadhesives [154–157]	Polyacrylamide-based copolymer with hydroxyl and hexyl groups	Repeatable and robust underwater adhesion to various substrates Material transfer, temporary fixation (orthopaedics), and material separation/Bovine bone adhesion	Tensile shear strength of 2 MPa Enhanced toughness and cohesion strength Rapid and reversible adhesion in water	Poor adhesion to bovine bone approx. 363 kPa Low mechanical strength

<p><i>Mytilus edulis</i> blue mussel bioadhesives [139,140,144,145]</p>	<p>Adhesives based on complex interaction between different proteins</p>	<p>Strong attachment to inorganic/organic surfaces at dry/wet environment</p> <p>Reliable crosslinking using oxidation agents, such as iron</p> <p>Suitable for joining titanium implants to a bone and/or bonding sternal bones</p>	<p>Non-immunogenicity and low cytotoxicity</p> <p>Greater adhesion on various substrates with adhesion strength of up to 10 MPa</p> <p>Good biodegradability</p> <p>Low exothermic reaction for the bonding of sternal bones</p>	<p>Difficulties relating to protein extraction resulting in high production costs, hampering the practical use</p> <p>Further research needed to determine the suitability of this adhesive as bone adhesive</p>
<p><i>Californica</i> sandcastle worm bioadhesives [95,147,148,158]</p>	<p>Polyphenolic protein and phosphoserine-based adhesive</p>	<p>Strong attachment in a wet environment</p> <p>Reconstruction of craniofacial fractures</p> <p>Bonding of wet bone fragments</p> <p>Bond tissues to metallic and polymeric biomaterials</p>	<p>Maximum adhesion strength of 107 ± 24.7 kPa and hardness in <30 s</p> <p>Osteointegration, bone ingrowth, and resorbability</p> <p>Small amount of adhesive needed to achieve the optimal properties</p> <p>Biodegradable and osteoconductive</p>	<p>Further <i>in vitro</i> and <i>in vivo</i> studies need to be conducted to verify the suitability to natural bone adhesion</p>

1.6. Clinical Requirements of Adhesives

Bioadhesives present a promising approach for bone fracture stabilisation, repair and regeneration applications, with the potential to overcome the limitations of existing fracture repair techniques. In addition to the clinical imperative to develop adhesives that can replace the surgical requirement for metal hardware, there is also a high demand for the development of an adhesive that could be used in conjunction with traditional metal hardware to improve fracture stabilisation and potentially reduce the risk of micromotion and loosening of these devices over time. In order for a bone adhesive to be suitable for use in bone fracture stabilisation and repair applications, it must meet several clinical requirements (Figure 1.8) [92]. In particular, adhesives must provide early mechanical stability, combining optimal adhesive and cohesive properties such as an adhesion strength greater than 2.5 MPa following orthopaedic recommendations. Appropriate adhesion to the bone under clinically relevant situations such as a moist environment, presence of bleeding and uneven surfaces, as well as stability under internal or external forces (e.g., tensile, compression or shear forces), must be achieved. Biocompatibility is also an important requirement in order to avoid cytotoxic responses and facilitate fracture healing through osteogenesis and, ultimately, bone regeneration.

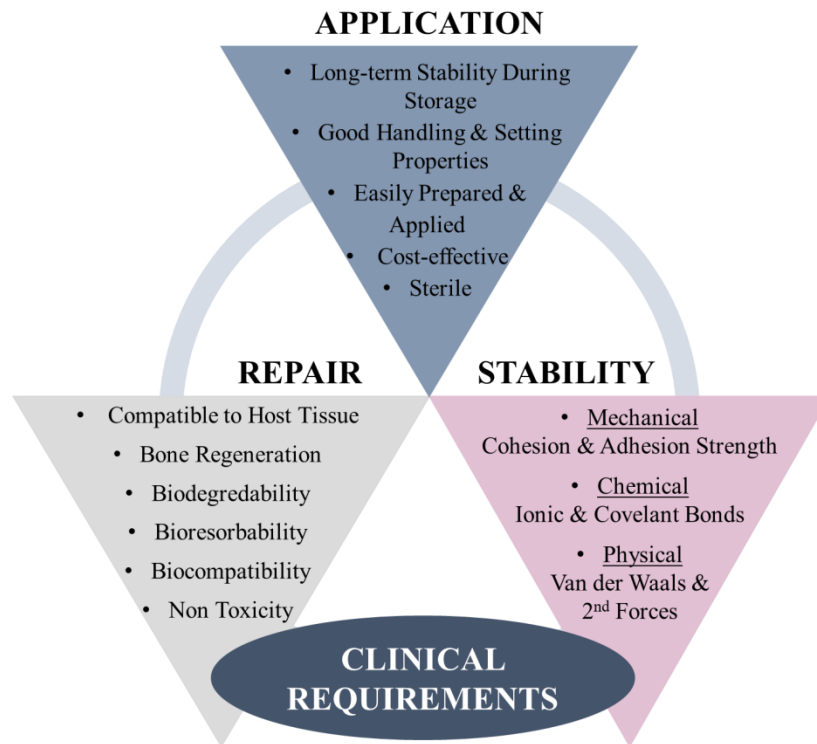


Figure 1.8: Clinical requirements - Requirements for suitable application of adhesive for bone repair and stabilisation.

1.7. Reinforcement of Current Adhesives

In recent years, bone adhesives with improved mechanical properties that can provide effective and faster bone fracture healing (e.g., osseointegration or stable microenvironment, osteoinduction and osteoconduction) have been developed. This has been achieved through the incorporation of fibres or organic/inorganic fillers (i.e., poly(lactic acid) (PLA), poly(glycolic acid) (PGA), poly(lactic-co-glycolic acid) (PLGA), and polycaprolactone (PCL)). For instance, a mussel inspired bone adhesive was developed containing tetracalcium phosphate enhanced with PLGA fibres, leading to a biodegradable bone adhesive with excellent osseointegration properties [159]. Incorporation of PLGA fibres into the formulation resulted in a compressive strength of 62 ± 8 MPa, shear strength of 3.5 ± 0.6 MPa, stability of shape on setting and rapid setting time in a wet environment. Excellent bioresorbability and osteoconductivity was also observed.

An alternative reinforcement strategy involved using different percentages of chitosan lactate solution instead of pure water, leading to finer and more homogeneously dispersed pores within the adhesive, has been shown to achieve higher mechanical strength than the PLGA reinforced adhesive [160]. While the bone adhesive provided biocompatibility, biodegradability, and osteoconductivity, a lack of elasticity was observed indicating that further research, using higher percentages of polymer, is required.

Enhancement of the covalent, ionic and hydrogen bonding between adhesive and bone has become an area of interest, for improving the osseointegration properties. Initial attempts involved the addition of guar gum into soybean protein isolate (SPI) glues that resulted in an approximately three times higher bond strength of SPI bone adhesives onto porcine bones [161]. The higher strength was achieved due to increase in the hydrogen bonding, density of protein aggregates and zero-shear viscosity of SPI adhesives. Enhancement of hydrogen bonding has also been achieved by incorporating a supramolecular hydrogel network [162].

This bone adhesive provided improvement of the interfacial toughness between disparate substrates and additional functionality such as reversibility and self-healable adhesion. Similar biomechanical strength with PMMA, while significantly enhancing biodegradability and osteointegrative capacities, was achieved by Liu *et al.* [163] by incorporating starch and barium sulphate into a CPC. In addition to these properties, this new cement demonstrated appropriate injectability and setting time, highlighting the attractive potential of this composite bone adhesive for bone applications.

Another class of bioactive pore forming bone adhesive was developed by incorporating poly(ethylene glycol) (PEG) porogens with encapsulated bioactive glass in 2-octyl cyanoacrylate (OCA) [164]. The reinforced adhesive exhibited rapid hydroxyapatite (HA) formation abilities and excellent bioactivity under physiological conditions with superior mechanical properties, instant bonding and a high efficiency of bone regeneration compared to cement containing calcium phosphate alone. This method is defined as a strategy to design bone adhesives with high cell ingrowth efficacy. Poly propylene fumarate-based adhesives have been also enhanced with nanobioactive glass particles [165]. *In vitro* bioactivity, biodegradability, biocompatibility, bone adhesion and high cell viability verified the potential of this composite as a biodegradable glue for use in orthopaedic surgery. Due to the excellent osteoconductivity of calcium phosphates such as HA and tricalcium phosphate (TCP) and their very good mechanical properties, they have been used widely in bone fractures. Another study evaluated the reinforcement of adhesives based on chitosan hydrogels with HA and calcium carbonate particles [166]. The new formulation demonstrated a potential candidate for clinical use in orthopaedics since it presents superior adhesion strength in both dry and aqueous conditions combined with normal cell growth and excellent biocompatibility *in vitro*. Polyurethane-based bone adhesive with the incorporation of nano sized HA were developed and characterised by Schreder *et al.* [103]. Increased adhesion was demonstrated compared

to other conventional adhesives while biocompatibility was demonstrated through *in vitro* and preliminary *in vivo* analysis. However, long-term observations and additional tests are needed to demonstrate full biocompatibility. Erken *et al.* [167] and Lie *et al.* [168] fabricated polyurethane-based adhesives with β -TCP enhancing the mechanical properties and osteoconductivity. In addition, high cell viability was recorded, and the ability of the material to facilitate the growth of cells and bone tissues was demonstrated.

1.8. Summary

Considering the disadvantages of existing surgical approaches for the treatment of complex bone fractures, bone adhesives for bone tissue engineering applications present significant potential as an alternative minimally invasive surgical approach. One main challenge relating to development of bone adhesives is the requirement to achieve high bond strength within the challenging clinical environment (i.e., wet environment). However, bone adhesives have the potential to offer advantageous properties including biocompatibility, biodegradation/bioresorbability, osteoconductivity and high bond strength to hard tissue (i.e., bone), and to date a range of such bone adhesives have been investigated including synthetic-polymer-, biological-polymer- and biomimetic-based adhesives. Many studies have focused on the development of bone adhesives with the ability to provide a high bond strength within a wet environment, while at the same time combining the requirement for biocompatibility, and biodegradability. Despite these challenges, several promising approaches, such as polysaccharide- or protein-based bone adhesives that achieve high levels of adhesion through covalently bonding to hard/soft tissue, are currently at the early stages of clinical testing. However, these bone adhesives are not suitable for application within a wet environment due to the low adhesive strength, which presents a significant limitation for clinical use.

Biomimetic-based bone adhesives that have been inspired by examples of adhesives found in nature present an attractive alternative approach and are rapidly gaining momentum in the

field of biologically applicable bone adhesives. They offer a significant advantage as they can function in a wet environment. Currently the scientific knowledge and understanding of the mechanisms involved in achieving successful adhesion in a wet environment is limited and thus considerable research efforts are being invested to study adhesion in living systems. With more substantial and exhaustive investigation relating to the interplay of environmental and chemical/biological factors, chemistries, and mechanisms for effective natural adhesion, it has been demonstrated that biomimetic-based bone adhesives have a potential role to play in the effective stabilisation and repair in bone tissue engineering applications, including the treatment of complex bone fractures. Comparing these biomimetic-based bone adhesives, systems that mimic the sandcastle worm are considered the most promising. For instance, the sandcastle worm-inspired bone adhesive that uses the addition of a phosphorylated amino acid (e.g., phosphoserine) to calcium phosphate-based adhesives can be considered as a highly effective bone adhesive for bone fracture stabilisation and repair. Phosphoserine can create novel properties in bioceramics, such as high adhesion within a few seconds and a reduction in the inherent brittleness displayed by bioceramic materials.

Research development of the bone adhesives is focused on exploring the potential of these materials as a vehicle for the controlled and localised delivery of cells, growth factors and small molecules [169–171], focusing on the synchronisation of the load and release of these bioactive elements in line with the timeline of normal tissue healing/repair. Another area of research focus relates to the tuning of the *in vivo* biodegradation of bone adhesives, which would complement localised delivery of a particular cargo [95,148,158,171].

In conclusion, bone adhesives have gained increasing recognition for their potential in fracture repair, bone filling, and implant augmentation. However, due to the different clinical requirements across different applications there is need to optimise bone adhesives for specific clinical scenarios, aiming to facilitate bone repair and formation. In order to achieve that, it is

essential to emphasise on the understanding of how various factors influence the properties of these adhesives which remains limited in the current research. Despite substantial progress has been made, there is still significant room for improvement in enhancing the mechanical and physical properties of these adhesives, particularly when considering large-scale production. Parameters such as handling properties, adhesion strength and injectability need further refinement, especially in the context of promoting biocompatibility for supporting tissue integration, particularly in wet conditions. Simultaneously, there is a growing demand for adhesives that can be easily administered through minimally invasive surgical techniques and offer on-demand and precise mixing/delivery capabilities. For those reasons the novelty of the developed bone adhesive formulation within this thesis lies in its unique composition and enhanced performance characteristics compared to existing phosphoserine-based adhesives. Unlike conventional formulations, this adhesive incorporates a synergistic blend of bioactive components that significantly improve its mechanical properties, such as adhesion strength and durability, particularly in wet conditions, which are critical for effective bone repair and integration. Furthermore, the formulation has been optimised for better handling properties and injectability, making it more suitable for minimally invasive surgical techniques. This adhesive also features an innovative on-demand mixing and delivery system, allowing for precise application and reducing the risk of premature setting. These advancements address the specific clinical needs for different applications, facilitating more efficient bone repair and formation.

1.9. Aim and Objectives

Considering the complexity of the bone defects and the increased proportion of incidence that require very complicated surgical intervention, this PhD is focused on the development of a bone adhesive with unique physical and mechanical properties, able to adhere or bond to biological-based tissues. The overall aim is to develop an optimised injectable phosphoserine-modified calcium phosphate cements (PM-CPC) comprised of α -TCP, phosphoserine, calcium silicate and deionised water, capable of achieving effective repair of bone fractures using an on-demand minimally invasive surgical approach.

The specific objectives of this project are:

Objective 1: Design and formulation of phosphoserine-modified calcium phosphate adhesive.

Objective 2: Characterisation of biomechanical properties of phosphoserine-modified calcium phosphate adhesive.

Objective 3: Design and fabrication of a dual syringe-mixed phosphoserine modified calcium phosphate adhesive for on-demand mixing and minimally invasive delivery.

Objective 4: *In vitro* evaluation of phosphoserine-modified calcium phosphate adhesive.

Objective 5: *In vivo* evaluation of phosphoserine-modified calcium phosphate adhesive.

**Chapter 2: Analysis and Optimisation of
the Phosphoserine-modified Calcium
Phosphate (PM-CPC) Adhesive
Composition**

Sections of this Chapter have previously been presented in a scientific article published in Acta Biomaterialia, Elsevier (2023): **A. Tzagiollari, J. Redmond, H.O. McCarthy, T.J. Levingstone, N.J. Dunne**, *Multi-objective property optimisation of a phosphoserine-modified calcium phosphate cement for orthopaedic and dental applications using Design of Experiments methodology*, Acta Biomaterialia, 2023

2.1. Introduction

Apatite form cements named alpha- and beta-tricalcium phosphate (α - and β -TCP) are currently used in several clinical applications in dentistry, maxillo-facial surgery and orthopaedics, with α -TCP being the major constituent of the powder component of various bone cements [172]. It can remain in a metastable state at room temperature and its stability range is influenced by ionic substitutions. It is as biocompatible as β -TCP, but more soluble, and hydrolyses rapidly to calcium-deficient hydroxyapatite (HA), which makes α -TCP useful in the development of self-setting osteoconductive bone cements and biodegradable bioceramics and composites for bone repair [173]. The increasing interest in α -TCP as a bone implant material stems from its biodegradability. It is more easily absorbed by the body compared to HA, β -TCP, and biphasic bioceramics (HA/ β -TCP) commonly used in clinical practice [174,175]. From a biological point of view, α -TCP is non-toxic, osteoconductive and bioactive, both *in vitro* and *in vivo* [176]. This characteristic makes α -TCP an ideal implant material that can be replaced by new bone at a faster rate than other calcium-phosphate-based materials available on the market [172,177]. In summary, α -TCP presents an appealing option for designing new biomaterials for emerging bone repair therapies based on tissue engineering and regenerative medicine [178,179]. Despite their advantages, α -TCP based cements lack of injectability and biomechanical integrity limiting their effectiveness as bone substitute.

The physical and biological properties of calcium phosphate cements (CPCs) are still inferior to native tissue due to their inorganic chemistry, which results in randomly-organised networks of entangled crystals, however they are brittle with poor tensile and shear properties [180,181]. The lack of effective bone adhesives can be attributed to the multiple and complex criteria for adequate bone repair, including adequate mechanical stability in wet conditions, sufficient working time for the surgeon to apply the adhesive, osteogenesis and biocompatibility [16]. For that reason, inorganic and organic compounds, such as citric, tannic

acid, silicic acid salt, etc., have been used widely to recreate biological and mechanical properties through physicochemical modifications, providing effective and faster bone fracture healing [182–186]. The addition of these compounds improves mechanical properties with stability of shape, reduces setting time in wet environments, and provides excellent bioresorbability and osteoconductivity [94].

Inorganic silicic acid salt such as calcium silicate can affect the properties of an adhesive-based material. Calcium silicate (Ca_2SiO_4) is known for its osteoconductive nature and its capacity to facilitate the formation of hydroxyapatite [187]. The beneficial effects of Ca_2SiO_4 based materials on inducing bone formation were first found on glass by Hench *et al.* in the early 1970s [188]. Glasses with this composition were able to bond to soft and hard tissues forming a carbonated HA layer when exposed to biological fluid. The fabrication process, mechanical properties, biocompatibility and the degradation and osteoconductivity of Ca_2SiO_4 based glass and glass-ceramics have been well documented [189–191]. Enhanced cell attachment and proliferation were found in an *in vitro* study using Ca_2SiO_4 based glasses, compared to β -TCP ceramics, while the release of calcium (Ca) and silicate (Si) ions enhanced the expression of osteoblast-related genes and promoted differentiation [191,192]. Incorporation of calcium silicate into magnesium phosphate cements not only enhanced the mechanical properties, but also demonstrated apatite mineralisation, bioactivity and biodegradation ability *in vitro* [193,194]. This interaction with the body's natural processes promotes integration between the adhesive and the surrounding bone, promoting enhanced bonding and overall stability [189,195]. An *in vivo* study further demonstrated that calcium silicate bioceramics could stimulate osteogenesis by accelerating new bone formation at defective sites in the femur [196]. Furthermore, calcium silicate's unique physicochemical properties can influence the setting time, viscosity, and workability of the adhesive, thus affecting the ease of surgical application and the subsequent performance of the adhesive in

clinical scenarios [197]. However, these materials also have some disadvantages such as low flowability and mechanical properties, dry consistency, and rapid degradation (dissolution rate should be properly controlled for improved biological outcomes) [198,199].

The addition of organic acids such as amino acids offer an attractive alternative to synthetic monomers, organic acids, or chemical modification. Specifically, amino acid additives can enhance handling and setting properties, template mineralisation of nanoscale amorphous calcium phosphate, and stabilise metastable ceramic phases—thereby improving mechanical properties and cell attachment, survival and proliferation [17,18]. Interestingly, amino acids can create macroscale disorder in cements by adsorbing to crystal surfaces or directly incorporating into the crystal lattice, potentially increasing the dissolution rate and release of bioactive ions such as calcium and phosphate [200–203]. Phosphoserine is an amino acid predominantly found in phosphoproteins such as osteopontin (OPN). OPN is a non-collagenous bone sialoprotein involved in mineralisation in vertebrates. It is also involved in a wide range of biological processes, including adhesion/cohesion of hard and soft tissue under wet environments, load dissipation in animals, and biomineralisation of calcium phosphate precipitation via matrix proteins and matrix vesicles [204,205]. In biological fluids α -TCP, transforms to metastable phases (i.e., octacalcium phosphate (OCP)), or directly to HA within a relatively short period. This results in a relatively short resorption and mineralisation of cells to the cement surface (i.e., the release of bioactive ions) [13,206,207]. Phosphoserine significantly influences α -TCP dissolution and improves HA morphology, as well as cell proliferation and mechanical strength [205]. The use of phosphoserine as an adjuvant can recreate complex architectural and material properties in α -TCP-based cements, producing entirely novel properties and stability under wet environments [101,148,150]. In particular, a strength of 40-100 times higher than that of commercial cyanoacrylates and surgical fibrin glues has been achieved under wet conditions, creating a

nanoscale organic/inorganic microstructure and templating of nanoscale amorphous calcium phosphate nucleation [148,160]. In addition to its high adhesion strength, the safety of this adhesive has been proven without any harmful effects on the surrounding soft tissue [119], while also enhancing cell proliferation and differentiation [205]. However, they lack of elasticity [208] and degradability [160,209].

While several studies show the potential of phosphoserine-based adhesives for tissue repair, an in-depth understanding of the influence of various process parameters on the properties of these adhesives is lacking [141,210–216]. The ideal combination of liquid and powder constituents remains uncertain, and there is a lack of clarity regarding potential interactions among adjustable factors, including the liquid-to-powder ratio (LPR), the weight percentage of calcium phosphates, and the particle size of the powder. The optimised adhesive composition needs to meet the specific requirements (e.g., handling and mechanical properties) of different application sites and fracture types. Thus, it is necessary to identify a composition that can effectively tailor the relevant properties to achieve efficacy and effectiveness given the diverse range of clinical applications for bone adhesives.

By systematically investigating the different compositions and properties using scientific methods, researchers can design and develop adhesives suitable for orthopaedic and dental applications, which demonstrate improved mechanical properties, biocompatibility, and durability. However, the development process is often limited by a single component, and as a result, computer-based optimisation technique such as a Design of Experiments (DoE) approach based on response surface methodology (RSM) are commonly used [217]. DoE is a systematic and scientific approach to planning, conducting, analysing, and interpreting experiments or tests [218]. To date, DoE has been used in various fields (including

engineering, manufacturing, chemistry, biology, and social sciences) to improve product quality, reduce costs, increase efficiency, and solve problems [219].

The first stage of the DoE process involves identifying the critical factors that affect the process or product performance using a structured experimental design [220]. The critical factors affecting bone adhesive properties can be divided into two categories: material and environmental factors. Material factors include the composition, molecular weight, surface chemistry, and morphology of the adhesive material. These factors can affect the adhesive strength, setting time, viscosity, and biocompatibility of the adhesive.

The second stage of DoE involves finding the optimal levels of the significant factors that maximise or minimise the response variable [221].

The third stage of DoE involves verifying the validity and reliability of the optimised process or product performance under different operating conditions or in different environments. This can be achieved using additional experiments or tests to ensure that the optimised process or product performance meets the desired specifications and requirements. DoE can provide significant benefits over traditional trial-and-error methods, as it provides a systematic and scientific approach by identifying and optimising the critical factors that affect process or product performance and validating the optimised performance under different conditions.

2.2. Chapter Aim

The primary aim of this chapter was to develop greater understanding of influence of different properties on process responses, thereby contributing to a more comprehensive understanding of the adhesive. The research involves evaluating a variety of phosphoserine-modified calcium phosphate adhesives, referred to as PM-CPC, to assess their physical, handling, and mechanical properties, as well as adequate adhesion/cohesion strength under wet-field conditions—with the optimal properties benchmarked against industry defined values. The initial focus of the chapter was on the synthesis and analysis of an α -TCP powder, which forms the primary component of the PM-CPC bone adhesive. DoE software was used to optimise the fabrication and experimental processes, allowing the refinement of experimentation resource usage and time, and establishing a cost-effective approach compared to conventional methods.

The specific objectives of this chapter were to:

- Synthesise and analytically assess micro-sized α -TCP ceramic particles.
- Investigate the influence of process parameter on the properties of PM-CPC using the DoE approach, with the key inputs being the molar ratios of the α -TCP, phosphoserine, and calcium silicate, LPR ratio and particle morphology.
- Optimise the composition of PM-CPC using DoE and validate the DoE studies by comparing the optimal predicted values with the actual experimental properties through t-test analysis.

2.3. Material and Methods

2.3.1. Synthesis of Micro-sized Ceramic Particles (α -TCP)

The α -TCP powder was obtained by thermal transformation of a mixture of calcium phosphate (CaHPO_4) and calcium carbonate (CaCO_3) (both from Sigma Aldrich, Ireland) at a molar ratio of $\text{Ca/P} \approx 3:2$ (both from Sigma Aldrich). The two powders were turbo-blended and heat-treated in a furnace (Elite BRF1600°, Elite Thermal Systems Ltd., UK) for 6 h at 1400°C [178]. For the heat-treatment, the powder mixture was transferred to alumina cylindrical crucibles (CC30A Alumina Cylindrical, Almath Crucibles, with Product No. 30019) suitable for high temperatures. Following the heating process, rapid quenching using compressed air with a pressure of 500 kPa was carried out. Upon synthesis of the α -TCP powder, the powder was categorised as non-passivated α -TCP, with a number of defects within the boundaries of the α -TCP-microstructure. To reduce the number of defects or impurities, a passivation process was carried out. In particular, the passivation of α -TCP powder involves reducing defects and impurities to enhance the material's properties. The defects present in non-passivated α -TCP include point defects like vacancies and interstitials, line defects such as dislocations, planar defects at grain boundaries, and volume defects like voids and inclusions. Grain boundaries, being high-energy interfaces between different crystalline grains, are particularly prone to defects and can significantly affect the material's mechanical and chemical stability. The passivation process typically includes surface treatment to remove contaminants, annealing to reduce internal stresses and heal defects, chemical stabilisation to form a protective layer, and sintering to bond particles and reduce porosity. These steps collectively improve the mechanical strength, chemical stability, and powder properties. For this process to take place, the α -TCP powder was transferred to zirconium dioxide (ZrO_2) crucibles, prior to the grinding process, and placed back in the furnace for an additional thermal treatment [222]. The thermal treatment for the passivation

of the powder included the heating of the furnace from the room temperature to 500°C at a rate of 5°C/min. The powder was held at this temperature for 24 h, before the temperature was returned to room temperature at a rate of 5°C/min.

The α -TCP powder was mixed with ethanol and then was subjected to particle attrition/grinding using 50 agate balls with a diameter of 10 mm in a planetary mill (Pulverisette 6, Frisch, Germany) at a rotating speed of 600 ± 5 RPM for 2, 6, 9, 10, 11, 13, 15 and 17 cycles. Each grinding cycle consisted of 5 min of grinding followed by a 5 min dwell time between each grinding cycle.

2.3.2. Analytical Assessment of α -TCP Powder

2.3.2.1 Chemical Properties: Identification of α -TCP Phase – Purity

The purity of the fabricated α -TCP powder was assessed using X-ray diffraction (XRD, Bruker D8 diffractometer, Bruker, Germany). Scans were conducted with a scan speed of $2 \text{ } 2\theta^\circ/\text{s}$ at 30 kV and 10 mA, with Cu-K α radiation in a range of 2θ between 20° to 60° . The peaks in the spectra were identified using Rietveld analysis and compared to the International Centre for Diffraction Data (ICDD) diffraction patterns for α -TCP (ICDD923) and beta-TCP (ICDD619).

High-quality Fourier transform infrared (FTIR) spectroscopy (Perkin Elmer Spectrum 100) equipped with a room-temperature lithium tantalate detector and a standard optical system with KBr windows for data collection was used. FTIR spectroscopy is a valuable technique for the qualitative identification of functional groups and crystalline phases in materials validated the accuracy of quantitative XRD results. Dried α -TCP powder was placed into the sample holder and the spectral range of $4500\text{-}400 \text{ cm}^{-1}$ was selected. Each test included 64 scans to account for a satisfactory signal-to-noise ratio. Characteristic functional groups were

identified based on reported absorbance ranges for similar organic and inorganic compounds within the literature.

2.3.2.2 Physical Properties: Particle Size-Morphology-Zeta Potential

The average particle size distribution of the α -TCP powder was determined using the Malvern Mastersizer Particle Analyser (Mastersizer 3000, Malvern Panalytical, UK). The measurement of the size distribution of particles was guided by the ISO 13320 standard, which is applicable to particle size ranging from approximately 0.1 μm to 3 mm. The identification of particle size was conducted by analysis of the particle (spherical or non-spherical) angular light scattering pattern. The particle size analyser was set up for non-spherical calcium-based particles with a particle refractive index between 1.53-1.63, with water selected as the dispersant. The values of D_{10} , D_{50} and D_{90} were recorded, which corresponded to the cumulative distribution at 10%, 50% and 90% of the total distribution of particle sizes. An average of six readings was recorded for every sample, with the results calculated in μm .

Scanning electron microscopy (SEM) was used to examine powder morphology using the Zeiss EVOLS15 Scanning Electron Microscope (ZEISS, Germany) with an acceleration voltage of 15 kV extra-high tension (EHT). Prior to imaging, powder samples were sputter-coated with gold to enhance conductivity. Each SEM images ($n=6$) with a magnification of $\times 20 \mu\text{m}$ was analysed using Image J software (Version 1.53t, Image Processing and Analysis in Java, National Institutes of Health and Laboratory for Optical and Computational Instrumentation) to determine the circularity of the particles, with a circularity of 1 denoting a spherical shape, while a circularity of 0 corresponds to a straight line.

Surface analysis was conducted to measure the zeta potential of the powder with Laser Diffraction (LD) (Zetasizer Advance Range, Malvern Panalytical, UK) analysis. High purity

deionised (DI) water filtered through a 0.22 μm membrane was used as the dispersion medium for α -TCP powder. α -TCP powder of 100 mg was carefully dispersed into 100 mL of water in a clean glass beaker and stirred at low speeds with a magnetic stirrer. The dispersed α -TCP sample was transferred into a disposable zeta potential cell specifically designed for LD analysis which then was placed in the instrument. The LD instrument was set to measure the zeta potential at a scattering angle of 90° . The instrument exposed the α -TCP particles to the laser beam, and the scattering pattern was captured by the detector.

2.3.3. Box-Behnken Factorial Design

After the verification of purity and suitability of the α -TCP powders comparing to the literature data, the Box-Behnken Factorial Design from Design of Experiments software (Design-Expert V5 Software, Stat-Ease Inc., USA) was used to specify the factors in the process that affects the process performance to the greatest extent. The design includes four numerical factors: A) (liquid:powder ratio [LPR], B) weight % [wt.%] phosphoserine, C) wt.% Ca_2SiO_4 , and D) number of grinding cycles; and one categorical factor denoted as E) post-process (Table 2.1). Three different studies were conducted with the number of grinding cycles increased for each study. In Study 1 (Appendix 2.1): the particles underwent 2, 6 and 10 grinding cycles, Study 2 (Appendix 2.2): 9, 11 and 13 grinding cycles, and Study 3 (Appendix 2.3): investigated 13, 15 and 17 grinding cycles. Each study employed a Box-Behnken design that consisted of 46 experimental runs, combining the min, max and midpoint of each factor.

2.3.4. Formulation of PM-CPC Adhesive

Various compositions of the PM-CPC bone adhesive were fabricated by premixing the liquid phase (DI water) with the powder phase [α -TCP, phosphoserine (Flamma, S.p.A. Italy) and calcium silicate (Sigma Aldrich)]. DI water was added at a predetermined LPR ranging from

0.2 mL/g to 0.5 mL/g as specified by the DoE. The powder phase consisted of defined weights (wt.%) of each component in accordance with the DoE, ranging between 60-90% for α -TCP, 10-40 wt.% for phosphoserine and 0-2 wt.% for calcium silicate (Table 2.1). To determine the limits for the factors for the DOE study, a comprehensive approach was utilised. Initially, an extensive review of relevant literature was conducted to understand the known effects and typical ranges of each factor. This helped establish a theoretical foundation and identify commonly studied boundaries. Following this, a series of preliminary experimental tests was performed to empirically assess the behaviour of the factors within these ranges. The preliminary testing allowed the identification of values where changes had negligible or no observable effects, thus refining the practical limits to those that were most meaningful for the study. This two-step process ensured that the selected limits were both scientifically grounded and empirically validated, enhancing the robustness and relevance of the experimental design.

For every run specified by DoE, 1 g of PM-CPC was hand mixed until all the components were homogeneously combined, achieving uniformity and consistency. The completion of mixing time was estimated by visually observing the mixture and looking for signs of complete homogeneity, specifically when no remaining powder particles were visible, and the texture became smooth and shiny. The homogeneous mixture was placed in different moulds to fabricate specimens with the required shape and dimensions for subsequent characterisation techniques. All specimens were incubated for 72 h in Ringer's solution (Ringer Tablets, Merck, Ireland) at 37°C and 100% relative humidity to simulate the biological environment.

2.3.5. Analytical Assessment of PM-CPC Adhesive

2.3.5.1 Initial and Final Setting Time

Initial (t_i) and final (t_f) setting times (i.e., the handling properties) of the PM-CPC adhesive were determined using the Gillmore needle apparatus, in accordance with ASTM C266–99. The apparatus consisted of a weighted needle of 113.4 ± 0.5 g and a weighted needle of 453.6 ± 0.5 g for measuring t_i and t_f respectively (Figure 2.1). For every run specified by the DoE study, 1 g of PM-CPC, with the appropriate amount of α -TCP, phosphoserine and calcium silicate, was solubilised in DI water at the required LPR. The completion of mixing time was estimated by visually observing the mixture and looking for signs of complete homogeneity, such as texture (smooth and shiny). The homogenous mixture of PM-CPC was transferred into polytetrafluoroethylene (PTFE) moulds ($h=8$ mm, $d=10$ mm). The specimens were stored in an incubator at 37°C to simulate the clinical environment. The t_i and t_f values were defined as the time when the adhesive could resist the indentation from the lighter and heavier needles without causing damage to the adhesive surface.

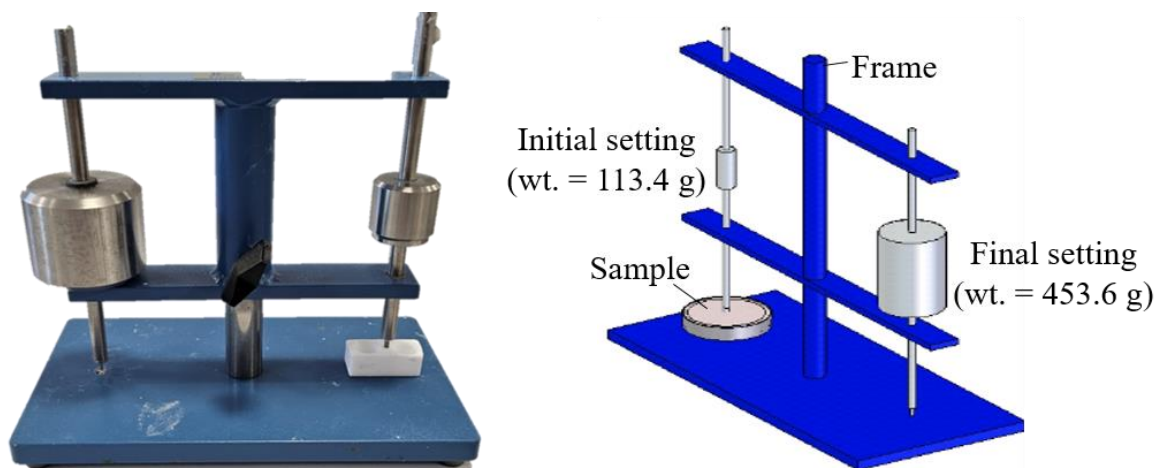


Figure 2.1: Setting Time Analysis – Set up of the Gillmore needle used for the determination of initial and final setting time of the different PM-CPC adhesives.

Table 2.1: Numerical and categorical factors and their levels used for the three different DoE studies, changing the levels of grinding cycles.

Numerical Factors				Responses
Factors	Units	Lower Limit	Upper Limit	
LPR	mL/g	0.2	0.5	
α-TCP	wt. %	60	90	
Phosphoserine	wt. %	10	40	
Ca₂SiO₄	wt. %	0	2	t_i (s)
Grinding Cycles	Study 1	2	10	t_f (s)
	Study 2	9	13	Compressive Strength (MPa)
	Study 3	13	17	Adhesive Strength (MPa)
Categorical Factors				
Passivation	-	NO	YES	

2.3.5.2 Mechanical Properties

The compressive strength of the PM-CPC adhesive was determined in accordance with ISO5833:2002 [223]. For mechanical testing, the PM-CPC formulation was placed into custom-made polytetrafluoroethylene (PTFE, Radionics, RS Stock No.:680-678) moulds (h=8 mm, d=10 mm), resulting in the fabrication of cylindrical-shaped specimen, as can be seen in Figure 2.2. The cylindrical-shaped specimens were placed in Ringer's solution (Ringer's tablets from Sigma Aldrich) for 72 h in an incubator set to 37°C. Compressive strength was recorded using the Zwick Testing Machine (Zwick Roell, UK), fitted with 5kN load cell. Each compression specimen was placed in the test rig between two platens and loaded at a crosshead speed of 1 mm/min. A load vs. deformation plot was subsequently produced. The load at failure/fracture, or the offset load or the upper yield-point load, whichever occurred first, was recorded. (Figure 2.2) Compressive strength was then determined as per (Equation 2.1). A total of 6 compression specimens were tested per run (as stipulated by the DoE design) and the mean and standard deviation for compressive strength were determined.

2.3.5.3 Adhesion Properties

Adhesion properties of the PM-CPC adhesive were assessed by performing the bond strength test on stainless steel cubes. Stainless steel cubes with a 1 cm² contact area were used. For the adhesion/bond strength testing, a 0.25 g layer of PM-CPC was applied to one surface of a 1 cm² stainless steel cube, and a second stainless steel cube was placed on top of the PM-CPC layer. The two cubes were clamped together using universal grips, and then incubated in Ringer's solution at 37°C for 72 h before testing. Each sample was then loaded to failure using the set up that can be seen Figure 2.3 on a Zwick mechanical testing machine, fitted with a 5 kN load cell with a crosshead speed of 1 mm/min. The specimens were tested until

failure, and the compressive strength and bond strength were determined from the resultant stress–strain curves.

Equation 2.1: Conversion of compression force (N) to compressive strength (MPa)

$$\text{Compressive strength (MPa)} = \frac{\text{Force (N)}}{\text{Original Cross Section Area (mm}^2\text{)}} \quad (2.1)$$

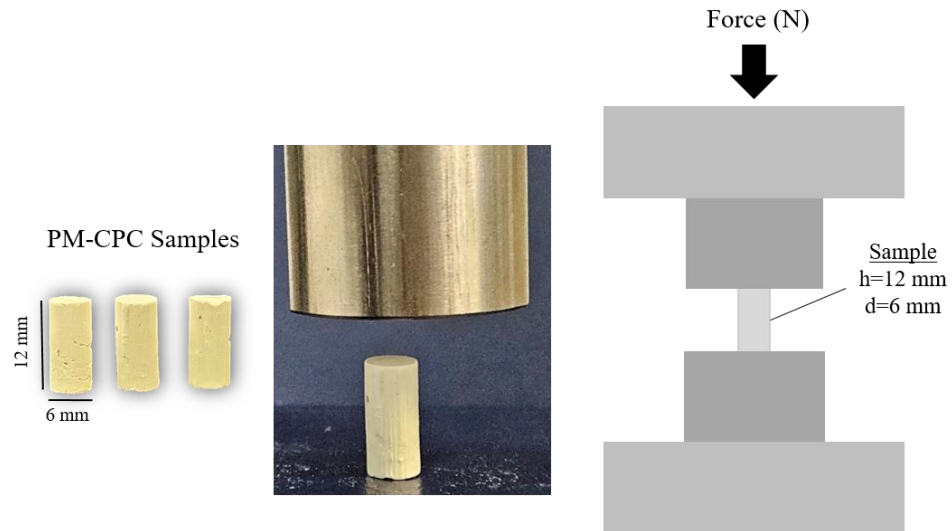


Figure 2.2: Compression Test – Set up of 5kN Zwick machine for the compression test of PM-CPC cylindrical-shaped specimens.

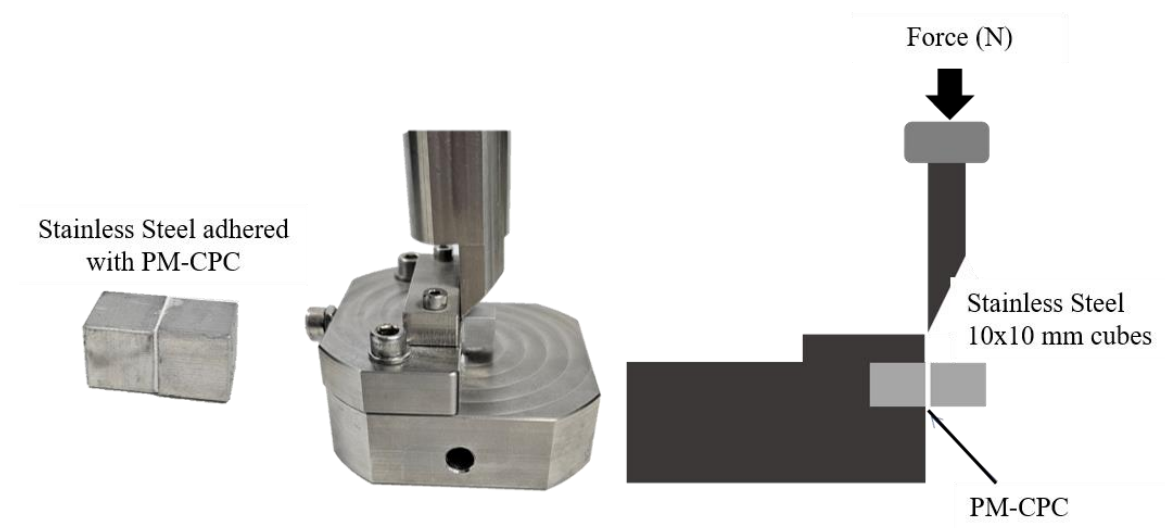


Figure 2.3: Adhesive Shear Test – Set up of 5kN Zwick machine for the adhesive shear test of PM-CPC adhesive within two stainless steel cubes.

2.3.6. DoE Modelling and Optimisation

Upon completion of the experimental testing, the data collected was analysed using Design Expert software. Models that relate the study inputs and outputs were developed. Regression equations were derived to ascertain the significance of the terms within each equation, employing sequential F-tests, lack-of-fit evaluations, and the Analysis of Variance (ANOVA) method. Statistical significance was established for p-value below 0.05. The Whitcomb Score, a recognised metric in the field [224], was used to select the most suitable model(s) and determined the influence of every factor on every response.

To determine the optimal composition of the PM-CPC adhesive, a numerical optimisation approach was used, guided by the following criteria: initial setting time (t_i) ≥ 60 s, final setting time (t_f) ≤ 200 s, compressive strength ≥ 10 MPa [225], and adhesive strength ≥ 2.5 MPa [12]. Inputs from the orthopaedic surgical community were sought to establish the setting times (t_i and t_f) that would facilitate rapid setting, fragment stability, and prevent adhesive leakage [226]. The DoE optimisation was conducted using the desirability function approach, where each response was assigned a desirability function (d_i). The d_i value ranged between 0 and 1, with 0 representing the worst acceptable value and 1 denoting the optimal performance with respect to the studied factors. Subsequently, the optimal composition of PM-CPC was identified, followed by synthesis and evaluation to validate the DoE study.

2.4. Results

2.4.1. Analytical Assessment of α -TCP Powder

2.4.1.1 Chemical Properties: Identification of α -TCP Phase - Purity

The XRD patterns were analysed using Rietveld software and were compared with database patterns for HA, β -TCP, and beta-calcium pyrophosphate (β -CPP) phases. The characteristic peaks indicative of all these phases were observed in the 2θ range of $22\text{--}35^\circ$ (Table 2.2). The XRD spectra revealed prominent peaks at 2θ of 22.74° , 22.93° , 30.70° , 34.16° , corresponding to the (211), (112), and (202) crystallographic planes. The presence of these peaks confirmed the presence of an α -TCP only phase (Figure 2.4). No additional phases were detected, indicating the complete transformation of the CaHPO_4 and CaCO_3 into α -TCP, resulting in 100% phase purity without any residual calcium phosphates.

The purity of the α -TCP phase was also validated from the FTIR spectra, as seen in Figure 2.5. According to spectra the α -TCP phase was observed from the bands between $960\text{--}1120\text{ cm}^{-1}$ and two bands within $559\text{--}597\text{ cm}^{-1}$ wavenumber. All bands refer to high energy phosphate bonds. The four bands within $960\text{--}1120\text{ cm}^{-1}$ and the five bands within $559\text{--}597\text{ cm}^{-1}$ wavenumbers indicate the existence of P-O (PO_4^{3-}) and O-P-O bonding respectively.

Table 2.2: Characteristic peaks of α -TCP, HA, β -TCP, β -CPP phases as appeared in Rietveld software after analysing XRD data.

	α-TCP	β-TCP	β-CPP	HA
Diffraction Angle (2θ)	22.74°	26.25°	26.20°	25.99°
	22.93°	27.82°	26.41°	29.05°
	30.70°	30.90°	27.30°	31.93°
	34.16°	34.42°	28.92°	33.01°
			29.45°	34.17°
		32.25°		

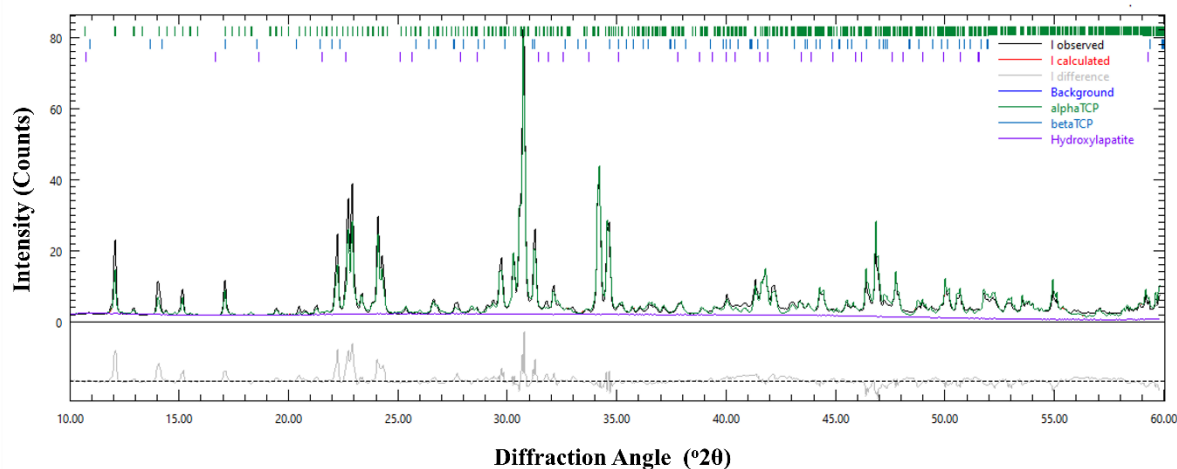


Figure 2.4: X-ray Diffraction (XRD) Analysis – Assessment of α -TCP powder confirmed the presence of a highly pure α -TCP phase, with a purity of 100%. This was evident from the pronounced peaks observed at 2θ angles of 22.74°, 22.93°, 30.70° and 34.16°. The patterns matched the reference patterns ICDD923 for α -TCP, further confirming the phase purity.

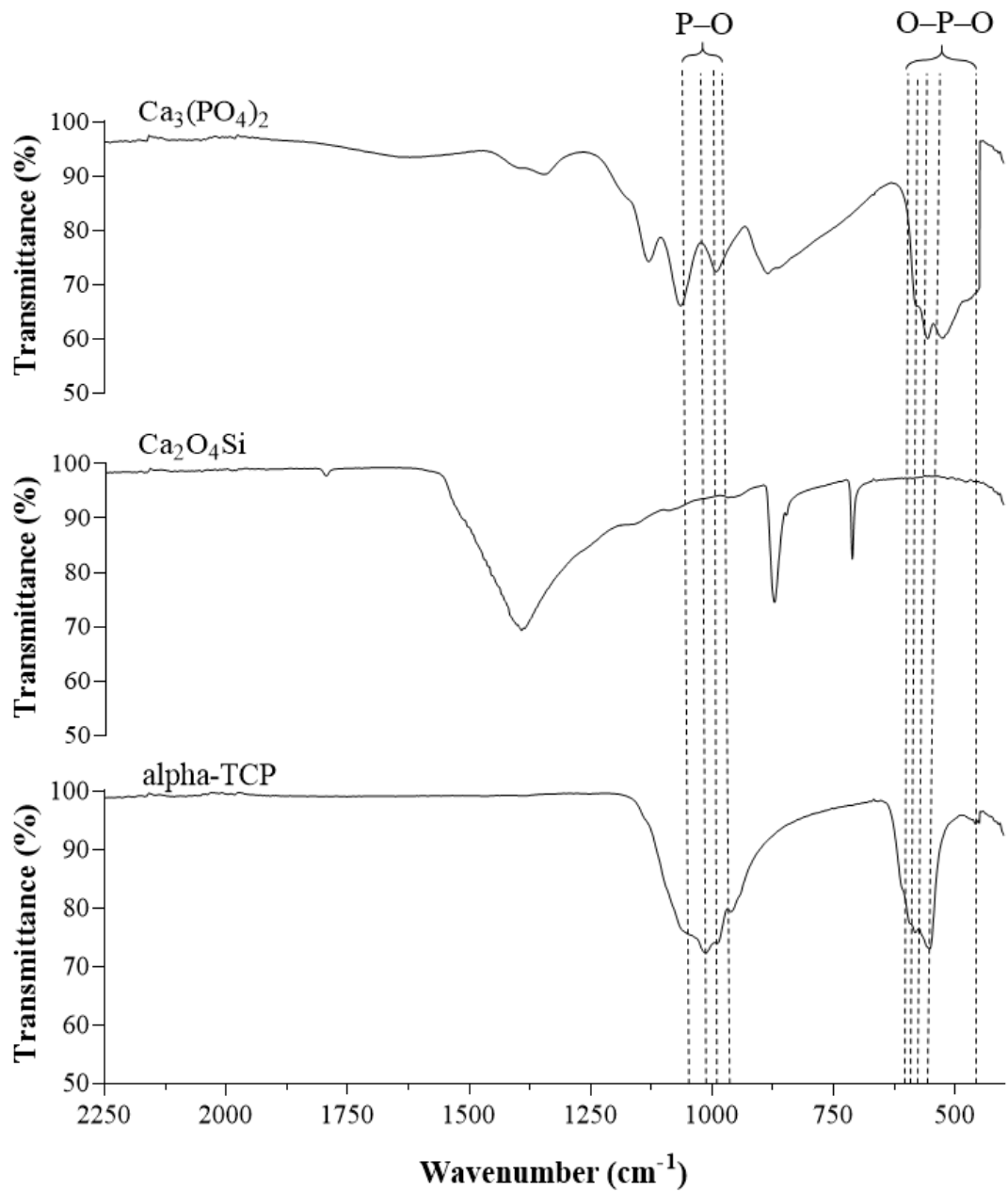


Figure 2.5: FT-IR Analysis – FT-IR spectra of α -TCP powder after the rapid quenching using compressed air for the identification of α -TCP purity.

2.4.1.2 Physical Properties: Particle Size-Morphology-Zeta Potential

The morphology of α -TCP particles as a function of different grinding cycles (i.e., 2, 6, 10, and 11, 13 and 17 cycles) can be observed in Figure 2.6. SEM analysis confirmed a correlation between particle size and attrition time, with a decrease in mean particle size distribution as a function of increasing milling times. Image J analysis demonstrated a circularity of 0.35 ± 0.2 , with a normal distribution of non-spherical particles. There was no significant effect on the particle size distribution after passivation of the α -TCP powder.

Particle size of the micro-sized powders was determined using laser diffraction, with cumulative particle size distribution results summarised in (Table 2.3). Micro-sized α -TCP powder exhibited a decrease in particle size from $D_{10} 6.7 \pm 0.4 \mu\text{m}$, $D_{50} 25.3 \pm 0.7 \mu\text{m}$, $D_{90} 58.6 \pm 4.9 \mu\text{m}$ for 2 cycles to $D_{10} 0.92 \pm 0.2 \mu\text{m}$, $D_{50} 4.05 \pm 1.3 \mu\text{m}$, $D_{90} 12.6 \pm 2.5 \mu\text{m}$ for 17 cycles of particle attrition. The particle size D_{50} of the powder reduced as a function of the number of attrition cycles.

The zeta potential of the α -TCP ranged from -13.2 mV to -18.4 mV (Table 2.3). The negative zeta potential suggests that the particles have a relatively strong negative surface due to the negatively charged functional groups or ions on the particle surface, which indicates a stable colloidal system. The stability of the colloidal system can be attributed to the electrostatic repulsion between the negatively charged particles, preventing aggregation and ensuring dispersion. No significant variation in zeta potential was observed between α -TCP powders with varying particle sizes (p-value > 0.05). This indicates that the particle size did not have an impact on the surface charge, demonstrating that other factors such as surface chemistry and composition were the dominant factors affecting the surface charge.

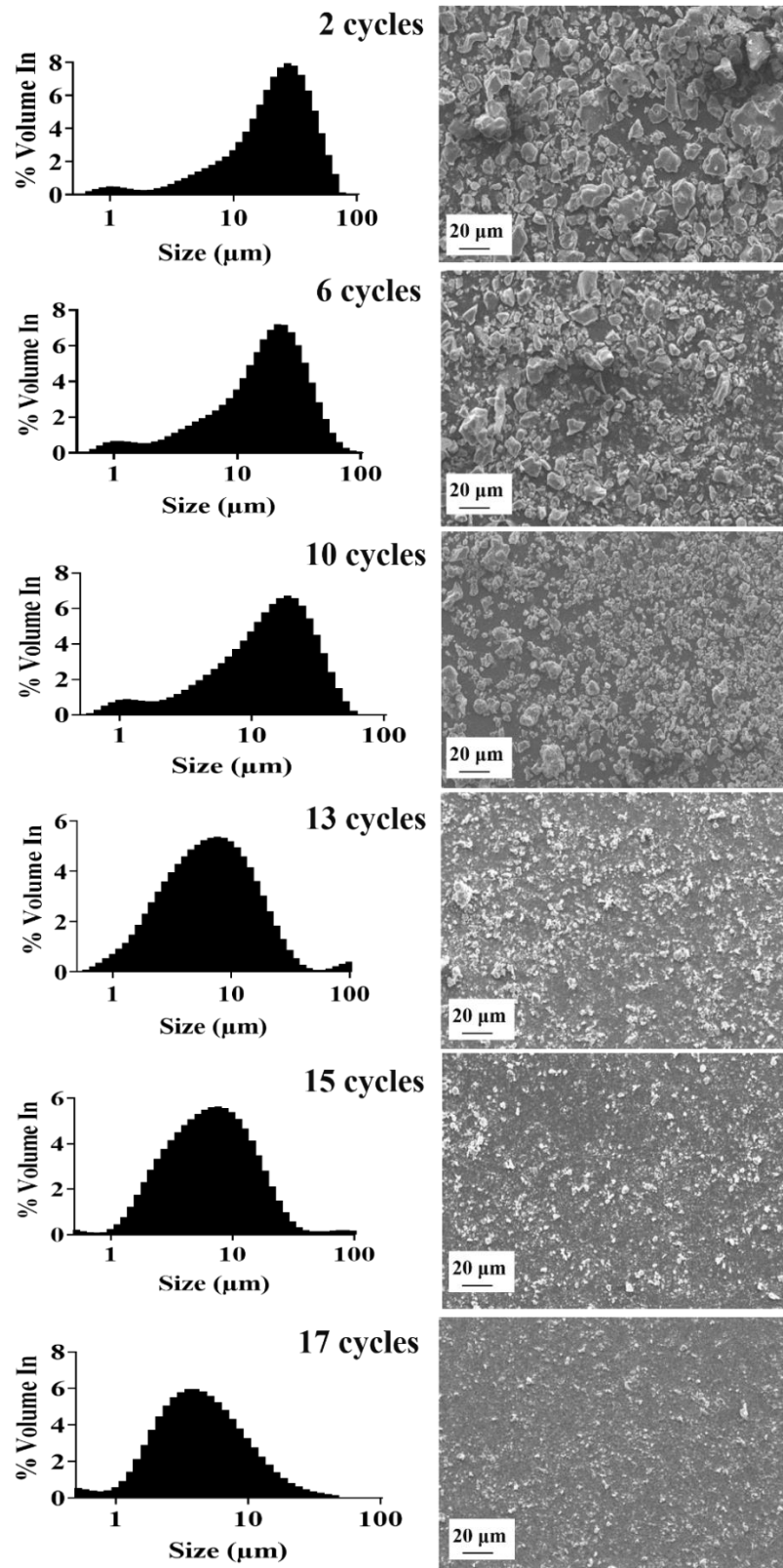


Figure 2.6: SEM Analysis and Particle Size – Distribution plot of α -TCP particles at different grinding cycles and accompanying SEM images of α -TCP powder. For all cycles non-spherical particles with an average circularity of 0.35 ± 0.2 resulted.

Table 2.3: Particle size distribution and zeta potential of α -TCP powder as a function of increasing the particle attrition cycles.

Attrition cycles	D₍₁₀₎ (μm)	D₍₅₀₎ (μm)	D₍₉₀₎ (μm)	D_{span}	Zeta Potential (mV)
2	6.7 ± 0.4	25.3 ± 0.7	58.6 ± 4.9	1.8	-15.9 ± 2.0
6	3.7 ± 0.5	13.3 ± 2.4	30.5 ± 5.8	2.0	-13.2 ± 1.3
10	2.5 ± 0.5	11.7 ± 1.5	28.8 ± 3.2	2.1	-14.8 ± 3.2
11	2.1 ± 0.4	6.9 ± 1.5	21.0 ± 2.8	2.5	-17.1 ± 3.0
13	1.9 ± 0.3	6.2 ± 1.5	17.2 ± 3	2.6	-16.4 ± 4.6
15	1.7 ± 0.3	5.1 ± 1.3	15.8 ± 2.5	2.7	-18.4 ± 2.1
17	0.9 ± 0.2	4.1 ± 1.3	12.6 ± 2.5	2.9	-15.8 ± 3.2

2.4.2. DoE Assessment of Different PM-CPC Composition

2.4.2.1 Initial and Final Setting Time

From all the three DoE studies it was observed that the setting times was significantly affected by both the LPR and phosphoserine content, with a linear relationship observed as suggested by the Fit summary (p-value < 0.05). All parameters and their values presenting the relative importance of each factor for all the three Doe studied and indicate the significant interactions found between factors are presented in Appendix 2.4 (1st Study) Appendix 2.5 (2nd Study) and Appendix 2.6 (3rd Study). According to the sum of squares provided by ANOVA analysis for both the LPR and phosphoserine, the percentage of contribution to the setting properties (i.e., the initial and final setting times) was greater than 40%, while the other factors (amount of calcium silicate and amount of α -TCP) provided a contribution of 2-7%. All three DoE studies demonstrated that the increase of the LPR influenced both the initial (p-value<0.05) and final setting times (p-value<0.01) (Figure 2.7a, Figure 2.7b). In particular, when the amount of DI water was increased and the phosphoserine amount was held constant at 25 wt.%, both t_i and t_f increased by 30-40%. Conversely, increasing the phosphoserine content from 25% to 40%, while maintaining a constant LPR of 0.35 mL/g, resulted in a three-fold increase in the setting properties (t_i and t_f), as seen in Figure 2.8a and Figure 2.8b. The addition of high amounts of phosphoserine (> 25wt.%) within the PM-CPC composition delayed the setting times, with t_i increasing to 6-9 min from 0.5-1.5 min and t_f to 7-10 min from 1-2 min. Furthermore, the interaction between LPR and phosphoserine content was observed for both setting times at low levels of LPR. Figure 2.9a and Figure 2.9b illustrates that in order to achieve fast setting times (t_i =1-3 min and t_f =2-5 min) at low levels of LPR (< 0.35 mL/g), a low amount of phosphoserine is required. The higher quantity of phosphoserine within the formulation can delay the setting reaction instead of speeding it up, resulting in setting times of 10-20 min (initial) and 15-25 min (final).

Notably, the duration of setting times decreased significantly with higher grinding cycles. In the first set of experiments (1st study), grinding cycles of 2, 6, and 10 were used, resulting in an t_i ranging from 3 min to 10 min and a t_f between 4 min to 12 min. The second study involved grinding cycles of 9, 11, and 13, which yielded a t_i of 1 min to 5 min and a t_f of 3 min to 6 min—these values have greater similarity to those set out by the clinical requirements. Lastly, the third study involving grinding cycles of 13, 15 and 17 cycles resulted in a t_i range of 0.5-1.0 min and a t_f between 0.7-1.0 min. The results indicate a notable trend in the impact of α -TCP grinding cycles on the setting time of the PM-CPC composition. As the number of grinding cycles increased, there was a consistent reduction in both t_i and t_f . Additionally, the smaller particle sizes facilitated easier mixing of the PM-CPC, leading to a significantly reduced mixing time of 20 s for α -TCP powders that underwent 10-17 grinding cycles, compared to 90 s for α -TCP powders that underwent 2-9 grinding cycles (p -value<0.01). The grinding process has a significant influence on the solidification properties of the composition. The observed decrease in setting time can be due to several mechanisms. For instance, the grinding cycles contribute to a reduction in particle size and an increase in surface area, leading to enhanced reactivity and faster setting kinetics. Additionally, the grinding process may introduce defects and microstructural changes, facilitating nucleation and growth of solidification products.

Examining the influence of passivated and non-passivated α -TCP on the handling properties of PM-CPC, showed an interaction was observed between passivation and grinding cycles. The passivated α -TCP powder at grinding cycles between 2-9 cycles led to slower setting ($t_i = 4.2$ - 8.4 min and $t_f = 5.6$ - 9.5 min) while the non-passivated powder provided faster setting and reduced setting times ($t_i = 3.4$ - 3.8 min and $t_f = 4.8$ - 5.5 min) (Figure 2.9c and Figure 2.9e). However, by increasing the number of grinding cycles (10-17 cycles) and thus reducing the

particle size, the non-passivated powder demonstrated setting properties closer to clinical ranges, as can be seen in Figure 2.9d and Figure 2.9f.

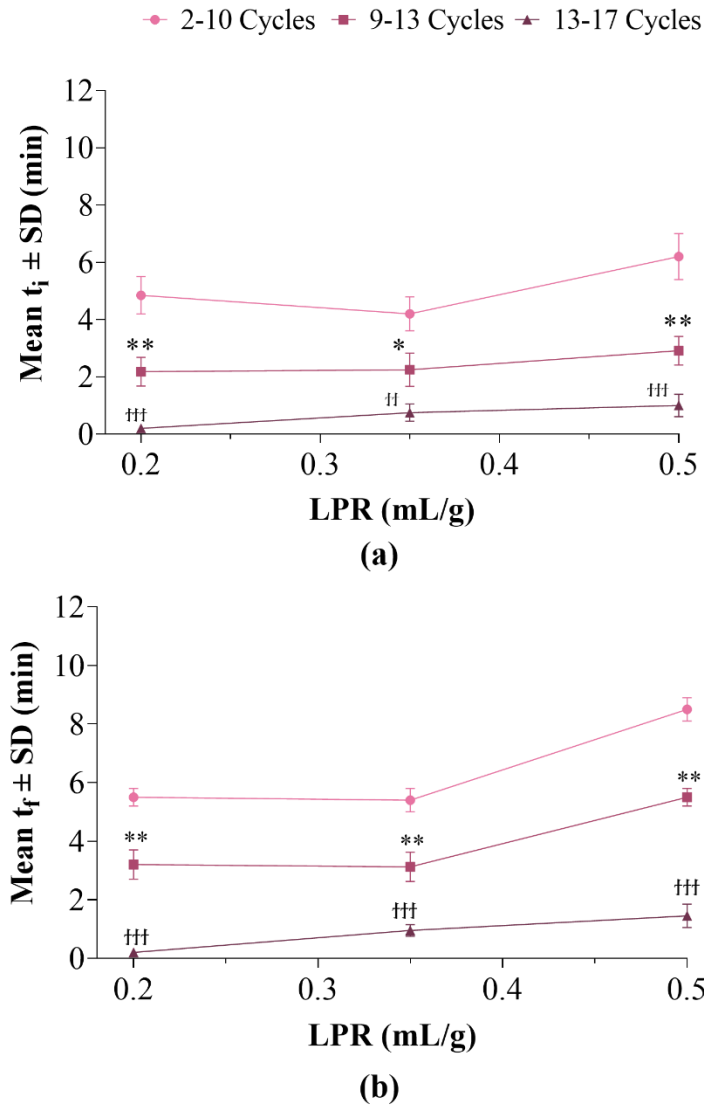


Figure 2.7: LPR Influence on Setting Properties – DoE graphs illustrating the impact of LPR on the (a) initial (t_i) and b) final (t_f) setting time of PM-CPC adhesive using α -TCP at different grinding cycles. *p-value < 0.05, **p-value < 0.01 and ††p-value < 0.001, †††p-value < 0.001 indicate the decrease of setting time at 9-13 cycles and 13-17 cycles respectively, compared with the values from 2-6 cycles.

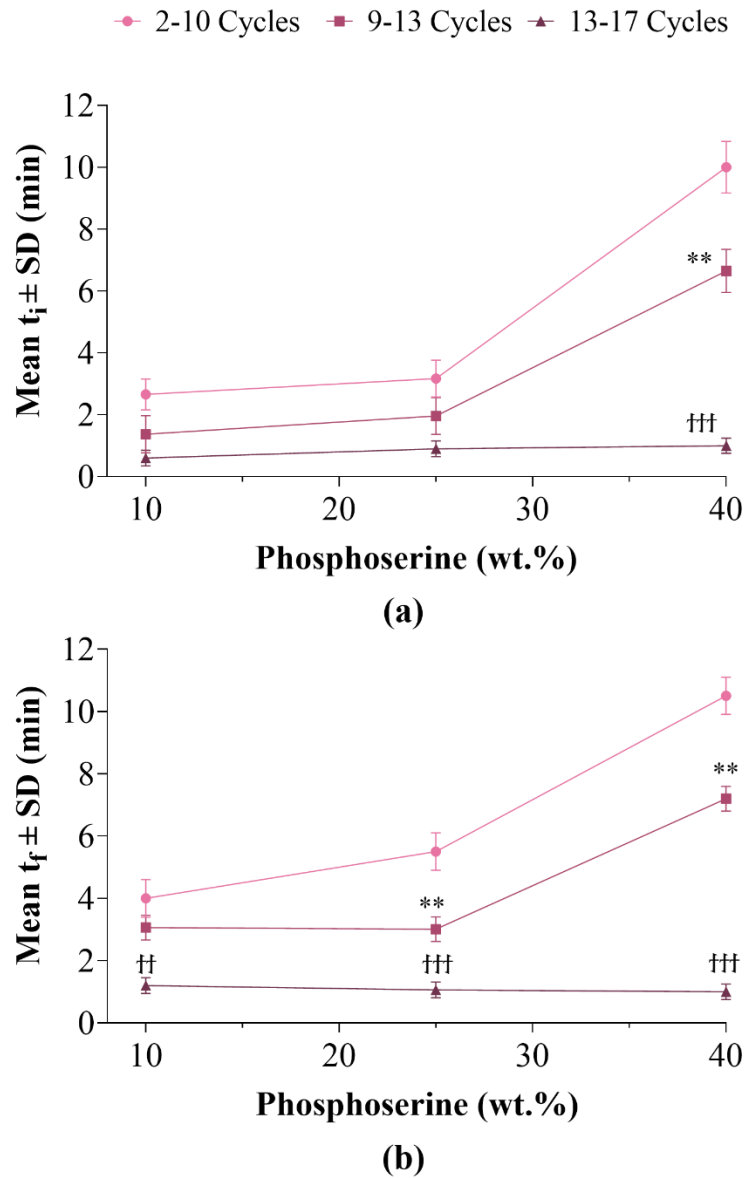


Figure 2.8: Phosphoserine Influence on Setting Properties – DoE graphs illustrating the impact of phosphoserine amount on the (a) initial (t_i) and (b) final (t_f) setting time of PM-CPC adhesive using α -TCP at different grinding cycles. **p-value < 0.01 and ††p-value < 0.01, †††p-value < 0.001 indicate the decrease of setting time at 9-13 cycles and 13-17 cycles respectively, compared with the values from 2-6 cycles.

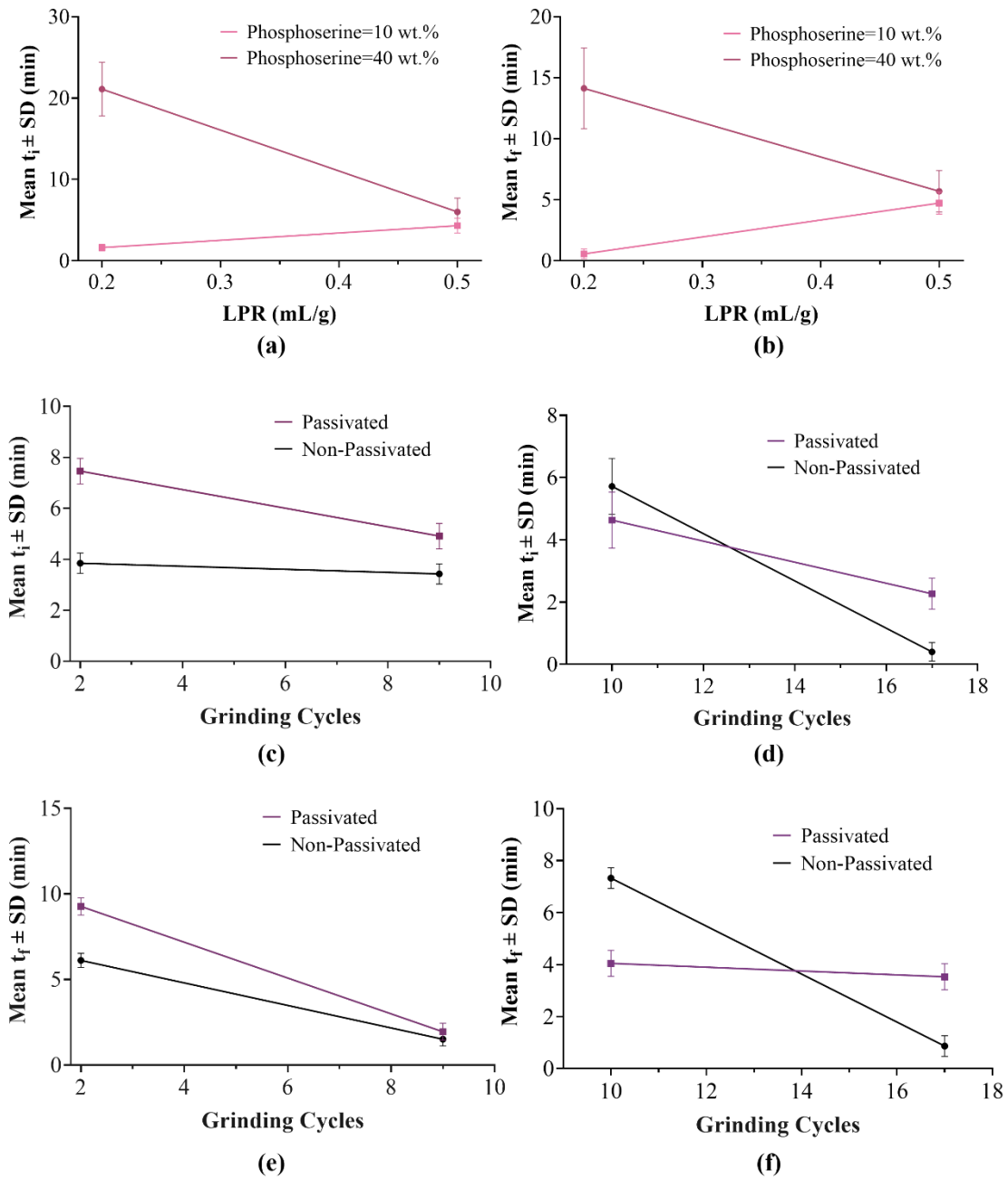


Figure 2.9: Interactions on Setting Properties – LPR and amount of phosphoserine interaction for (a) initial and (b) final setting time obtained from DoE analysis. Interaction between passivation process and α -TCP grinding cycles after analysing initial setting time at (c) 2-9 cycles and (d) 10-17 cycles and final setting time at (e) 2-9 cycles and (f) 10-17 cycles.

2.4.2.2 Mechanical Properties

The use of passivated α -TCP powder showed no statistically significant difference in compressive strength compared to non-passivated α -TCP. In the first study group (after 2, 6, and 10 cycles), the PM-CPC specimens exhibited compressive strengths ranging from 17 MPa to 23 MPa. This results indicate that decreasing the particle size by adding more grinding cycles there is an increase in the mechanical properties, presenting the influence of particle size on the mechanical integrity of the sample. In the second study, increasing more the number of grinding cycles (9, 11 and 13 cycles) and thus decreasing particle size, the PM-CPC specimens displayed an average compressive strength of 23.5 ± 3 MPa. Lastly, the third study (13, 15 and 17 cycles) obtained the lowest compressive strengths between 18 MPa to 20 MPa (Figure 2.10a). The trend of decreasing compressive strength values observed in the third study suggests a potential loss of structural integrity over time. Comparing the three different DoE studies, it can be observed that varying the numbers of particle grinding cycles demonstrated an increase in the compressive strength ($p\text{-value} < 0.001$) when the grinding cycle number increased from 2 cycles to 11 cycles (Figure 2.10a). The increase of grinding for more than 11 cycles led to reduction on mechanical properties.

The DoE analysis found that the compressive strength of PM-CPC was influenced by two factors, the LPR and the amount of phosphoserine within the PM-CPC. According to the sum of squares and the contribution of each factor provided from ANOVA analysis, the factor with the greatest influence on this response is the LPR with a contribution greater than 20%. The effect of the factors on the compressive properties is shown in Figure 2.10b and Figure 2.10c. A reduction in compressive strength was observed with increasing the LPR (Figure 2.10b), while a non-linear influence of compressive strength was observed when increasing the phosphoserine content (Figure 2.10c). Increasing the phosphoserine content from 10 wt.% to 25 wt.% led to an increase of compressive strength while a decrease of compressive

strength was demonstrated with more than 25 wt.% of phosphoserine within the PM-CPC adhesive.

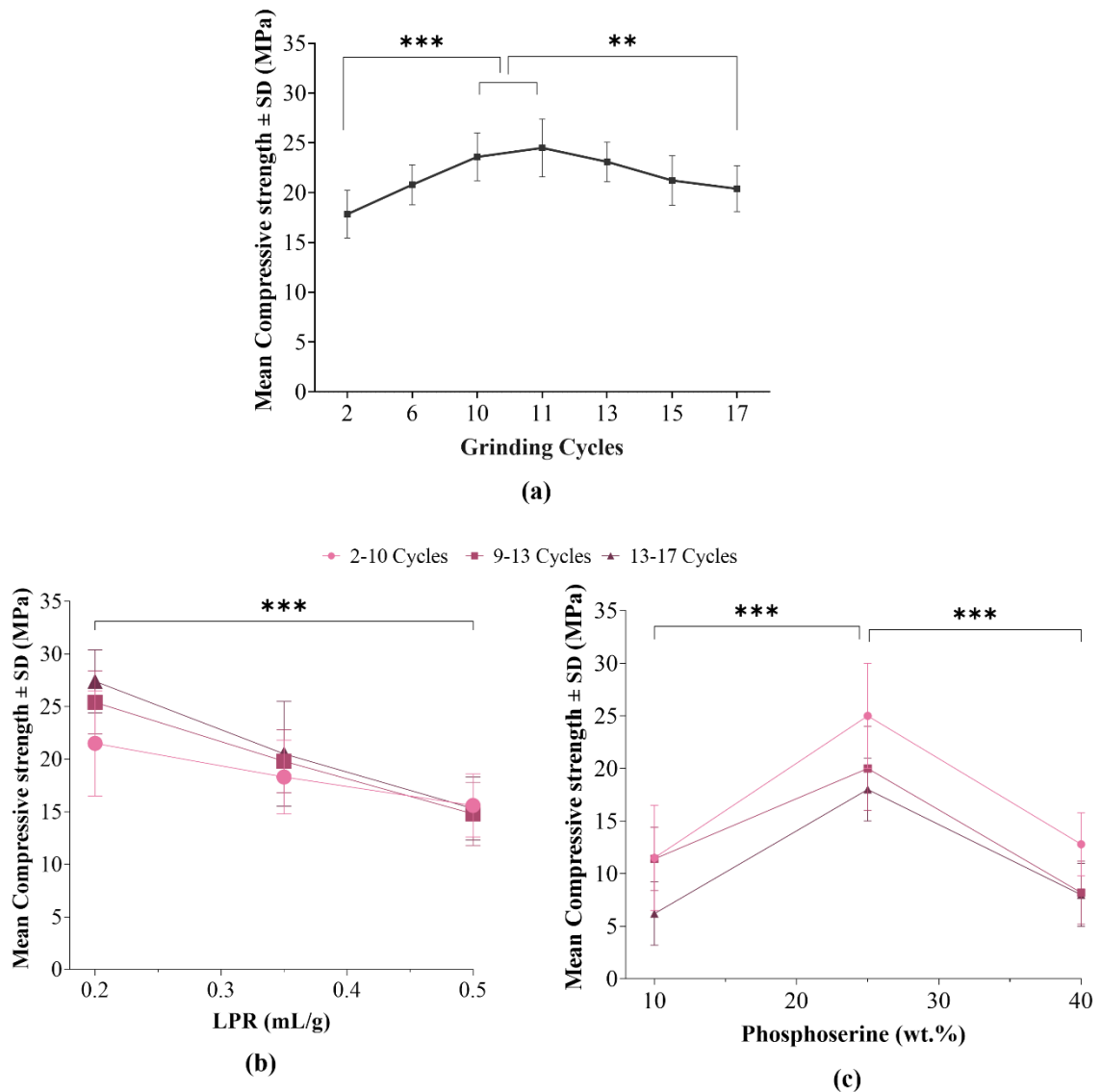


Figure 2.10: LPR and Phosphoserine Influence on Compressive Strength – DoE graphs describing the impact of (a) grinding cycles, (b) LPR and (c) phosphoserine content on the compressive strength of PM-CPC adhesive for α -TCP at different grinding cycles. The results demonstrate that increasing the LPR leads to a reduction while the increase in phosphoserine up to 25% enhanced the strength. The significance levels are denoted as **p-value < 0.01, ***p-value < 0.001.

2.4.2.3 Adhesion Properties

Increase of adhesive strength was observed for smaller particle sizes of α -TCP (higher number of grinding cycles). Specifically, the adhesive strength was significantly (p -value <0.01) increased at 5.5 ± 0.8 MPa after 13 cycles compared to 4 ± 0.5 MPa after 2 cycles (Figure 2.11a). Further increase of grinding cycles led to a decrease in the adhesive strength by 1 MPa leading to an adhesive strength 4.5 ± 0.5 MPa. In all three separate studies, an increase in the LPR from 0.2 mL/g to 0.5 mL/g resulted in an average adhesive strength of 4.5 ± 0.5 MPa and 4.0 ± 0.3 MPa, as illustrated in (Figure 2.11b). Conversely, there was a statistically significant (p -value <0.001) enhancement in adhesive strength with an increase in the amount of phosphoserine, leading to a strength of 5.0 ± 0.5 MPa from an initial strength of 2.4 ± 0.8 MPa, as shown in (Figure 2.11c). The highest adhesive strength values were observed when α -TCP was ground through more than 10 grinding cycles.

The LPR and amount of phosphoserine were the factors that most significantly influenced the adhesive strength for all three DoE studies (Figure 2.11b and Figure 2.11c)—a similar finding to compressive strength. A higher contribution (approx. 44%) was demonstrated from LPR to the final model, with increasing LPR leading to the linear decrease in adhesive strength. Increasing the phosphoserine content enhanced through a non-linear relationship the adhesion properties compared to the addition of DI water, indicating an interrelationship between these two factors. Furthermore, the results demonstrate that increasing the phosphoserine content up to 25% enhanced adhesive strength. The higher number of grinding cycles did not have a significant impact on adhesive strength (p -value > 0.05).

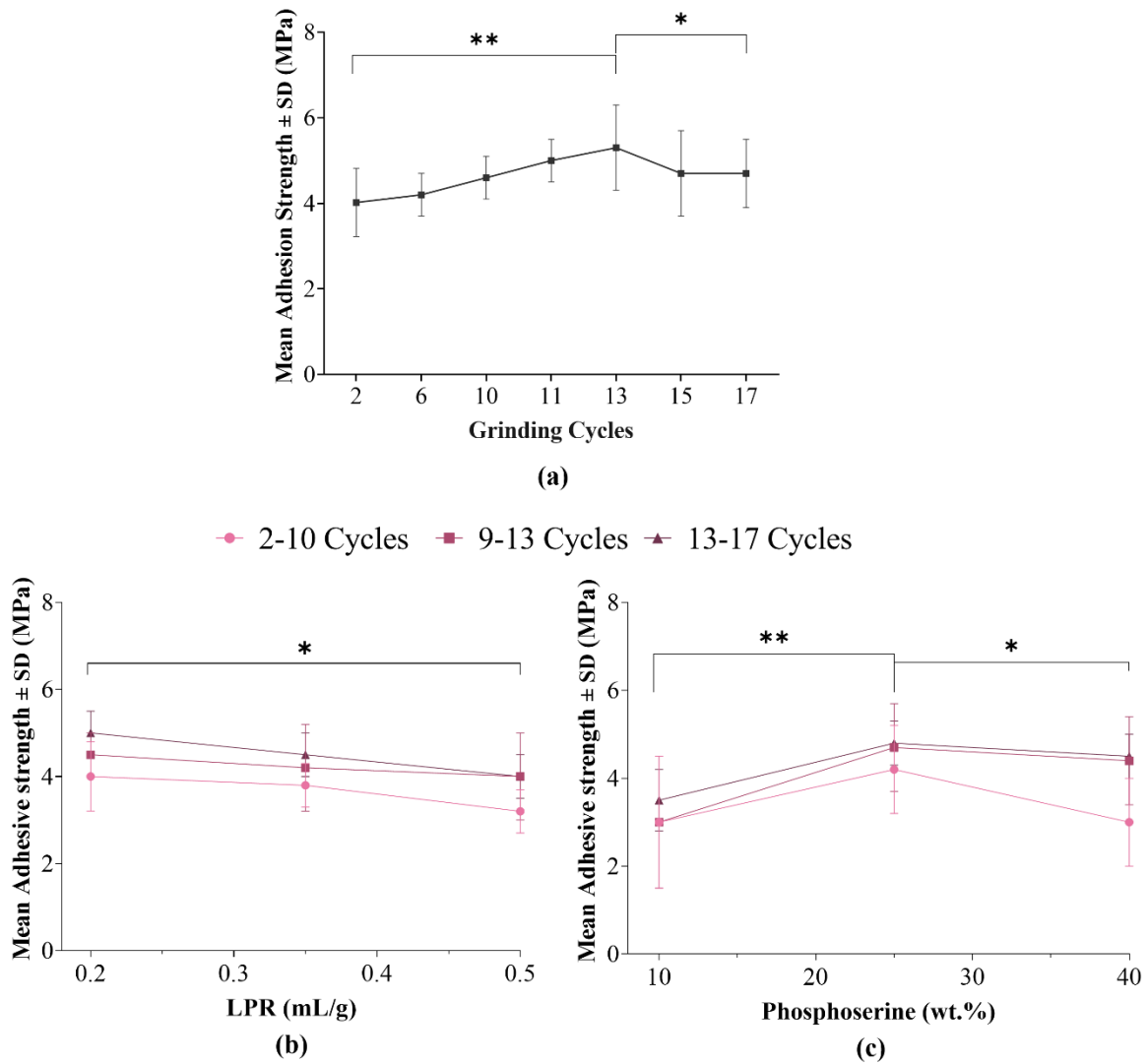


Figure 2.11: LPR and Phosphoserine Influence on Adhesive Strength – DoE graphs demonstrating the impact of (a) grinding cycles, (b) LPR and (c) phosphoserine content on the adhesive strength of adhesive for the three DoE studies. The significance levels are denoted as *p-value < 0.05, **p-value < 0.01, indicating significant changes observed in all three studies (i.e., 2-6, 9-13, and 13-17 grinding cycles).

2.4.3. DoE Optimisation and Validation

The models generated for each response from the DoE analysis were then used to optimise the PM-CPC according to a set of clinical informed optimisation criteria as per Table 2.4. The optimal PM-CPC composition was determined to be 74 wt.% α -TCP (after 11 grinding cycles), 25 wt.% phosphoserine, 1 wt.% calcium silicate, with a LPR of 0.3 mL/g. This composition achieved a di of 0.92, indicating an optimal performance. The predicted responses for the optimal composition of PM-CPC and the experimental values are shown in Table 2.4. To verify the accuracy of these predicted values, an experimental validation study was conducted using t-test analysis. The results showed a non-significant difference (p-value = 0.1) between the predicted and experimental values, with a percentage of difference of 5% for both setting properties (Table 2.4) and lower than 14% difference for mechanical properties (Table 2.4). Furthermore, the DoE studies demonstrated high accuracy, as the experimental values were within the standard deviation of the predicted responses, with a non-significant difference between experimental and predicted values.

Table 2.4: Results of DoE optimisation of the PM-CPC composition showing the acceptable clinical ranges for each factor and validation of the models by comparing the difference between predicted responses for the optimal PM-CPC composition and the actual values from experimental data.

<u>DoE Optimal PM-CPC Adhesive Composition</u>				
74 wt.% non-passivated αTCP after 11 cycles		25 wt.% phosphoserine		1 wt.% calcium silicate
Responses	Clinical Requirements	DoE Prediction	Experimental Values	Difference (%)
Initial Setting Time (s)	$60 \geq t_i \geq 120$	110 ± 10	115 ± 10	4.4
Final Setting Time (s)	$120 \geq t_f \geq 200$	200 ± 20	192 ± 10	4.1
Compressive Strength (MPa)	≥ 10	25.7 ± 3	29.5 ± 4.6	13.8
Adhesive Strength (MPa)	≥ 2.5	4.2 ± 0.3	3.9 ± 0.9	7.4

2.5. Discussion

This chapter aimed to evaluate a range of PM-CPC adhesive compositions, to gain an in-depth understanding of the influence of variable factors on PM-CPC properties under wet field conditions for bone repair and stabilisation. Initially, the α -TCP powder was synthesised and analytically characterised and this was then followed by investigating the influence of various process parameters (setting time, compressive and adhesive strength) on the properties of PM-CPC using DoE studies. DoE analysis highlighted the influence of the most significant factors (LPR, amount of phosphoserine and α -TCP powder particle size) on the final properties of the adhesive. Optimisation of the process yielded an injectable bone adhesive with setting, mechanical and adhesion properties suitable for clinical bone defect repair.

Phase pure α -TCP was fabricated, with XRD and FT-IR analysis confirming the presence of α -TCP without any evidence of other calcium phosphates present, such as β -TCP [227] or HA [228]. The presence of other phases could compromise the mechanical and biological properties of the resultant adhesive, therefore, achieving high phase purity is crucial to ensure biocompatibility and desired functionality, and to reduce the risk of implant failure or rejection [229–231]. The synthesised α -TCP powder had an irregular, non-spherical, and polyhedral shape, with a circularity of 0.35 ± 0.2 —values which align with the reported morphology for α -TCP powders obtained through mechanical milling [232]. As expected, there was a negative correlation ($R^2 = 0.90$) between particle size and number of grinding cycles, consistent with previous findings [13]. The reduction in particle size can be attributed to the mechanical force exerted during the grinding process, which breaks down larger particles into smaller ones. The negative zeta potential obtained herein is advantageous for bone tissue engineering applications as it facilitates the adsorption of Ca^{2+} ions, promoting cell adhesion, proliferation and new bone formation [233,234].

A DoE study was then conducted to gain a comprehensive understanding of the factors influencing the handling, mechanical and adhesion properties of the PM-CPC adhesives. An interesting outcome of this study was the lack of a statistically significant difference in handling and mechanical properties between passivated and non-passivated α -TCP. The likely expectation would have been that passivation—a process aimed at creating a protective coating or layer to reduce chemical reactivity—would cause distinct changes in the properties of α -TCP [235]. However, a number of studies obtained minimal difference in the mechanical properties after passivation process similar to our findings [222,236]. Furthermore, as mentioned already passivation offers a protective barrier without inducing significant changes to the material's surface roughness or porosity which can explain the low effect on handling properties.

Another important finding was the effect of the number of grinding cycles, which had a significant impact on the setting behaviour of PM-CPC. It has been determined from the results that the particle size of α -TCP significantly influences the setting properties of PM-CPC. Fine-tuning the particle size through grinding can be a strategic approach to achieving optimal handling properties for specific clinical scenarios. In the case of lower grinding cycles or bigger particle sizes for α -TCP powder, the DoE indicated a slower setting time. This delay in setting may be attributed to the surface area of particles, which plays a crucial role in determining their reactivity [237]. Having a powder of a larger particle size mean there is a reduced surface area available for dissolution, which is a critical step in the setting reaction of many bone cements, thus slowing down the overall setting time [238,239]. This observation suggests that for specific clinical applications requiring a more extended working time, α -TCP of larger particle size may be a suitable choice. Conversely, when α -TCP particle size was small the setting process was accelerated. This rapid setting could be advantageous in situations demanding quick surgical procedures and immediate fixation of

bone fragments. However, this faster setting might pose challenges in terms of handling and application precision. The findings in this study corroborate previous works [240,241], further emphasising the importance of optimising particle size and grinding conditions for desired properties in applications using α -TCP. The understanding of this fundamental principle is essential especially when balancing factors like mechanical strength, setting time.

In addition to grinding cycles, the DoE analysis demonstrated that the LPR, phosphoserine content, had a significant impact on both handling and mechanical properties, with the LPR showing the highest contribution. Increasing the LPR resulted in a more injectable adhesive with slow setting and low mechanical properties. These results align with findings from previous studies which similarly observed that increasing LPR values in adhesive formulations resulted in a more malleable and injectable mixture [13,242,243]. Conversely, increasing the phosphoserine content led to faster setting times and higher mechanical properties, particularly for low levels of LPR. This observation is consistent with prior research examining the setting and mechanical characteristics of cements based on α -TCP and β -TCP in relation to varying phosphoserine concentrations [148,244]. With the trade-offs between setting time, and mechanical properties brought about by variations in LPR and phosphoserine content, careful calibration of these parameters is required.

A challenge when attempting to produce optimal PM-CPC is that the material properties are interrelated [242], therefore improving the compressive strength has a negative effect on the handling properties. The influence of the LPR on mechanical properties can be attributed to the effect of water content on the porosity of the adhesive after setting, where a higher water content results in increased porosity and poorer mechanical properties [245]. A larger amount of water resulted in an increase in the porosity content of the cement and consequently, a material demonstrating poorer mechanical properties [246]. This interaction mechanism on mechanical properties is an area of research that requires further investigation. The DoE

analysis exhibited a non-linear relationship between phosphoserine content and the mechanical properties. As the phosphoserine content is increased from 10 wt.% to 25 wt.%, there is a linear increase in compressive strength. This indicates a positive correlation between phosphoserine content and the mechanical properties of the CPC. However, beyond 25 wt.% of phosphoserine, a linear reduction in compressive strength was observed. This non-linear relationship between phosphoserine content and the mechanical properties of the PM-CPC suggests the presence of an optimum or threshold concentration. At lower phosphoserine levels (10-25 wt.%), the incorporation of phosphoserine enhances the interfacial bonding and chemical interactions within the matrix, leading to improved compressive strength. However, at higher phosphoserine levels (beyond 25 wt.%), an excess of phosphoserine might disrupt the formation of the adhesive matrix or introduce structural irregularities, resulting in a decrease in compressive strength. Overall, the DoE modelling provided important insight into the relationships between multiple input and output variables in the context of the PM-CPC synthesis, enabling efficient optimisation of the process.

Optimisation of the PM-CPC adhesive was then completed using the DoE models to identify the optimal PM-CPC composition for clinical use, that demonstrates a satisfactory injectability and workability, and setting times within an appropriate range, along with enhanced mechanical and adhesion performance. The optimal composition for PM-CPC adhesive, meeting these clinical requirements, was determined to be 74 wt.% α -TCP (after 11 grinding cycles), 25 wt.% phosphoserine, 1 wt.% calcium silicate, and an LPR of 0.3 mL/g. The optimal composition proposed by the DoE studies resulted in an injectable adhesive with setting times and static mechanical properties that met the required clinical specifications for the treatment of challenging bone fractures.

2.6. Conclusions

In conclusion, this chapter successfully addressed its primary aim, which was to contribute to a more comprehensive understanding of the factors affecting the responses of the PM-CPC adhesive. The successful fabrication and analytical assessment of α -TCP powders was achieved, confirming their phase purity through XRD and FTIR analysis. Monitoring α -TCP purity ensures that the final adhesive's characteristics remain consistent, avoiding potential deviations in its behaviour. By employing a DoE approach, the particle size of α -TCP, LPR and phosphoserine content were found to significantly influence the handling, mechanical, and bond properties of the PM-CPC adhesive. Optimisation through DoE allowed us to identify an optimal composition of PM-CPC, aligning with clinical requirements for setting times as well as compressive and bond/shear strength after a 24-h setting reaction. The adaptability of a DoE model extends its relevance beyond single-use optimisation. As clinical requirements evolve, the established DoE model can be recalibrated appropriately, eliminating the need to start the analysis from scratch. Thus, it not only facilitates in-depth initial analysis and understanding of the key process parameters affecting PM-CPC properties, but also streamlines future improvements, making it an enduring tool in adhesive formulation and optimisation.

These studies can be considered as a preliminary design to understand the factors and levels that had the greatest impact on fabrication of the adhesive. The transition from lab-scale volumes to industry-relevant volumes presents challenges and the implications of scaling up remain to be seen. Given the promising properties of the PM-CPC adhesive, its optimal composition was selected for further analysis and validation in larger and more varied settings. This will confirm its suitability for clinical use as a calcified tissue adhesive under wet conditions and assess its scalability for industrial production volumes.

**Chapter 3: Functional Assessment of
Optimal Phosphoserine-modified Calcium
Phosphate Adhesive (PM-CPC) for Bone
Repair and Implant Augmentation**

Sections of this Chapter have previously been presented in a scientific article published in Acta Biomaterialia, Elsevier (2023): **A. Tzagiollari, J. Redmond, H.O. McCarthy, T.J. Levingstone, N.J. Dunne**, *Multi-objective property optimisation of a phosphoserine-modified calcium phosphates for orthopaedic and dental applications using Design of Experiments methodology*, Acta Biomaterialia, 2023

3.1. Introduction

While the natural healing process of bone fractures is generally effective at repairing bones, some bone fractures, defects or loss often require the use of metal hardware to achieve effective stabilisation [32,62]. In recent research efforts, phosphoserine-modified calcium phosphate cement has emerged as a potential standout in the realm of biomedical adhesives under wet environments [101,148,150,215,247,248].

Although most research studies in the field focus on evaluating specific phosphoserine-modified adhesive compositions and comparing them with existing cement formulations, they lack knowledge about the mechanical and physical properties of these adhesives, particularly when considering large-scale production. Furthermore, parameters such as adhesion strength, degradation rate and bioactivity of the bone adhesive on bones or the ability to stabilise metallic implants and enhance their mechanical properties are unclear, particularly in wet conditions [16].

Following the initial DoE study (Chapter 2), the optimal composition was determined based on its handling and mechanical attributes, which are key criteria for orthopaedic and dental applications. Given these initial promising findings, this chapter focus on a thorough analytical assessment of the selected composition. The aim is to validate its efficacy in broader settings, ensuring its suitability as a wet-condition calcified tissue adhesive, and to evaluate its potential for large-scale production. Scaling up can introduce challenges, from ensuring consistent material quality to batch-to-batch variability and batch size. Hence, part of this chapter will explore the implications and potential obstacles of scaling up the adhesive, ensuring that the properties we have observed in controlled settings are maintained when produced in larger volumes. With this focused approach the optimal PM-CPC composition will be translated from promising laboratory results to practical, large-scale applications, particularly in orthopaedic and dental application.

3.2. Chapter Aim

The overall aim of this chapter is to conduct a comprehensive characterisation of the properties exhibited by the optimal PM-CPC composition, as previously identified in Chapter 2. This in-depth analysis is essential to verify its suitability for clinical application as a calcified tissue adhesive. The initial focus was the hand-mixing of the optimal PM-CPC composition in higher batch sizes to determine whether it is feasible for the adhesive to be produced in industry-relevant volumes properties. Once mixed, the adhesive was characterised to assess their handling and mechanical properties. Furthermore, chemical, architectural, biological and degradative properties were determined. The ability of the adhesive to be used as an augmentation material for both orthopaedic and dental application was also investigated.

The specific objectives of this chapter are to:

- Assess of the increased batch size from 1g to 10 g determining the setting and mechanical properties.
- Assess of the stability, degradation and bioactivity of the PM-CPC bone adhesive.
- Assess of the pull-out and removal torque properties to ensure that the adhesive meets the requirements to be used as implant augmentation.

3.3. Material and Methods

3.3.1. Formulation of Optimal PM-CPC Adhesive

The optimal PM-CPC adhesive was formulated by mixing the powder phase (74 wt.% α -TCP, 25 wt.% phosphoserine and 1 wt.% calcium silicate) with 0.3 mL/g DI water. The liquid and powder phases were mixed with a spatula for 15-20 s and then placed in different moulds to fabricate specimens with the required shape and dimensions for the

various characterisation techniques. All specimens were incubated for 72 h in Ringer's solution at 37°C and 100% relative humidity to simulate the biological environment.

3.3.2. Analytical Assessment of Optimal Hand-mixed PM-CPC Adhesive

3.3.2.1 Handling and Mechanical Properties

To assess the clinical applicability of the adhesive, additional characterisation of the optimal PM-CPC was conducted. In particular, the scalability of the optimal PM-CPC was evaluated by increasing the batch size from 1 g to 10 g to determine whether it is feasible for the adhesive to be produced in industry-relevant volumes. The influence of the increased batch size on the optimal PM-CPC properties was evaluated by determining the mixing, setting and mechanical properties (i.e., compressive and adhesive shear strength) as per Section 2.3.5.1. for setting time, and Section 2.3.5.2 and Section 2.3.5.3 for compressive and adhesion strength respectively.

3.3.2.2 Washout Resistance

The stability of the PM-CPC in a wet-field environment simulating the biological environment was assessed using a washout resistance test [249]. The washout resistance test was performed using two different configurations: (1) manually shaped PM-CPC with a volume of approximately 0.50 mm³, and (2) injected PM-CPC, which was delivered through a syringe without a nozzle (extrusion diameter = 2.25 mm), these techniques mimics the shear forces and dynamic environment the material would encounter during actual injection into a bone defect or cavity. The larger extrusion diameter compared to the manually shaped configuration ensures that the material's flow characteristics and resistance to washout are accurately represented under realistic conditions.

In both cases, the specimens were transferred to a beaker containing 20 mL of phosphate buffered solution (PBS). The specimens were incubated at 37°C, with visual inspections every

minute for 5 min (qualitative analysis). The specimen was considered to have passed the washout resistance test if it did not visibly disintegrate in the solution. In addition, for quantitative measurement, the weight of manually shaped PM-CPC was recorded before the immersion in PBS. The weight of the specimens was measured every 1 min for the next 5 min. The disintegrated amounts (percentage of mass loss) were then calculated.

3.3.2.3 Degradation and *In vitro* Degradation Properties

Cylindrical PM-CPC specimens (12 mm height, 6 mm diameter) were incubated in PBS solution (pH 7.4) at 37°C on a plate shaker for time intervals of 4, 6, 8, 14, 30, 60, 90, and 120 days. The solution was replaced every 4 weeks. At each time-point, three specimens were removed from the degradation media, washed with DI water, and dried under vacuum for 2 days at 37°C. The dry mass of the specimens was then determined. Enzymatic-based *in vitro* degradation was also assessed. Here specimens were placed in a porcine pancreas lipase-phosphate buffer solution (PPL)-PBS solution. The PPL concentration was 10 U/mL PPL ($\geq 3,000$ U/g, Merck Life Science Limited, Ireland). The same procedure as with PBS-only was followed.

3.3.2.4 Biological Activity

To evaluate the bioactivity, the formation of bonelike apatite on the specimens (4 mm height, 8 mm diameter) was examined in a simulate body fluid solution, at 37°C and a pH of 7.4. The ion concentrations in the solution was almost identical to those in human blood plasma [250]. The solution was replenished every 3 days, with specimens removed from incubation after 24 h, 3 days and 7 days. Subsequently, the specimens were washed with DI water and dried in an oven at 50°C for 3 h. Changes in the surface morphology of specimens were characterised using SEM, equipped with energy-dispersive X-ray spectroscopy (EDX). The SEM images

were further analysed using Image J for the determination of the crystal's morphology and size.

Additionally, XRD analysis as per Section 2.3.2.1 was performed to evaluate the crystalline phases present in PM-CPC adhesive at different time points, including after mixing and during the setting reactions. The XRD analysis was performed on hardened specimens following immersion in Ringer's solution at timepoints of 24 h, 3 days, and 7 days post fabrication to assess the time-dependent phase transition. For this analysis, each sample was dried and ground to a powder using a mortar and pestle.

3.3.2.5 Adhesion Strength on Dental Implants

Sockets (4.0 mm inner hole and 8.4 mm outer) were created in blocks of low-density synthetic bone material (5PCF solid rigid polyurethane foam (Sawbones Europe AB, Sweden)), as can be seen in Figure 3.1. The PM-CPC adhesive was manually mixed prior to injection into predrilled sockets followed by the insertion of a dental implant (augmented) while as control was used the dental implant without PM-CPC adhesive (non-augmented). The injection was completed at ambient conditions ($T=22\text{ }^{\circ}\text{C}$ and humidity= $45\pm 5\%$) while simultaneously ensuring that the adhesive adequately covered the entire endosteal area (surface-modified region). The dental implant (Strauman ITI standard non-octagon Morse taper, Switzerland) was inserted using an implant driver (Hexagonal screwdriver, Straumann, Switzerland) into the "wet" adhesive before the final setting time and left to set for 20 min. Pull-out and removal torque testing was conducted for both augmented and non-augmented dental implants to determine the effect of PM-CPC on the mechanical stability of dental implants.

The effect of blood on the adhesive properties of PM-CPC was also investigated during both pull-out and removal torque tests to account for any potential bleeding at the implant site when delivering the adhesive in an *in vivo* environment. The tests were conducted using

porcine blood (obtained from a Dublin-based butcher) to simulate the *in vivo* environment. The blood was added in the socket one min before the injection of PM-CPC (Figure 3.1), which was manually mixed at ambient conditions.

The pull-out force was measured using a Zwick Testing System with a 5 kN load cell. The system was fitted with tensile grips and equipped with an extensometer for strain measurements. Experiments were conducted according to American Society for Testing and Materials International (ASTM) F543 standards, with a speed rate of 5 mm/min and a 0.1 N pre-load force. All samples (non-augmented implant, augmented implant and augmented implant + porcine blood) were tested to failure (n=6). The torque force was measured using a digital torque screwdriver. The removal torque forces without PM-CPC, with PM-CPC and with blood and PM-CPC were recorded and compared.

3.3.2.6 Adhesion Strength on Orthopaedic Screws

The ability of PM-CPC to augment the mechanical stability of orthopaedic screws was also determined through a pull-out force test (Figure 3.2). For the pull-out test, two different types of screws were selected: (1) the Cortex screw (Smith & Nephew, UK) (cortical screw, diameter 2.7 mm, h=36 mm) and (2) Osteopenia screw (Smith & Nephew, UK) (cancellous screw, diameter 4.0 mm, h=36 mm). Initially, the predrilled hole with a diameter of 2 mm in low-density synthetics blocks (5PCF solid rigid polyurethane foam (Sawbones Europe AB, Sweden)) was filled with PM-CPC, followed by the insertion of each screw to a depth of 20 mm within the defect while the PM-CPC is still in liquid-paste form and has not been fully set. The axial pull-out test was conducted 10 min after PM-CPC mixing in PM-CPC accordance with ASTM F543 at a crosshead rate of 5 mm/min and a 0.1 N pre-load force (n=6).

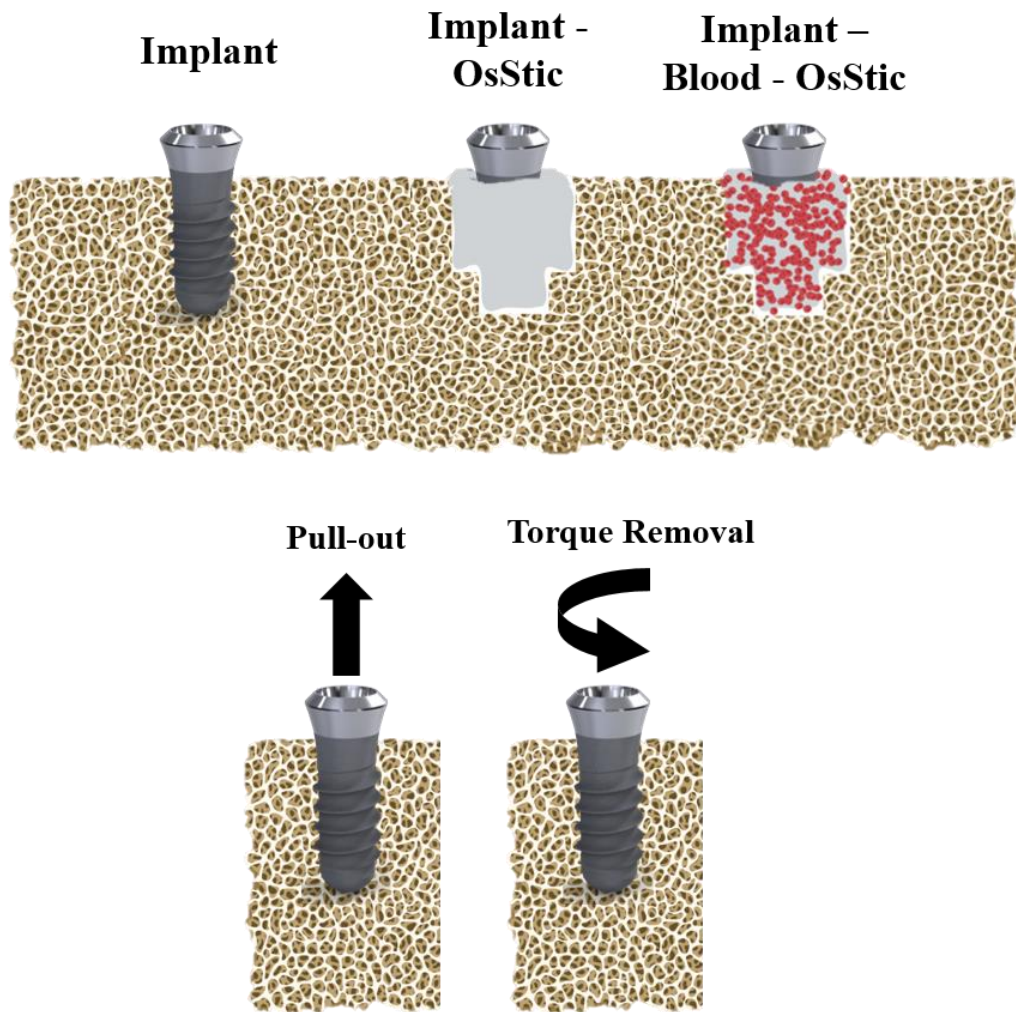


Figure 3.1: Set-up of Pull-out and Torque Removal Test for Dental Implants – Schematic representation of the set-up for mechanical characterisation of non-and augmented dental implants with and without the presence of blood.

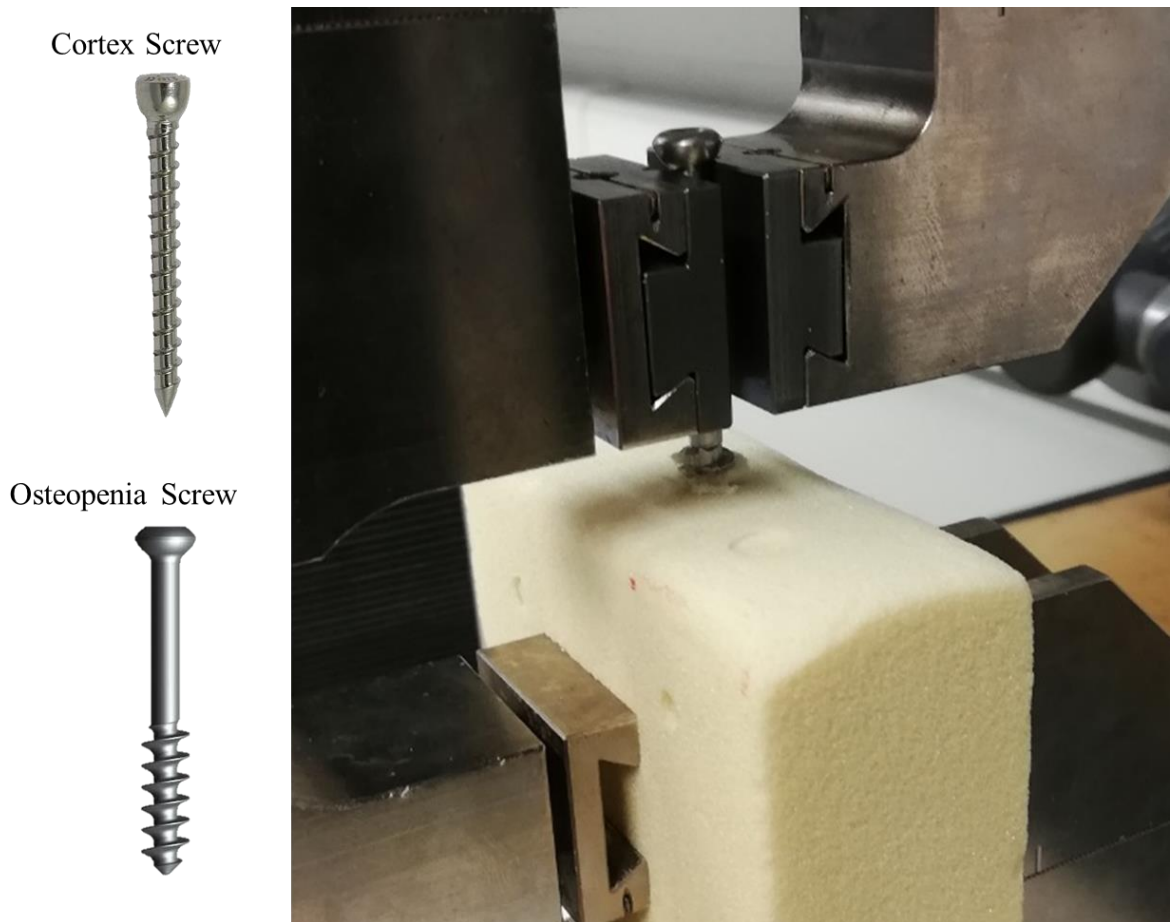


Figure 3.2: Set-up of Pull-out Test for Orthopaedic Implants – Illustration of the pull-out test set up in terms of the grip and sample position for the application of the axial force.

3.3.2.7 Bone-to-Bone Adhesion Properties

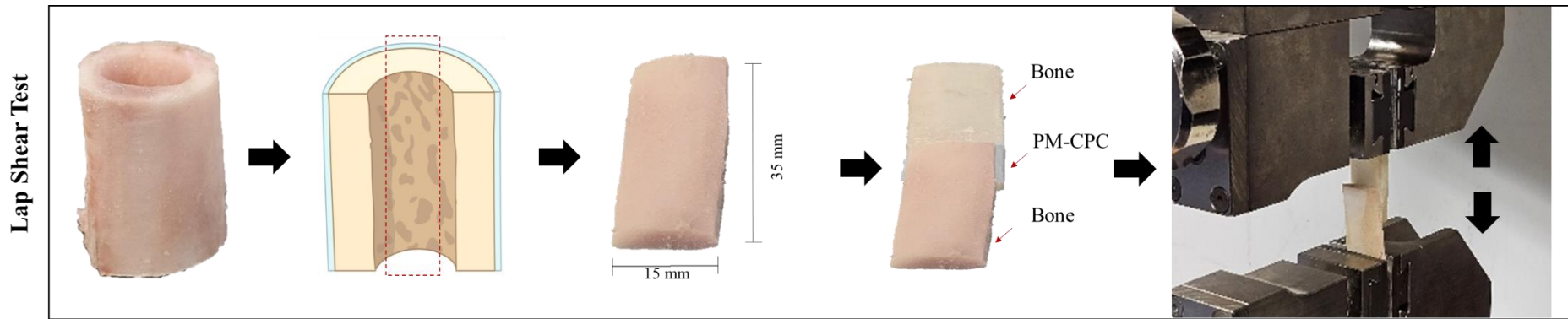
Sample Preparation

Bovine femur bones were selected for use in bone-to-bone adhesion testing, due primarily to their favourable cortical thickness. Bovine femora were purchased from a Dublin-based butcher to obtain both cortical (Figure 3. 3a) and cancellous (Figure 3. 3b) bone specimens. After removal of soft tissue, each femoral bone was wrapped in PBS-soaked gauze. During all cutting and machining operations, the bone material was frequently and liberally sprayed with saline solution to keep it cool and wet. Each bone was sectioned into rectangular slices measuring Length×Width×Thickness of 35×15×3 mm (n=6) and cuboid-shaped specimens measuring 20×10×10 mm (n=6) using a Titan TTB705BDS electric bandsaw (Screwfix,

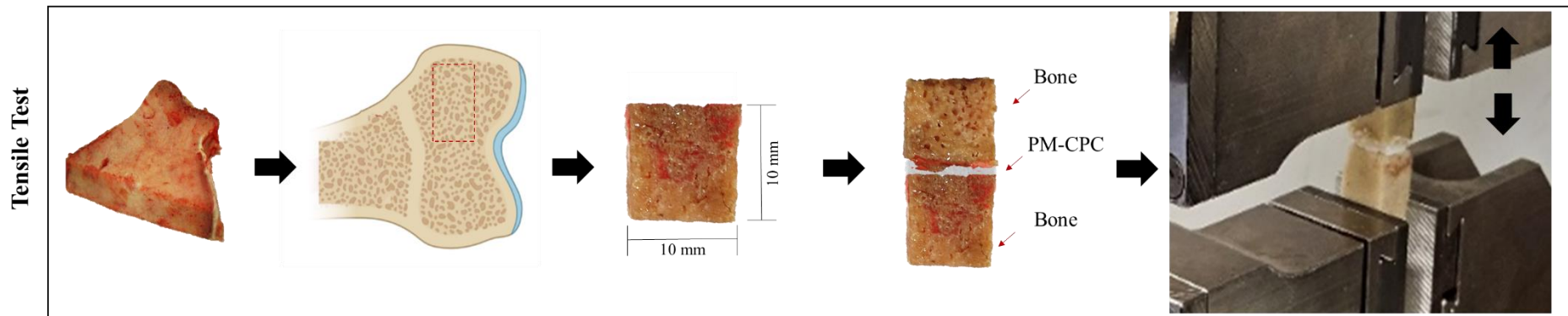
Ireland) with water cooling. To ensure uniform thickness, each bone specimens was ground using a Metkon Forcimat (Bursa, Turkey) grinding-polishing machine with P80 grade silicon carbide paper (TMQ Ltd., Ireland).

Testing

Lap shear and tensile tests were conducted to assess bone-to-bone adhesion under wet conditions (n=6 specimens). The lap shear test used rectangular-shaped bone specimens, while the tensile test employed cuboid shaped bone specimens. Each test sample was prepared by applying a 0.2 g layer of the optimal PM-CPC adhesive onto one surface of a bone sample, covering a surface area of 100 mm². A second bone sample was then placed on top. The specimens were immersed in Ringer's solution and incubated at 37°C for 24 h and 72 h. Each sample was tested to failure using a Zwick Testing System, fitted with a 5 kN load cell. The system was fitted with tensile grips and equipped with an extensometer for strain measurements. Lap shear and tensile test specimens were designed so that the highest strains would occur in the central portion or gauge region of the specimen. Fracture surfaces were examined using SEM to identify the mode of failure, which could be adhesive (failure between adhesive and bone substrate), cohesive (failure within the adhesive), or mixed (involving both cohesive and adhesive failure).



(a)



(b)

Figure 3. 3: Bovine Femur Specimens for Bone-to-Bone Adhesion Test – Porcine bovine femur bone sample preparation from the (a) cortical bone for lap shear testing and (b) cancellous bone for tensile testing.

3.4. Statistical Analysis

All experiment testing was completed using a minimum of three repeats (n=3) and a maximum of 6 samples (n=6). Data is presented as the mean \pm SD. The statistical significance of data for difference comparison was determined using t-test, with a $p < 0.05$ defined as the minimal level of significance. All statistical analysis was performed using GraphPad (GraphPad_Prism Software, Version 8.0.2).

3.5. Results

3.5.1. Handling and Mechanical Properties

After adjusting the batch size of PM-CPC powder and mixing, a homogeneous paste was obtained within 20 s. As illustrated in Figure 3.4a, this consistency was observed for the 1g, 5g, and 10g batch sizes after manually mixing with a spatula. A similar texture was observed irrespective of batch size, with a smooth and shiny PM-CPC mixture achieved within 20 s (Figure 3.4b). Similarly, the initial and final setting times for all three batch sizes remained within the clinical specifications (Figure 3.4c). There was no significant difference ($p\text{-value} > 0.05$) between the setting times for the different batch sizes tested.

The average compressive and adhesive strength were unaffected by the change in batch size leading to non-significant difference ($p\text{-value} > 0.05$). With average compressive strength of 29.5 ± 4.6 MPa and adhesive strength of $\sim 3.9 \pm 0.9$ MPa across the three different batch sizes (Figure 3.5a). The values for compressive and adhesive strength align with the clinical requirements for bone adhesives.

Analysis of the fracture surfaces showed cohesive failure modes (n=6), characterised by a noticeable adhesive layer. This layer was found on both fractured surfaces in four instances (n=4 out of 6), and solely on one of the metallic (stainless steel) surfaces in two instances (n=2 out of 6), as depicted in (Figure 3.5b). These observations demonstrate the cohesive and

adhesive properties of the optimised PM-CPC bone adhesive, particularly in its interactions with stainless steel surfaces.

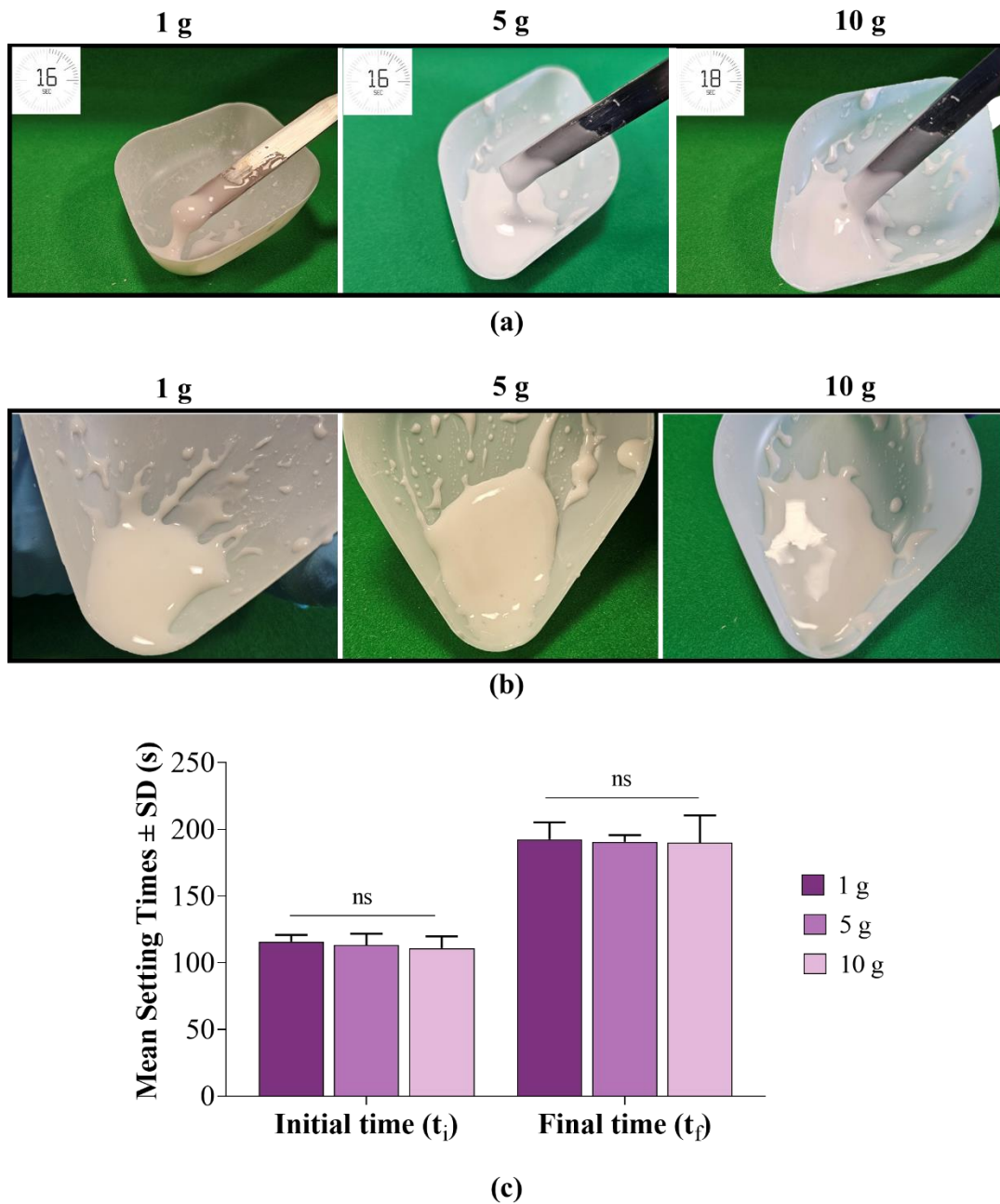
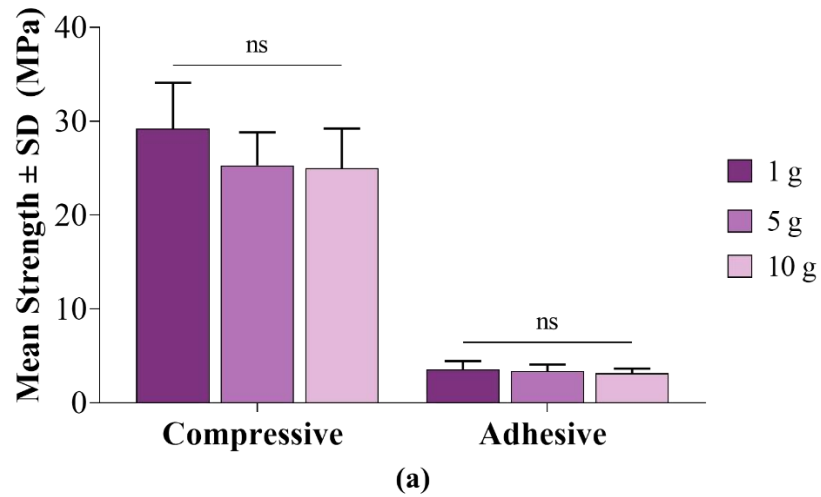
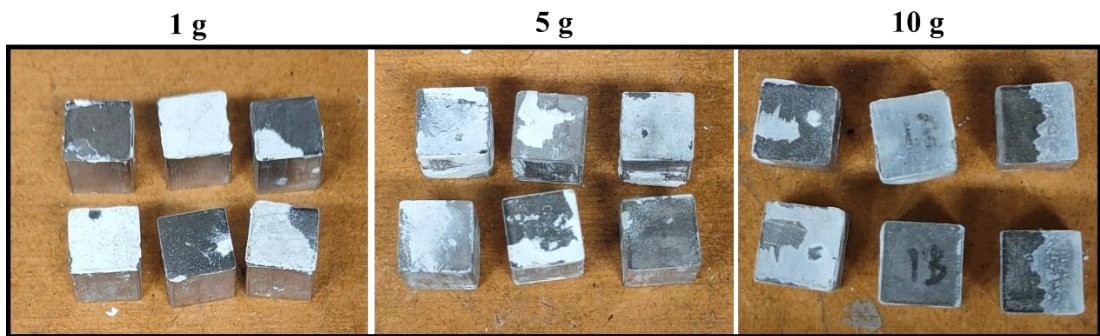


Figure 3.4: Setting Times of PM-CPC Adhesive – (a) mixing time, (b) mixture texture after homogenisation and (c) setting properties of the optimal PM-CPC composition were not affected by the increase of batch size from 1 g to 10 g. ns= non-significant, (n=6).



(a)



(b)

Figure 3.5: Static-Mechanical Properties of PM-CPC Adhesive – (a) Mean compressive strength and adhesive strength of the PM-CPC adhesive were not affected by increase of batch size from 1 g to 10 g. (b) Images of the stainless steel cubes after testing of the adhesive properties, with both cohesive and adhesive failure modes observed. ns= non-significant, (n=6).

3.5.2. Washout Resistance

Qualitative analysis of the adhesive demonstrated stability and integrity after 5 min, showing no visible signs of dissolution, as seen in Figure 3.6a. Within the first two timepoints (i.e., two minutes), despite the adhesive not being completely set, it maintained a stable shape within the PBS solution. When injected directly into the PBS bath, the injected PM-CPC retained a stable shape without displaying any signs of disintegration (Figure 3.6b). This observation demonstrates the adhesive's capacity to maintain its structural integrity even when injected in a wet environment. Subsequent washout resistance testing demonstrated that PM-CPC set before any visible disintegration occurred, thus the material passed the washout resistance test.

The quantitative analysis showed that the PM-CPC adhesive maintained good stability and strength when immersed in a PBS solution at 37°C (Figure 3.6c). Within the first minutes of immersion, before the adhesive fully set, a minimal mass loss of $2.9 \pm 0.1\%$ was noted, demonstrating the adhesive's robust resistance to degradation in wet conditions. Despite this, no visible disintegration was observed, indicating the adhesive's structural integrity and excellent stability under wet-field conditions.

3.5.3. Degradation and *In vitro* Degradation Properties

The degradation behaviour of the PM-CPC adhesive in PBS was evaluated over a 120-day period, with an approximate total mass loss of $18 \pm 4\%$ observed (Figure 3.7a). Over the initial five days, the degradation led to a roughly $5 \pm 0.5\%$ reduction in mass. Subsequently, the degradation rate decelerated, with an average daily mass loss of approximately 0.55% observed between Day 5 and Day 30. From Day 30 onward, the mass loss stabilised once again, with no statistical difference between values recorded between Day 30 until Day 120 with an average daily mass loss of 0.05%.

Furthermore, the enzymatic degradation of the PM-CPC adhesive was investigated. During the initial five days of enzymatic degradation, the mass loss was 11.8%. Subsequently, the rate of mass loss slowed, exhibiting a degradation pattern like that observed in the PBS-only study. The addition of PPL accelerated the degradation rate, leading to an approximate $25 \pm 6\%$ mass loss by Day 30 (Figure 3.7a).

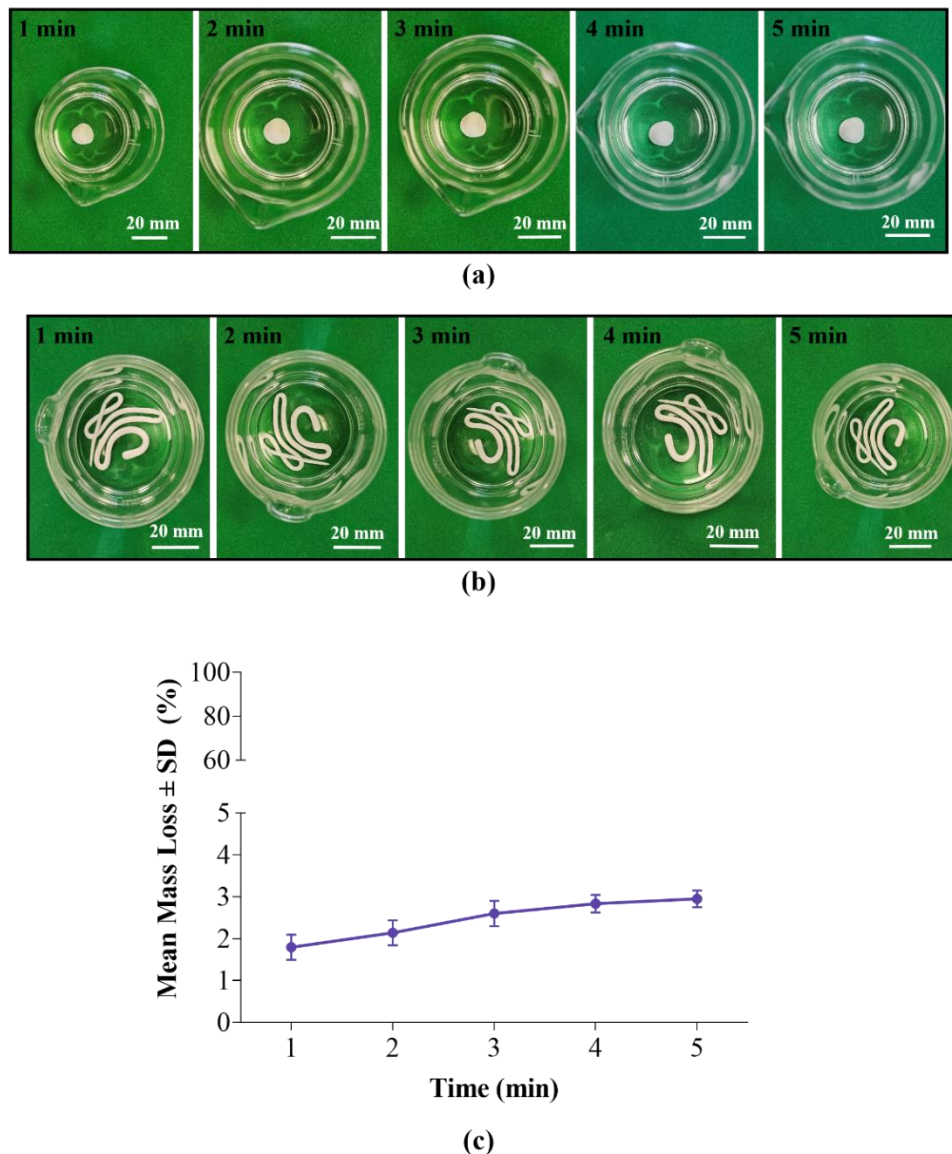
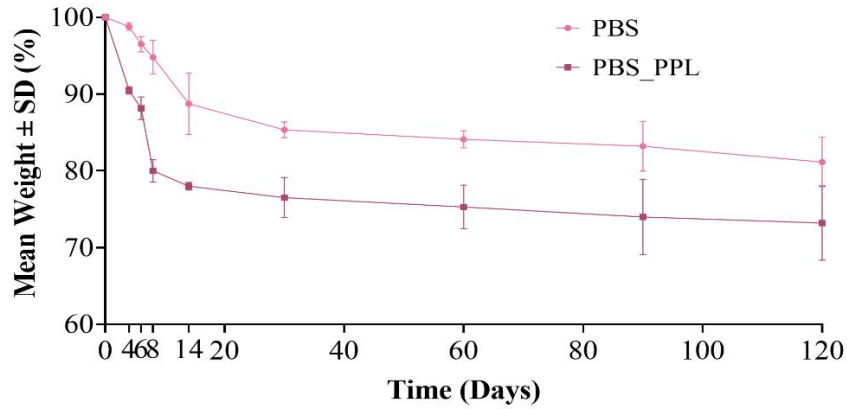


Figure 3.6: Washout Resistance of PM-CPC Adhesive – Evaluation of the washout resistance of the PM-CPC in PBS after being (a) manually shaped and (b) injected in the beaker through a syringe showing no disintegration at 5 min after setting. (c) Measurement of mass loss for PM-CPC at different timepoints for a total of 5 min after setting.

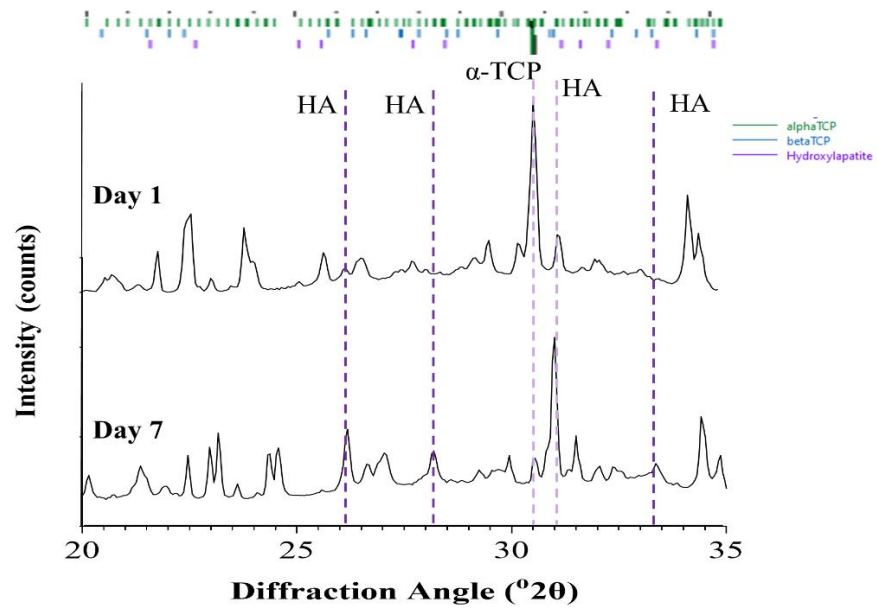
3.5.4. Biological Activity

After 24 hours of immersion in SBF, around 30% of the α -TCP phase transformed into HA crystals, a progression that continued over the next four days. XRD analysis verified this transformation, showing that ~50% of the calcium phosphate phase had converted into HA after a span of seven days (Table 3.1). This phenomenon is shown in Figure 3.7b, where the appearance of three distinct peaks attributed to HA at 26° , 28.5° and 33.1° are highlighted (indicated by the purple dashed line). Furthermore, the primary peak corresponding to the α -TCP structure at 30.7° undergoes a shift towards higher angles, reaching 31.9° . Notably, this angle aligns with the principal peak exhibited by HA-based structures.

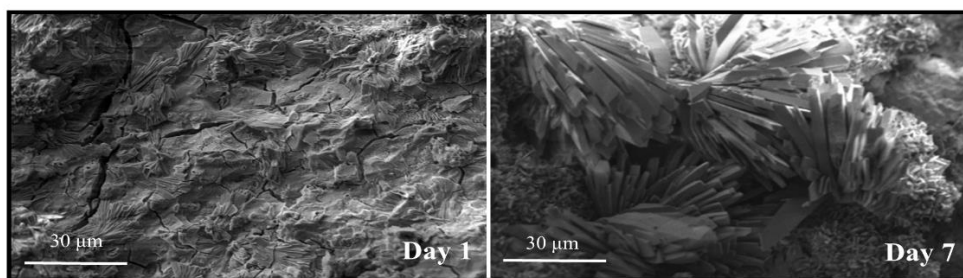
SEM images depicted a newly formed layer of HA crystals on the surface of the PM-CPC after 24 h of SBF immersion (Figure 3.7c). The formation of needle-shaped crystals was observed, with a length ranging from $7.7 \pm 0.4 \mu\text{m}$ to $27.0 \pm 1.3 \mu\text{m}$, and diameters between $1.5 \pm 0.2 \mu\text{m}$ and $3 \pm 0.4 \mu\text{m}$. After three days of immersion, specimens displayed a rise in the quantity and size of HA crystals, compared to those seen after 24 h. These crystals formed clusters on the surface of the PM-CPC adhesive. In contrast, the PM-CPC immersed for 7 days demonstrated a complete apatite layer consisting of needle-shaped crystals with lengths between $70.2 \pm 4.3 \mu\text{m}$ and $145.1 \pm 7.1 \mu\text{m}$ and a diameter of $7.1 \pm 2.6 \mu\text{m}$. Additionally, medium-sized (length= $8.3 \pm 1.7 \mu\text{m}$, thickness= $3.4 \pm 0.4 \mu\text{m}$) and large-sized (length= $82.3 \pm 5.3 \mu\text{m}$, thickness= $19.9 \pm 4.1 \mu\text{m}$) platelike HA crystals were observed. The SEM-EDX analysis confirmed the predominance of Ca and P elements on the surface, exhibiting chemical similarity to HA. The PM-CPC adhesive after 7 days exhibited Ca/P and Ca/O molar ratios of 1.6 and 0.44 respectively Table 3.1, demonstrating an increase of both molar ratios from the typical ratios of α -TCP (Ca/P =1.5, Ca/O=0.38).



(a)



(b)



(c)

Figure 3.7: Degradation and Biological Activity of PM-CPC Adhesive – (a) Degradation analysis of the PM-CPC immersed in PBS and PBS-PPL at 37°C, demonstrated a total mass loss of 20% and 28% respectively after 120 days. (b) XRD analysis and (c) SEM images showing the bioactivity and conversion of the α -TCP to HA crystals with approximately 50% conversion after 7 days showing a needle-shaped morphology compared to Day 1.

Table 3.1: Percentage of α -TCP and HA phase from XRD data and Ca/P and Ca/O molar ratios after 1-, 3- and 7-days immersion of PM-CPC bone adhesive in Ringer's solution.

XRD Analysis

Day	α-TCP (%) \pm SD	HA (%) \pm SD
1	71.7 \pm 7.1	28.3 \pm 6.1
3	66.5 \pm 6.8	33.5 \pm 6.8
7	49.2 \pm 7.3	50.8 \pm 7.3

SEM-EDX Analysis

Day	Ca (wt.%)	P (wt.%)	O (wt.%)	Ca/P Ratio	Ca/O Ratio
1	23.9 \pm 1.5	15.2 \pm 1.2	56.63 \pm 2.0	1.58	0.42
3	24.1 \pm 1.5	14.8 \pm 1.2	52.4 \pm 2.2	1.62	0.46
7	24.5 \pm 1.7	14.9 \pm 1.3	49.8 \pm 2.2	1.64	0.49

3.5.5. Adhesion Strength on Dental Implants

The analysis of the torque force measured on removal the dental implant showed that the PM-CPC adhesive significantly improved the resistance to rotational forces in augmented dental implants. The average torque removal force for the augmented implants of 53.8 ± 3.5 Ncm was greater than the non-augmented implants (30 ± 4 Ncm) (p -value <0.001) (Figure 3.8). These results indicate that the PM-CPC improved the adhesive strength between the implant and the surrounding bone. Additionally, the impact of the presence of blood within the socket on the adhesive properties of PM-CPC was evaluated, which had a negligible effect on the adhesive strength when PM-CPC was used. For the augmented implant group with the presence of blood, the torque removal force was measured at 43.8 ± 2.1 Ncm compared to 53.0 ± 3.6 Ncm without blood ($n=6$) (Figure 3.8). This difference between the augmented group with and without blood was not statistically significant (p -value >0.05).

The analysis of the pull-out force measurements demonstrated that augmenting the screw fixation with PM-CPC led to a significant enhancement in the bonding strength. The non-augmented dental implant exhibited a pull-out force of 241.3 ± 17.5 N, while the augmented implants showed higher pull-out forces of 639.4 ± 24.0 N and 610 ± 18.7 N with and without the present of blood, respectively (p -value <0.001 and p -value <0.01) (Figure 3.9a). This substantial increase indicates that augmenting the screw fixation with PM-CPC, led to a much stronger and more stable connection between the implant and the surrounding bone. The presence of blood did not have a significant impact (p -value >0.05) on the pull-out force (from 639.4 ± 24.0 N to 610 ± 18.7 N) (Figure 3.9a).

When a pull-out force was applied, synthetic bone particles were observed on the surface of the implant. The existence of synthetic bone residue indicates that the implant resistance encountered during the pull-out test was attributed to the implant's structural features and design, which contributed to its stability. Observation of the failure modes after the pull-out

test for the augmented implant with and without blood provided valuable insights into the behaviour of the adhesive and its interaction with the bone. The predominant failure mode, observed in both cases, occurred within the interface of adhesive and bone, as seen in Figure 3.9b. This indicates that the adhesive strength achieved using PM-CPC played a crucial role in determining the overall adhesive strength between the implant and the bone. The observed failure mode indicated that the PM-CPC effectively bonded to both the implant surface and the bone, creating a strong adhesive interface that resisted pull-out forces. The presence of blood during the implant procedure did not appear to influence the type of failure mode, as both cases showed similar patterns with failures occurring mainly within the adhesive.

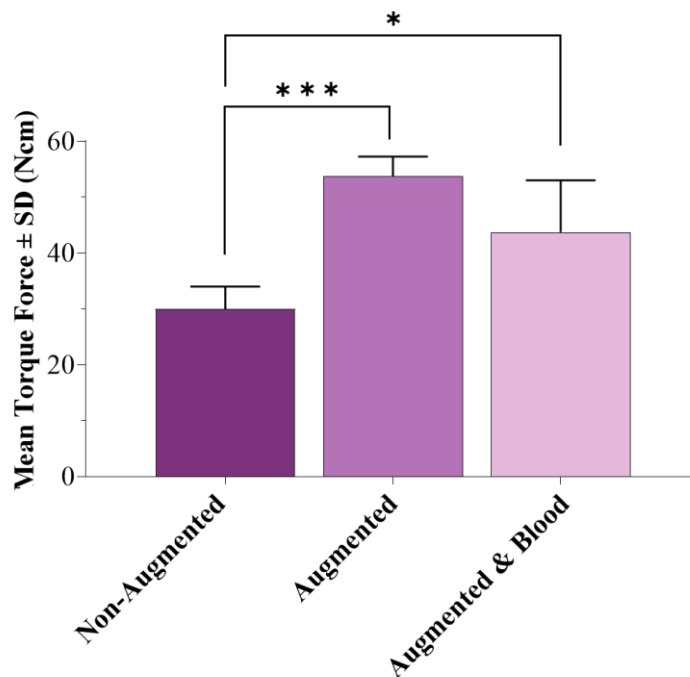


Figure 3.8: Torque Removal Forces of Dental Implants – An increase in torque force was observed after implant augmentation with PM-CPC bone adhesive with and without blood compared to the non-augmented group. Statistical significance is denoted by *p-value < 0.05 and ***p-value < 0.001, (n=6).

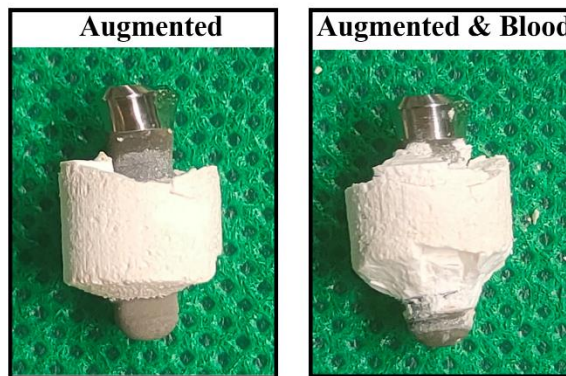
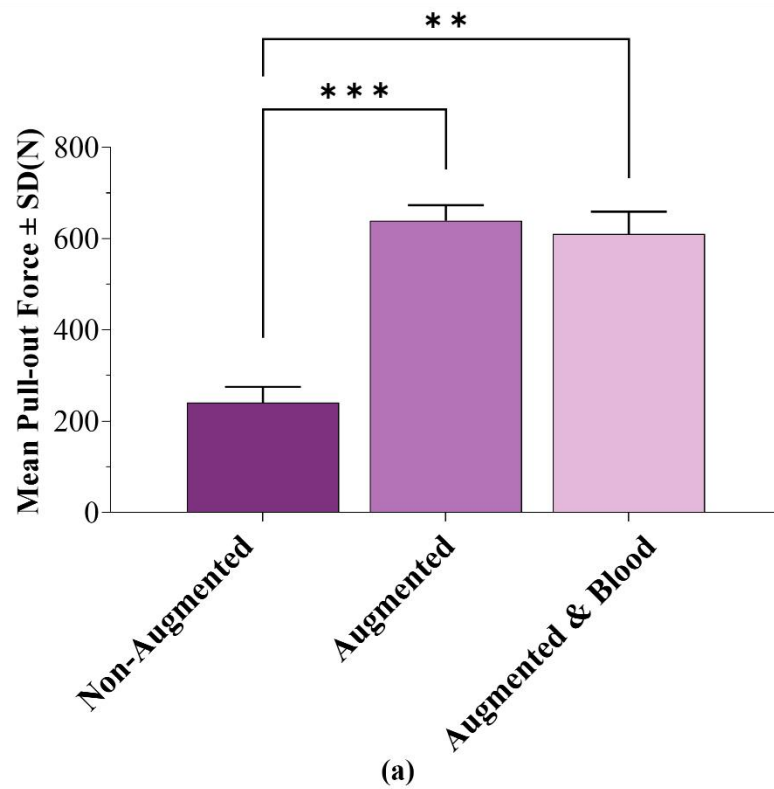


Figure 3.9: Pull-out Forces of Dental Implants – (a) Pull-out forces of dental implants before and after augmentation with and without PM-CPC bone adhesive and blood. Images revealing the (b) cohesive failure mode after the test. Statistical significance is denoted by **p-value < 0.01 and ***p-value < 0.001, indicating an increase in pull-out forces observed after implant augmentation with and without blood compared to non-augmented. (n=6).

3.5.6. Adhesion Strength on Orthopaedic Screws

The pull-out testing results for both the Osteopenia and Cortex bone screws, conducted on a synthetic bone, demonstrated a significant force difference between the non-augmented and PM-CPC-augmented configurations. Specifically, the non-augmented Osteopenia screw obtained a pull-out force of 65.8 ± 9.5 N, whereas the PM-CPC-augmented group showed a significant (p -value <0.001) force increase, reaching 343.4 ± 22.4 N (Figure 3.10a). Similarly, the results from the pull-out testing of the non-augmented Cortex screw were found to be 46.7 ± 7.3 N, while the augmentation of the screw with the PM-CPC adhesive yielded a significantly increased force of 299.8 ± 14.0 N (Figure 3.10a). A significant ($p<0.001$) five-fold increase in pull-out forces was observed when contrasting the non-augmented arrangement with the PM-CPC-augmented configuration for both screw types. These findings demonstrate the impact of the PM-CPC adhesive on the pull-out forces for both cancellous and cortical bone screws, thus underscoring its potential to enhance the stability and efficacy of these screws across varying bone types.

After pull-out testing, it was observed that the non-augmented screws were stripped out of the foam (Sawbone) without any traces of foam remaining adhered to the screw, while the augmented screws demonstrated cohesion failure since traces of foam were observed on the adhesive around the screw. The samples failed at the bone-adhesive interface, leading to the removal of the adhesive as a single mass with no remaining adhesive within the defect (Figure 3.10b). PM-CPC was evenly distributed along the length of the screw threads and along the inner surfaces of the defect. The PM-CPC was mainly contained within the threads indicating that there was a strong bonding between the adhesive and screw.

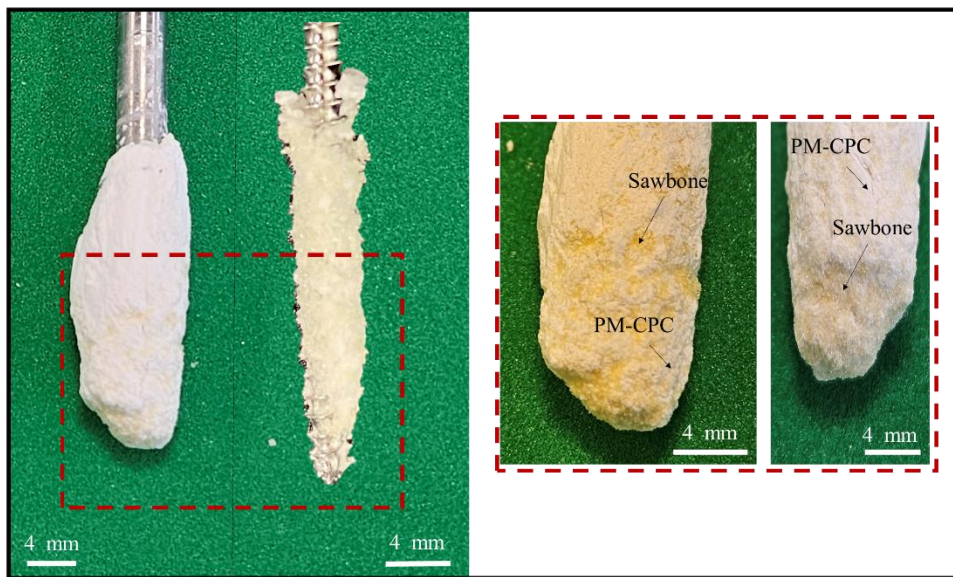
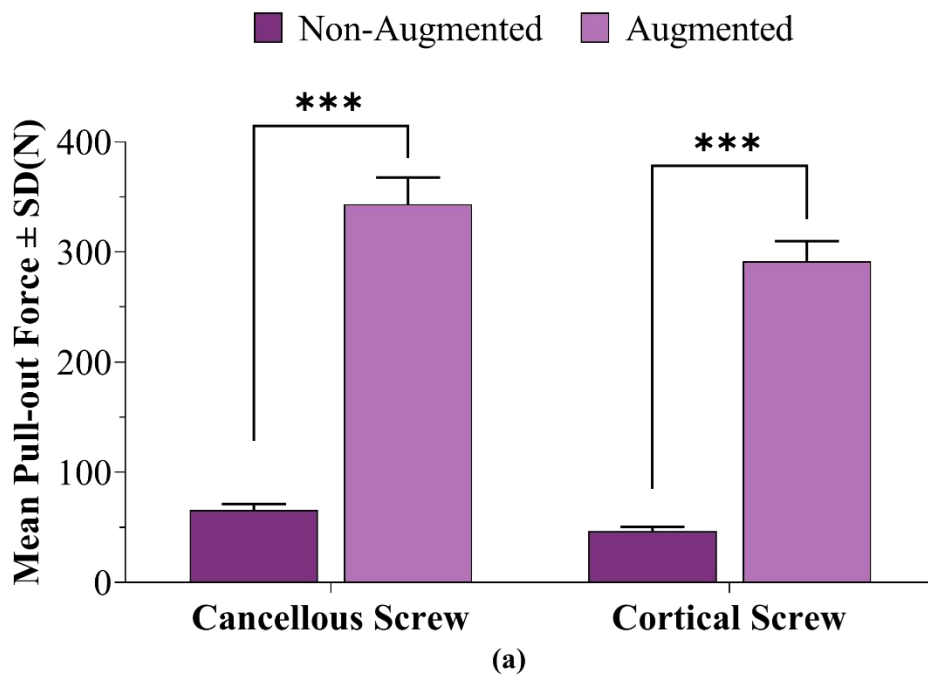


Figure 3.10: Pull-out Forces of Orthopaedics Implants – (a) Graph presenting the pull-out forces and (b) images revealing the bone-adhesive interface failure mode observed in orthopaedic screws before and after augmentation with PM-CPC bone adhesive. Statistical significance is denoted by ***p-value < 0.001, indicating the increase in pull-out forces (n=6).

3.5.7. Bone-to-Bone Adhesion using PM-CPC

The adhesive strength of the optimal PM-CPC adhesive was evaluated using cancellous and cortical bone samples. Two different bond tests, tensile and lap shear testing, were conducted in wet environments. Results showed that the optimal PM-CPC demonstrated lap shear strength at 0.95 ± 0.28 MPa and tensile strength at 0.64 ± 0.14 MPa (p -value <0.001) for cancellous bone samples (Figure 3.11a). Similar trends were observed for the cortical bone samples, where lap shear and tensile strength values of 0.80 ± 0.15 MPa and 0.50 ± 0.10 MPa, respectively were recorded. Bone specimens bonded with PM-CPC and tested under wet conditions demonstrated strong resistance to shear and tensile forces. They were able to withstand forces of 100 N prior to exhibiting signs of failure. Additionally, the adhesive strength displayed by both the cortical and cancellous bone specimens was higher to that of traditional tissue adhesives like Histoacryl, Palacos LV, and BSA-Glue [251] (p -value <0.05) (Figure 3.11a). Testing using a lap shear joint configuration produced higher forces at failure compared to testing using a tensile joint arrangement due to the increased exposure of osteons resulting from the cross-sectional cut, potentially enhancing micro-mechanical bonding, and consequently the adhesive strength [252].

To examine the failure mode of the optimal PM-CPC, SEM analysis was conducted on the surfaces of cortical and cancellous bone specimens following failure. The results showed a mixed-mode failure in both lap shear and tensile testing of cancellous and cortical bone specimens. PM-CPC was present on approximately 50% of the fractured surfaces of the cortical bone after analysing three fracture sites, indicating that cohesive failure occurred in these regions (covering an average area of 50 mm^2 out of 100 mm^2) and adhesive failure occurred in the remaining regions (representative Figure 3.11b). After the tensile and lap testing of cancellous bone samples, fully adhesive-mode failure and mixed-mode failure,

comprising of cohesive-mode failure (average area=82.6 mm²) and adhesive-mode (average area=17.4 mm²), was observed as can be seen in the representative Figure 3.11c.

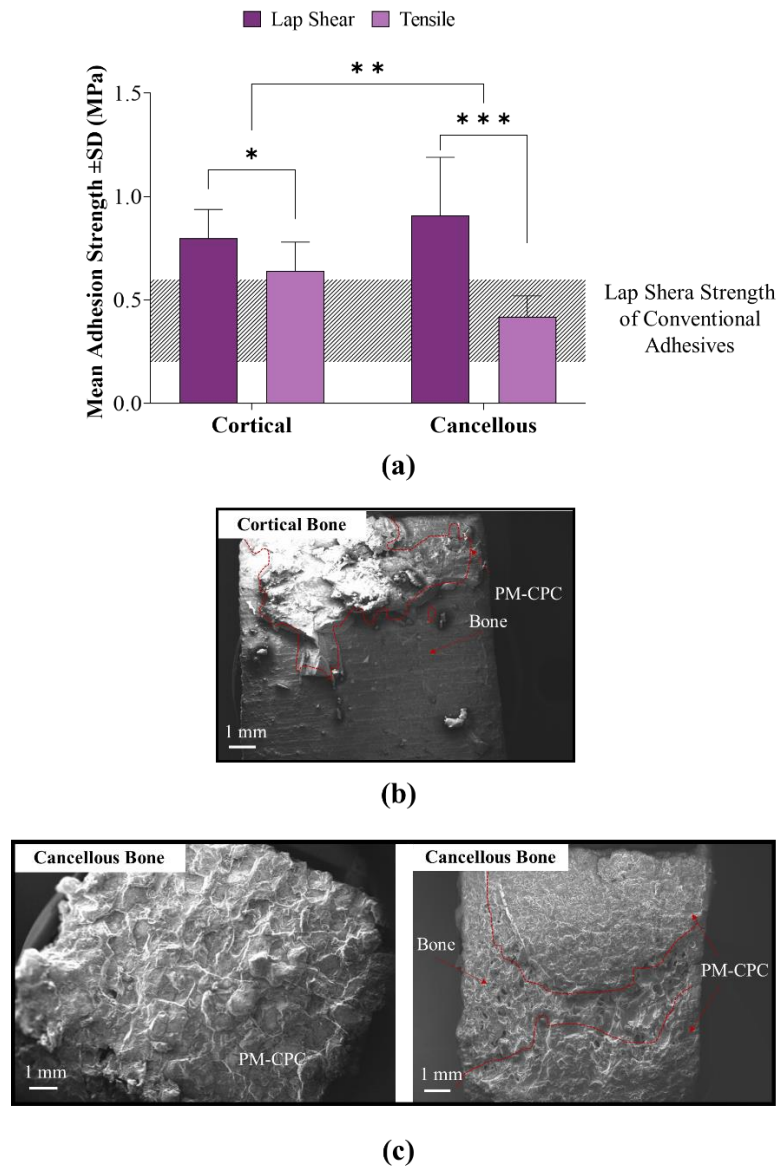


Figure 3.11: Bone-to-Bone Adhesion Properties – (a) Lap shear and tensile strength (n=6) shows the ability of optimal PM-CPC to adhere both cortical and cancellous bones withstanding a force of approx. 100 N at 37°C in a wet-field environment significantly higher than conventional adhesives (Histoacryl, Palacos LV, and BSA-Glue). SEM images (n=3) illustrating representative images of mixed-mode failure mode at the fracture surfaces of (b) cortical and (c) cancellous bone after failure. *p-value < 0.05, **p-value < 0.01 and ***p-value < 0.001.

3.6. Discussion

This chapter focuses on the comprehensive evaluation of the optimal PM-CPC composition for its suitability as a bone adhesive in both orthopaedic and dental applications. The assessment includes the PM-CPC's handling and mechanical properties, particularly its ability to retain these characteristics when produced in larger batches. The aim was to ensure that the material's efficacy, observed in controlled laboratory conditions, could be translated to practical, large-scale applications without compromising its desirable properties. Furthermore, properties, which are crucial for potential use in clinical settings were evaluated such as the adhesive's performance under wet conditions, the stability, and the consistency of the degradation properties.

In terms of PM-CPC's performance, the main observation was the consistency in achieving a homogenous adhesive within a short span of 20 s, irrespective of the batch size. This not only implies a consistent mixability but also suggests that the PM-CPC adhesive maintains its inherent characteristics even when the volume is scaled up. The optimal PM-CPC composition after increasing the batch size demonstrated average initial and final setting times of 2.5 min to 3.5 min, respectively, without any significant difference. The fast setting indicates accelerated HA nucleation in the presence of phosphoserine, providing working and setting times within an acceptable range for surgeons to apply and stabilise bone fractures, thereby, eliminating batch size as a variable affecting the setting phase [119,253]. The average compressive and adhesive strength values remained unaffected despite changes in the batch size further emphasising its reliability. The ability of PM-CPC to maintain its qualitative and quantitative properties irrespective of batch size enhances its potential to be produced in industry-relevant volumes.

The optimal PM-CPC demonstrated the ability to remain stable after mixing and before setting in a wet-field environment. The absence of disintegration in the adhesive suggests its

ability to effectively bond to the bone surface and withstand external stresses. This characteristic is crucial for ensuring long-term durability and reliability in clinical applications. The optimal PM-CPC also demonstrated suitable degradation properties, with ~25% degradation observed by week 2. The degradation results were consistent with previous studies of CPC [254,255], showing slow degradation rates under physiological conditions. For instance, Ruhe *et al.* [256] fabricated calcium phosphate cements enhanced with PLGA that had degradation of 30-40% after 12 weeks, with only 10-20% degradation during the initial 6 weeks. The overall slow rate of degradation aligns with the normal rate of bone healing and new bone formation showing the potential of the adhesive to provide initial bone fragments stability [63]. Furthermore, the presence of an interfacial apatite layer on the PM-CPC surface, formed after immersion in SBF for seven days, confirms its bioactivity and suitability for biomedical applications. The formation of a chemically similar HA layer on the surface of the PM-CPC and the presence of characteristic needle-shaped and platelet crystals validates its potential for promoting osseointegration and bone regeneration. The formation of an interfacial apatite layer at the bone-biomaterials interface is a common characteristic of bioactive materials [257]. In addition to the HA crystal formation PM-CPC adhesive after 7 days exhibited Ca/P and Ca/O molar ratios of 1.60 and 0.44 respectively approaching the typical values of HA (Ca/P = 1.67, Ca/O = 0.55). Overall, the slow degradation rate means that the PM-CPC can provide effective support and stability to bone fragments during the initial stages of the natural bone healing process [258,259].

The pull-out and removal torque testing conducted on both augmented and non-augmented dental and orthopaedic implants aimed to assess the effect of PM-CPC as an adhesive enhancer. The analysis of the results indicates that PM-CPC effectively enhances the bonding strength of implants, facilitating better adhesion. These results are in line with existing literature, which used tetracalcium phosphate and Tetranite Stabilisation-Material

(LaunchPad Medical) respectively [213,214]. Both studies have shown that the use of PM-CPC effectively enhances mechanical properties and stability. However, the force obtained using the PM-CPC adhesive was found to be approximately twice the torque force obtained from Tetranite, with an average torque force of 45 Ncm compared to 22.2 Ncm. Additionally, *in vivo* investigations have further substantiated the method's efficacy, highlighting that implants positioned in oversized osteotomies can be securely stabilised during placement through the application of a highly osteoconductive, and resorbable adhesive [248]. Furthermore, the presence of blood during the implant procedure had no impact on the adhesive properties of PM-CPC, indicating that its effectiveness was not significantly compromised by the existence of blood. These findings highlight the potential clinical significance of PM-CPC as an adhesive enhancer for both dental implants and orthopaedic screws, particularly in augmented cases. The results demonstrated that the application of PM-CPC in implant surgeries can contribute to improved implant stability and success rates.

The observation of failure modes following the pull-out testing provides valuable information about the effectiveness of PM-CPC at enhancing the adhesion to metallic-based implants. The adhesive failure observed demonstrates a strong bond between the implant and adhesive. This type of failure thus highlights the importance of achieving a robust and continuous interface between the adhesive and the bone surface. Failure at the interface could be attributed to various factors, such as inadequate surface preparation, poor penetration of the adhesive into the bone's micro-structure, or potential contamination during the implantation process.

In addition to the optimal handling and mechanical properties, the PM-CPC provided effective bone-to-bone bonding when used to adhere cancellous and cortical bovine femoral bone. The setting condition (dry or wet) significantly influenced the bond strength, with the optimal PM-CPC adhesive exhibiting a higher bond strength in dry environments compared

to wet environments for both cancellous and cortical bone samples. This finding is consistent with previous studies reporting the adverse effects of moisture on the bonding properties of various biomaterials, including dental adhesives and bone cements [260]. Lower bond strength values under wet-field conditions can be attributed to the presence of moisture, which interferes with the PM-CPC-bone interface and induces hydrolytic degradation of the adhesive. Despite lower bond strength values under wet-field conditions, all femora bone samples withstood forces > 50 N before fracture, with a maximum load of 100 N recorded. This provides significantly higher adhesion compared to other available adhesives, which demonstrated an average force of 47 N and a max load of 55 N [261]. The mixed-mode failure observed in the lap shear and tensile testing of cancellous and cortical bone samples indicates the presence of both molecular and physical bonds at the PM-CPC-bone interface [251,261]. The cohesive failure obtained leads to 100% adhesion between the adhesive and substrate, improving mechanical stability and reducing stress concentrations within the PM-CPC adhesive. This cohesive failure observed during SEM analysis of the fracture surfaces indicates the formation of strong bonding between the PM-CPC and the substrate of the bone specimen, a desirable property for clinical applications. The adhesive provided early mechanical stability, tuning of the resorption time to the rate of new bone substitution promoted by the material [247] and exhibit optimal adhesive and cohesive properties in wet-field conditions.

3.7. Conclusions

Overall, the optimal composition of PM-CPC demonstrated clinically relevant handling properties, allowing for homogenous mixing and precise delivery. Notably, PM-CPC demonstrated a high bone-to-bone and implant adhesive bond strength under wet-field conditions displaying its potential for effective bonding in challenging clinical scenarios in both orthopaedic and dental application. Furthermore, PM-CPC exhibited a slow degradation

rate during the initial five days, which could provide initial stability to bone fragments during the critical early stages of the natural bone healing process.

In conclusion, the optimal composition of PM-CPC shows promise in meeting the clinical requirements for a calcified tissue adhesive used in bone and implant stabilisation and repair. However, a significant challenge lies in the current requirement for manual mixing of the powder and liquid phases before injection, coupled with limited setting time. While premixed injectable CPCs have been developed, they still have limitations related to thorough powder-liquid mixing and precise injection timing as well as phase separation. So, there is still a need for the development of an adhesive designed to be mixed on demand and delivered minimally invasively.

**Chapter 4: Development of an Injectable
Phosphoserine-modified Calcium
Phosphate (PM-CPC) and a Minimally
Invasive Delivery Device**

4.1. Introduction

Despite promising properties offered by CPCs, there are still challenges relating to their application [262–264]. In particular, the in-theatre powder to liquid mixing of CPCs within a surgical environment has been shown to lead to variations in adhesive properties and poor injectability restricting their applicability [178,265,266]. CPC must meet specific handling requirements to enable effective mixing and delivery for minimally invasive procedures such as spinal applications, vertebroplasty, bone void filling in closed fractures, and osteoporotic bone reinforcement [267]. One critical issue is the continuous change in material properties during the working phase which leaves a limited window for preparation and application. There is a growing need to develop injectable, ready-to-use CPCs to address these limitations. Consequently, numerous studies have been conducted to enhance the minimally invasive delivery of CPCs and thus expand their clinical applications [249,268,269].

For traditional formulations of CPCs, phase separation during injection has been a significant obstacle, as it can result in a higher-than-desired liquid content, potentially leading to leakage from the surgical site and compromising the final properties of the set CPC [262,270,271]. New formulations that aim to overcome these challenges have been explored. For example, aqueous injectable CPCs have been developed, but these face challenges related to thorough powder-liquid mixing and the requirement for precisely controlled timing of injection to the surgical site [272]. Premixed injectable CPCs have also been explored, but issues such as phase separation and the inability to regain the original consistency upon stimulus removal have posed challenges [273]. Furthermore, previous injectable CPCs had poor mechanical properties [249,274].

Furthermore, new delivery systems for the minimally invasive delivery of CPCs have also been explored. Prior investigations on cements for dental application have demonstrated the benefits associated with the minimally invasive administration of a biphasic calcium

phosphate adhesive, facilitated through the use a dual-phase syringe system [211,262,275]. Therefore, it is envisaged that transitioning from the current manual mixing approach to a mechanised on-demand mixing technique will enable the precise and minimally invasive application of the PM-CPC developed herein.

To address the drawbacks of the existing PM-CPCs and contribute to the field's advancement, there is a need to develop premixed PM-CPCs that can be prepared in advance under controlled conditions and remain stable in storage and within syringes. This approach offers advantages such as reduced processing time, lower risk of contamination, enhanced reproducibility, and immediate injection of the mixture into the host tissue defect. Previous studies achieved stability of CPC when mixed with non-aqueous solutions such as poly(propylene glycol), glycerol, chitosan malate, etc. [181,249,276]. However, this formulation had a relatively long setting time due to the poor mixing between the powder and liquid phases, when exposed to a physiological solution, which could be clinically problematic. Therefore, there is need to develop an approach that will provide an improved and rapid-setting, mixing time and adequate homogeneity.

This study proposed using a dual (paste-paste) syringe-mixed PM-CPC adhesive. This adhesive with the new mixing technique should provide rapid setting, adhesion and sufficient mechanical strength immediately after placement in a defect site. This approach aims to address the limitations of current systems associated with setting time, moisture effects during storage, and the material shelf life, ultimately offering an adhesive that will enhance the clinical use of CPC in bone defect treatments.

4.2. Chapter Aim

The overall aim of this chapter was to adapt the optimal PM-CPC adhesive composition from Chapter 3 to achieve a two component adhesive that can be delivered minimally invasively

using a dual syringe system, without affecting the setting, mechanical, biological and adhesion properties of the final product. The chapter focuses on the development of a new dual syringe-mixed PM-CPC adhesive and assessment of the physical, handling, mechanical properties, and adhesion/cohesion strength under wet-field conditions—with the optimal properties benchmarked against industry defined values.

The specific objectives of this chapter were the:

- Synthesis and analytical assessment of a two-component PM-CPC adhesive designed for minimally invasive delivery using a dual syringe system.
- Systematic comparison of the dual syringe-mixed PM-CPC with the optimal hand-mixed PM-CPC bone adhesive to gain insights into the potential advantages and applicability of the new premixed formulation in bone adhesive applications.

4.3. Material and Methods

4.3.1. Formulation of Hand-Mixed PM-CPC Adhesive

The liquid phase 0.3 mL/g of DI water was added to the optimal powder phase (α -TCP, phosphoserine and calcium silicate) composition as defined in Chapter 2 and subsequently hand-mixed for 20 s as described in Section 3.3.1.

4.3.2. Formulation of Dual Syringe-Mixed PM-CPC Adhesive

Component 1 – Accelerator Paste:

The first component of the dual syringe-mixed PM-CPC adhesive formulation was the accelerator paste. This component consisted of two key powder phases: phosphoserine and calcium silicate. Phosphoserine was incorporated at a specific weight percentage, serving as a significant bioactive agent and accelerator, whereas calcium silicate provides desirable mechanical properties and biocompatibility. The two powders were manually mixed in a

predetermined weight percentages as per optimal PM-CPC adhesive composition (25 wt.% phosphoserine and 1 wt.% calcium silicate).

The powder phase of each component was mixed with biocompatible oil phase (Kolliphor EL) and its components are often used to increase the solubility of both hydrophilic and hydrophobic substances by reducing surface tension [277]. The Koliphor oil was prepared by combining two surface-active agents, Polyoxyl 35 castor oil (Kolliphor® EL, Merck Life Sciences Ltd, Ireland) and hexadecyl-phosphate (Merck Life Sciences Ltd, Ireland) (ratio of 0.3 wt./wt.) [276]. This property is particularly useful in ensuring that phosphoserine, which might otherwise have limited solubility, is evenly distributed throughout the cement mixture. The improved solubility and dispersion of phosphoserine can lead to better integration and performance of the cement, enhancing its adhesive properties and overall functionality as a bone adhesive.

The powder and oil phase were combined at different oil/powder weight ratios, ranging from 0.3 mL/g to 0.6 mL/g, enabling adjustments to achieve the desired consistency and workability of the paste. A mortar and pestle were used to mix and ensure uniform dispersion and homogeneous mixture of the powder and oil phase. The final homogenous paste was dispensed into 3 mL and 5 mL syringes, which were shielded with a female Luer lock caps. The filled syringes were then stored at room temperature, until further use.

Component 2 – α -TCP Paste:

The second component, the α -TCP paste, forms an integral part of the PM-CPC paste adhesive system. This paste was designed to provide the necessary mechanical properties and structural support to the adhesive composition. This paste contains a predominant powder phase consisting of α -TCP (74 wt.% of the total powder phase of PM-CPC adhesive). α -TCP powder and Koliphor oil were mixed, at different oil/powder weight ratios, ranging from 0.3

mL/g to 0.6 mL/g, to achieve the desired consistency and workability of the paste. Initial mixing was conducted using a stainless steel mixer (IKA-Labortechnik RW 20 digital overhead stirrer, Merck Life Sciences Ltd, Ireland) until homogenous. The mixed paste was then transferred into a 500 mL zirconia beaker and further mixed and homogenised with 8 zirconia balls of 100 g each in a planetary ball mill for 3 h at 300 RPM. The final homogenous paste was dispensed into 3 mL and 5 mL shielded syringes. The filled syringes were then stored at room temperature (22 °C) with a humidity of 45-50%, until further use.

Dual Syringe-mixed PM-CPC Adhesive:

The mixing of the two components (Component 1: accelerator and Component 2: α -TCP pastes) was achieved using a double syringe mixing system through a mixing nozzle (Figure 4.1).

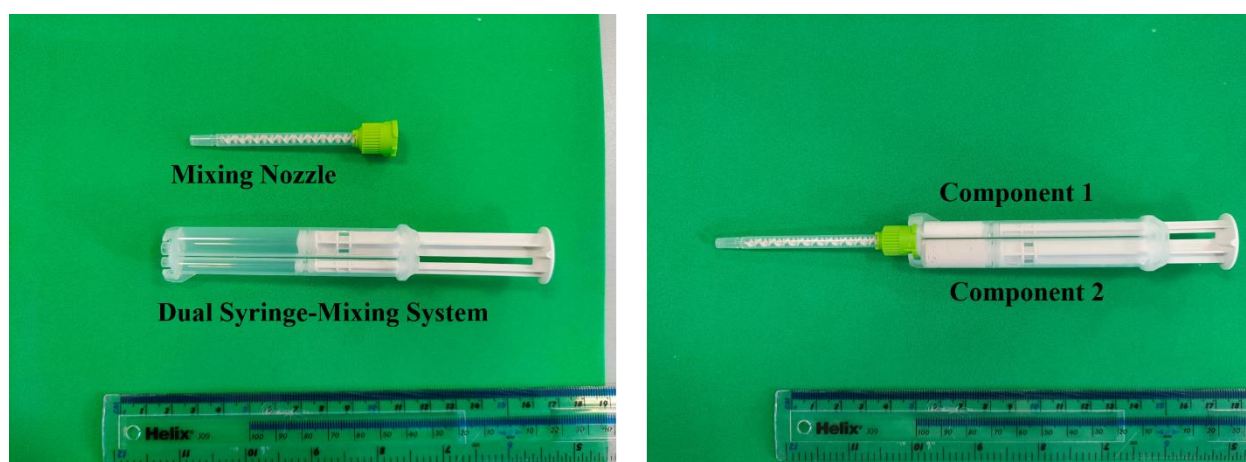


Figure 4.1: Double Syringe Mixing System used for the injectable and on-demand mixed PM-CPC adhesive.

4.3.3. Analytical Assessment of Individual Components

4.3.3.1 Phase Separation

To assess the influence of varying oil content on phase separation within the paste, an oil-to-powder phase separation test was conducted following centrifugation [276,278]. Paste

formulations were prepared by systematically adjusting the oil to powder ratio within the paste from 0.3 mL/g to 0.6 mL/g. 2 g of prepared paste samples were transferred to 15 mL tubes followed by centrifugation at 2400 RPM for 20 min. Following centrifugation, the centrifuge tubes were inverted and the volume of oil drops separating from the paste was determined. The percentage of phase separation was then quantified (Eq. 4.1). The paste was considered stable when no oil drops separated from the paste.

Equation 4.1 – Percentage of Phase Separation between oil and powder phase:

$$\text{Phase Separation (\%)} = \frac{\text{Separated Oil Phase Volume}}{\text{Initial Paste Volume}} \times 100$$

4.3.3.2 Injectability

Quantitative evaluation of injectability was carried out by determining the percentage of the paste delivered prior to solidification under set loading conditions [270,279,280]. The paste (volume of 5 ml) was transferred to a commercial syringe with an aperture of 2 mm (13 mm diameter cartridge with nominal capacity of 10 mL). Loading was applied vertically on the top of the plunger using the Zwick Universal Testing Machine fitted with a 500 N load cell. A crosshead speed rate of 10 mm/min was applied until the max force of 140 N was reached and the paste was no longer injectable. The samples tested were narrowed down based on the phase separation results for that reason the injectability test was conducted for the oil to powder phases of 0.3 mL/g to 0.4 mL/g. The force-displacement curves obtained from Zwick machine were generated and compared while the percentage of the paste delivered under these conditions was then quantified (Eq. 4.2).

Equation 4.2 –Injectability:

$$\text{Injectability (\%)} = \frac{\text{Wt. before test } (W_f) - \text{Wt. after the test } (W_a)}{\text{Wt. before test } (W_f) - \text{Wt. of empty syringe } (W_b)}$$

4.3.3.3 Paste Stability

The structural integrity and homogeneity of the optimal oil to powder phase paste (0.4 mL/g), as defined after testing the phase separation and injectability characteristics, was assessed by monitoring the viscosity at regular time intervals. The paste was transferred within a syringe and stored at room conditions (T=22 °C, humidity=45±5%) over a period of 48 Weeks. At different time points the paste samples were transferred to a 100 mL beaker and the viscosity was obtained using a viscometer (IKA ROTANISC hi-vi II, IKA-Werke GmbH & Co, Germany) at a rotation speed of 100 RPM at room temperature (22 °C). The spindle SP12 was used from the standard spindle set SP set-2 (IKA-Werke GmbH & Co, Germany).

4.3.4. Analytical assessment of dual syringe-mixed PM-CPC Adhesive

The comprehensive analysis of the two-component PM-CPC adhesive mixed using a double-syringe mixing system (Double Syringe, 5mL, 4:1, Medmix, Baar, Switzerland), with a mixing nozzle (Mixer, DN3,4:1, Medmix, Baar, Switzerland) was carried out to assess its performance across various aspects using the detailed methodologies presented in a Chapter 3. The evaluation included a thorough investigation of its handling and mechanical properties, washout resistance, degradation behaviour, and biological activity. A number of 6 specimens were used for each test. In addition, as per the analytical assessment of optimal PM-CPC adhesive, the ability of the dual syringe-mixed PM-CPC adhesive to enhance adhesion of dental and orthopaedic implants as well as facilitating bone-to-bone bonding. The double-syringe mixed PM-CPC adhesive was systematically compared with the optimal hand-mixed PM-CPC bone adhesive from Chapter 3.

4.4. Statistical Analysis

Each test was repeated a minimum of three and up to a maximum of six times. Where feasible, results were analysed for statistical significance. One-way or two-way analysis of variance (ANOVA) was conducted for the comparison of means, following confirmation of normality of data and homogeneity of variance. Where data from two independent samples were required to be tested for statistical significance a two-tailed t test was used. For all other dependents, regression analysis was used. A probability value of less than 0.05 was considered significant. All statistical analysis was performed using GraphPad (GraphPad_Prism Software, Version 8.0.2).

4.5. Results

4.5.1. Analytical Assessment of Individual Components

4.5.1.1 Phase Separation

During the analysis, the mixing of individual Component 1 and 2 was carried out using varying oil/powder ratios, ranging from 0.3 mL/g to 0.6 mL/g. Smooth and uniform pastes were achieved for all ratios. However, the ratios were found to significantly impact ($p\text{-value}<0.05$) the paste consistency and mixing behaviour. Ratios exceeding 0.5 mL/g led to separation of the oil phase, which is clearly visible in Figure 4.2a. Specifically, a ratio of 0.5 mL/g resulted in low viscosity pastes, displaying 4.67% phase separation for Component 1 and 1.47% for Component 2 upon centrifugation (Figure 4.2b). Similarly, at a 0.6 mL/g ratio, phase separation reached 7.5% for Component 1 and 2.5% for Component 2 (Figure 4.2b). Conversely, using oil phase ratios below 0.3 mL/g yielded granular materials, thereby rendering such ratios unfit for further analysis. Both Component 1 and 2 exhibited a complete absence of phase separation when maintained at 0.3 mL/g and 0.4 mL/g oil ratios, demonstrating 0% phase separation under these conditions.

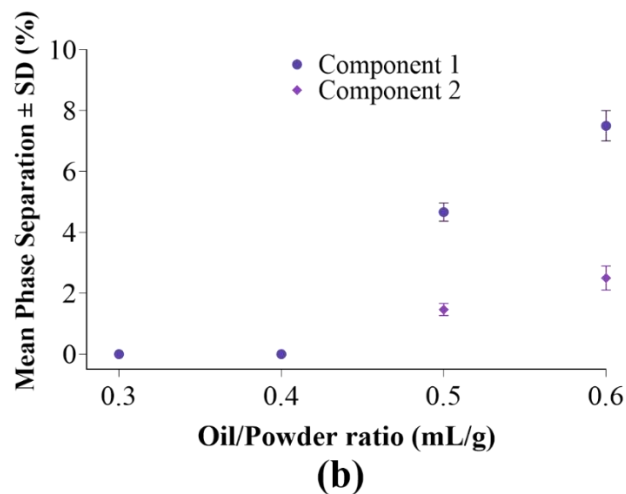
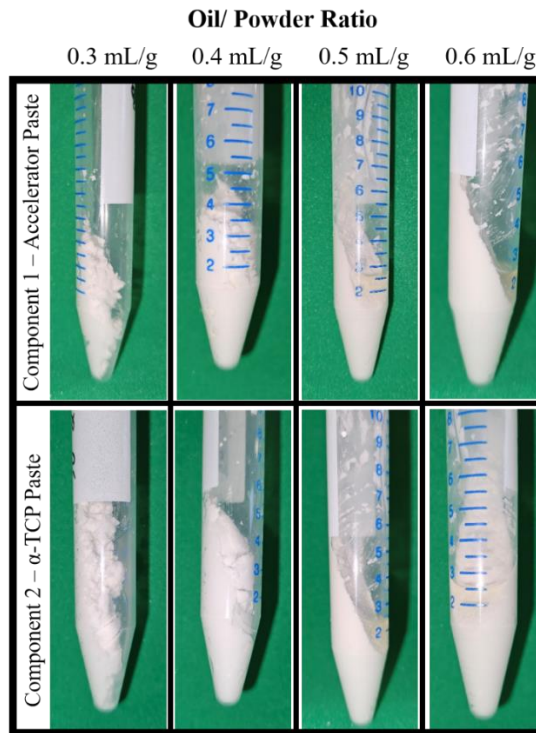


Figure 4.2: Phase Separation of Individual components – (a) Visual representation of oil separation observed in Component 1 and 2 pastes with varying oil/powder ratios ranging from 0.3 mL/g to 0.6 mL/g. (b) Graphical illustration of the relationship between the applied ratios and the extent of phase separation observed in the paste formulations (n=3).

4.5.1.2 Injectability

Due to the phase separation at ratios ≥ 0.5 mL/g, the mixing of individual components was carried out using ratios ranging from 0.3 mL/g to 0.4 mL/g. The force-displacement graph

shows the extrusion characteristics of the material exhibiting an initial escalation in force—representing the yield stress required to instigate paste flow—progressing into a stable plateau phase indicative of consistent material flow, concluding with a rapid increase in force when the material has finished coming out.

In Component 1, the extrusion force showed an initial steady state, or a slight elevation for both 0.35 mL/g and 0.4 mL/g compositions Figure 4.3a. Notably, a rapid increase in the extrusion force was observed for the 0.3 mL/g paste, possibly attributed to phase separation effects. Similarly, Component 2 exhibited analogous behaviour, with the 0.4 mL/g composition displaying the longest displacement/smooth plateau as can be seen in force-displacement graph Figure 4.3b. This prolonged displacement indicates enhanced injectability compared to the other two compositions. Comparing the maximum forces required for initial paste injection, of Component 1, as the oil/powder ratio varied from 0.3 mL/g to 0.4 mL/g led to a significant force reduction, dropping from 61.2 N to 22.2 N. Similarly, for Component 2, the maximum force dropped from 43.3 N to 15.9 N as the ratio increased from 0.3 mL/g to 0.4 mL/g. This trend indicates the influence of the oil/powder ratio on extrusion force, implying that higher ratios result in lowered forces necessary for initiating paste extrusion.

The percentage of injectability for both individual pastes was notably influenced by variations in the oil/powder ratio. The ratio of 0.35 mL/g significantly (p -value <0.01) improved the injectability percentage, with the accelerator paste reaching 63.9% and the α -TCP paste achieving 49.4%, as shown in Figure 4.3c. This represents an injectability that is roughly two to three times higher than what was observed with a 0.3 mL/g ratio. Which refers to approximately 2-3 times greater injectability compared to 0.3 mL/g ratio. With a further increase in the oil/powder ratio to 0.4 mL/g, the injectability of the adhesive reached an upper threshold, registering at about 71.2% for the accelerator paste and 67.6% for the α -TCP paste

Figure 4.3c. This pattern demonstrated that increasing the oil-to-powder ratio enhances the injectability, presenting as the ideal ratio the 0.4 mL/g for optimal performance.

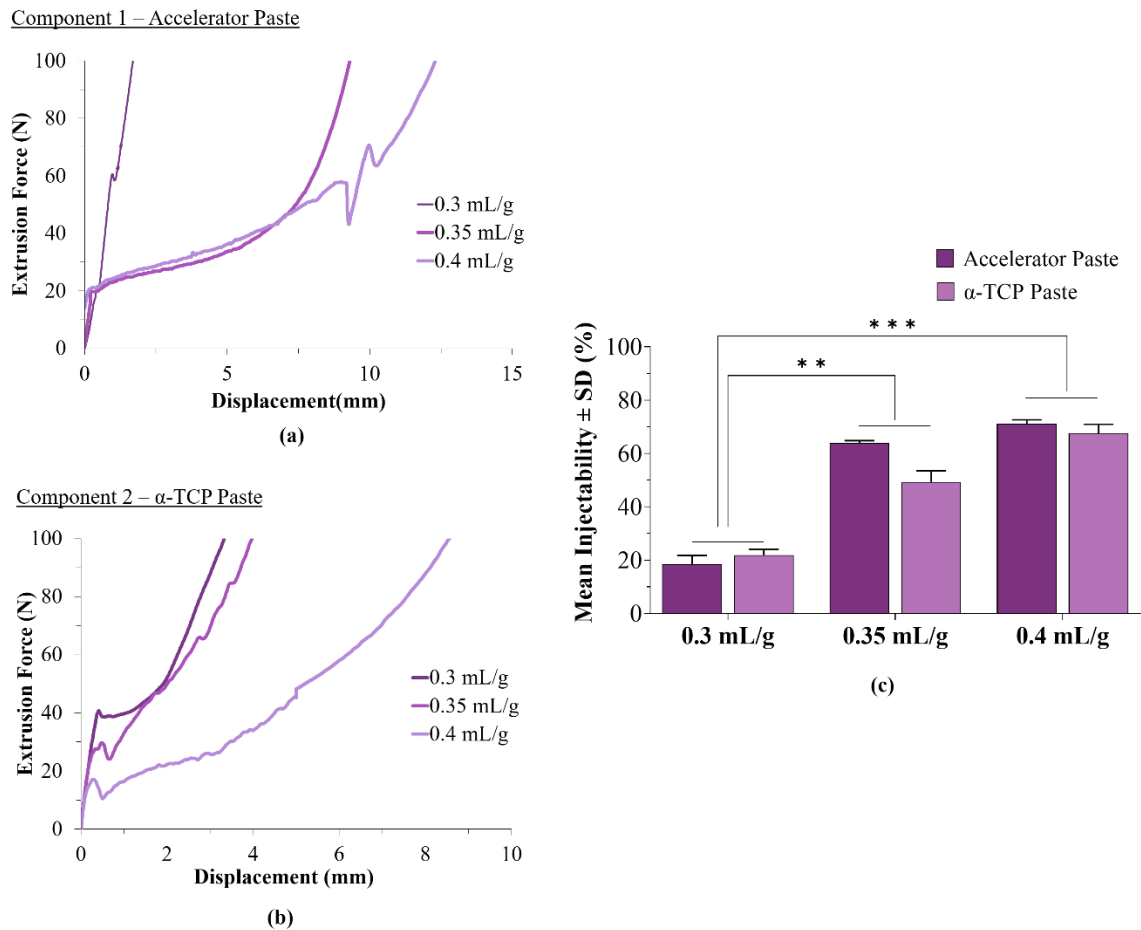
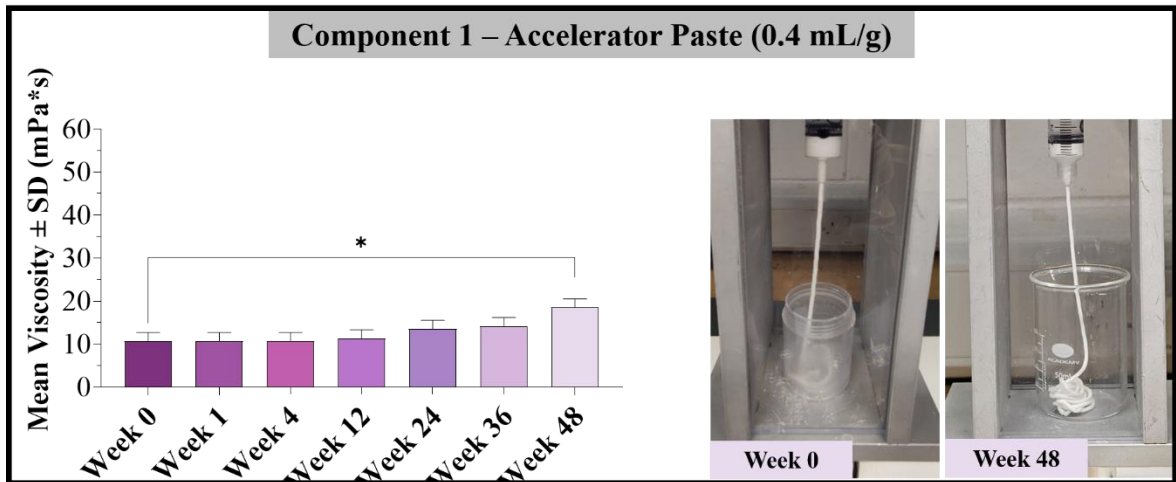


Figure 4.3: Injectability of Individual Pastes – Extrusion curves for (a) Component 1 and (b) Component 2 with different oil/powder ratios, (c) the percentage of injectability increasing the ratio from 0.3-0.4 mL/g. Statistical significance is denoted by **p-value < 0.01 and ***p-value < 0.001 (n=6).

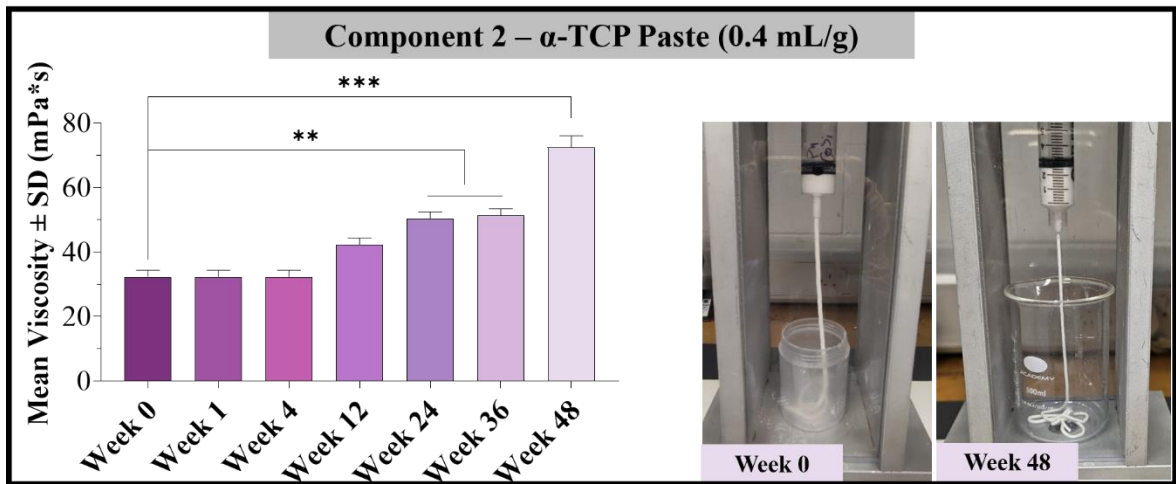
4.5.1.3 Paste Stability

A paste stability test was conducted to assess the injectability and viability (through viscosity) of the paste over an extended period, crucial for its applicability through a dual syringe system. The viscosity of the accelerator paste was initially determined on Day 1, referred to as Week 0, and was measured to be 10.7 mPa*s (Figure 4.4a), indicating a relatively low viscosity, which generally suggests good injectability. The viscosity remained consistent over the first 12 weeks of observation. Subsequent evaluations at Week 24 and Week 36 obtained a slight non-significant ($p\text{-value}>0.05$) increase in viscosity, with values of 13.6 mPa*s, indicating a sustained stability without significant alterations. However, a significant increase ($p\text{-value}<0.05$) was observed at Week 48, with a viscosity of 18.5 mPa*s, nearly twice the value recorded on Day 1. Despite the increase, the paste remained injectable, indicating its sustained usability even after an extended period of 48 weeks. In particular, the injectability forces was found to be stable during the first 12 weeks with force values of 70 ± 10 N. Slightly increase was observed at week 24 and week 36 with the force reaching 85 ± 8 N, however, the paste was still injectable with no significant ($p\text{-value}>0.05$) increase in extrusion forces.

For Day 1, the viscosity of α -TCP paste was measured at 32.35 mPa*s. This viscosity remained consistent for 4 weeks, with an increase of approximately 30% noted at Week 12. Following this, at Weeks 24 and 36, a significant increase ($p\text{-value}<0.01$) in viscosity was observed, with the value reaching 50.5 mPa*s. Similarly at Week 48, a statistically significant increase in viscosity was observed ($p\text{-value}<0.001$), reaching 72.5 mPa*s—twice the value of Day 1. Importantly, Figure 4.4b illustrates that despite this increase, the paste maintained its injectability, underlining its ongoing suitability for application even after an extensive 48-week period.



(a)



(b)

Figure 4.4: Variation of Viscosity over Time for the Optimal Components– Change of viscosity for (a) Component 1 and (b) Component 2 paste with oil/powder ratio of 0.4 mL/g over a 1-year duration (48 weeks) as well as the injectability of the pastes. Despite the observed variations in viscosity, the paste maintained its injectable characteristics. Statistical significance is denoted by *p value < 0.05, **p value < 0.01 and ***p-value < 0.001 (n=3).

4.5.2. Analytical Assessment of Dual Syringe-mixed PM-CPC Adhesive

4.5.2.1 Handling Properties

The initial and final setting times were determined for hand-mixed adhesive as $t_i = 2.01$ min and $t_f = 3.15$ min, respectively (Figure 4.5). While the setting times of the dual syringe-mixed PM-CPC adhesive were found to be significantly higher (p -value < 0.05) with a $t_i = 3.10$ min and $t_f = 3.80$ min. Despite this observation, both initial and final setting times remained within the clinical specifications ($t_i = 1.5$ min, $t_f = 4$ min, (Figure 4.5), ensuring the adhesive's suitability for practical usage. This finding underlines the dual syringe-mixed PM-CPC adhesive's ability to meet the essential criteria for setting time while offering the advantage of being conveniently mixed and delivered on site using the double syringe mixing system (Figure 4.5).

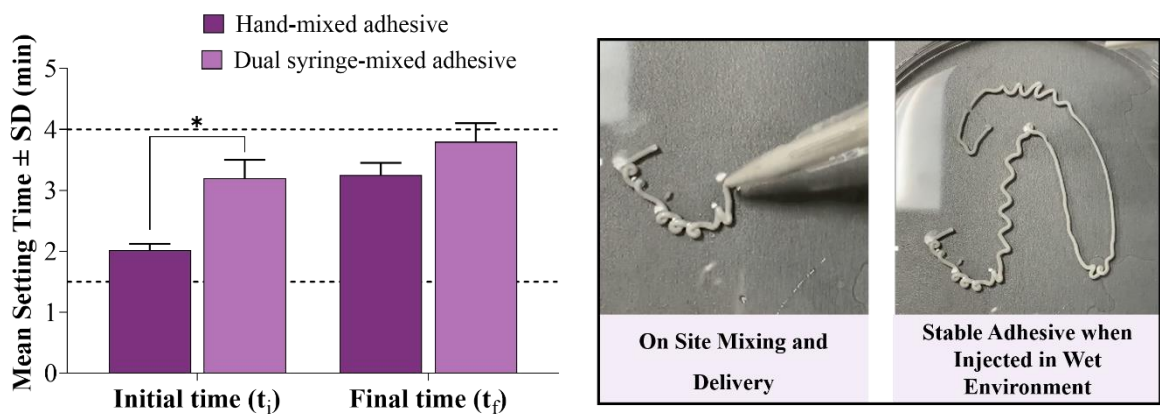


Figure 4.5: Handling Properties of the Dual Syringe-mixed and Hand-mixed PM-CPC Adhesive – Handling properties of the dual syringe-mixed PM-CPC adhesive in comparison with the hand-mixed PM-CPC adhesive. Statistical significance is denoted by * p -value < 0.05 ($n=6$).

4.5.2.2 Mechanical Properties

The mechanical properties of the adhesive as a consequence of different mixing techniques were determined. The compressive strength was found to be ~ 20 MPa for the dual syringe-mixed PM-CPC adhesive and ~ 25 MPa for the hand-mixed adhesive Figure 4.6a. The mean adhesive strength of the hand-mixed adhesive was determined to be 3.15 MPa while the dual syringe-mixed adhesive obtained a 2.95 MPa adhesive strength as can be seen in Figure 4.6b. When compared the two adhesives mixed using different techniques no significant difference ($p\text{-value}>0.05$) was observed with the mechanical properties meeting the clinical requirements (compressive strength >10 MPa and adhesive strength >2.5 MPa) for both.

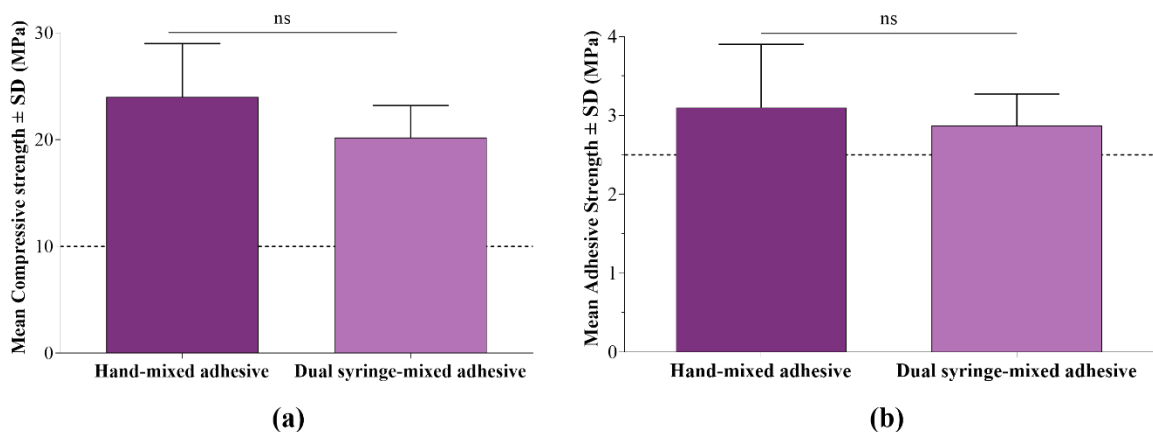


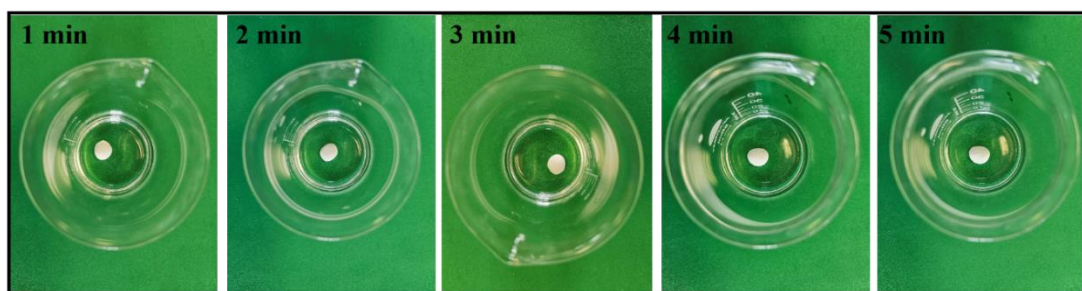
Figure 4.6: Mechanical Properties of the Adhesive as a Consequence of Different Mixing Techniques – (a) The compressive and (b) adhesive strengths of dual syringe-mixed PM-CPC adhesive in comparison with the hand-mixed PM-CPC adhesive.

4.5.2.3 Washout Resistance

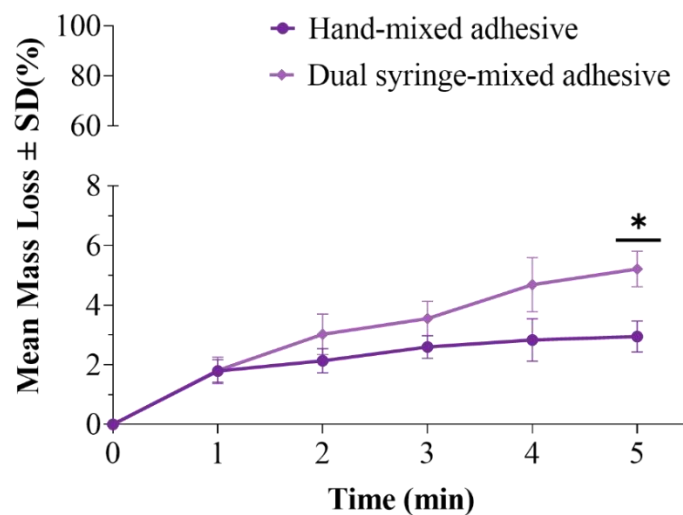
The qualitative assessment of the washout resistance of the dual syringe-mixed PM-CPC adhesive showed that it maintained its stability and integrity when applied in a wet environment. During the initial three-minute timepoint, the adhesive was seen to maintain its structural integrity within the PBS solution despite not being fully set. No observable signs

of dissolution were present after 5 min, indicating the adhesive's ability to set before encountering any visible disintegration (Figure 4.7a).

Through quantitative analysis, it was established that the dual syringe-mixed PM-CPC adhesive exhibited only a minimal mass loss of 5.2% after a 5 min immersion, signifying its limited degradation during its early stages (Figure 4.7b). The dual syringe-mixed PM-CPC adhesive when compared to the hand-mixed PM-CPC adhesive presented a similar promising trend displaying a significantly (p -value <0.01) lower mass loss of 2.95%.



(a)



(b)

Figure 4.7: Washout Resistance of the Dual Syringe-mixed and Hand-mixed PM-CPC Adhesive – (a) Qualitative and (b) quantitative assessment of the washout ability of the dual syringe-mixed and hand-mixed PM-CPC adhesive, showing no disintegration within the first 5 min. Statistical significance is denoted by * p -value < 0.05 ($n=3$).

4.5.2.4 *In vitro* Degradation

The assessment of the degradation behaviour of the dual syringe-mixed PM-CPC adhesive was carried out over a 120-day duration. The adhesive exhibited a cumulative mass loss of approximately 35% (Figure 4.8a). The initial five days were characterised by a relatively fast degradation phase, accounting for a mass loss of about 12%. Post this phase, a noticeable decrease in the degradation rate was observed, with the dual syringe-mixed PM-CPC adhesive obtaining an average daily mass loss of roughly 0.65% from Day 5 to Day 30. Beyond Day 30, the mass loss stabilised, displaying a statistically insignificant variance in the values until Day 120, maintaining an average daily mass loss of approximately 0.085%.

A comparison between the dual syringe-mixed and the hand-mixed PM-CPC adhesive in terms of degradation behaviour highlighted similar trends within the 120-day period. Despite variation in formulation techniques and composition, both adhesives showed comparable degradation behaviours. The initial phase of rapid degradation, followed by a phase of high mass loss and final stabilisation of the degradation rate, highlighted the similarities in the degradation dynamics of the two adhesive variants (Figure 4.8a). However, it is worth highlighting that the dual syringe-mixed adhesive exhibited a relatively higher degree of degradation within the 120-day period, with a total mass loss of 35%, in contrast to the hand-mixed adhesive, which displayed a total mass loss of 28%.

4.5.2.5 Biological Activity

The investigation into the biological activity of the dual syringe-mixed adhesive within a 7-day timeframe involved SEM analysis of the adhesives prepared using the different techniques. The micrographs showed the surface characteristics and crystal formations resulting from the interaction with simulated body fluid (SBF). After 24 h of SBF immersion, newly formed layer of needle-shaped HA crystals were evident the surface of the adhesive with lengths spanning from 8.26 μm to 16.56 μm and diameters averaging at $2.4 \pm 0.3 \mu\text{m}$

(Figure 4.8b). Upon extending the immersion period to 7 days, the dual syringe-mixed PM-CPC adhesive exhibited a more developed apatite structure, which consisted of medium-sized platelike HA crystals (Figure 4.8b). These crystals had dimensions of approximately $15.6\pm 0.7\ \mu\text{m}$ in length and $10.4\pm 0.4\ \mu\text{m}$ in thickness. Furthermore, the presence of larger-sized platelike HA crystals was observed with a length of $63.8\pm 0.5\ \mu\text{m}$ and thickness of $31.4\pm 0.6\ \mu\text{m}$.

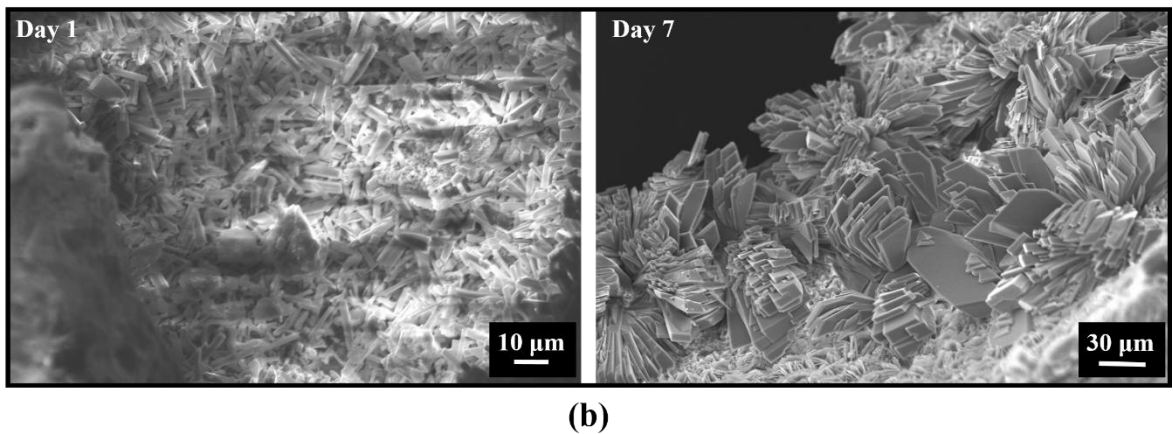
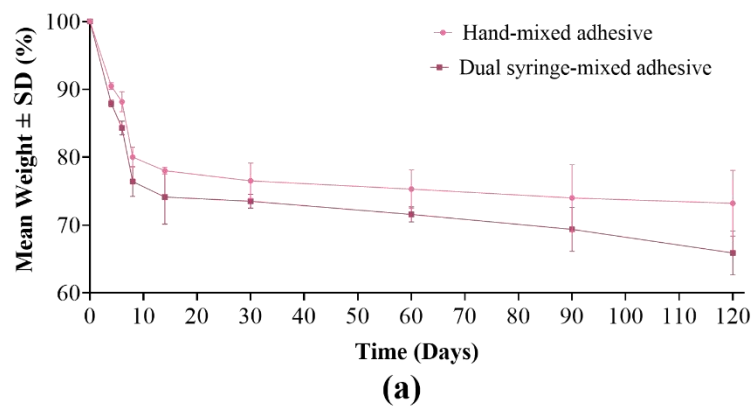


Figure 4.8: Degradation of the Dual Syringe-mixed and Hand-mixed PM-CPC Adhesive and Biological Activity of the Dual Syringe-mixed Adhesive – (a) Degradation analysis of the dual syringe-mixed PM-CPC adhesive immersed in PBS-PPL at 37°C, demonstrated a total mass loss of 28% respectively after 120 days, and (c) SEM images showing the bioactivity and conversion of the α -TCP to platelike HA crystals after 7 days.

4.5.2.6 Adhesion Strength on Orthopaedic Screws

Pull-out testing results for both the cancellous and cortical screws presented significant (p -value <0.001) differences in forces between the non-augmented and augmented screws. For the non-augmented cancellous screw, the pull-out force registered at 65.7 ± 3.2 N. However, with the incorporation of the dual syringe-mixed adhesive before screw insertion, a significant increase (p -value <0.001) was observed, elevating the pull-out force to 330.4 ± 25.5 N, which was slightly below the force of 343.4 ± 25.8 N achieved with the augmented screw using the hand-mixed adhesive (Figure 4.9). Similarly, in the case of the non-augmented cortex screw, the pull-out force was recorded as 46.7 ± 2.5 N. Upon augmentation with the dual syringe-mixed adhesive, a substantial and statistically significant (p -value <0.001) force enhancement was obtained, resulting in a force of 275 ± 13.7 N (Figure 4.9). A fivefold increase in pull-out forces was noted when comparing the non-augmented configurations to both augmentation methods with either dual syringe-mixed PM-CPC adhesive or hand-mixed adhesive PM-CPC for both screw types.

4.5.2.7 Bone-to-Bone Adhesion

The investigation of bone-to-bone adhesion using the dual syringe-mixed PM-CPC adhesive led to significantly (p -value >0.05) high strength (Figure 4.10). In wet conditions, cancellous bones adhered with the dual syringe-mixed PM-CPC adhesive exhibited a lap shear strength of 0.98 ± 0.21 MPa, a value comparable to the strength achieved by bone samples adhered with the hand-mixed PM-CPC adhesive. Similar trends were evident in the case of cortical bone samples, where wet conditions yielded a lap shear strength of 0.68 ± 0.11 MPa. Although the adhesion values for the dual syringe-mixed PM-CPC adhesive used in augmentation were lower compared to the hand-mixed version, the consistency of the dual syringe-mixed adhesive was higher. This was indicated by lower standard deviations in its measurements. A lower standard deviation implies that the adhesion values were closer to the mean, suggesting

a more reliable and predictable performance of the dual syringe-mixed adhesive in clinical applications. These outcomes indicate the ability of the dual syringe-mixed PM-CPC adhesive to establish robust bone-to-bone adhesion strength.

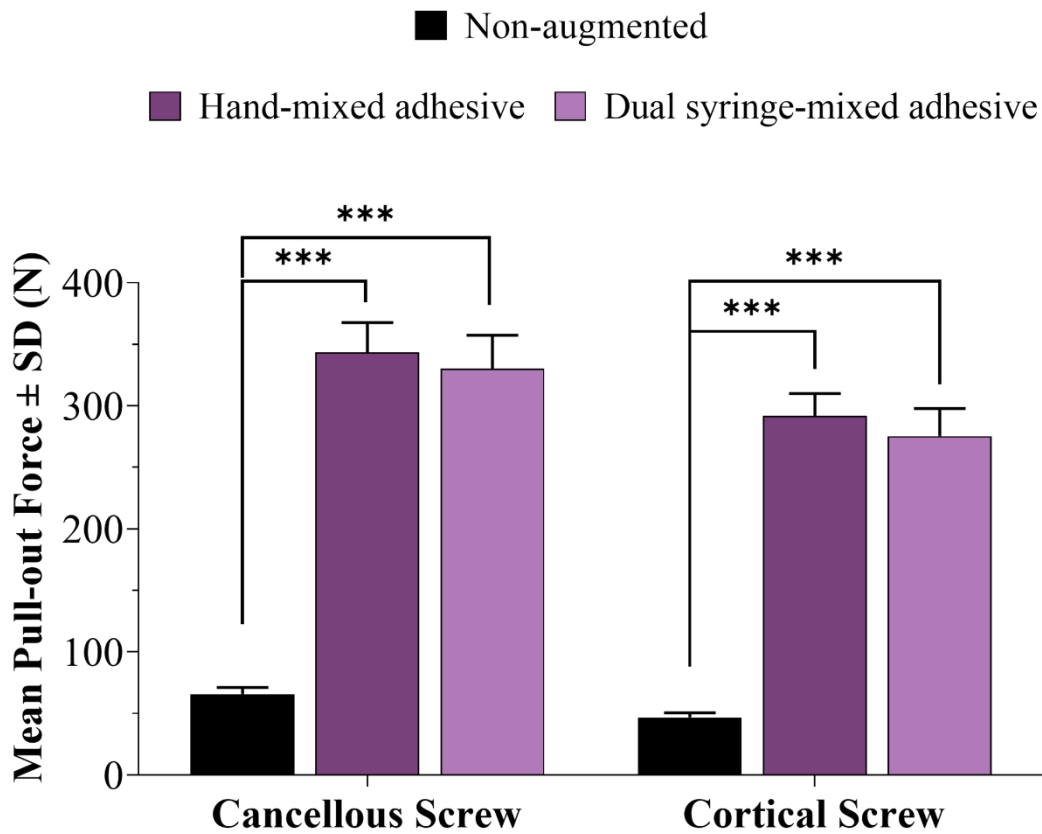


Figure 4.9: Maximum Pull-out Forces of Augmented Orthopaedics Screws – Graph presenting the pull-out forces in orthopaedic screws before and after augmentation with dual syringe-mixed and hand-mixed PM-CPC adhesive. Statistical significance is denoted by ***p-value < 0.001, indicating the increase in pull-out forces (n=6).

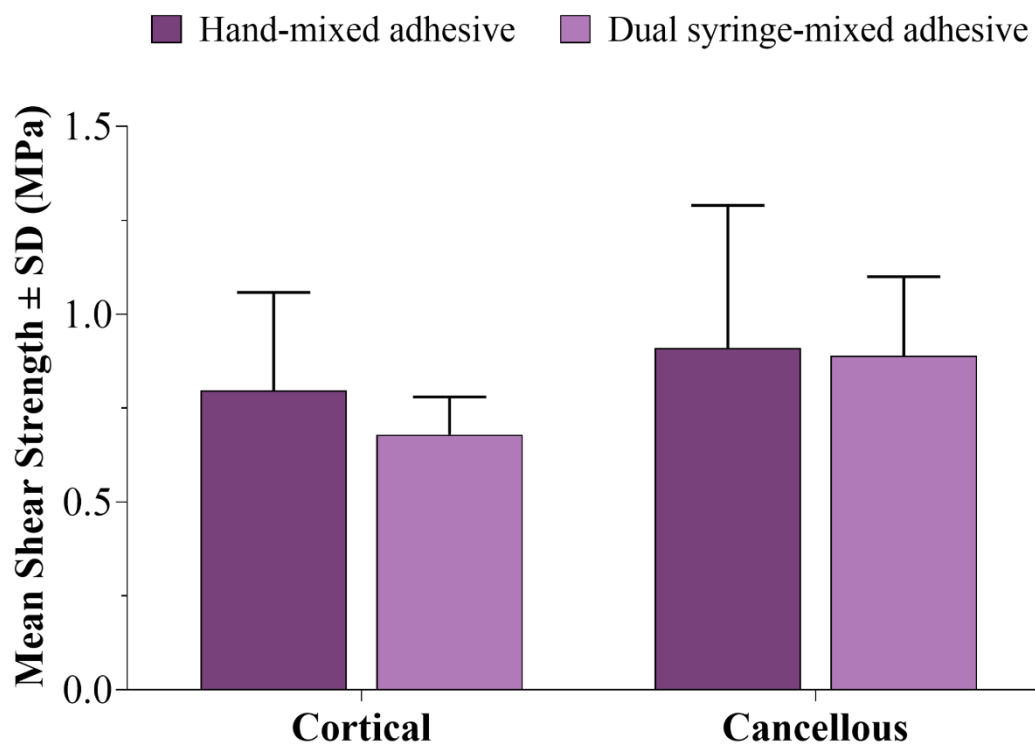


Figure 4.10: Bone to Bone Adhesion Properties – Lap shear strength shows the ability of dual syringe-mixed and hand-mixed adhesive to adhere both cortical and cancellous bones withstanding a force of ~100 N at 37°C in a wet-field environment. Statistical significance is denoted by *p value < 0.051, indicating the increase in lap shear strength (n=6).

4.6. Discussion

In this Chapter, the optimal PM-CPC adhesive composition was used for the development of a dual syringe-mixed adhesive with the aim of successful injectability without affecting the setting, mechanical, biological and adhesion properties of the final product.

Initially, ratios above 0.5 mL/g, decreased the structural integrity of the mixture, leading to separation in oil and powder phases in phase separation tests. The investigation of the effect of varying oil/powder ratios on Component 1 and Component 2 led to the determination of key characteristics and behaviours critical to their eventual application as injectable on-demand mixed adhesive. The decreased extrusion forces required for both components as the ratio approached 0.4 mL/g indicates a determining effect of ratio on ease of application. This trend not only indicates reduced mechanical limitations, but also highlights the potential for a smoother, less disruptive delivery mechanism, which is fundamental to clinical settings [281–283]. Whereas the separation of powder granules was seen below 0.3 mL/g. In particular, separation in the needle was observed during injectability since the added force caused the liquid phase to flow along the needle quicker than the solid [280,284].

Following this analytical assessment of each component and their behaviour at different powder/oil ratios, the optimal ratio was determined to be 0.4 mL/g for both paste components. This formulation achieved uniformity in consistency and stability, preventing phase separation, while ensuring smooth extrusion. The viscosity analysis of this optimal components over an extended period showed a time-dependent increase in viscosity [285]. The observed increase in viscosity over time could be theoretically linked to the slow evaporation of the oil phase or possible polymerisation reactions within the components, leading to a denser network and consequently, higher viscosity [286]. The measured increase in viscosity, although significant, did not affect the applicability of the pastes over a 48-week

period. This consistent stability is essential to ensure consistent performance and reliability in real-time applications.

The investigation into the setting time, mechanical properties, stability, degradation behaviour, and biological activity of the 0.4 mg/L formulation of the dual syringe-mixed PM-CPC adhesive were then investigated to assess the impact of the new formation on its clinical applicability. For instance, the handling properties demonstrated the ability of the dual syringe-mixed PM-CPC adhesive to maintain the handling properties of the hand-mixed adhesive, meeting the essential criteria for setting time while offering the advantage of being mixed and delivered on-demand using the double syringe mixing system. The results further reinforce the suitability of the adhesive for various clinical scenarios where proper setting within the specified time range is crucial for successful outcomes. Rapid setting is essential since it provides initial mechanical stability after injection, avoiding implant disintegration as proved from the wash-out test. Proper cohesion and shape retention in a wet environment was found which is in line with other studies [249,287] and indicate potential reduction of associated inflammatory reactions observed previously [288].

In addition, the mechanical performance of the adhesive, including its compressive and adhesive strength, aligns with the necessary clinical requirements. Comparing the dual syringe-mixed adhesive with the hand-mixed adhesive slightly lower mechanical strengths (~8.70%) were observed. Nonetheless, the observed consistency in results, as indicated by lower standard deviations, demonstrates a more reliable and reproducible performance of the dual syringe-mixed PM-CPC adhesive compared to the hand-mixed adhesive [289,290]. The mechanical performance of the dual syringe-mixed PM-CPC adhesive (>20 MPa) was found to be also significantly higher than a previously reported injectable CPC which consisted of CPC combined with glycerol which led to a strength of 6 MPa [274]. Similarly, a CPC-glycerol paste-based system developed in another study investigated the performance of CPC-

chitosan, CPC-tartaric and CPC-monocalcium phosphate monohydrate adhesives, however none of them exceeded the strength of 10 MPa [249].

Over the first few days of a 120-day observation period, both the hand-mixed and dual syringe-mixed PM-CPC adhesives demonstrated a rapid mass loss of about 35%. This suggests that chemical dissolution and the body's natural resorption processes begin early after implantation. This finding aligns with previous research indicating early-stage degradation is a common characteristic for these types of materials [291]. The SEM analysis showed the formation of an apatite layer and HA crystals within a short period of immersion in Ringer's solution indicative of its bioactivity and potential for osseointegration. The variation in crystal morphology and size over the immersion period aligns with the theories suggesting that the ionic exchange and supersaturation levels in the SBF influence the crystallisation process [292,293]. The degradation rate combined with the SEM results demonstrate the high *in vitro* bioactivity of those materials. This degradation rate and apatite formation were found to be more similar to natural bone than other CPCs therefore exhibits a higher resorbability than other CPCs [249,276,294,295].

Furthermore, it was observed that the dual syringe-mixed PM-CPC adhesive not only exhibited satisfactory handling and mechanical characteristics but also demonstrated effective adhesion to bovine femur samples and potential in augmenting orthopaedic and dental implants. Specifically, all femur bone samples bonded with the dual syringe-mixed adhesive withstood forces exceeding 50 N, with some reaching up to 100 N, which is comparable to the hand-mixed adhesive's performance. Notably, despite the adhesion strength being marginally lower for the dual syringe-mixed adhesive compared to the hand-mixed form, its consistency was superior, as reflected by the lower standard deviations. This suggests a more uniform and predictable bonding, which is advantageous for clinical reliability.

4.7. Conclusion

In conclusion, the study successfully formulated a two-component PM-CPC adhesive system that can be efficiently mixed via a syringe-based method. The adhesive's comprehensive evaluation revealed that its quality, including setting time, mechanical strength, stability, degradation behavior, and bioactivity, is comparable to that of the traditionally hand-mixed adhesive. This innovation offers a practical solution for on-demand mixing and precise application, significantly enhancing the efficiency of minimally invasive surgical procedures in orthopedic and dental settings. It stands as a testament to the progress in surgical adhesives, promising improved clinical outcomes through enhanced handling and application control. This advancement represents a significant progress in the development of surgical adhesives, with the potential for better clinical outcomes due to their improved handling and application control.

Even if these studies demonstrated the handling mechanical and adhesion properties of the hand-mixed and dual syringe-mixed PM-CPC adhesive, there is still need to investigate their interaction with surrounding tissues and cells. *In vitro* studies are essential to assess the adhesive's biocompatibility, and ability to support cell attachment and proliferation. Also, the study was conducted in a controlled laboratory environment, which does not entirely replicate the *in vivo* conditions within the human body. Therefore, *in vivo* studies would be suitable to understand the adhesive's behaviour and performance in a more physiological context.

**Chapter 5: *In Vitro* and *In Vivo*
Evaluation of PM-CPC Adhesive:
Biocompatibility and Efficacy as a
Bioadhesive for Implant Stabilisation and
Bone Repair**

5.1. Introduction

The incorporation of phosphoserine into α -TCP leads to a composite that more closely resembles the structure and physical characteristics of natural bone tissue. Studies conducted *ex vivo* on organisms have shown that adhesives modified with phosphoserine exhibit a quicker remodelling rate compared to traditional α -TCP cement [119,148]. These modified adhesives tend to transition into brushite rapidly instead of the gradual conversion into HA observed in unmodified variants which mimic the natural mineralisation process seen in bone healing [296]. When phosphoserine is added, the modified adhesives exhibit a much faster transition into brushite (dicalcium phosphate dihydrate, DCPD). Brushite formation occurs more rapidly due to the presence of phosphoserine, which likely acts as a catalyst or facilitator for this specific crystallization pathway. This accelerated conversion is beneficial because brushite is more soluble and can remodel more quickly in biological environments, leading to faster integration and replacement by natural bone tissue compared to the slower-forming and more stable HA seen in unmodified α -TCP cements.

There have been not many *in vitro* studies evaluating the cellular mechanisms underlying the cell-level and tissue-level changes that occur during healing, which are unique to phosphoserine-based cements. In particular, there is one study by Billström *et al.* [119] that have investigated how cells react to phosphoserine modified cements. However, in this study there is no information on how the composition of phosphoserine modified adhesive affects the cells involved in bone regeneration. Vrchovecka *et al.* [210] published the first study that evaluated how phosphoserine modified cements formulation affects osteogenic cell differentiation, cytocompatibility, and ion release, using *in situ* curing conditions similar to conditions *in vivo*. This *in vitro* study demonstrated cytocompatibility after curing the adhesive. However, the study was mainly focused on investigating ion release and pH

influence on different cell types, aiming to develop an *in vitro* environment closer to the *in vivo*.

Furthermore, the incorporation of calcium silicate into magnesium phosphate cements has been documented to not only enhance mechanical properties but also to exhibit *in vitro* apatite mineralisation, bioactivity, and biodegradation capabilities [187,193,194]. This interaction with the body's natural processes promotes integration between the adhesive material and the surrounding bone tissue, thereby augmenting bonding strength and overall stability [189,195]. Moreover, *in vivo* investigations have demonstrated that biomaterials containing calcium silicate can stimulate osteogenesis by accelerating new bone formation [196]. However, some studies have reported cytotoxic effects [297–299].

Taking into account the positive results for PM-CPCs further *in vitro* exploration need to be conducted for the specific PM-CPC formulations developed during this study. Specifically, the injectable dual syringe adhesive need to be analysed *in vitro* and compared to the standard adhesive.

Early *in vivo* studies have investigated phosphoserine modified cements formulations with low (<5%) percentages of phosphoserine in rats and mini pigs [215,300]. One *in vivo* study was conducted in rats demonstrating high bone remodelling rates and bone formation, while the second one it was conducted in mini pigs showing accelerated resorption. Furthermore, *in vivo* studies have shown osteointegration and histocompatibility of phosphoserine cements [119,212,215,301], where the tissue healing response is improved without pathological inflammation, and is remodelled into new bone rapidly [119]. The current *in vivo* studies have explored bone stabilisation while phosphoserine modified adhesives have not been investigated previously for implant stabilisation and possible dental applications.

Besides biological requirements, dental materials must exhibit functional properties that ensure their long-term reliability [302–304]. Among these properties, the resistance to fracture and wear (interaction between surfaces which leads to the gradual removal of material) holds significant importance [305,306]. This is particularly crucial in preventing various wear-related modes that are often implicated in implant failures [307]. The success and long-term use of dental implants depend on biological and mechanical properties. The biological aspect refers to proper osseointegration, precise implant placement, bone augmentation procedures, and the absence of implant-related toxicity. On the mechanical front, implant strength, resistance to fractures, stability of screw joints, and prevention of loosening are key considerations [308]. Key for this assessment is exploring mechanical stability following *in vivo* implantation.

5.2. Chapter Aim

This chapter aims to evaluate the cytotoxicity and cell proliferation of the dual syringe-mixed and hand-mixed PM-CPC adhesives in comparison to other materials such as HydroSet (commercial control) and α -TCP cement. Furthermore *in vivo* study was conducted focusing on the stability of the interfaces between the PM-CPC adhesive and bone and between the adhesive and the implant surface over time through implant stability quotients (ISQ), pull-out and torque out values. More specifically, the use of PM-CPC adhesive for stabilising implants under sub-optimal geometrical conditions (conditions that would normally cause low or no primary implant stability) was examined.

The specific objectives of this chapter were the:

- Assess and compare the cytotoxicity of PM-CPC adhesives mixed using different technique, HydroSet, and α -TCP cement, in two cell types.

- Assess the cell proliferation induced by the dual syringe-mixed and hand-mixed PM-CPC adhesives.
- Investigation of the *in vivo* stability of the interfaces between the hand-mixed PM-CPC adhesive and different bone types and hand-mixed PM-CPC adhesive and the implant surface over time.

5.3. Material Methods

5.3.1. *In Vitro* Assessment of the Dual Syringe-mixed and Hand-mixed PM-CPC adhesives

5.3.1.1 Sample Preparation

PM-CPC adhesive was created by hand-mixing powder phase with liquid phase as described previously (Chapter 3) with a defined weight percentage of each component (n=6). Dual syringe-mixed PM-CPC adhesive specimens (n=6) were prepared by mixing the two components through the dual syringe mixing system as described in Chapter 4. To investigate the effect of phosphoserine in the PM-CPC adhesive, α -TCP cements were also prepared without phosphoserine combining α -TCP powder with 0.35 mL/g of 1 M sodium dihydrogen phosphate (Na_2HPO) [309]. HydroSet (HydroSet®, HA bone Adhesive, Stryker, Michigan, US) cement samples (n=6), as a commercial control, were also prepared as per instructions to compare the HA-based and α -TCP-based cements. Specifically, HydroSet was selected as a comparison adhesive in this study because it is a commercially available HA-based bone adhesive widely recognised for its clinical efficacy and mechanical properties. This choice provides a benchmark for evaluating the performance of the newly developed PM-CPC and phosphoserine-modified α -TCP cements. By comparing the novel adhesives to HydroSet, which is well-documented and extensively used in clinical settings, the study can effectively assess the relative advantages and improvements offered by the new formulations. This comparison allows for a direct evaluation of how the new adhesives measure up to a standard,

ensuring that any observed benefits or differences are meaningful and relevant to current medical practices. Additionally, HydroSet's established performance metrics offer a reliable baseline for evaluating properties such as setting time and biocompatibility, thus providing a comprehensive context for interpreting the results of the experimental adhesives. Disc-shaped specimens, with dimensions of 12 mm in diameter and 2 mm in thickness, were formed using silicone moulds. These specimens were examined in two states: as initially cast without any curing (non-cured), and after being incubated in Ringer's solution at 37°C for over 24 h (cured) [310]. Prior to cell culture experiments the non-cured and cured discs were sterilised through immersion in 70% ethanol for 10 min and washed thrice with PBS to remove any residues.

5.3.1.2 Cell Culture

The mouse mesenchymal stem cells (Gibco™ MSCs, generally isolated from tibia and femoral marrow, Thermo Fisher Scientific, Ireland) were cultured in Dulbecco's modified Eagle's medium (Gibco™ DMEM, Thermo Fisher Scientific, Ireland).

The pre-osteoblast cell line (MC3T3 E1, Mouse C57BL/6 calvaria, Merck Life Science Limited, Ireland) was expanded in alpha modified Eagles medium (Gibco™ MEM α , nucleosides, no ascorbic acid, Thermo Fisher Scientific, Ireland).

Each medium was supplemented with 10% Foetal Bovine Serum (FBS, Merck Life Science Limited, Ireland) and 1% penicillin/streptomycin (Merck Life Science Limited, Ireland) at 37 °C in a 5% CO₂ atmosphere. For *in vitro* procedures, cells were trypsinised with 0.25% trypsin (Thermo Fisher Scientific, Hemel Hempstead, UK), collected via centrifugation (800 RPM for 5 min) and resuspended in fresh media to be used in below studies. The cell morphology was observed by an inverse phase-contrast microscope (Olympus Microscope, EVIDENT, Ireland) at x10 magnification.

5.3.1.3 Cytotoxicity Analysis

The cytotoxicity, of the dual syringe-mixed and hand-mixed PM-CPC adhesive, HydroSet and α -TCP cement to the MSCs and MC3T3 cells, was investigated. Cytotoxicity was analysed in accordance with the extraction method outlined in ISO 10993-12 and ISO 10993-5 [311]. The ISO standards for toxicity set 70% cell survival as the limit for “non” cytotoxicity. The extract based method is routinely used to evaluate if biomaterial composition is cytotoxic to cells [312–315]. The disc-shaped samples were immersed in culture medium at a ratio of 0.2 g/mL and incubated for a total of 72 h at 37°C.

MSCs were seeded in a 96-well plate at a density of 5×10^3 cells/well and allowed to adhere for 24 h. The cells were exposed to the disc extract for 24 h, 48 h, and 72 h. After incubation periods, cell viability was assessed using the 5 mg/mL multi-transaction translator (MTT) assay (Thiazolyl Blue tetrazolium bromide, Thermo Fisher Scientific, Ireland dissolved in sterile 1xPBS, yellow). MTT solution was added to each well, and the plate was incubated at 37 °C for 4 h, allowing viable cells to convert MTT to formazan crystals. The formazan crystals were dissolved in DMSO (Dimethyl sulfoxide $\geq 99.9\%$, Merck Life Science Limited, Ireland) with the use of a shaker (Microplate shaker, MTS 2/4 digital, VWR International Ltd., Ireland) and the absorbance was measured at 570 nm using a microplate reader (Infinite 200 PRO plate reader, TECAN, Switzerland). A DMSO-only background blank was subtracted from all readings as Negative Control (NC). NC readings were averaged and set as 100% viable. Cell viability (%) was then determined by Equation 5.1.

Equation 5.1– Calculation of cell viability %:

$$\left(\frac{\text{Experimental Abs } 540 \text{ nm}}{\text{Mean Negative Control Abs } 540 \text{ nm}} \right) \times 100\%$$

MC3T3-E1 cells were seeded at a density of 4×10^3 cells/cm² on a 96-well plate and were cultivated for 48 h until reaching approximately 60% confluency. As per MSC cells, the medium was subsequently replaced with the bone adhesive disc extract medium after 24 h, and cells were exposed in the extract for an additional 24, 48 and 72 h. The metabolic activity of MC3T3-E1 cells was measured by alamarBlue. The alamarBlue assay is based on the measurable reduction of resazurin to resorufin by metabolically active cells [316]. After the incubation period the cells were washed with sterile PBS and the 10% alamarBlue diluted in the α -MEM media was added. The plates were incubated for 4 h to allow the reduction of resazurin and 100 μ L of new reduced media from each well was transferred to a 96-well plate for measurement. A 10% alamarBlue-only background blank was subtracted from all readings as Negative Control (NC). Reduction of alamarBlue was determined by measuring absorbance at wavelengths of 570 nm and 600 nm and comparing the standard curve. Cell viability (%) was determined as the percentage of alamarBlue reduction (Equation 5.2). The manufacturer guidelines provided the relevant values for the molar extinction coefficients (E) for oxidised (E_{oxi}) and reduced (E_{red}) alamarBlue.

Equation 5.2– Percentage (%) reduction of alamarBlue reagent:

$$\left(\frac{(E_{oxi}600 \times A570) - (E_{oxi}570 \times A600)}{(E_{red}570 \times C600) - (E_{red}600 \times C570)} \right) \times 100 \%$$

Where, A_{570/600} – Absorbance (sample) at 570/600 nm, C_{570/600} – Absorbance (NC) at 570/600 nm, E_{oxi} 570 = 80,586, E_{oxi} 600 = 117,216, E_{red} 570 = 155677 and E_{red} 600 = 14,652.

5.3.1.4 Cell Proliferation

MC3T3-E1 cells were collected from 75 cm² culture flasks via trypsin treatment and resuspended in 1-2 mL MEM α media and then were counted using the trypan blue exclusion method. Specifically, 10 μ L of cells/trypan blue suspension was added to a haemocytometer

and cells in the four corner quadrants were counted to determine the volume needed for cell seeding. MC3T3-E1 cells were seeded onto the bone adhesive discs at a density of 25×10^3 MC3T3-E1 cells. The discs were placed in a 24-well plate, and 1 mL of the supplemented α -MEM was added to each well. The cells were then incubated for predetermined time intervals (Day 1, 4, 7, 14 and 21) to assess proliferation.

Cell proliferation was assessed using the alamarBlue assay. The culture medium was removed from the wells, and cells were washed with PBS. Then, 10% v/v alamarBlue reagent was added to each well in fresh culture medium. The plates were then incubated at 37°C for 4 h in a humidified atmosphere with 5% CO₂. A 10% alamarBlue-only background blank was subtracted from all readings as Negative Control (NC). Reduction of alamarBlue was determined by measuring absorbance at wavelengths of 570 nm and 600 nm and comparing the standard curve. Cell viability (%) was determined as the percentage of alamarBlue reduction Equation 5.2.

5.3.2. *In Vivo* Assessment of PM-CPC Adhesives

Because I contributed to the optimisation and development of the optimal PM-CPC formulation, I was part of an *in vivo* study conducted on mini pigs for that reason HydroSet was not used as a comparison. The main hypothesis of this study was that the interfaces associated with the adhesive material (bone/adhesive and adhesive/implant) are stable over time when the material is used in artificial extraction sockets (native trabecular bone) and that the use of the material can enable bone healing. In order to prove this hypothesis, the stability of the interfaces between adhesive-bone and adhesive implant was evaluate over time. Additionally, the objective of this study was to assess the healing and resorption behaviour in response to the hand-mixed PM-CPC adhesive (this decision was primarily driven by the partnering company that had a particular interest in the hand-mixed version of the adhesive), when used in conjunction with implant placement. This focused approach allowed for a

detailed assessment of the new adhesive's performance in a realistic biological environment, providing critical insights into its potential clinical application and effectiveness. Including HydroSet in the *in vivo* study would have shifted the focus from optimising and understanding the novel PM-CPC adhesive to a comparative analysis, which was not the primary goal of this specific investigation.

During the surgeries, my primary responsibility involved the preparation of the PM-CPC adhesives, ensuring they were optimally formulated for application within the surgical cavities. Post-surgery, my involvement was focused on the mechanical evaluation (ISQ, pull-out and torque out test) of the implants. This critical phase of the study was conducted in collaboration with the research team from Institute Straumann. My role was the assessment of the mechanical stability and integrity of the implants of each mini pig's involvement in the study, providing vital insights into the performance and efficacy of our PM-CPC formulation in a realistic biological context.

While I was not directly involved in the histological studies conducted by Institute Straumann and the University of Bern, their findings played a complementary role in my research. The histological images they provided were instrumental in reinforcing the evidence gathered from my mechanical analysis. These images, showcasing the adhesive-bone and implant-adhesive interfaces, were incorporated into this chapter to enhance the understanding of the implant stabilisation process and to support the mechanical results I had observed. The integration of these histological observations with my mechanical findings offered a more comprehensive view of the PM-CPC's behaviour and effectiveness *in vivo*.

5.3.2.1 Animal Model and Management

A total of 13 female Göttingen Minipigs (20–23 months, Ellegaard Gottingen Minipigs A/S, Dalmoose, Denmark), weighing 31–51 kg at the time of teeth extraction, were employed for

the *in vivo* study. Göttingen Minipigs were chosen due to their close resemblance to human bone anatomy, structure, healing, and remodelling, thereby being representative for investigations in bone regeneration in implant dentistry [317,318]. The minipig mandible shares similarities in movement, shape, size, and anatomy with humans, and the bone regeneration rate of adult minipig mandible is comparable to that of young skeletal mature humans [319,320]. Essential parameters related to the bone physiology of the minipigs and their similarities in bone mineral density and concentration to human bone were taken into consideration. One animal was sacrificed 2 h post-implantation (T=0), to allow for full blood coagulation at the surgery sites. Four animals were sacrificed at 2 (T+2), 4 (T+4) and 8 (T+8) weeks post implantation (Figure 5.1). Termination was performed by inducing cardiac arrest with an injection of Euthanimal (400 mg/mL, at a dose of 0.3 mL/kg).

The study was conducted at Ellegaard Gottingen Minipigs A/S, Dalmose, Denmark. The study adhered to the ethical guidelines and received approval from the Ministry of Food, Agriculture and Fisheries of Denmark (Ethics approval number: 2021-15-0201-00876). This study was performed in accordance with ISO 10993-6 Biological evaluation of medical devices – Part 6: Tests for local effects after implantation. Strict adherence to the principles of replacement, refinement, or reduction (3Rs) was maintained, and the derived data were intended to provide valuable insights into tissue behavior at different biomaterials, devices, or implant surfaces, given the ethical constraints for similar studies in humans.

5.3.2.2 PM-CPC Adhesive Preparation

The adhesive assessed as part of the *in vivo* study was the hand-mixed PM-CPC adhesive (total mass=1.5 g) as described in Chapter 3. Each PM-CPC adhesive was double packed in Tyvek/Film pouches to maintain sterility and integrity. The adhesive underwent gamma irradiation sterilisation (STERIS Radiation Technology Centre, UK), with a dose ranging

between 26.7 to 31.1 kGy, ensuring the material remained free of any contaminants or microbial agents.

Prior to implant placement, sterile deionised water was added to the powder phase and the PM-CPC adhesive was hand mixed thoroughly for 20 s to achieve a uniform consistency. Post-mixing, the adhesive was transferred to a conventional syringe within a time frame of 50 s. This timely transfer was crucial to ensure the application of the adhesive before the onset of the final setting time (3.4 ± 0.6 min). The mixed adhesive, now in the syringe, was accurately injected into the prepared osteotomies.

5.3.2.3 Surgical Procedures

Minipigs underwent two surgical procedures under general anaesthesia after overnight fasting. All medications were administered following standard veterinary practice. One-sided extractions of mandibular premolars and molars (P2-P4, M1) were performed 12 weeks prior (T-12) to implant placement, and on the day of the surgery (T=0), extractions were performed on the remaining side (ES) as shown in Figure 5.1, followed by immediate implant placement. The mandibular alveolar ridge was exposed and prepared. Five oversized osteotomies (diameter of 5.3 mm x depth of 9 mm) were created in the mandible. PM-CPC adhesive was applied to the osteotomy prior to implant (Bone Level (BL) implants, Ø3.3 mm x 8mm endosteal length, materials: Roxolid, surface: SLActive) (Straumann Holding AG, Basel, Switzerland) placement, ensuring a 1 mm subcrestal placement. Excess adhesive was removed, and closure caps and membranes were applied.

5.3.2.4 Mechanical Characterisation

The mechanical stability including implant stability quotients (ISQ), pull-out and torque values were determined over the duration of the study (0, 2, 4 and 8 weeks). However, prior to harvesting the hemi-mandibles, the mechanical stability was measured determining the ISQ

values on the BL implants 30 min after the implant placement. Subsequently, ISQ was assessed at the point of termination by exposing the implants, prior to removing the hemimandibles.

The hemi-mandibles were then harvested and mounted in the material testing machine for the determination of the pull-out force under tensile loading as described in Section 3.3.6. Furthermore, the torque values required for implant removal were determined using a handheld torque meter fitted with a 350 Ncm torque cell (Mark-10, NY, USA). During the measurement, the peak removal torque required to release the implant from the implantation site, at the various time points, was recorded. The pull-out was implemented to assess the interface between the adhesive and the bone while the torque-out was implemented to assess the interface between the adhesive and the implant.

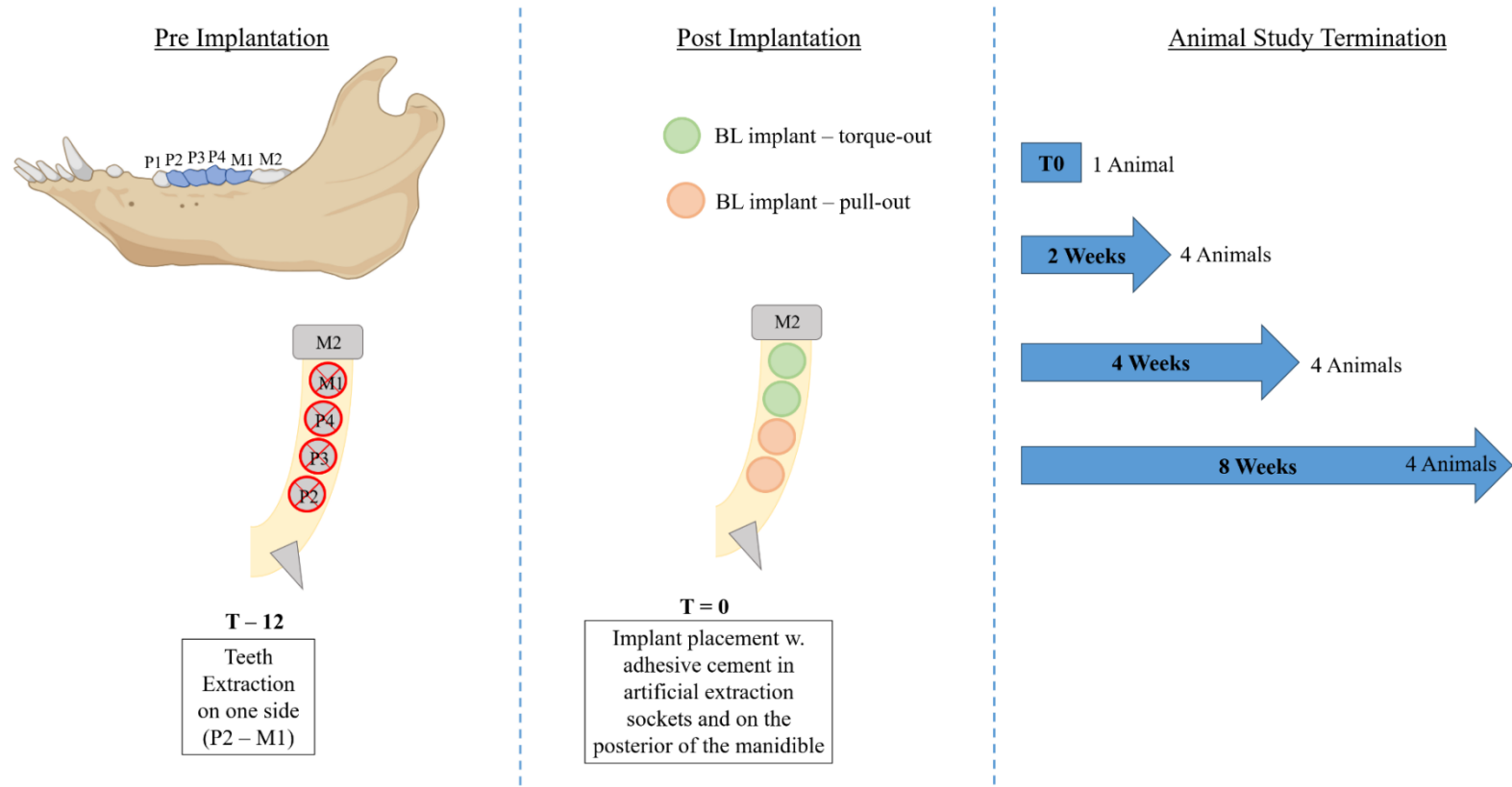


Figure 5.1: Overall *in vivo* study design – The scheme demonstrated only one layout of the sample distribution. The “Artificial extraction sockets”, in the form of Ø5.3 mm osteotomies (green for torque out and orange for pull-out) were used to assess the changes at the PM-CPC/Trabecular bone interface. Following implantation, one animal was terminated at T=0, 4 animals at T+2 w, 4 animals at T+4 w and 4 animals at T+8 w.

5.4. Results

5.4.1. *In Vitro*–Cytotoxicity Analysis

The cytotoxicity of HA-based (HydroSet), α -TCP cements and dual syringe-mixed and hand-mixed PM-CPC adhesives were tested using two cell types after 24 h and 72 h cell exposure to sample extract. Initially, the samples were tested non-cured. The data from the non-cured samples showed that the viability of the MC3T3-E1 cells was below the 70% threshold at both 24 h and 72 h timepoints (Figure 5.2). For the MSC cells after 24 h exposure to the sample extract, the PM-CPC adhesive showed the highest viability (percentage viability= $95.4 \pm 20.8\%$), and no statistically significant differences (p -value >0.05) in viability were observed compared to the negative control for all samples except HydroSet (p -value <0.001) (Figure 5.2). Similarly, after 72 h, there was no significant (p -value >0.05) difference, when MSC cell used, between the α -TCP cement, hand-mixed and dual syringe-mixed PM-CPC adhesive groups, and the NC (Figure 5.2). Even though low cell viability was observed for non-cured samples, the α -TCP-based adhesives (α -TCP cement, hand-mixed and dual syringe-mixed PM-CPC adhesive) showed to be more cytocompatible than HydroSet (HA-based cement).

After curing, all samples showed viability of $>70\%$ indicating an acceptable level of cytocompatibility (Figure 5.3). Higher cell viability (p -value <0.01) was observed on hand-mixed and dual syringe-mixed PM-CPC adhesive groups compared to HydroSet for both cell types at both time points (24 h and 72 h). Furthermore, for both cell types at both timepoints, higher viability (p -value <0.05), with values close to 100%, was observed for the hand mixed and dual syringe-mixed PM-CPC adhesives compared to α -TCP cements, indicating that the addition of phosphoserine and calcium silicate positively influenced cell viability and promoted cell proliferation. After 72 h exposure of cells to the undiluted extract non-significant change of cell viability was observed for hand-mixed and dual syringe-mixed

PM-CPC adhesive, while HydroSet appeared slightly toxic. Overall, the cured materials showed greater cytocompatibility with cell viability of >70% achieved for hand-mixed and dual syringe-mixed PM-CPC adhesive and α -TCP cement. Furthermore, MSC maintained higher cell viability than MC3T3 when in contact with the extract.

The higher MSC cell viability observed in the α -TCP cement and the PM-CPC adhesive compared to HydroSet can be attributed to several key factors related to the material composition and properties. Firstly, the incorporation of phosphoserine into the α -TCP cement likely enhanced the bioactivity and biocompatibility of the adhesive. Phosphoserine, being a naturally occurring amino acid derivative, may promote better cell adhesion and proliferation by providing bioactive sites that facilitate cellular interactions. Additionally, the microstructure and porosity of the α -TCP cement can significantly influence cell viability. The optimized PM-CPC formulation, with its tailored porosity and surface characteristics, may have provided a more favourable environment for MSC attachment and growth compared to the denser, less porous structure of HydroSet.

Furthermore, the chemical composition of the α -TCP cement, which transitions more rapidly into brushite rather than hydroxyapatite (HA), could create a more conducive environment for early cell proliferation and differentiation. Brushite is known for its higher solubility and faster resorption rates, which can lead to quicker remodelling and integration with the host tissue, thereby supporting better initial cell viability and activity. In contrast, the slower-converting HA in HydroSet might not provide the same level of initial bioactivity and resorption dynamics, resulting in comparatively lower MSC viability. Overall, these factors combined to make the α -TCP cement and PM-CPC adhesive more conducive to supporting MSC viability and promoting better overall cellular responses.

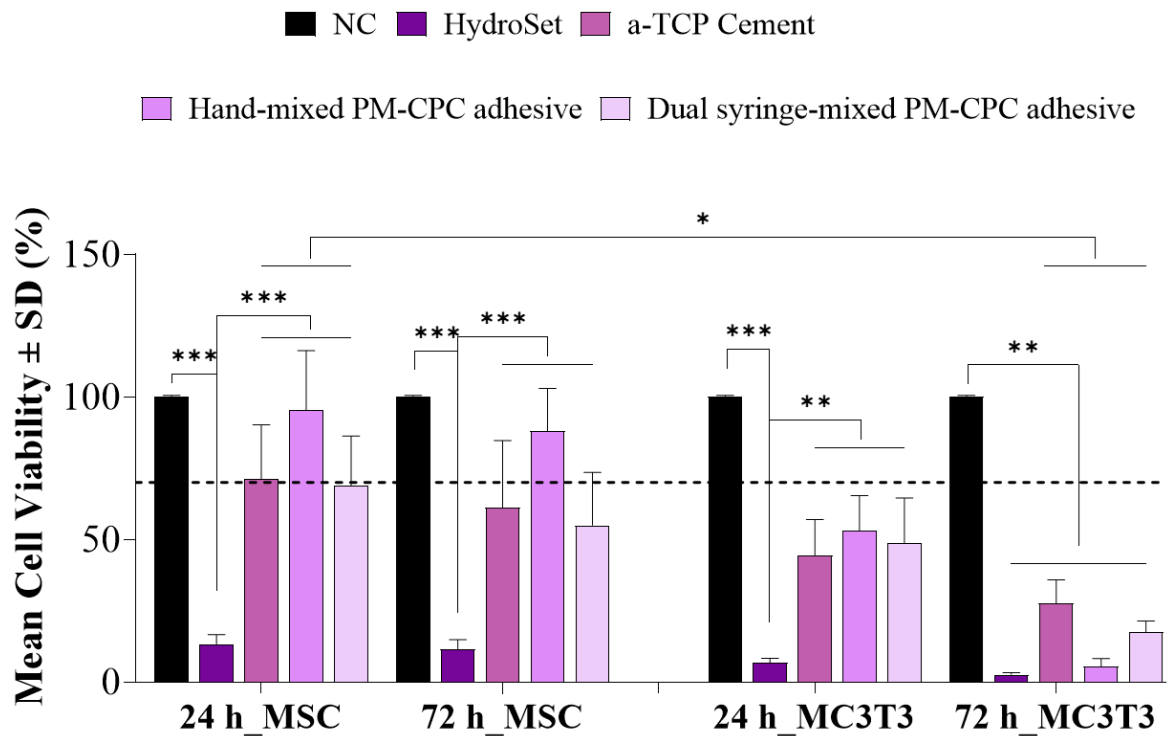


Figure 5.2: Cell Viability of Non-Cured Samples – Cytotoxicity analysis in viability level of two cell lines incubated with samples extracts at either 24 h or 72 h. Dashed line at 70% represents the threshold whereby materials are considered cytotoxic if cell viability decreases below this value. Statistical significance is denoted by *p value < 0.05, **p value < 0.01 and ***p-value < 0.001, (n ≥ 3).

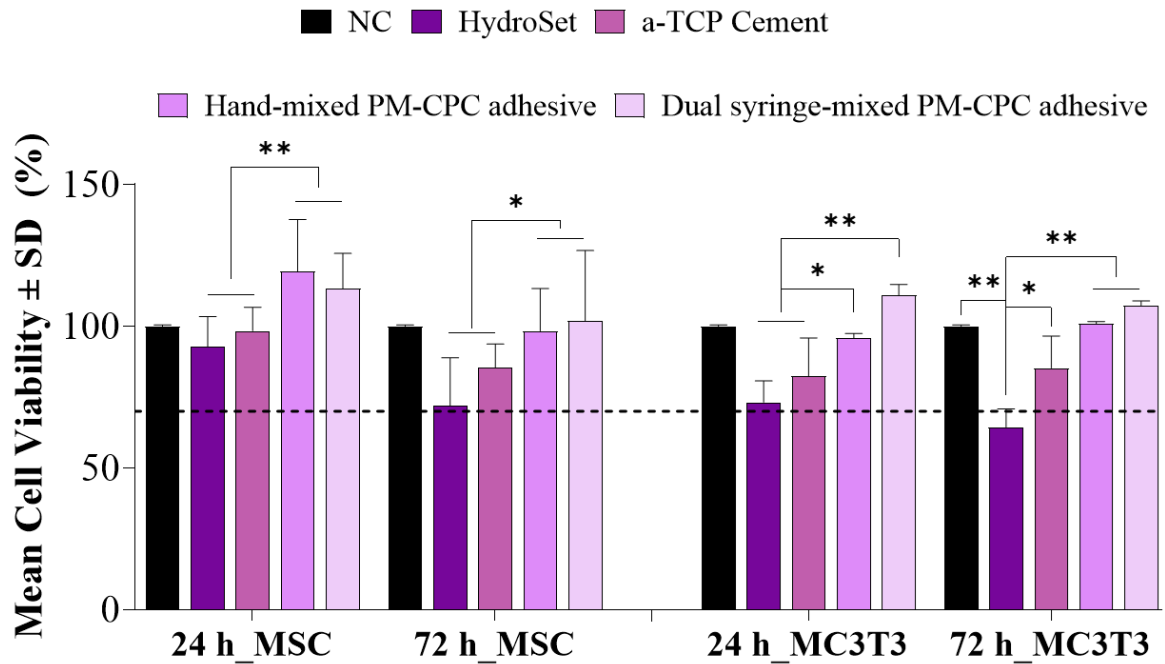


Figure 5.3: Cell Viability of Cured Samples – Cytotoxicity analysis in viability level of two cell lines incubated with samples extracts at either 24 h or 72 h. Dashed line at 70% represents the threshold whereby materials are considered cytotoxic if cell viability decreases below this value. Results shown are mean \pm SD ($n \geq 3$).

5.4.2. *In Vitro*–Cell Proliferation

The 21-day alamarBlue study (Figure 5.4) showed that both PM-CPC adhesive had a significant increase in the reduction of alamarBlue when compared to their Day 1, 4 and 7 counterparts ($p\text{-value} \leq 0.001$) indicating that cells. During the first week (Day 1- Day 7) there was no significant difference in the reduction of alamarBlue. At Day 14, a significant ($p\text{-value} < 0.01$) alamarBlue reduction was observed in both adhesives, which was further increased ($p\text{-value} < 0.01$) after 21 days reaching a mean reduction of 50-59%. These results indicate that cell proliferation leads to an increase in cell numbers at Day 14 and Day 21. Comparing the PM-CPC adhesive under different mixing conditions no significant difference ($p\text{-value} > 0.05$) was observed on their ability to promote cell proliferation.

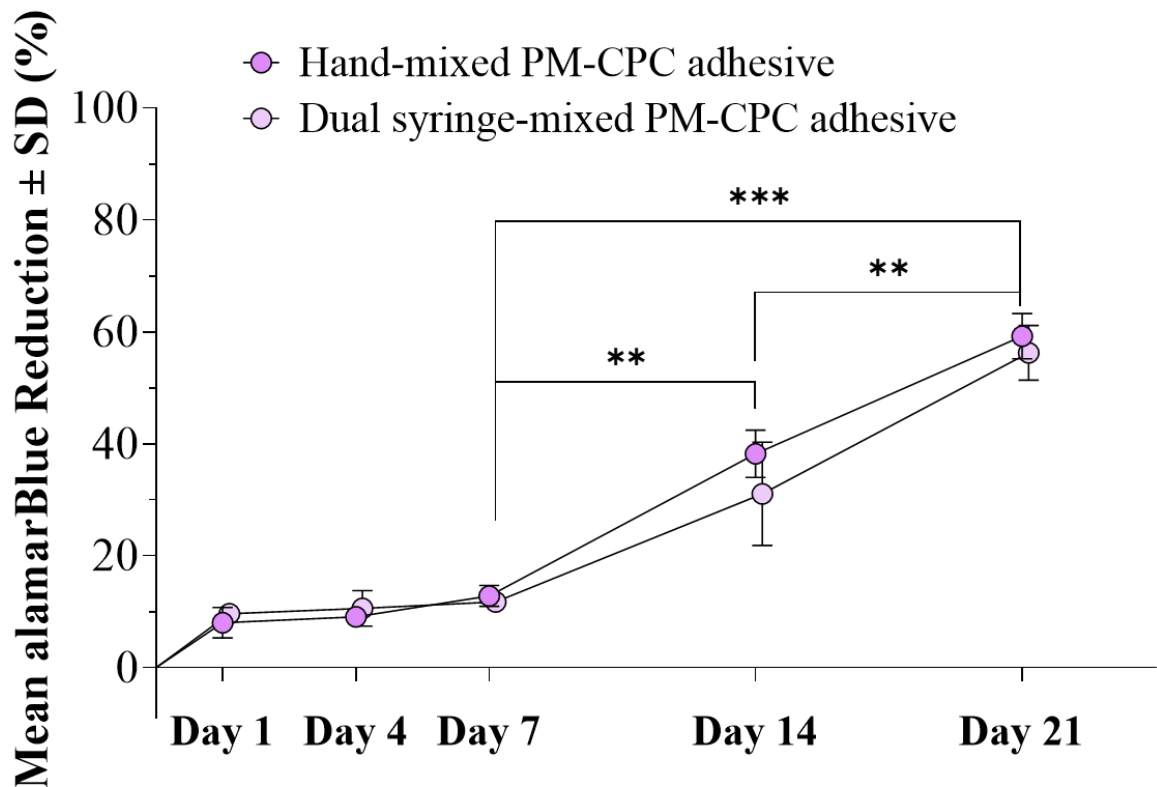


Figure 5.4: Cell Proliferation – Significant reduction of alamarBlue by MC3T3-E1 cells on hand-mixed and dual syringe-mixed PM-CPC adhesive at Day 14 and Day 21. No significant difference was observed between hand-mixed and dual syringe-mixed PM-CPC adhesive. Statistical significance is denoted by **p value < 0.01 and ***p-value < 0.001, (n = 6).

5.4.3. *In Vivo*–Mechanical Characterisation

In vivo experiments demonstrated the ability of PM-CPC adhesive to mechanically stabilise the implant within the trabecular bone (8 weeks post-implantation). The primary ISQ values of 45 were found 15 min post implantation, however, a high standard deviation was observed (Figure 5.5a). However, over time and specifically 24 h after surgery the ISQ values were increased and stabilised obtaining lower standard deviation. This indicates that the system is further stabilising which might be related to blood coagulation at the surgical site. Similar observations have been reported previously [321] where ISQ values increased and stabilised within the first 24-48 hours post-implantation, attributing this to early biological processes including blood clot formation and initial wound healing responses. This pattern suggests that ISQ is more reliable for assessing functional stability after the initial healing phase rather than immediate post-implantation stability. The adhesive material showed a slight expansion, over time. This might also explain the increased ISQ values over the first 24 hours as it could potentially mean that the material is applying pressure to the walls of the bone defect. This, however, has yet to be confirmed in future studies. Therefore, ISQ might not be a reliable measurement to assess immediate stabilisation but might be useful to assess functional loading after healing. Over the 8-week period the ISQ values remained stable averaging at 70, indicating that the implant was not loosening over time.

In terms of the pull-out forces no significant differences were found between the groups, however, there appears to be a trend toward increasing average values, relative to the 24 h time point. As can be seen from Figure 5.5b after 4 weeks, the average pull-out force increased by ~16% compared to Day 1, reaching 287 N. Pull-out increase significantly (p -value <0.01) from 24 h to 4 weeks post-implantation indicate positive effects at the PM-CPC–bone interface. These results are in line with other studies [322,323] where it was reported that bioactive bone adhesives can enhance the mechanical integration of implants. Their studies

showed similar increases in pull-out forces over time, correlating with the bone formation and maturation around the adhesive material. The gradual increase in pull-out strength in your study suggests effective osseointegration, a critical factor for long-term implant success. The pull-out force remained at values above 150 N for the next 8 Weeks, without any significant change. The pull-out setup consistently allowed for assessing the strength of the bone/adhesive interface (as indicated by the adhesive still being attached to the implant, following the pull-out procedure). As a result, the data indicates that the bone/adhesive interface is further stabilised, over time, suggesting that the adhesive provides a platform for osseointegration.

The torque required for the removal of the implant was above 35 Ncm on Day 1, with similar values recorded at Day 14 and Day 28. Torque increases significantly (p -value <0.05) at later timepoints (Day 56 and Day 84) post implantation, with a 50% at Day 56 compared to Day 24, reaching ~75 Ncm (Figure 5.5c). The consistent trend for the first time points indicate that the integrity of the material is maintained over time and the increased maximum values at the 8-week time point indicates that new bone is being formed around the implant that was mature enough to have a measurable mechanical effect. Comparable findings are reported by Wang *et al.* [324], who observed that the removal torque of implants stabilized with bioactive cements increased significantly over a similar timeframe. This increase was attributed to the maturation and mineralization of new bone, enhancing the overall mechanical interlock between the implant and the surrounding bone tissue. No significant differences were found between the groups; however, it is noted that the removal torque values appear consistent over the first time points of the study and with a tendency for increased maximum forces at the 8-week time points.

5.4.4. Histological Analysis

The histological images were obtained and used as evidence for mechanical stability. The assessment was made by an expert with extensive experience in the field of histological assessment (Dieter Bosshard, University of Bern, Switzerland).

Observing the histological images 24 h after implantation (Figure 5.6a), direct contact between the adhesive and bone is observed for the artificial extraction socket, indicated the direct contact of bone-adhesive and implant-adhesive. This image also presents the homogenous application and distribution of the PM-CPC adhesive between implant and bone. At 2 weeks as can be seen from Figure 5.6b both primary contact (PC) and secondary contact (SC) points are observed. This indicates that the adhesive-bone contact is maintained, and bone formation has started to take place at the surface of the adhesive material. As a result, the observed increase in pull-out force after 2 weeks of implantation can be correlated with the formation of new bone and the existence of both the PC and SC points. At 4 weeks (Figure 5.6c), there is still direct contact between the dense cortical bone and the adhesive while signs of adhesive resorption are shown the defect site along with the formation of new bone. Eight weeks following the implantation, there is a noticeable development where the newly formed bone reaches the surface of the implant (Figure 5.6d). Concurrently, there's a reduction in the volume of the adhesive, predominantly around the coronal part of the implant. This change in the bone-adhesive interface significantly enhances the mechanical stability and characteristics of the implant. This improvement is further corroborated by the observed increase in both pull-out and torque forces, indicating a successful integration of the implant with the surrounding bone tissue. However, on left side it can be observed the existence of periodontal ligament (PDL) which has occupied the space between the root and the implant.

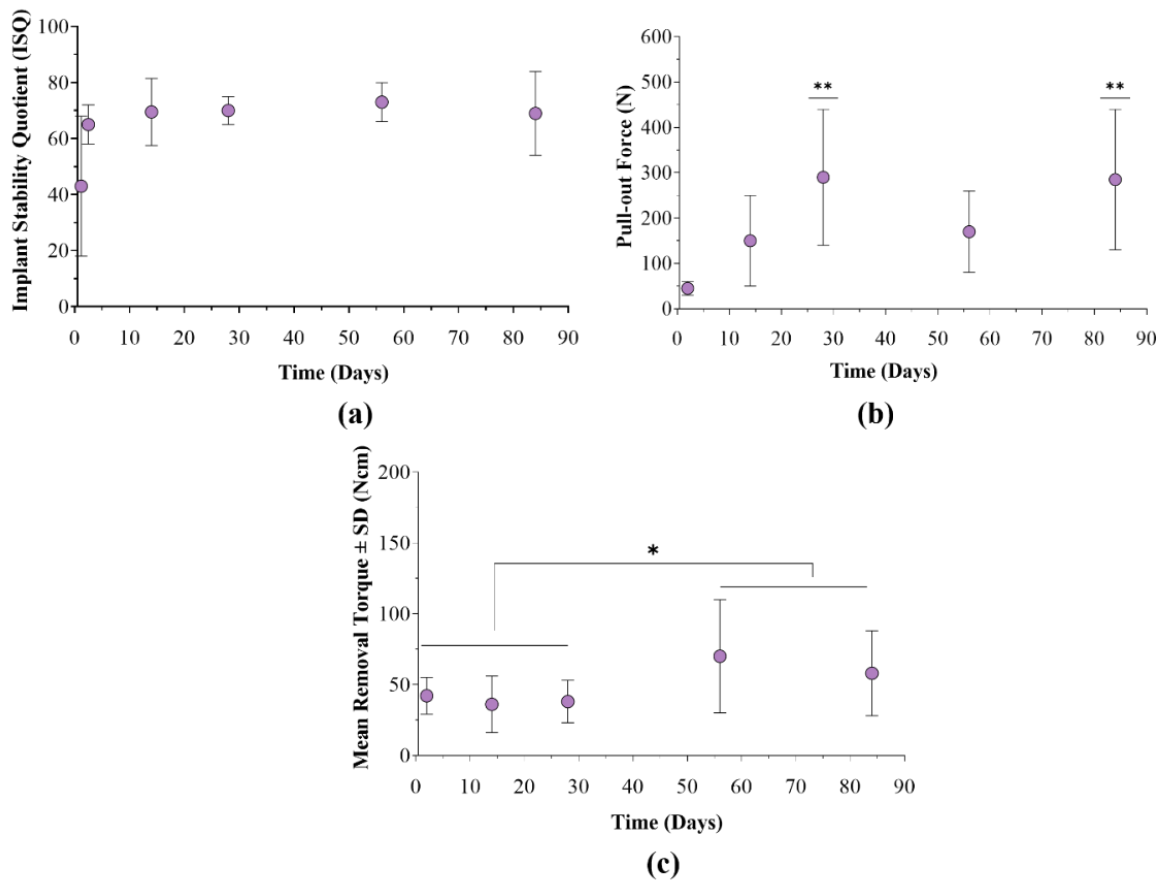


Figure 5.5: Mechanical Characterisation of the PM-CPC–Bone and Implant–PM-CPC Interface – (a) ISQ values and (b) pull-out forces indicating forced between bone-adhesive and c) implant removal torque indicating forced between implant-adhesive over 86 days *in vivo*. The results demonstrate the mechanical characteristics and stability of the dental implants over time. Statistical significance is denoted by **p value < 0.01, (n = 4).

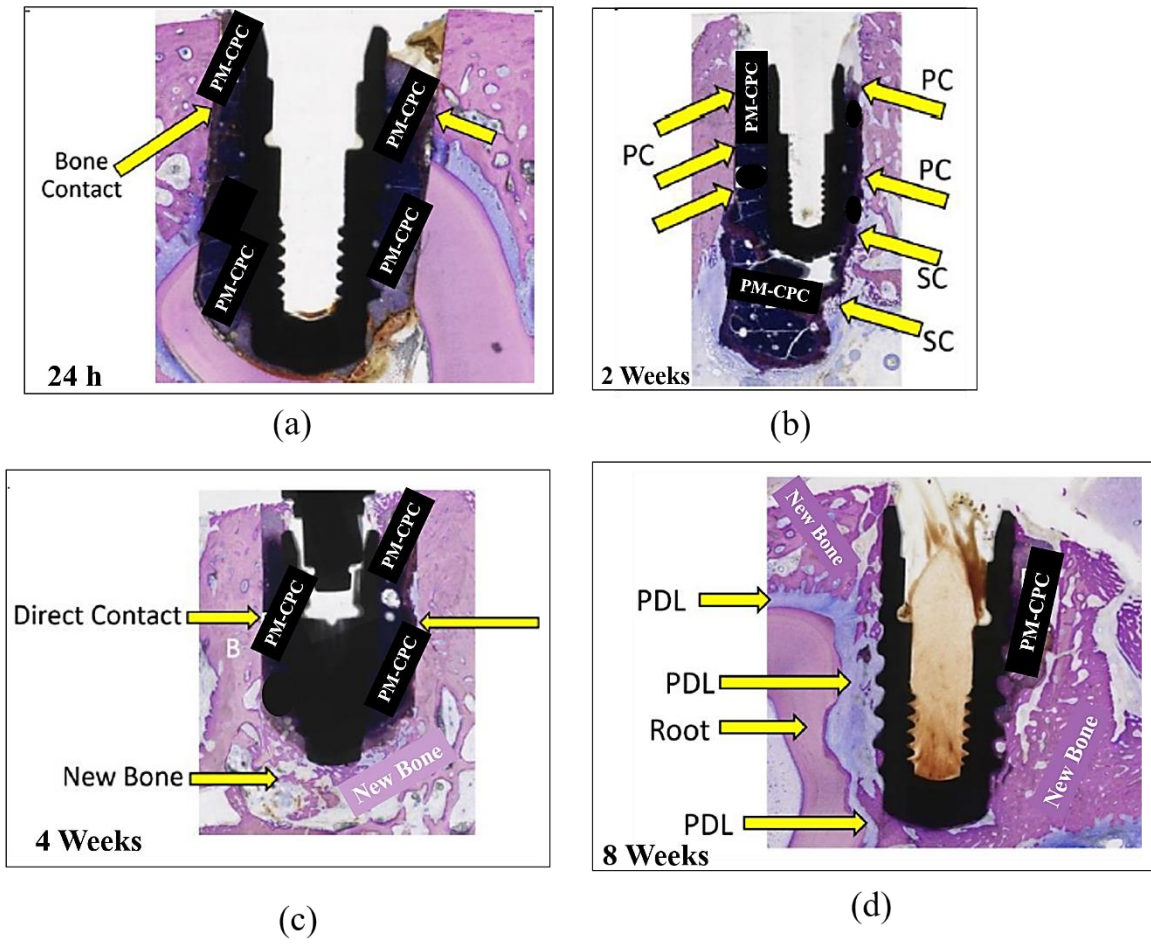


Figure 5.6: Representative images from the histological sections prepared from specimens of artificial extraction sockets –Analysis at (a) 24 h, and (b) 2 weeks, (c) 4 weeks, and (d) 8 weeks post-implantation, showing adhesive-implant and bone-adhesive interface and new bone formation.

5.5. Discussion

Within this chapter two PM-CPC adhesives—one mixed using a dual syringe system and the other mixed by hand—were evaluated *in vitro* against a commercial control and α -TCP cement. Furthermore the *in vivo* study was designed to examine the performance of the hand mixed PM-CPC adhesive within artificial extractions sockets. Following the various healing periods, mechanical fixation was assessed by removal torque and pull-out measurements.

When comparing the behaviour of the two different cell types (MC3T3-E1 and MSC), it was observed the variation in cellular sensitivity, with the MC3T3-E1 exhibiting greater sensitivity. The MC3T3-E1 cells exhibited lower survival rates post-exposure to the materials, highlighting the necessity of considering cell-specific responses when evaluating biomaterial cytocompatibility. Similar behaviour in terms of the sensitivity of MC3T3-E1 cells was observed by Pujari-Palmer *et. al.*, [210] when carrying out cytotoxicity testing using three different cell types including MC3T3-E1.

The hand-mixed and dual syringe-mixed PM-CPC adhesives demonstrated significantly enhanced cytocompatibility across both cell types compared to the HA-based (HydroSet). The consistently higher cell viability observed with α -TCP based adhesives confirming their ability to promote cellular activity and viability, a crucial property for successful tissue integration and regeneration [325–329]. Another finding was the impact of phosphoserine and calcium silicate on cellular behaviour, which is in line with other studies on phosphoserine modified adhesives [148,212,330–332]. The PM-CPC adhesive either hand-mixed or mixed using the dual syringe-mix system demonstrated high cell viability, approaching 100%. The obtained cell viability not only demonstrated its compatibility but also its ability to promote cell proliferation, [333,334].

Post-curing, all samples were non-cytotoxic, with an important increase in cell viability[299,335]. The 21-day alamarBlue study presented the behaviour of the hand-mixed

and dual syringe-mixed PM-CPC adhesive regarding cell proliferation over time. During the initial week it was observed no significant differences in the reduction of alamarBlue. This suggests that both PM-CPC adhesives obtained an initially stable phase, wherein the cellular activities remain constant. While at Day 14, a significant increase in alamarBlue reduction was observed for both PM-CPC forms, indicating the enhancement in cell proliferation. The increase continued, reaching a mean reduction between 50-59% by Day 21. The results show that PM-CPC adhesives promote cell growth over time, making this adhesive suitable for long-term use in bone healing and regeneration. Furthermore, similar behaviour was observed between hand-mixed and dual syringe-mixed PM-CPC adhesives. The lack of significant difference between the two PM-CPC adhesives in promoting cell proliferation demonstrate a consistent performance even if different mixing technique was used. This consistency is advantageous as it broadens the applicability of PM-CPC, allowing for flexibility in choosing the most suitable form for specific clinical scenarios without compromising the biological outcomes.

Considering the positive outcomes regarding cytocompatibility and cell proliferation, both the PM-CPC adhesives are considered as promising candidates for further research and potential clinical applications. However, the osteogenesis and polymerase chain reaction (PCR) of both hand-mixed and dual syringe-mixed PM-CPC adhesive should be explored to determine changes in gene expression profiles.

In vivo experiments clearly demonstrated the ability of PM-CPC to rapidly stabilise the implant within the trabecular bone with primary ISQ values of 65–85 after 15 min. By 4 weeks, the average pull-out force was increased ~16% compared to Day 0, reaching 287 N. Torque increased by 50% between days 28 and 56 reaching ~80 Ncm, indicating that newly formed bone that had reached the implant was mature enough to have a measurable mechanical effect. The tendency towards an increase from the 8-week time point indicate that

the material is being remodelled and replaced by bone which is also confirmed by the histological images. These findings parallel previous works indicating that stable ISQ values and increasing pull-out forces are indicative of positive bone-implant interactions, which is fundamental for the long-term success of dental implants [214]. Furthermore, long-term stability throughout a 12-month follow-up period was achieved when tetracalcium phosphate (61.5% w/w of solids), phosphoserine (38.5% w/w of solids), and water was used as adhesive formulation [248].

Additionally histological images showed bone infiltrated the PM-CPC adhesive and new bone grew into and through the material implanted without detectable gaps or voids, further confirming the adhesive's suitability in a clinical setting. These positive outcomes not only reflect the potential of PM-CPC adhesives to replace traditional options but also highlight their role in advancing minimally invasive surgical techniques. The PM-CPC adhesives offer a balance of biocompatibility and mechanical integrity necessary for successful dental and orthopaedic implant surgeries. However, some data showed that when non-erupted wisdom tooth was impacted during the preparation of the socket the PDL was often found to have proliferated to fill the space between the bone and the adhesive, which resulted in no direct contact between adhesive and bone and, therefore, non-optimal mechanical stabilisation.

While the *in vivo* study provided valuable insights into the stabilisation capabilities of PM-CPC adhesive in a live model, it is important to note the limitation due to the absence of a control group. Without comparing the outcomes against a baseline or control—such as non-augmented implant, bones treated with a different adhesive, or a placebo—the results lack a point of reference to contextualise the efficacy of PM-CPC adhesive. This makes it challenging to draw definitive conclusions about the material's performance, as the observed improvements cannot be definitively attributed to the adhesive without comparative data. Future studies would benefit from including a control to fully understand the adhesive's

relative effectiveness. Also, quantitative analysis, possibly with higher resolution or cross-sectional images, would be necessary to make a more definitive assessment, including the determination of the bone volume present and the degree of osseointegration.

5.6. Conclusion

These *in vitro* and *in vivo* studies have provided pivotal insights into the potential of PM-CPC in dental implantology, demonstrating its promising properties in cytocompatibility, and mechanical stability compared to HydroSet and α -TCP cements. Key findings include the differential cellular sensitivity between MC3T3-E1 and MSC cell lines, emphasising the importance of a diverse cellular approach in evaluating biocompatibility. Remarkably, PM-CPC formulations, demonstrated superior cytocompatibility across both cell types, reinforcing α -TCP's potential as a preferred material for bone regeneration. The incorporation of phosphoserine and calcium silicate in PM-CPC adhesive led to significant enhancements in cell viability and proliferation, highlighting a promising strategy for optimising biological performance of bone cements. Additionally, the study underscored the crucial role of the curing process in ensuring material biocompatibility and highlighted the consistent performance of both hand-mixed and dual syringe-mixed PM-CPC adhesives. Significant cell proliferation observed from Day 14 and consistent ISQ values alongside increased pull-out forces, point towards positive bone-implant interactions and long-term implant success. Furthermore, histological analysis demonstrated new bone formation and adhesive resorption with sufficient contact between implant adhesives. Overall, the data show that if the ingrowth of soft connective tissues is prevented, the material is a promising candidate for providing primary stability to non-stable dental implants.

**Chapter 6: Overall Discussion,
Concluding Remarks and Future
Perspectives**

6.1. Overall Discussion

CPCs are considered highly attractive for orthopaedic and dental applications due to their ease of moulding, osteoconductive and natural biodegradability, however they still lack mechanical integrity and injectability [11,172,181,336]. To align with bone's mechanical strength and promote bioactivity, CPCs are frequently enhanced with organic and inorganic additives [337–339]. Innovations in this area include adhesives inspired by nature, known as biomimetic adhesives. These are particularly promising because they work well in wet environments, which is crucial for stabilising and repairing bone tissue in engineering applications. The development of an effective bone adhesives wide ranging potential applications, avoiding the complications associated with metal hardware, offering surgical efficiency and enhanced patient safety [16,151].

This research specifically focuses on a bioinspired adhesive, using phosphorylated amino acids to improve the characteristics of calcium phosphate-based adhesives. The thesis aims to design, characterise, and evaluate a PM-CPC, targeting the unmet clinical need for a bone adhesive that provides substantial and instant fragment stability and suitable mechanical properties under wet environment. Within this chapter, the key findings of this thesis are presented.

1. Synthesis of a highly pure α -TCP powder with different sizes: A range of α -TCP powders were successfully and repeatably synthesized using heat treatment followed by rapid quenching with compressed air. This controlled-rate fabrication technique allowed for the synthesis of a highly pure powder of 100% α -TCP phase with an irregular non-spherical shape (0.35 ± 0.2). According to literature, the phase purity is crucial for biocompatibility and functionality in clinical applications, thus mitigating the risk of implant failure [340–342]. The resultant powder obtained a variety of particle sizes presenting the effect of grinding

cycles on the particle size distribution as observed from previous studies on calcium phosphate powders [13,343,344]. Furthermore, a negative zeta potential (-17.1 ± 3.0) was obtained, which has been reported to be an important property for effective cell adhesion and bone formation [345,346].

2. In-depth understanding of the individual factors on the final properties of PM-CPC

adhesive: The DoE approach was used to analyse and understand the influence of each component as well as of the α -TCP particle size, identifying α -TCP particle size, LPR and amount of phosphoserine as significant factors influencing both handling and mechanical properties of the adhesive. The number of grinding cycles had a significant impact on the setting behaviour of PM-CPC. Particle sizes with a $D_{50} < 11.7 \pm 1.5 \mu\text{m}$ led to faster setting times, which can be beneficial for quick surgical procedures. Conversely, the D_{50} values of the particle sizes closer to $25.3 \pm 0.7 \mu\text{m}$, due to slower setting may be more appropriate for clinical scenarios that need longer working times. The LPR had the highest contribution ($p\text{-value} < 0.001$) to handling and mechanical properties. However, improvements in compressive strength negatively affected handling properties due to increased porosity from higher water content. In addition, this study presented a non-linear relationship between phosphoserine content and mechanical properties, indicating a threshold concentration for phosphoserine that maximises adhesive strength without compromising other properties [347]. Optimisation of the PM-CPC adhesive was then carried out using the DoE models to identify the optimal PM-CPC composition for clinical use, guided by the following criteria: initial setting time (t_i) ≥ 60 s, final setting time (t_f) ≤ 200 s, compression strength ≥ 10 MPa [225], and bond strength ≥ 2.5 MPa [12]. Inputs from the orthopaedic surgical community were sought to establish clinically relevant setting times (t_i and t_f) that would facilitate rapid setting, achieve the required fragment stability and prevent adhesive leakage [226]. These

setting times were considered as the most important responses in the optimisation process. Experimental validation has shown that these models are both accurate and reliable. They enhance efficiency and adaptability by allowing for the assessment of many variables at once. This approach also quickly indicates the most important factors and their best levels, requiring fewer tests than conventional methods.

Overall, this is considered a pivotal study in this as it advanced knowledge about how the composition of PM-CPC adhesives affects their performance in wet conditions for bone healing, contributing new insights to existing research. Presently, research on phosphoserine-based adhesives primarily examines the properties of a single composition, which restricts the range of application sites [152,332,348]. By varying the composition and particle size distribution of the ceramic powder, a broader spectrum of uses could be achieved. The development of the BBD for factorial analysis not only clarifies the impact of each separate factor but also provides a reusable framework. This allows for various numerical optimisation studies to be conducted, adapting to new clinical needs based on the specific site of application, in order to create an appropriate PM-CPC adhesive composition.

3. Development of an optimal hand-mixed PM-CPC adhesive composition suitable for clinical bone defect repair: The study identified that the optimal PM-CPC composition can achieve a homogenous mixture within 20 s, regardless of the batch size underscoring the adhesive's reliability. The setting times for the PM-CPC adhesive ranged from 2.5-3.5 min. The findings of this study highlight the efficacy of PM-CPC in providing rapid setting times, which is critical for time-sensitive surgical procedures such as bone fracture and implant stabilisation. This timeframe for setting achieved by the incorporation of phosphoserine, meets the immediate needs of surgical intervention.

The homogeneous mixing capability, consistent handling and mechanical properties of PM-CPC, regardless of batch size, ensures that biomaterials can be scaled up for widespread clinical use without compromising quality. The successful application in wet conditions and the controlled degradation that aligns with the natural bone healing timeline extend the material's applicability to a range of clinical scenarios, from dental to orthopaedic applications. The slow degradation rate of PM-CPC, combined with its resistance to washout, provides insights into the design of materials that offer initial stability and gradually transfer load to regenerating tissue.

PM-CPC adhesive significantly improved the mechanical stability of both dental and orthopaedic implants, as evidenced by pull-out and removal torque testing. The results demonstrated that PM-CPC could enhance the bond strength between implants and bone, a crucial factor for the success of surgical interventions. Under wet-field conditions, all femoral bone samples withstood forces > 50 N before fracture, with a maximum load of 100 N recorded. This provides significantly higher bonding compared to other commercially available cements [261]. The adhesive significantly improved the bonding strength of implants, as evidenced by pull-out and removal torque testing [214], while the presence of blood during the implant procedure did not compromise the effectiveness of PM-CPC adhesive, indicating its robust performance in realistic surgical scenarios. In summary, the study concludes that PM-CPC, exhibits excellent mechanical and adhesive properties, stability, and bioactivity, making it a highly suitable adhesive for clinical applications in orthopaedics and dentistry.

4. Development of a dual-syringe mixed PM-CPC adhesive with suitable setting, mechanical, and adhesion properties for clinical bone defect repair:

On a broader scientific scale, the shift from manual to on-demand mixing and delivery techniques for PM-CPC adhesive, as suggested by the research, progress the movement in the biomedical sciences toward precision medicine and minimally invasive procedures [211,262,275]. Such innovations are vital not only for improving patient outcomes, but also for advancing the current scientific methodologies and biomedical engineering techniques. As highlighted previously a rapid setting time was identified as being clinically preferable for the PM-CPC adhesive as it enables rapid fixation and stabilisation. However, this rapid setting time poses challenges relating to its injectability, particularly when being mixed by hand. A dual-syringe system was developed ensuring precise, on-demand mixing and delivery of PM-CPC adhesive, allowing for a more accurate and less invasive application during surgical procedures.

For the development of this injectable dual component syringe mixed adhesive Koliphor oil was used as gelling agent in each component. Initially an optimal balance was achieved between the oil/powder ratio to ensure stability, prevent phase separation, and maintain injectability and viscosity over time, which is crucial for its clinical applicability. With this new system, the PM-CPC adhesive maintains its beneficial properties, such as injectability and phase stability, over extended periods (48 weeks), indicating its suitability for clinical use. For the scientific community, this work provides insights into the design of advanced biomedical materials, emphasising the importance of injectability, stability, and mechanical strength in developing effective bone adhesives.

The adhesive also demonstrates robust mechanical strength and the ability to adhere bones or to enhance orthopaedic and dental implant stability in wet conditions, providing a practical solution for surgical applications. Another observation was that the dual-syringe mixed PM-CPC adhesive exhibited smaller standard deviations in mechanical and adhesion property measurements. This consistency is important because it ensures predictable and reliable

performance, essential in clinical applications where precision and reproducibility are needed. In the context of current hand-mixed adhesives, which can show significant variability in properties due to human error during mixing, the dual-syringe system provides an improvement. The reduced variability ensures that surgeons can depend on the adhesive's performance during procedures, minimising the risk of failure due to the material's inconsistencies. For the scientific community, this advancement provides a clear pathway to refining the standardisation of biomedical materials, which can lead to more uniform outcomes in clinical trials and, eventually, in clinical practice. The impact of this finding extends beyond the operating room; by ensuring uniformity and reliability, such systems can greatly contribute to the evolution of surgical techniques and the development of next-generation biomaterials.

5. *In vitro* and *in vivo* evaluation of the PM-CPC adhesive, investigating its biocompatibility and efficacy as a bioadhesive for implant stabilisation and bone repair:

The fifth chapter of the thesis presents an investigation into the performance of the PM-CPC adhesive, focusing on its biocompatibility and potential for clinical applications in bone repair and implant stabilisation. The study explores the adhesive's cytocompatibility, and mechanical stability, providing an in-depth understanding of how this material interacts with biological tissues both *in vitro* and *in vivo*.

The PM-CPC adhesive has shown promising results regarding cell viability, significantly better than bone cements like HydroSet and α -TCP. The incorporation of phosphoserine into the adhesive's formula enhances its biological performance significantly, which is evidenced by the cell proliferation outcomes from alamarBlue assays. Furthermore, significant cell proliferation over time was observed, particularly after 14 days, suggesting the material's suitability for long-term bone regeneration.

Mechanical characterisation *in vivo* has demonstrated that the PM-CPC adhesive can effectively stabilise implants within trabecular bone. This was observed over an 8-week period, during which the adhesive's bond strength with the bone increased, indicating ongoing osseointegration. Histological assessments further supported these findings, showing new bone formation at the material-bone interface, which is indicative of the adhesive's pronounced osteoconductivity and biocompatibility. When positioned against the existing literature, the PM-CPC adhesive represents a considerable step forward in bioadhesive technology. The innovative addition of phosphoserine to the cement matrix not only improves its physical properties but also appears to actively support cellular viability and proliferation, which are critical for tissue integration.

The research conducted enhances existing knowledge by demonstrating the multifaceted advantages of the PM-CPC adhesive, from its ease of handling and robust mechanical attributes to its supportive role in biological processes essential for bone healing.

6.2. Concluding Remarks

This research thesis has fabricated and characterised a range of phosphoserine-modified calcium phosphate adhesives aiming to develop an optimal formulation that not only aligns with the mechanical strength and bioactivity of natural bone but also overcomes the limitations of current cements in terms of mechanical integrity and injectability.

The synthesis of a highly pure α -TCP powder with controlled particle sizes marked the first step towards achieving this goal ensuring biocompatibility and functionality. Furthermore, an in-depth understanding was achieved of how PM-CPC adhesive composition and particle size can influence the adhesive's handling and mechanical properties, leading to the identification of the optimal PM-CPC composition. In particular, this optimal composition demonstrated rapid setting times and high adhesion forces, regardless of batch size, ensuring its scalability and reliability for clinical use. Moreover, the adhesive's performance in wet conditions and

its controlled degradation aligned with the natural bone healing timeline, extending its applicability across various clinical scenarios. A significant step and achievement was the development of a dual-syringe mixed PM-CPC adhesive without significantly affecting the handling and mechanical properties even if a gelling agent was added. The *in vitro* and *in vivo* evaluations of the PM-CPC adhesive further established its biocompatibility and efficacy as a bioadhesive for implant stabilisation and bone repair. The adhesive showed promising results in cell viability and mechanical stability, indicating its potential as a promising candidate and alternative to existing bone cements.

Overall, this research has successfully achieved its objectives by developing a PM-CPC adhesive that offers mechanical stability, biocompatibility, and ease of use. The findings from this research contribute valuable knowledge to the scientific community, offering new perspectives on the design, optimisation, and application of bioinspired adhesives.

6.3. Future Perspectives

Building upon the current research on the PM-CPC adhesive, several key areas of future work stand out as essential to providing a comprehensive understanding of this innovative material and to achieve the full potential of the study:

Development of the optimal dual-syringe system for on-demand mixing and precise delivery of the PM-CPC adhesive.

While the dual syringe-mixed PM-CPC adhesive was effective for the application, there is a need to further refine and optimise this dual-syringe delivery mechanism. Future work could focus on enhancing the precision, control, and ease of use of the delivery system, potentially through automation or the integration of smart technologies that can adjust to the varying conditions of surgical procedures.

Assessment of long-term stability and effects of product sterilisation in terms of physicochemical, rheological, setting, mechanical and degradation properties.

This evaluation includes a detailed analysis of the physicochemical properties to ensure that the optimal composition and structure of the adhesive are maintained over extended periods, especially after sterilisation processes. For instance, rheological properties, after sterilisation and long-term storage, need to be investigated since they are related to the ease and consistency of application during surgical procedures. Additionally, the setting and mechanical properties to ensure that the adhesive's curing time and strength remains optimal for clinical use even after undergoing sterilisation, ensuring reliable performance in bone repair and implant stabilisation. Finally, the degradation properties can be assessed to confirm that the adhesive degrades at a controlled rate, aligning with the natural bone healing timeline, and does not undergo any adverse changes.

Investigate *in vitro* and *in vivo* proprieties in terms of osteoconductive properties.

Future research can be focused deeply into investigating the osteoconductive properties of the optimal hand-mixed and dual syringe-mixed PM-CPC adhesive, both *in vitro* and *in vivo*. This comprehensive approach can lead to a deeper understanding of how the adhesive supports and facilitates bone growth under various conditions. From the *in vitro* study the adhesive's ability to create a conducive environment for bone cell growth can be identified. This aspect of research is crucial for understanding the bioactive properties of the adhesive and its potential to enhance bone formation at the cellular level.

In vivo assessments of the optimal PM-CPC adhesive need to be conducted in fracture models in animals such as rabbits or rats, closely mirroring human bone fractures. This will enable an in-depth evaluation of the adhesive's ability to aid in bone healing and integration. To validate its efficacy, the adhesive can be benchmarked against the current gold standard

treatments, such as clinically established bone cements or fixation methods, in these models. The study needs to include both negative controls (untreated fractures or those treated with inert materials) and positive controls (fractures treated with standard methods), providing a comprehensive comparison. This approach aims to establish the adhesive as a viable alternative for fracture management, focusing on its potential benefits over existing therapies in terms of healing efficiency and patient outcomes.

Bibliography

- [1] Wu, et al., Global, regional, and national burden of bone fractures in 204 countries and territories, 1990–2019: a systematic analysis from the Global Burden of Disease Study 2019, *Lancet Heal. Longev.* 2 (2021) e580–e592.
- [2] H.S. Gupta, P. Zioupos, Fracture of bone tissue: The “hows” and the “whys,” *Med. Eng. Phys.* 30 (2008) 1209–1226. <https://doi.org/10.1016/j.medengphy.2008.09.007>.
- [3] T.J. de Villiers, S.R. Goldstein, Bone health 2022: an update, *Climacteric.* 25 (2022) 1–3. <https://doi.org/10.1080/13697137.2021.1965408>.
- [4] W.J. Metsemakers, B. Smeets, S. Nijs, H. Hoekstra, Infection after fracture fixation of the tibia: Analysis of healthcare utilization and related costs, *Injury.* 48 (2017) 1204–1210. <https://doi.org/10.1016/j.injury.2017.03.030>.
- [5] D.S. Elliott, K.J.H. Newman, D.P. Forward, D.M. Hahn, B. Ollivere, K. Kojima, R. Handley, N.D. Rossiter, J.J. Wixted, R.M. Smith, C.G. Moran, A unified theory of bone healing and nonunion, *Bone Jt. J.* 98B (2016) 884–891. <https://doi.org/10.1302/0301-620X.98B7.36061>.
- [6] H.K. Uthoff, P. Poitras, D.S. Backman, Internal plate fixation of fractures: Short history and recent developments, *J. Orthop. Sci.* 11 (2006) 118–126. <https://doi.org/10.1007/s00776-005-0984-7>.
- [7] M.S. Tonetti, S. Jepsen, L. Jin, J. Otomo-Corgel, Impact of the global burden of periodontal diseases on health, nutrition and wellbeing of mankind: A call for global action, *J. Clin. Periodontol.* 44 (2017) 456–462. <https://doi.org/10.1111/jcpe.12732>.
- [8] E.J. Law, H. Taib, Z. Berahim, Amniotic Membrane: An Approach to Periodontal Regeneration, *Cureus.* 14 (2022). <https://doi.org/10.7759/cureus.27832>.
- [9] R. Di Tinco, G. Bertani, A. Pisciotta, L. Bertoni, J. Bertacchini, B. Colombari, E. Conserva, E. Blasi, U. Consolo, G. Carnevale, Evaluation of antimicrobial effect of air-polishing treatments and their influence on human dental pulp stem cells seeded on titanium disks, *Int. J. Mol. Sci.* 22 (2021) 1–15. <https://doi.org/10.3390/ijms22020865>.
- [10] S. Piglionico, J. Bousquet, N. Fatima, M. Renaud, P.Y. Collart-dutilleul, P. Bousquet, Porous tantalum vs. Titanium implants: Enhanced mineralized matrix formation after stem cells proliferation and differentiation, *J. Clin. Med.* 9 (2020) 1–15.

<https://doi.org/10.3390/jcm9113657>.

- [11] H.H.K. Xu, P. Wang, L. Wang, C. Bao, Q. Chen, M.D. Weir, L.C. Chow, L. Zhao, X. Zhou, M.A. Reynolds, Calcium phosphate cements for bone engineering and their biological properties, *Bone Res.* (2017). <https://doi.org/10.1038/boneres.2017.56>.
- [12] K.O. Böker, K. Richter, K. Jäckle, S. Taheri, I. Grunwald, K. Borchering, J. von Byern, A. Hartwig, B. Wildemann, A.F. Schilling, W. Lehmann, Current state of bone adhesives-Necessities and hurdles, *Materials (Basel)*. 12 (2019) 1–19. <https://doi.org/10.3390/ma12233975>.
- [13] V. Jack, F.J. Buchanan, N.J. Dunne, Particle attrition of α -tricalcium phosphate: Effect on mechanical, handling, and injectability properties of calcium phosphate cements, *Proc. Inst. Mech. Eng. Part H J. Eng. Med.* (2008). <https://doi.org/10.1243/09544119JEIM312>.
- [14] G. Lewis, Properties of acrylic bone cement: State of the art review, *J. Biomed. Mater. Res.* (1997). [https://doi.org/10.1002/\(SICI\)1097-4636\(199722\)38:2<155::AID-JBM10>3.0.CO;2-C](https://doi.org/10.1002/(SICI)1097-4636(199722)38:2<155::AID-JBM10>3.0.CO;2-C).
- [15] G. Lewis, Alternative acrylic bone cement formulations for cemented arthroplasties: Present status, key issues, and future prospects, *J. Biomed. Mater. Res. - Part B Appl. Biomater.* 84 (2008) 301–319. <https://doi.org/10.1002/jbm.b.30873>.
- [16] A. Tzagiollari, H.O. McCarthy, T.J. Levingstone, N.J. Dunne, Biodegradable and Biocompatible Adhesives for the Effective Stabilisation, Repair and Regeneration of Bone, *Bioengineering*. 9 (2022) 250. <https://doi.org/10.3390/bioengineering9060250>.
- [17] Z. Wang, Z. Xu, W. Zhao, N. Sahai, A potential mechanism for amino acid-controlled crystal growth of hydroxyapatite, *J. Mater. Chem. B*. 3 (2015) 9157–9167. <https://doi.org/10.1039/c5tb01036e>.
- [18] F. Manoli, J. Kanakis, P. Malkaj, E. Dalas, The effect of aminoacids on the crystal growth of calcium carbonate, *J. Cryst. Growth*. 236 (2002) 363–370. [https://doi.org/10.1016/S0022-0248\(01\)02164-9](https://doi.org/10.1016/S0022-0248(01)02164-9).
- [19] R.K. Fuchs, W.R. Thompson, S.J. Warden, *Bone biology*, Second Edi, Elsevier Ltd, 2018. <https://doi.org/10.1016/B978-0-08-102451-5.00002-0>.
- [20] H. Fonseca, D. Moreira-Gonçalves, H.J.A. Coriolano, J.A. Duarte, *Bone quality: The*

- determinants of bone strength and fragility, *Sport. Med.* 44 (2014) 37–53. <https://doi.org/10.1007/s40279-013-0100-7>.
- [21] M. Cardinale, R. Newton, K. Nosaka, *Strength and Conditioning: Biological Principles and Practical Applications*, John Wiley Sons. (2011) 179–192.
- [22] R.O. Ritchie, M.J. Buehler, P. Hansma, Plasticity and toughness in bone, *Phys. Today.* (2009) 41–47.
- [23] N.H. Hart, R.U. Newton, J. Tan, T. Rantalainen, P. Chivers, A. Siafarikas, S. Nimphius, Biological basis of bone strength: Anatomy, physiology and measurement, *J. Musculoskelet. Neuronal Interact.* 20 (2020) 347–371.
- [24] B. Clarke, Normal bone anatomy and physiology., *Clin. J. Am. Soc. Nephrol.* 3 Suppl 3 (2008) 131–139. <https://doi.org/10.2215/CJN.04151206>.
- [25] A. Singh, A. Mehdi, R. Srivastava, N. Verma, Immunoregulation of bone remodelling, *Int. J. Crit. Illn. Inj. Sci.* 2 (2012) 75. <https://doi.org/10.4103/2229-5151.97271>.
- [26] J.C. Crockett, M.J. Rogers, F.P. Coxon, L.J. Hocking, M.H. Helfrich, Bone remodelling at a glance, *J. Cell Sci.* 124 (2011) 991–998. <https://doi.org/10.1242/jcs.063032>.
- [27] E.F. Eriksen, Cellular mechanisms of bone remodeling, *Rev. Endocr. Metab. Disord.* 11 (2010) 219–227. <https://doi.org/10.1007/s11154-010-9153-1>.
- [28] E.N.E. Marieb, K. Hoehn, *Human Anatomy & Physiology*, Ninth Edition, 2006.
- [29] P. Augat, S. Schorlemmer, The role of cortical bone and its microstructure in bone strength, *Age Ageing.* 35 (2006) 27–31. <https://doi.org/10.1093/ageing/afl081>.
- [30] D. Carnelli, P. Vena, M. Dao, C. Ortiz, R. Contro, Orientation and size-dependent mechanical modulation within individual secondary osteons in cortical bone tissue, *J. R. Soc. Interface.* 10 (2013). <https://doi.org/10.1098/rsif.2012.0953>.
- [31] A.G. Robling, A.B. Castillo, C.H. Turner, Biomechanical and molecular regulation of bone remodeling, *Annu. Rev. Biomed. Eng.* 8 (2006) 455–498. <https://doi.org/10.1146/annurev.bioeng.8.061505.095721>.
- [32] G. Zhu, T. Zhang, M. Chen, K. Yao, X. Huang, B. Zhang, Y. Li, J. Liu, Y. Wang, Z. Zhao, Bone physiological microenvironment and healing mechanism: Basis for future

- bone-tissue engineering scaffolds, *Bioact. Mater.* 6 (2021) 4110–4140. <https://doi.org/10.1016/j.bioactmat.2021.03.043>.
- [33] E.F. Morgan, G.U. Unnikrisnan, A.I. Hussein, Bone Mechanical Properties in Healthy and Diseased States, *Annu. Rev. Biomed. Eng.* 20 (2018) 119–143. <https://doi.org/10.1146/annurev-bioeng-062117-121139>.
- [34] S. Amin, S.J. Achenbach, E.J. Atkinson, S. Khosla, L.J. Melton, Trends in fracture incidence: A population-based study over 20 years, *J. Bone Miner. Res.* 29 (2014) 581–589. <https://doi.org/10.1002/jbmr.2072>.
- [35] K.A. Alswat, Gender Disparities in Osteoporosis, *J. Clin. Med. Res.* 9 (2017) 382–387. <https://doi.org/10.14740/jocmr2970w>.
- [36] C.H. Turner, M.R. Forwood, J. -Y Rho, T. Yoshikawa, Mechanical loading thresholds for lamellar and woven bone formation, *J. Bone Miner. Res.* 9 (1994) 87–97. <https://doi.org/10.1002/jbmr.5650090113>.
- [37] I. Sevostianov, M. Kachanov, Impact of the porous microstructure on the overall elastic properties of the osteonal cortical bone, *J. Biomech.* 33 (2000) 881–888. [https://doi.org/10.1016/S0021-9290\(00\)00031-2](https://doi.org/10.1016/S0021-9290(00)00031-2).
- [38] [Boston Medical and Surgical Journal 2006-may 25 vol. 354 iss. 21] Seeman, Ego_Delmas, Pierre D. - Bone Quality — The Material and Structural Basis of Bone Strength and Fragility (2006) [10.1056_nejmra053077] - .pdf, (n.d.).
- [39] R. Florencio-Silva, G.R.D.S. Sasso, E. Sasso-Cerri, M.J. Simões, P.S. Cerri, Biology of Bone Tissue: Structure, Function, and Factors That Influence Bone Cells, *Biomed Res. Int.* 2015 (2015). <https://doi.org/10.1155/2015/421746>.
- [40] M.S. Rahman, N. Akhtar, H.M. Jamil, R.S. Banik, S.M. Asaduzzaman, TGF- β /BMP signaling and other molecular events: Regulation of osteoblastogenesis and bone formation, *Bone Res.* 3 (2015). <https://doi.org/10.1038/boneres.2015.5>.
- [41] A.M.F.S. Mohamed, An overview of bone cells and their regulating factors of differentiation, *Malaysian J. Med. Sci.* 15 (2008) 4–12.
- [42] M. Ehlinger, H. Favreau, D. Eichler, P. Adam, F. Bonnomet, Early mechanical complications following fixation of proximal femur fractures: From prevention to treatment, *Orthop. Traumatol. Surg. Res.* 106 (2020) S79–S87.

<https://doi.org/10.1016/j.otsr.2019.02.027>.

- [43] S.R. Cummings, L.J. Melton, Osteoporosis I: Epidemiology and outcomes of osteoporotic fractures, *Lancet*. 359 (2002) 1761–1767. [https://doi.org/10.1016/S0140-6736\(02\)08657-9](https://doi.org/10.1016/S0140-6736(02)08657-9).
- [44] E. Hernlund, A. Svedbom, M. Ivergard, J. Compston, et al, Osteoporosis in the EU : medical management , epidemiology and economic burden. Key findings of the IOF / EFPIA EU 27 report, *Arch. Osteoporos*. 8 (2013).
- [45] D. Ring, J.B. Jupiter, Complex fractures of the distal humerus and their complications, *J. Shoulder Elb. Surg*. 8 (1999) 85–97. [https://doi.org/10.1016/S1058-2746\(99\)90063-0](https://doi.org/10.1016/S1058-2746(99)90063-0).
- [46] L. Jiang, E. Chen, L. Huang, C. Wang, Arthroscopy-Assisted Reduction Percutaneous Internal Fixation Versus Open Reduction Internal Fixation for Tibial Plateau Fracture: A Systematic Review and Meta-analysis, *Orthop. J. Sport. Med*. 9 (2021) 1–7. <https://doi.org/10.1177/23259671211027838>.
- [47] K. Malik-Tabassum, K. Pillai, Y. Hussain, S. Bleibleh, S. Babu, P. V. Giannoudis, T.H. Tosounidis, Post-operative outcomes of open reduction and internal fixation versus circular external fixation in treatment of tibial plafond fractures: A systematic review and meta-analysis, *Injury*. 51 (2020) 1448–1456. <https://doi.org/10.1016/j.injury.2020.04.056>.
- [48] K.W. Nellans, E. Kowalski, K.C. Chung, The Epidemiology of Distal Radius Fractures, *Hand Clin*. (2012). <https://doi.org/10.1016/j.hcl.2012.02.001>.
- [49] M. Muraoka, Y. Nakai, Twenty years of statistics and observation of facial bone fracture, *Acta Oto-Laryngologica, Suppl*. 6489 (1998) 261–265. <https://doi.org/10.1080/00016489850183043>.
- [50] G. Kasimova, D. Yunusov, M. Sakhibova, E. Yaxudaev, B. Batirova, Analysis of fracture of the foot bones in children according to the andijan region, *Ann. Rom. Soc. Cell Biol*. 25 (2021) 6186–6192.
- [51] S. Meena, P. Sharma, A.K. Sambharia, A. Dawar, Fractures of distal radius: an overview, *J. Fam. Med. Prim. Care*. 3 (2014) 325–332. <https://doi.org/10.4103/2249-4863.148101>.

- [52] F. Souyris, F. Klersy, P. Jammet, C. Payrot, Malar bone fractures and their sequelae, *J. Cranio-Maxillofacial Surg.* 17 (1989) 64–68. [https://doi.org/10.1016/s1010-5182\(89\)80047-2](https://doi.org/10.1016/s1010-5182(89)80047-2).
- [53] R.D. Welling, J.A. Jacobson, D.A. Jamadar, S. Chong, E.M. Caoili, P.J.L. Jebson, MDCT and radiography of wrist fractures: Radiographic sensitivity and fracture patterns, *Am. J. Roentgenol.* 190 (2008) 10–16. <https://doi.org/10.2214/AJR.07.2699>.
- [54] B. Erol, R. Tanrikulu, B. Görgün, Maxillofacial fractures. Analysis of demographic distribution and treatment in 2901 patients (25-year experience), *J. Cranio-Maxillofacial Surg.* (2004). <https://doi.org/10.1016/j.jcms.2004.04.006>.
- [55] N.J.V. Hogg, T.C. Stewart, J.E.A. Armstrong, M.J. Girotti, Epidemiology of maxillofacial injuries at trauma hospitals in Ontario, Canada, between 1992 and 1997, *J. Trauma - Inj. Infect. Crit. Care.* (2000). <https://doi.org/10.1097/00005373-200009000-00007>.
- [56] K. Hwang, S.H. You, Analysis of facial bone fractures: An 11-year study of 2,094 patients, *Indian J. Plast. Surg.* 43 (2010) 42–48. <https://doi.org/10.4103/0970-0358.63959>.
- [57] O. Johnell, J.A. Kanis, An estimate of the worldwide prevalence and disability associated with osteoporotic fractures, *Osteoporos. Int.* (2006). <https://doi.org/10.1007/s00198-006-0172-4>.
- [58] W.D. Fisher, D.L. Hamblen, Problems and pitfalls of compression fixation of long bone fractures: a review of results and complications, *Injury.* (1979). [https://doi.org/10.1016/S0020-1383\(79\)80069-8](https://doi.org/10.1016/S0020-1383(79)80069-8).
- [59] S. Larsson, Treatment of osteoporotic fractures, *Scand. J. Surg.* (2002). <https://doi.org/10.1177/145749690209100202>.
- [60] L.T. Xue X., Yan S., Cai X., Shi M., Intramedullary nailing versus plating for extra-articular distal tibial metaphyseal fracture: A systematic review and meta-analysis, *Injury.* (2014).
- [61] A. Misra, R. Kapur, N. Maffulli, Complex proximal humeral fractures in adults- A systematic review of management, *Injury.* 32 (2001) 363–372. [https://doi.org/10.1016/S0020-1383\(00\)00242-4](https://doi.org/10.1016/S0020-1383(00)00242-4).

- [62] T.K. Kovach, A.S. Dighe, P.I. Lobo, Q. Cui, Interactions between MSCs and Immune Cells.pdf, *J. Immunol. Res.* 2015 (2015).
- [63] C.S. Bahney, R.L. Zondervan, P. Allison, A. Theologis, J.W. Ashley, J. Ahn, T. Miclau, R.S. Marcucio, K.D. Hankenson, Cellular biology of fracture healing, *J. Orthop. Res.* 37 (2019) 35–50. <https://doi.org/10.1002/jor.24170>.
- [64] M.B. Mucha, Peter; Farnell, Analysis of Pelvic Fracture Management, (1984) *The Journal of Trauma Injury Infection and Critica.*
- [65] V. Hallett H. Mathews, Richmond, Method for Subcutaneous Suprafascial Pedicular Internal Fixaton, (1992).
- [66] S.W. Mardam-Bey, D.L. Bernholt, L. Bogunovic, R.W. Wright, Treatment of Tibial Eminence Fractures, Second Edi, Elsevier, 2018. <https://doi.org/10.1016/B978-0-323-38962-4.00138-7>.
- [67] J. Aginsky, Intramedullary Compression Nail for the Treatment of Bone Fractures, (1978) 2–6.
- [68] D.E. Murphy, Charles P., D. Ambrosia, Robert D., “Complex Fe”, *The Journal of Trauma Injury Infection and Critical Care* Volume 28 issue 11, (1988).
- [69] K. Kang, J. Park, S. Hyoun, J.Y. Oh, Methods and Devices for Treatment of Bone Fractures, 2 (2014).
- [70] M.E. Lynch, M.C.H. Van Der Meulen, Mechanical properties of bone tissue, *Biomech. Dent. Implant. Handb. Res.* (2012) 1–20.
- [71] J.L. Berger, “Methods and device for internal fixation of bone fractures” United States Patent, 1996, *Prog. Med.* 28 (2008) 3077–3080.
- [72] A.T. Fragomen, S.R. Rozbruch, The mechanics of external fixation, *HSS J.* 3 (2007) 13–29. <https://doi.org/10.1007/s11420-006-9025-0>.
- [73] C. Collinge, R. Sanders, T. DiPasquale, Treatment of complex tibial periarticular fractures using percutaneous techniques, *Clin. Orthop. Relat. Res.* (2000) 69–77. <https://doi.org/10.1097/00003086-200006000-00009>.
- [74] S. Principles, *Complications of Fracture Repair*, 1968 (1969) 1–4.
- [75] External Fixation – Orthopedic Implants Industry, (2016).

<https://orthopedicimplantsindia.wordpress.com/2016/04/14/top-benefits-of-external-fixation/>.

- [76] Hoffmann 3 _ Stryker External Fixation System, (2018). <https://www.stryker.com/us/en/trauma-and-extremities/products/hoffmann-3-external-fixation-system.html>.
- [77] S. Saha, S. Roy, Metallic Dental Implants Wear Mechanisms, Materials, and Manufacturing Processes: A Literature Review, *Materials (Basel)*. 16 (2023) 1–33. <https://doi.org/10.3390/ma16010161>.
- [78] H.A. Bulaqi, M. Mousavi Mashhadi, F. Geramipناه, H. Safari, M. Paknejad, Effect of the coefficient of friction and tightening speed on the preload induced at the dental implant complex with the finite element method, *J. Prosthet. Dent.* 113 (2015) 405–411. <https://doi.org/10.1016/j.prosdent.2014.09.021>.
- [79] D. Burtscher, D. Dalla Torre, Dental implant procedures in immunosuppressed organ transplant patients: a systematic review, *Int. J. Oral Maxillofac. Surg.* 51 (2022) 380–387. <https://doi.org/10.1016/j.ijom.2021.06.008>.
- [80] T.M. Smith, Current Trends in Dental Morphology Research, *J Korean Assoc Oral Maxillofac Surg.* (2014) 50–60.
- [81] J.H. Lee, V. Frias, K.W. Lee, R.F. Wright, Effect of implant size and shape on implant success rates: A literature review, *J. Prosthet. Dent.* 94 (2005) 377–381. <https://doi.org/10.1016/j.prosdent.2005.04.018>.
- [82] S. Winkler, H.F. Morris, S. Ochi, Implant survival to 36 months as related to length and diameter., *Ann. Periodontol.* 5 (2000) 22–31. <https://doi.org/10.1902/annals.2000.5.1.22>.
- [83] C.J. Ivanoff, K. Gröndahl, L. Sennerby, C. Bergström, U. Lekholm, Influence of variations in implant diameters: a 3- to 5-year retrospective clinical report., *Int. J. Oral Maxillofac. Implants.* 14 (2023) 173–80. <http://www.ncbi.nlm.nih.gov/pubmed/10212533>.
- [84] J. Bumgardner, G. Boring, R. Cooper, C. Gao, S. Givaruangswat, Preliminary Evaluation of a new Dental Implant Design in Canine Models, *J. Penelit. Pendidik. Guru Sekol. Dasar.* 6 (2016) 128.

- [85] L.I. Linkow, S. Winkler, M. Shulman, L.D. Carlo, M.E. Pasqualini, F. Rossi, M. Nardone, A new look at the blade implant, *J. Oral Implantol.* 42 (2016) 373–380. <https://doi.org/10.1563/aaid-joi-D-16-00015>.
- [86] H.W. Jang, J.K. Kang, K. Lee, Y.S. Lee, P.K. Park, A retrospective study on related factors affecting the survival rate of dental implants, *J. Adv. Prosthodont.* 3 (2011) 204–215. <https://doi.org/10.4047/jap.2011.3.4.204>.
- [87] F. Javed, H. Ahmed, R. Crespi, G. Romanos, Role of primary stability for successful osseointegration of dental implants: Factors of influence and evaluation, *Interv. Med. Appl. Sci.* 5 (2013) 162–167. <https://doi.org/10.1556/IMAS.5.2013.4.3>.
- [88] A.A.H. Alzahrani, B.J. Gibson, Scoping review of the role of shared decision making in dental implant consultations, *JDR Clin. Transl. Res.* 3 (2018) 130–140. <https://doi.org/10.1177/2380084418761340>.
- [89] J.M.C. Lima, L.C. Anami, R.M. Araujo, C.A. Pavanelli, Removable partial dentures: Use of rapid prototyping, *J. Prosthodont.* 23 (2014) 588–591. <https://doi.org/10.1111/jopr.12154>.
- [90] H.F. Turner, Ramus frame implant technique., *J. Am. Dent. Assoc.* 121 (1990) 418–420. <https://doi.org/10.14219/jada.archive.1990.0164>.
- [91] H.B. Bingol, J.C.M.E. Bender, J.A. Opsteen, S.C.G. Leeuwenburgh, Bone adhesive materials: From bench to bedside, *Mater. Today Bio.* 19 (2023) 100599. <https://doi.org/10.1016/j.mtbio.2023.100599>.
- [92] M.J. Sánchez-Fernández, H. Hammoudeh, R.P. Félix Lanao, M. van Erk, J.C.M. van Hest, S.C.G. Leeuwenburgh, Bone-Adhesive Materials: Clinical Requirements, Mechanisms of Action, and Future Perspective, *Adv. Mater. Interfaces.* 6 (2019) 1–11. <https://doi.org/10.1002/admi.201802021>.
- [93] A. Tzagiollari, H. Mccarthy, T. Levingstone, Bioadhesives for Bone Fracture Repair, (2019).
- [94] M.R. Norton, G.W. Kay, M.C. Brown, D.L. Cochran, Bone glue - The final frontier for fracture repair and implantable device stabilization, *Int. J. Adhes. Adhes.* 102 (2020) 102647. <https://doi.org/10.1016/j.ijadhadh.2020.102647>.
- [95] A. Kirillova, C. Kelly, N. von Windheim, K. Gall, Bioinspired Mineral-Organic

- Bioresorbable Bone Adhesive, *Adv. Healthc. Mater.* (2018). <https://doi.org/10.1002/adhm.201800467>.
- [96] C. Gao, S. Peng, P. Feng, C. Shuai, Bone biomaterials and interactions with stem cells, *Bone Res.* 5 (2017) 1–33. <https://doi.org/10.1038/boneres.2017.59>.
- [97] Z. Sheikh, S. Najeeb, Z. Khurshid, V. Verma, H. Rashid, M. Glogauer, Biodegradable materials for bone repair and tissue engineering applications, *Materials (Basel)*. 8 (2015) 5744–5794. <https://doi.org/10.3390/ma8095273>.
- [98] M. Alizadeh-Osgouei, Y. Li, C. Wen, A comprehensive review of biodegradable synthetic polymer-ceramic composites and their manufacture for biomedical applications, *Bioact. Mater.* 4 (2019) 22–36. <https://doi.org/10.1016/j.bioactmat.2018.11.003>.
- [99] A. Gardziella, R. Mueller, Phenolic Resins, *Kunststoffe, Ger. Plast.* 80 (1990) 66–68. <https://doi.org/10.4011/shikizai1937.64.710>.
- [100] M. Donkerwolcke, F. Burny, D. Muster, Tissues and bone adhesives historical aspects, *Biomaterials*. 19 (1998) 1461–1466. [https://doi.org/10.1016/S0142-9612\(98\)00059-3](https://doi.org/10.1016/S0142-9612(98)00059-3).
- [101] V. Bhagat, M.L. Becker, Degradable Adhesives for Surgery and Tissue Engineering, *Biomacromolecules*. 18 (2017) 3009–3039. <https://doi.org/10.1021/acs.biomac.7b00969>.
- [102] E. Brandeis, D. Katz, M. Silbermann, C. Zinman, A new bioadhesive for in vivo bone adhesion, *J. Mater. Sci. Mater. Med.* (1993). <https://doi.org/10.1007/BF00125591>.
- [103] K.J. Schreder, I.S. Bayer, D.J. Milner, E. Loth, I. Jasiuk, A polyurethane-based nanocomposite biocompatible bone adhesive, *J. Appl. Polym. Sci.* 127 (2013) 4974–4982. <https://doi.org/10.1002/app.38100>.
- [104] M. Pmma, A. Update, M.S. Zafar, Prosthodontic Applications of Polymethyl, *Polymers (Basel)*. 12 (2020) 1–35.
- [105] S.S. Phull, A.R. Yazdi, M. Ghert, M.R. Towler, Bone cement as a local chemotherapeutic drug delivery carrier in orthopedic oncology: A review, *J. Bone Oncol.* 26 (2021) 100345. <https://doi.org/10.1016/j.jbo.2020.100345>.
- [106] X. Cui, C. Huang, M. Zhang, C. Ruan, S. Peng, L. Li, W. Liu, T. Wang, B. Li, W.

- Huang, M.N. Rahaman, W.W. Lu, H. Pan, Enhanced osteointegration of poly(methylmethacrylate) bone cements by incorporating strontium-containing borate bioactive glass, *J. R. Soc. Interface.* 14 (2017). <https://doi.org/10.1098/rsif.2016.1057>.
- [107] K. Ishihara, N. Nakabayashi, Adhesive bone cement both to bone and metals: 4-META in MMA initiated with tri-n-butyl borane, *J. Biomed. Mater. Res.* 23 (1989) 1475–1482. <https://doi.org/10.1002/jbm.820231209>.
- [108] L. Wistlich, A. Rücker, M. Schamel, A.C. Kübler, U. Gbureck, J. Groll, A Bone Glue with Sustained Adhesion under Wet Conditions, *Adv. Healthc. Mater.* 6 (2017). <https://doi.org/10.1002/adhm.201600902>.
- [109] H. Matras, The use of fibrin sealant in oral and maxillofacial surgery, *J. Oral Maxillofac. Surg.* 40 (1982) 617–622. [https://doi.org/10.1016/0278-2391\(82\)90108-2](https://doi.org/10.1016/0278-2391(82)90108-2).
- [110] J. Keller, P.H. Jørgensen, Fixation of osteochondral fractures, (1985) 323–326.
- [111] H. Matras, Fibrin seal: The state of the art, *J. Oral Maxillofac. Surg.* 43 (1985) 605–611. [https://doi.org/10.1016/0278-2391\(85\)90129-6](https://doi.org/10.1016/0278-2391(85)90129-6).
- [112] X. Wu, J. Ren, J. Li, Fibrin glue as the cell-delivery vehicle for mesenchymal stromal cells in regenerative medicine, *Cytotherapy.* 14 (2012) 555–562. <https://doi.org/10.3109/14653249.2011.638914>.
- [113] S. Hasan, M. Weinberg, O. Khatib, L. Jazrawi, E.J. Strauss, The Effect of Platelet-rich Fibrin Matrix on Rotator Cuff Healing in a Rat Model, *Int. J. Sports Med.* 37 (2015) 36–42. <https://doi.org/10.1055/s-0035-1554637>.
- [114] P. Bösch, F. Lintner, H. Arbes, G. Brand, Experimental investigations of the effect of the fibrin adhesive on the Kiel heterologous bone graft, *Arch. Orthop. Trauma. Surg.* 96 (1980) 177–185. <https://doi.org/10.1007/BF00457781>.
- [115] G.P. Pini Prato, P. Coltellini, G. Agudio, C. Clauser, Human Fibrin Glue Versus Sutures in Periodontal Surgery, *J. Periodontol.* 58 (1987) 426–431. <https://doi.org/10.1902/jop.1987.58.6.426>.
- [116] G. Giannini, V. Mauro, T. Agostino, B. Gianfranco, Use of autologous fibrin-platelet glue and bone fragments in maxillofacial surgery, *Transfus. Apher. Sci.* 30 (2004) 139–144. <https://doi.org/10.1016/j.transci.2003.11.009>.

- [117] A. Khodakaram-Tafti, D. Mehrabani, H. Shaterzadeh-Yazdi, An overview on autologous fibrin glue in bone tissue engineering of maxillofacial surgery, *Dent. Res. J. (Isfahan)*. 14 (2017) 79–86. <https://doi.org/10.4103/1735-3327.205789>.
- [118] X. Liu, M. Pujari-Palmer, D. Wenner, P. Procter, G. Insley, H. Engqvist, Adhesive cements that bond soft tissue ex vivo, *Materials (Basel)*. 12 (2019) 1–13. <https://doi.org/10.3390/ma12152473>.
- [119] G. Hulsart-Billström, C. Stelzl, P. Procter, M. Pujari-Palmer, G. Insley, H. Engqvist, S. Larsson, In vivo safety assessment of a bio-inspired bone adhesive, *J. Mater. Sci. Mater. Med.* 31 (2020). <https://doi.org/10.1007/s10856-020-6362-3>.
- [120] D. Le Nihouannen, A. Saffarzadeh, O. Gauthier, F. Moreau, P. Pilet, R. Spaethe, P. Layrolle, G. Daculsi, Bone tissue formation in sheep muscles induced by a biphasic calcium phosphate ceramic and fibrin glue composite, *J. Mater. Sci. Mater. Med.* 19 (2008) 667–675. <https://doi.org/10.1007/s10856-007-3206-3>.
- [121] C.V. Cassaro, L.A. Justulin, P.R. De Lima, M. De Assis Golim, N.P. Biscola, M.V. De Castro, A.L.R. De Oliveira, D.P. Doiche, E.J. Pereira, R.S. Ferreira, B. Barraviera, Fibrin biopolymer as scaffold candidate to treat bone defects in rats, *J. Venom. Anim. Toxins Incl. Trop. Dis.* 25 (2019) 1–17. <https://doi.org/10.1590/1678-9199-jvatitd-2019-0027>.
- [122] S.G. Kumbar, U.S. Toti, M. Deng, R. James, C.T. Laurencin, A. Aravamudhan, M. Harmon, D.M. Ramos, Novel mechanically competent polysaccharide scaffolds for bone tissue engineering, *Biomed. Mater.* 6 (2011). <https://doi.org/10.1088/1748-6041/6/6/065005>.
- [123] B. Hoffmann, E. Volkmer, A. Kokott, P. Augat, M. Ohnmacht, N. Sedlmayr, M. Schieker, L. Claes, W. Mutschler, G. Ziegler, Characterisation of a new bioadhesive system based on polysaccharides with the potential to be used as bone glue, *J. Mater. Sci. Mater. Med.* 20 (2009) 2001–2009. <https://doi.org/10.1007/s10856-009-3782-5>.
- [124] B.H. Choi, H. Cheong, J.S. Ahn, C. Zhou, J.J. Kwon, H.J. Cha, S.H. Jun, Engineered mussel bioglue as a functional osteoinductive binder for grafting of bone substitute particles to accelerate in vivo bone regeneration, *J. Mater. Chem. B*. 3 (2015) 546–555. <https://doi.org/10.1039/c4tb01197j>.

- [125] N.L. Millar, T.A. Bradley, N.A. Walsh, R.C. Appleyard, M.J. Tyler, G.A.C. Murrell, Frog glue enhances rotator cuff repair in a laboratory cadaveric model, *J. Shoulder Elb. Surg.* (2009). <https://doi.org/10.1016/j.jse.2008.12.007>.
- [126] D.F. Farrar, Bone adhesives for trauma surgery: A review of challenges and developments, *Int. J. Adhes. Adhes.* 33 (2012) 89–97. <https://doi.org/10.1016/j.ijadhadh.2011.11.009>.
- [127] V. Bhagat, E. O'Brien, J. Zhou, M.L. Becker, Caddisfly Inspired Phosphorylated Poly(ester urea)-Based Degradable Bone Adhesives, *Biomacromolecules.* (2016). <https://doi.org/10.1021/acs.biomac.6b00875>.
- [128] E.M. Petrie, Cyanoacrylate adhesives in surgical applications: A critical review, *Rev. Adhes. Adhes.* 2 (2014) 253–310. <https://doi.org/10.7569/RAA.2014.097306>.
- [129] U. Kandalam, A.J. Bouvier, S.B. Casas, R.L. Smith, A.M. Gallego, J.K. Rothrock, J.Y. Thompson, C.Y.C. Huang, E.J. Stelnicki, Novel bone adhesives: A comparison of bond strengths in vitro, *Int. J. Oral Maxillofac. Surg.* (2013). <https://doi.org/10.1016/j.ijom.2013.04.005>.
- [130] J.F. Kukleta, C. Freytag, M. Weber, Efficiency and safety of mesh fixation in laparoscopic inguinal hernia repair using n-butyl cyanoacrylate: Long-term biocompatibility in over 1, 300 mesh fixations, *Hernia.* 16 (2012) 153–162. <https://doi.org/10.1007/s10029-011-0887-9>.
- [131] Y.J. Lee, G.B. Jung, S. Choi, G. Lee, J.H. Kim, H.S. Son, H. Bae, H.K. Park, Biocompatibility of a novel cyanoacrylate based tissue adhesive: Cytotoxicity and biochemical property evaluation, *PLoS One.* 8 (2013). <https://doi.org/10.1371/journal.pone.0079761>.
- [132] C.F. Chen, H.H. Shen, T.Y. Lin, Y.J. Yu, W.C. Chen, I.M. Chu, Studies on the preparation and characterization of mPEG-polyester biodegradable biogluce for bone defect repair, *J. Med. Biol. Eng.* 31 (2011) 13–17. <https://doi.org/10.5405/jmbe.683>.
- [133] H. Kobayashi, S. -H Hyon, Y. Ikada, Water-curable and biodegradable prepolymers, *J. Biomed. Mater. Res.* (1991). <https://doi.org/10.1002/jbm.820251206>.
- [134] Y. Shi, P. Zhou, V. Jérôme, R. Freitag, S. Agarwal, Enzymatically Degradable Polyester-Based Adhesives, *ACS Biomater. Sci. Eng.* 1 (2015) 971–977.

<https://doi.org/10.1021/acsbiomaterials.5b00217>.

- [135] M. Arora, E.K.S. Chan, S. Gupta, A.D. Diwan, Polymethylmethacrylate bone cements and additives: A review of the literature, *World J. Orthop.* 4 (2013) 67–74. <https://doi.org/10.5312/wjo.v4.i2.67>.
- [136] U. Ali, K.J.B.A. Karim, N.A. Buang, A Review of the Properties and Applications of Poly (Methyl Methacrylate) (PMMA), *Polym. Rev.* 55 (2015) 678–705. <https://doi.org/10.1080/15583724.2015.1031377>.
- [137] A.P. Duarte, J.F. Coelho, J.C. Bordado, M.T. Cidade, M.H. Gil, Surgical adhesives: Systematic review of the main types and development forecast, *Prog. Polym. Sci.* (2012). <https://doi.org/10.1016/j.progpolymsci.2011.12.003>.
- [138] J.H. Waite, Adhesion in Byssally Attached Bivalves, *Biol. Rev.* (1983). <https://doi.org/10.1111/j.1469-185x.1983.tb00387.x>.
- [139] H.G. Silverman, F.F. Roberto, Understanding marine mussel adhesion, *Mar. Biotechnol.* (2007). <https://doi.org/10.1007/s10126-007-9053-x>.
- [140] P. Flammang, A. Lambert, P. Bailly, E. Hennebert, Polyphosphoprotein-containing marine adhesives, *J. Adhes.* 85 (2009) 447–464. <https://doi.org/10.1080/00218460902996358>.
- [141] H.J. Cha, D.S. Hwang, S. Lim, Development of bioadhesives from marine mussels, *Biotechnol. J.* 3 (2008) 631–638. <https://doi.org/10.1002/biot.200700258>.
- [142] H. Yamamoto, Bonding Strength of Synthetic Poly(amino acid)s on Metals, *Nippon KAGAKU KAISHI.* (1986). <https://doi.org/10.1246/nikkashi.1986.90>.
- [143] A. Nagai, H. Yamamoto, Insolubilizing Studies of Water-Soluble Poly(Lys Tyr) by Tyrosinase, *Bull. Chem. Soc. Jpn.* (1989). <https://doi.org/10.1246/bcsj.62.2410>.
- [144] H. Yamamoto, S. Kuno, A. Nagai, A. Nishida, S. Yamauchi, K. Ikeda, Insolubilizing and adhesive studies of water-soluble synthetic model proteins, *Int. J. Biol. Macromol.* (1990). [https://doi.org/10.1016/0141-8130\(90\)90019-7](https://doi.org/10.1016/0141-8130(90)90019-7).
- [145] H.J. Meredith, C.L. Jenkins, J.J. Wilker, Enhancing the adhesion of a biomimetic polymer yields performance rivaling commercial glues, *Adv. Funct. Mater.* (2014). <https://doi.org/10.1002/adfm.201303536>.

- [146] S. Kaur, G.M. Weerasekare, R.J. Stewart, Multiphase adhesive coacervates inspired by the sandcastle worm, *ACS Appl. Mater. Interfaces.* (2011). <https://doi.org/10.1021/am200082v>.
- [147] A. Li, M. Jia, Y. Mu, W. Jiang, X. Wan, Humid bonding with a water-soluble adhesive inspired by mussels and sandcastle worms, *Macromol. Chem. Phys.* (2015). <https://doi.org/10.1002/macp.201400513>.
- [148] M. Pujari-Palmer, H. Guo, D. Wenner, H. Autefage, C.D. Spicer, M.M. Stevens, O. Omar, P. Thomsen, M. Edén, G. Insley, P. Procter, H. Engqvist, A novel class of injectable bioceramics that glue tissues and biomaterials, *Materials (Basel)*. 11 (2018) 1–15. <https://doi.org/10.3390/ma11122492>.
- [149] M.A. Lillie, G.J. David, J.M. Gosline, Mechanical role of elastin-associated microfibrils in pig aortic elastic tissue, *Connect. Tissue Res.* (1998). <https://doi.org/10.3109/03008209809028905>.
- [150] J.L. Bystrom, M. Pujari-Palmer, Phosphoserine functionalized cements preserve metastable phases, and reprecipitate octacalcium phosphate, hydroxyapatite, dicalcium phosphate, and amorphous calcium phosphate, during degradation, in vitro, *J. Funct. Biomater.* 10 (2019). <https://doi.org/10.3390/jfb10040054>.
- [151] D.F. Farrar, Bone adhesives for trauma surgery: A review of challenges and developments, *Int. J. Adhes. Adhes.* (2012). <https://doi.org/10.1016/j.ijadhadh.2011.11.009>.
- [152] V. Bhagat, E. O'Brien, J. Zhou, M.L. Becker, Caddisfly Inspired Phosphorylated Poly(ester urea)-Based Degradable Bone Adhesives, *Biomacromolecules*. 17 (2016) 3016–3024. <https://doi.org/10.1021/acs.biomac.6b00875>.
- [153] D.S. Singh, Synthesis of Caddisfly Inspired Polyester Adhesive, (2018). http://rave.ohiolink.edu/etdc/view?acc_num=akron1523308439000894.
- [154] H. Yamamoto, A. Nagai, T. Okada, A. Nishida, Synthesis and adhesive studies of barnacle model proteins, *Mar. Chem.* (1989). [https://doi.org/10.1016/0304-4203\(89\)90038-8](https://doi.org/10.1016/0304-4203(89)90038-8).
- [155] H. Yamamoto, A. Nagai, Polypeptide models of the arthropodin protein of the barnacle *Balanus balanoides*, *Mar. Chem.* (1992). [209](https://doi.org/10.1016/0304-</p></div><div data-bbox=)

4203(92)90061-E.

- [156] J. Nishida, Y. Higaki, A. Takahara, Synthesis and characterization of barnacle adhesive mimetic towards underwater adhesion, *Chem. Lett.* (2015). <https://doi.org/10.1246/cl.150311>.
- [157] H. Fan, J. Wang, J.P. Gong, Barnacle Cement Proteins-Inspired Tough Hydrogels with Robust, Long-Lasting, and Repeatable Underwater Adhesion, *Adv. Funct. Mater.* 2009334 (2020) 1–8. <https://doi.org/10.1002/adfm.202009334>.
- [158] H. Shao, K.N. Bachus, R.J. Stewart, A water-borne adhesive modeled after the sandcastle glue of *P. californica*, *Macromol. Biosci.* 9 (2009) 464–471. <https://doi.org/10.1002/mabi.200800252>.
- [159] M.R. Norton, G.W. Kay, M.C. Brown, D.L. Cochran, Bone glue - The final frontier for fracture repair and implantable device stabilization, *Int. J. Adhes. Adhes.* 102 (2020) 102647. <https://doi.org/10.1016/j.ijadhadh.2020.102647>.
- [160] A. Kirillova, O. Nillissen, S. Liu, C. Kelly, K. Gall, Reinforcement and Fatigue of a Bioinspired Mineral–Organic Bioresorbable Bone Adhesive, *Adv. Healthc. Mater.* 10 (2021) 1–19. <https://doi.org/10.1002/adhm.202001058>.
- [161] H. Chen, Z. Xu, J. Mo, Y. Lyu, X. Tang, X. Shen, Effects of guar gum on adhesion properties of soybean protein isolate onto porcine bones, *Int. J. Adhes. Adhes.* 75 (2017) 124–131. <https://doi.org/10.1016/j.ijadhadh.2017.03.001>.
- [162] J. Liu, O.A. Scherman, Cucurbit[n]uril Supramolecular Hydrogel Networks as Tough and Healable Adhesives, *Adv. Funct. Mater.* 28 (2018) 1–6. <https://doi.org/10.1002/adfm.201800848>.
- [163] H. Liu, B. Liu, C. Gao, B. Meng, H. Yang, H. Yu, L. Yang, Injectable, biomechanically robust, biodegradable and osseointegrative bone cement for percutaneous kyphoplasty and vertebroplasty, *Int. Orthop.* 42 (2018) 125–132. <https://doi.org/10.1007/s00264-017-3674-0>.
- [164] L. Xu, S. Gao, R. Zhou, F. Zhou, Y. Qiao, D. Qiu, Bioactive Pore-Forming Bone Adhesives Facilitating Cell Ingrowth for Fracture Healing, *Adv. Mater.* 32 (2020) 1–7. <https://doi.org/10.1002/adma.201907491>.
- [165] S. Shahbazi, F. Moztarzadeh, G.M.M. Sadeghi, Y. Jafari, In vitro study of a new

- biodegradable nanocomposite based on poly propylene fumarate as bone glue, *Mater. Sci. Eng. C.* 69 (2016) 1201–1209. <https://doi.org/10.1016/j.msec.2016.08.035>.
- [166] V. Granskog, S. García-Gallego, J. von Kieseritzky, J. Rosendahl, P. Stenlund, Y. Zhang, S. Petronis, B. Lyvén, M. Arner, J. Håkansson, M. Malkoch, High-Performance Thiol–Ene Composites Unveil a New Era of Adhesives Suited for Bone Repair, *Adv. Funct. Mater.* 28 (2018) 1–10. <https://doi.org/10.1002/adfm.201800372>.
- [167] M. Erken, A. Tevlek, P. Hosseinian, B. Topuz, H.M. Aydin, Effects of ceramic particle size on cell attachment and viability in polyurethane-based bone adhesive composites, *J. Compos. Mater.* 54 (2020) 2013–2022. <https://doi.org/10.1177/0021998319884729>.
- [168] K. Lei, Q. Zhu, X. Wang, H. Xiao, Z. Zheng, In Vitro and in Vivo Characterization of a Foam-Like Polyurethane Bone Adhesive for Promoting Bone Tissue Growth, *ACS Biomater. Sci. Eng.* 5 (2019) 5489–5497. <https://doi.org/10.1021/acsbiomaterials.9b00918>.
- [169] Z. Wang, Z. Wang, W.W. Lu, W. Zhen, D. Yang, S. Peng, Novel biomaterial strategies for controlled growth factor delivery for biomedical applications, *NPG Asia Mater.* 9 (2017) e435-17. <https://doi.org/10.1038/am.2017.171>.
- [170] S. Senapati, A.K. Mahanta, S. Kumar, P. Maiti, Controlled drug delivery vehicles for cancer treatment and their performance, *Signal Transduct. Target. Ther.* 3 (2018) 1–19. <https://doi.org/10.1038/s41392-017-0004-3>.
- [171] S.N. Tammam, H.M.E. Azzazy, A. Lamprecht, Biodegradable particulate carrier formulation and tuning for targeted drug delivery, *J. Biomed. Nanotechnol.* 11 (2015) 555–577. <https://doi.org/10.1166/jbn.2015.2017>.
- [172] X. Hou, L. Zhang, Z. Zhou, X. Luo, T. Wang, X. Zhao, Calcium Phosphate-Based Biomaterials for Bone Repair, (2022).
- [173] S. Dorozhkin, Self-Setting Calcium Orthophosphate Formulations, *J. Funct. Biomater.* 4 (2013) 209–311. <https://doi.org/10.3390/jfb4040209>.
- [174] J. Jeong, J.H. Kim, J.H. Shim, N.S. Hwang, C.Y. Heo, Bioactive calcium phosphate materials and applications in bone regeneration, (2019) 1–11.
- [175] M. Prakasam, J. Locs, K. Salma-ancane, D. Loca, Fabrication , Properties and Applications of Dense Hydroxyapatite : A Review, (2015) 1099–1140.

<https://doi.org/10.3390/jfb6041099>.

- [176] I. Palmer, J. Nelson, W. Schatton, N.J. Dunne, F. Buchanan, S.A. Clarke, Biocompatibility of calcium phosphate bone cement with optimised mechanical properties: an in vivo study, *J. Mater. Sci. Mater. Med.* 27 (2016). <https://doi.org/10.1007/s10856-016-5806-2>.
- [177] M. Canillas, P. Pena, A.H. De Aza, M.A. Rodríguez, Calcium phosphates for biomedical applications, *Boletín La Soc. Española Cerámica y Vidr.* 56 (2017) 91–112. <https://doi.org/10.1016/j.bsecv.2017.05.001>.
- [178] R.M. O’Hara, J.F. Orr, F.J. Buchanan, R.K. Wilcox, D.C. Barton, N.J. Dunne, Development of a bovine collagen-Apatitic calcium phosphate cement for potential fracture treatment through vertebroplasty, *Acta Biomater.* (2012). <https://doi.org/10.1016/j.actbio.2012.07.003>.
- [179] C. Zhou, X. Li, J. Cheng, H. Fan, X. Zhang, Bioactive Ceramics and Metals for Regenerative Engineering, *Regen. Eng.* (2018) 31–43. <https://doi.org/10.1201/9781315121079-3>.
- [180] H.H.K. Xu, J.B. Quinn, Calcium phosphate cement containing resorbable fibers for short-term reinforcement and macroporosity, *Biomaterials.* 23 (2002) 193–202. [https://doi.org/10.1016/S0142-9612\(01\)00095-3](https://doi.org/10.1016/S0142-9612(01)00095-3).
- [181] K.L. Low, S.H. Tan, S.H.S. Zein, J.A. Roether, V. Mouriño, A.R. Boccaccini, Calcium phosphate-based composites as injectable bone substitute materials, *J. Biomed. Mater. Res. - Part B Appl. Biomater.* 94 (2010) 273–286. <https://doi.org/10.1002/jbm.b.31619>.
- [182] B. Qiao, D. Zhou, Z. Dai, W. Zhao, Q. Yang, Y. Xu, X. Li, J. Wu, S. Guo, D. Jiang, Bone Plate Composed of a Ternary Nanohydroxyapatite/Polyamide 66/Glass Fiber Composite: Biocompatibility In Vivo and Internal Fixation for Canine Femur Fractures, *Adv. Funct. Mater.* 29 (2019) 1–9. <https://doi.org/10.1002/adfm.201808738>.
- [183] D. Barati, J.D. Walters, S.R. Pajoum Shariati, S. Moeinzadeh, E. Jabbari, Effect of organic acids on calcium phosphate nucleation and osteogenic differentiation of human mesenchymal stem cells on peptide functionalized nanofibers, *Langmuir.* 31 (2015) 5130–5140. <https://doi.org/10.1021/acs.langmuir.5b00615>.

- [184] J. Chung, I. Granja, M.G. Taylor, G. Mpourmpakis, J.R. Asplin, J.D. Rimer, Molecular modifiers reveal a mechanism of pathological crystal growth inhibition, *Nature*. 536 (2016) 446–450. <https://doi.org/10.1038/nature19062>.
- [185] L. Pastero, M. Bruno, D. Aquilano, Habit change of monoclinic hydroxyapatite crystals growing from aqueous solution in the presence of citrate ions: The role of 2D epitaxy, *Crystals*. 8 (2018) 1–12. <https://doi.org/10.3390/cryst8080308>.
- [186] M. Li, J. Zhang, L. Wang, B. Wang, C. V. Putnis, Mechanisms of Modulation of Calcium Phosphate Pathological Mineralization by Mobile and Immobile Small-Molecule Inhibitors, *J. Phys. Chem. B*. 122 (2018) 1580–1587. <https://doi.org/10.1021/acs.jpcc.7b10956>.
- [187] J. Singh, S.S. Chatha, H. Singh, Microstructural and in-vitro characteristics of functional calcium silicate topcoat on hydroxyapatite coating for bio-implant applications, *Prog. Biomater.* 11 (2022) 95–108. <https://doi.org/10.1007/s40204-022-00183-w>.
- [188] L.L. HENCH, R.J. SPLINTER, W.C. ALLEN, Bonding Mechanisms at the Interface of Ceramic Prosthetic Materials, 2 (n.d.).
- [189] M. Cerrutti, N. Sahai, *Silicate Biomaterials for Orthopaedic and Dental Implants*, (2014). <https://doi.org/10.2138/rmg.2006.64.9>.
- [190] A.R. Boccaccini, D. Ph, Effect of Bioactive Glasses on Angiogenesis : A Review of In Vitro and In Vivo Evidences, 16 (2010).
- [191] A. Hoppe, N.S. Güldal, A.R. Boccaccini, A review of the biological response to ionic dissolution products from bioactive glasses and glass-ceramics, *Biomaterials*. 32 (2011) 2757–2774. <https://doi.org/10.1016/j.biomaterials.2011.01.004>.
- [192] J. Sun, J. Li, X. Liu, L. Wei, G. Wang, F. Meng, Proliferation and gene expression of osteoblasts cultured in DMEM containing the ionic products of dicalcium silicate coating, *Biomed. Pharmacother.* 63 (2009) 650–657. <https://doi.org/10.1016/j.biopha.2009.01.007>.
- [193] Z. Du, H. Leng, L. Guo, Y. Huang, T. Zheng, Z. Zhao, X. Liu, X. Zhang, Q. Cai, X. Yang, Calcium silicate scaffolds promoting bone regeneration via the doping of Mg²⁺ or Mn²⁺ ion, *Compos. Part B Eng.* 190 (2020) 107937.

<https://doi.org/10.1016/j.compositesb.2020.107937>.

- [194] W. Liu, Z. Huan, C. Wu, Z. Zhou, J. Chang, High-strength calcium silicate-incorporated magnesium phosphate bone cement with osteogenic potential for orthopedic application, *Compos. Part B Eng.* 247 (2022) 110324. <https://doi.org/10.1016/j.compositesb.2022.110324>.
- [195] G.C. Wang, Z.F. Lu, H. Zreiqat, *Bioceramics for skeletal bone regeneration*, 2014. <https://doi.org/10.1533/9780857099037.2.180>.
- [196] P. Zhou, D. Xia, Z. Ni, T. Ou, Y. Wang, H. Zhang, L. Mao, K. Lin, S. Xu, J. Liu, Calcium silicate bioactive ceramics induce osteogenesis through oncostatin M, *Bioact. Mater.* 6 (2021) 810–822. <https://doi.org/10.1016/j.bioactmat.2020.09.018>.
- [197] C.C. Chen, C.C. Ho, C.H. David Chen, S.J. Ding, Physicochemical Properties of Calcium Silicate Cements for Endodontic Treatment, *J. Endod.* 35 (2009) 1288–1291. <https://doi.org/10.1016/j.joen.2009.05.036>.
- [198] D. Marković, B. Četenović, A. Vuković, V. Jokanović, T. Marković, Nanosynthesized calcium-silicate-based biomaterials in endodontic treatment of young permanent teeth, 2016. <https://doi.org/10.1016/B978-0-323-42867-5.00011-4>.
- [199] M.A. Saghiri, J. Orangi, A. Asatourian, J.L. Gutmann, F. Garcia-Godoy, M. Lotfi, N. Sheibani, Calcium silicate-based cements and functional impacts of various constituents, *Dent. Mater. J.* 36 (2017) 8–18. <https://doi.org/10.4012/dmj.2015-425>.
- [200] W. Jiang, M.S. Pacella, Di. Athanasiadou, V. Nelea, H. Vali, R.M. Hazen, J.J. Gray, M.D. McKee, Chiral acidic amino acids induce chiral hierarchical structure in calcium carbonate, *Nat. Commun.* 8 (2017) 1–13. <https://doi.org/10.1038/ncomms15066>.
- [201] M. Bohner, H.P. Merkle, P. Van Landuyt, G. Trophardy, J. Lemaitre, Effect of several additives and their admixtures on the physico-chemical properties of a calcium phosphate cement, *J. Mater. Sci. Mater. Med.* 11 (2000) 111–116. <https://doi.org/10.1023/A:1008997118576>.
- [202] K. Rubini, E. Boanini, A. Bigi, Role of aspartic and polyaspartic acid on the synthesis and hydrolysis of brushite, *J. Funct. Biomater.* 10 (2019). <https://doi.org/10.3390/jfb10010011>.
- [203] S. Li, L. Wang, Phosphorylated osteopontin peptides inhibit crystallization by resisting

- the aggregation of calcium phosphate nanoparticles, *CrystEngComm*. 14 (2012) 8037–8043. <https://doi.org/10.1039/c2ce26140e>.
- [204] C.W. Prince, T. Oosawa, W.T. Butler, M. Tomana, A.S. Bhowan, M. Bhowan, R.E. Schrohenloher, Isolation, characterization, and biosynthesis of a phosphorylated glycoprotein from rat bone., *J. Biol. Chem.* 262 (1987) 2900–2907.
- [205] A. Reinstorf, M. Ruhnnow, M. Gelinsky, W. Pompe, U. Hempel, K.W. Wenzel, P. Simon, Phosphoserine - A convenient compound for modification of calcium phosphate bone cement collagen composites, *J. Mater. Sci. Mater. Med.* 15 (2004) 451–455. <https://doi.org/10.1023/B:JMSM.0000021119.14870.3d>.
- [206] C. Combes, C. Rey, Amorphous calcium phosphates: Synthesis, properties and uses in biomaterials, *Acta Biomater.* 6 (2010) 3362–3378. <https://doi.org/10.1016/j.actbio.2010.02.017>.
- [207] S. Von Euw, W. Ajili, T.H.C. Chan-Chang, A. Delices, G. Laurent, F. Babonneau, N. Nassif, T. Azais, Amorphous surface layer versus transient amorphous precursor phase in bone – A case study investigated by solid-state NMR spectroscopy, *Acta Biomater.* 59 (2017) 351–360. <https://doi.org/10.1016/j.actbio.2017.06.040>.
- [208] J.L. Bystrom, M. Pujari-Palmer, Phosphoserine functionalized cements preserve metastable phases, and reprecipitate octacalcium phosphate, hydroxyapatite, dicalcium phosphate, and amorphous calcium phosphate, during degradation, in vitro, *J. Funct. Biomater.* (2019). <https://doi.org/10.3390/jfb10040054>.
- [209] R.T. Tran, L. Wang, C. Zhang, M. Huang, W. Tang, C. Zhang, Z. Zhang, D. Jin, B. Banik, J.L. Brown, Z. Xie, X. Bai, J. Yang, Synthesis and characterization of biomimetic citrate-based biodegradable composites, *J. Biomed. Mater. Res. - Part A.* 102 (2014) 2521–2532. <https://doi.org/10.1002/jbm.a.34928>.
- [210] K. Vrchovecká, M. Pávková-Goldbergová, H. Engqvist, M. Pujari-Palmer, Cytocompatibility and Bioactive Ion Release Profiles of Phosphoserine Bone Adhesive: Bridge from In Vitro to In Vivo, *Biomedicines*. 10 (2022). <https://doi.org/10.3390/biomedicines10040736>.
- [211] L. Yang, S. Chen, T. Shang, R. Zhao, B. Yuan, X. Zhu, M.G. Raucci, X. Yang, X. Zhang, M. Santin, L. Ambrosio, Complexation of Injectable Biphasic Calcium

- Phosphate with Phosphoserine-Presenting Dendrons with Enhanced Osteoregenerative Properties, *ACS Appl. Mater. Interfaces.* 12 (2020) 37873–37884. <https://doi.org/10.1021/acsami.0c09004>.
- [212] A. Reinstorf, U. Hempel, F. Olgemöller, H. Domaschke, W. Schneiders, R. Mai, B. Stadlinger, A. Rösen-Wolff, S. Rammelt, M. Gelinsky, W. Pompe, O-phospho-L-serine modified calcium phosphate cements - Material properties, in vitro and in vivo investigations, *Materwiss. Werksttech.* (2006). <https://doi.org/10.1002/mawe.200600026>.
- [213] R. Sugita, A.A. Jones, G.A. Kotsakis, D.L. Cochran, Radiographic evaluation of a novel bone adhesive for maintenance of crestal bone around implants in canine oversized osteotomies, *J. Periodontol.* 93 (2022) 924–932. <https://doi.org/10.1002/JPER.20-0876>.
- [214] D. Cochran, A. Jones, R. Sugita, M. Brown, T. Guda, H. Prasad, J. Ong, A. Pollack, G. Kay, Immediate Dental Implant Stabilization in a Canine Model Using a Novel Mineral-Organic Adhesive: 4-Month Results, *Int. J. Oral Maxillofac. Implants.* 35 (2020) 39–51. <https://doi.org/10.11607/jomi.7891>.
- [215] R. Mai, R. Lux, P. Proff, G. Lauer, W. Pradel, H. Leonhardt, A. Reinstorf, M. Gelinsky, R. Jung, U. Eckelt, T. Gedrange, B. Stadlinger, O-phospho-L-serine: A modulator of bone healing in calcium-phosphate cements, *Biomed. Tech.* 53 (2008) 229–233. <https://doi.org/10.1515/BMT.2008.040>.
- [216] N. Bandara, H. Zeng, J. Wu, Marine mussel adhesion: Biochemistry, mechanisms, and biomimetics, *J. Adhes. Sci. Technol.* 27 (2013) 2139–2162. <https://doi.org/10.1080/01694243.2012.697703>.
- [217] B. Vayre, F. Vignat, F. Villeneuve, Designing for additive manufacturing, *Procedia CIRP.* 3 (2012) 632–637. <https://doi.org/10.1016/j.procir.2012.07.108>.
- [218] M. Ruiz Espejo, *Design of Experiments for Engineers and Scientists*, 2006. <https://doi.org/10.1198/tech.2006.s381>.
- [219] J. Antoy, *Design of Experiments for Engineers and Scientists: Second Edition*, *Des. Exp. Eng. Sci. Second Ed.* (2014) 1–672. <https://doi.org/10.1016/C2012-0-03558-2>.
- [220] B. Durakovic, *Design of experiments application, concepts, examples: State of the art*,

- Period. Eng. Nat. Sci. 5 (2017) 421–439. <https://doi.org/10.21533/pen.v5i3.145>.
- [221] S. Ranga, M. Jaimini, S. Sanjay Kumar, B. Singh Chauhan, A. Kumar, A Review on Design OF Experiments (DOE), *Int. J. Pharmaceutical Chem. Sci.* 5 (2016) 196–200. <httpwww.ijpcsonline.comfiles17-10-161-1086.pdf>.
- [222] M. Bohner, R. Luginbühl, C. Reber, N. Doebelin, G. Baroud, E. Conforto, A physical approach to modify the hydraulic reactivity of α -tricalcium phosphate powder, *Acta Biomater.* 5 (2009) 3524–3535. <https://doi.org/10.1016/j.actbio.2009.05.024>.
- [223] INTERNATIONAL STANDARD ISO cements, 2002 (2002).
- [224] M.J. Anderson, P.J. Whitcomb, RSM simplified : optimizing processes using response surface methods for design of experiments, (n.d.).
- [225] J. Jansen, E. Ooms, N. Verdonschot, J. Wolke, Injectable calcium phosphate cement for bone repair and implant fixation, in: *Orthop. Clin. North Am.*, 2005. <https://doi.org/10.1016/j.ocl.2004.06.014>.
- [226] N.A. Caraan, R. Windhager, J. Webb, N. Zentgraf, K.D. Kuehn, Role of fast-setting cements in arthroplasty: A comparative analysis of characteristics, *World J. Orthop.* 8 (2017) 881–890. <https://doi.org/10.5312/wjo.v8.i12.881>.
- [227] H.S. Ryu, H.J. Youn, K. Sun Hong, B.S. Chang, C.K. Lee, S.S. Chung, An improvement in sintering property of β -tricalcium phosphate by addition of calcium pyrophosphate, *Biomaterials.* 23 (2002) 909–914. [https://doi.org/10.1016/S0142-9612\(01\)00201-0](https://doi.org/10.1016/S0142-9612(01)00201-0).
- [228] H. Eslami, M. Solati-Hashjin, M. Tahriri, The comparison of powder characteristics and physicochemical, mechanical and biological properties between nanostructure ceramics of hydroxyapatite and fluoridated hydroxyapatite, *Mater. Sci. Eng. C.* 29 (2009) 1387–1398. <https://doi.org/10.1016/j.msec.2008.10.033>.
- [229] G. Cicek, E.A. Aksoy, C. Durucan, N. Hasirci, Alpha-tricalcium phosphate (α -TCP): Solid state synthesis from different calcium precursors and the hydraulic reactivity, *J. Mater. Sci. Mater. Med.* 22 (2011) 809–817. <https://doi.org/10.1007/s10856-011-4283-x>.
- [230] M.R. Cohn, A. Unnanuntana, T.J. Pannu, S.J. Warner, J.M. Lane, Materials in fracture fixation, *Compr. Biomater. II.* 7 (2017) 278–297. <https://doi.org/10.1016/B978-0-12->

803581-8.10109-2.

- [231] Y. Pan, F. Xiao, Y. Dong, Optimization of the preparation process of α -tricalcium phosphate applied to bone cement, *Mater. Res. Express.* 6 (2019). <https://doi.org/10.1088/2053-1591/ab36fd>.
- [232] A. Bignon, J. Chevalier, G. Fantozzi, Effect of ball milling on the processing of bone substitutes with calcium phosphate powders, *J. Biomed. Mater. Res.* 63 (2002) 619–626. <https://doi.org/10.1002/jbm.10379>.
- [233] A. Fahami, G.W. Beall, Mechano-synthesis of carbonate doped chlorapatite–ZnO nanocomposite with negative zeta potential, *Ceram. Int.* 41 (2015) 12323–12330. <https://doi.org/10.1016/j.ceramint.2015.06.061>.
- [234] K. Cheng, W. Weng, H. Wang, S. Zhang, In vitro behavior of osteoblast-like cells on fluoridated hydroxyapatite coatings, *Biomaterials.* 26 (2005) 6288–6295. <https://doi.org/10.1016/j.biomaterials.2005.03.041>.
- [235] E.B. Montufar, Y. Maazouz, M.P. Ginebra, Relevance of the setting reaction to the injectability of tricalcium phosphate pastes, *Acta Biomater.* 9 (2013) 6188–6198. <https://doi.org/10.1016/j.actbio.2012.11.028>.
- [236] Z. Irbe, L. Berziņa-Cimdiņa, The effect of α -tricalcium phosphate powder preparation methods on cement properties, *Key Eng. Mater.* 614 (2014) 62–67. <https://doi.org/10.4028/www.scientific.net/KEM.614.62>.
- [237] R. Serra-Maia, S. Chastka, M. Bellier, T. Douglas, J.D. Rimstidt, F.M. Michel, Effect of particle size on catalytic decomposition of hydrogen peroxide by platinum nanocatalysts, *J. Catal.* 373 (2019) 58–66. <https://doi.org/10.1016/j.jcat.2019.03.026>.
- [238] M.B. Thürmer, C.E. Diehl, L.A.L. dos Santos, Calcium phosphate cements based on alpha-tricalcium phosphate obtained by wet method: Synthesis and milling effects, *Ceram. Int.* 42 (2016) 18094–18099. <https://doi.org/10.1016/j.ceramint.2016.08.115>.
- [239] T.J. Brunner, R.N. Grass, M. Böhner, W.J. Stark, Effect of particle size, crystal phase and crystallinity on the reactivity of tricalcium phosphate cements for bone reconstruction, *J. Mater. Chem.* 17 (2007) 4072–4078. <https://doi.org/10.1039/b707171j>.
- [240] U. Gibureck, J. Barralet, M. Hofmann, R. Thull, Mechanical Activation of

Tetracalcium Phosphate, (n.d.) 6–7.

- [241] U. Gbureck, O. Grolms, J.E. Barralet, L.M. Grover, R. Thull, Mechanical activation and cement formation of β -tricalcium phosphate, *Biomaterials*. 24 (2003) 4123–4131. [https://doi.org/10.1016/S0142-9612\(03\)00283-7](https://doi.org/10.1016/S0142-9612(03)00283-7).
- [242] R.M. O’Hara, N.J. Dunne, J.F. Orr, F.J. Buchanan, R.K. Wilcox, D.C. Barton, Optimisation of the mechanical and handling properties of an injectable calcium phosphate cement, *J. Mater. Sci. Mater. Med.* (2010). <https://doi.org/10.1007/s10856-009-3977-9>.
- [243] N. Dunne, R. O’Gara, F. Buchanan, J. Orr, Effect of liquid/powder ratio on the setting, handling and mechanical properties of collagen-apatitic cements, *Key Eng. Mater.* 493–494 (2012) 415–421. <https://doi.org/10.4028/www.scientific.net/KEM.493-494.415>.
- [244] L.M. Grover, U. Gbureck, D.F. Farrar, J.E. Barralet, Adhesion of a novel calcium phosphate cement to cortical bone and several common biomaterials, *Key Eng. Mater.* 309-311 II (2006) 849–852. <https://doi.org/10.4028/www.scientific.net/kem.309-311.849>.
- [245] R. Martínez-García, M.I. Sánchez de Rojas, P. Jagadesh, F. López-Gayarre, J.M. Morán-del-Pozo, A. Juan-Valdes, Effect of pores on the mechanical and durability properties on high strength recycled fine aggregate mortar, *Case Stud. Constr. Mater.* 16 (2022). <https://doi.org/10.1016/j.cscm.2022.e01050>.
- [246] J. Zhang, F. Tancret, J.M. Bouler, Mechanical properties of Calcium Phosphate Cements (CPC) for bone substitution: Influence of fabrication and microstructure, *Key Eng. Mater.* 493–494 (2012) 409–414. <https://doi.org/10.4028/www.scientific.net/KEM.493-494.409>.
- [247] L. Offer, V. Bastian, T. Pavlidis, C. Heiss, M. Gelinsky, A. Reinstorf, S. Wensch, K. Susanne Lips, R. Schnettler, Phosphoserine-modified calcium phosphate cements: bioresorption and substitution, *Ann. Am. Thorac. Soc.* 12 (2010) 181–204. <https://doi.org/10.1002/term>.
- [248] D.L. Cochran, A.A. Jones, R. Sugita, M.C. Brown, H. Prasad, G.W. Kay, Twelve-month evaluation of a novel mineral–organic adhesive material used to stabilize dental

- implants placed in oversized osteotomies in vivo in an animal model, *Clin. Oral Implants Res.* 33 (2022) 391–404. <https://doi.org/10.1111/clr.13899>.
- [249] L.E. Carey, H.H.K. Xu, C.G. Simon, S. Takagi, L.C. Chow, Premixed rapid-setting calcium phosphate composites for bone repair, *Biomaterials.* 26 (2005) 5002–5014. <https://doi.org/10.1016/j.biomaterials.2005.01.015>.
- [250] T. Kokubo, H. Takadama, How useful is SBF in predicting in vivo bone bioactivity?, *Biomaterials.* 27 (2006) 2907–2915. <https://doi.org/10.1016/j.biomaterials.2006.01.017>.
- [251] A. Bou-Francis, A. Ghanem, Standardized methodology for in vitro assessment of bone-to-bone adhesion strength, *Int. J. Adhes. Adhes.* 77 (2017) 96–101. <https://doi.org/10.1016/j.ijadhadh.2017.03.014>.
- [252] A. Redmann, V. Damodaran, F. Tischer, P. Prabhakar, T.A. Osswald, Evaluation of single-lap and block shear test methods in adhesively bonded composite joints, *J. Compos. Sci.* 5 (2021). <https://doi.org/10.3390/jcs5010027>.
- [253] F.P. Kesseli, C.S. Lauer, I. Baker, K.A. Mirica, D.W. Van Citters, Identification of a calcium phosphoserine coordination network in an adhesive organo-apatitic bone cement system, *Acta Biomater.* 105 (2020) 280–289. <https://doi.org/10.1016/j.actbio.2020.01.007>.
- [254] R.P. Félix Lanao, S.C.G. Leeuwenburgh, J.G.C. Wolke, J.A. Jansen, Bone response to fast-degrading, injectable calcium phosphate cements containing PLGA microparticles, *Biomaterials.* 32 (2011) 8839–8847. <https://doi.org/10.1016/j.biomaterials.2011.08.005>.
- [255] T. Lu, F. He, J. Ye, Physicochemical Properties, in Vitro Degradation, and Biocompatibility of Calcium Phosphate Cement Incorporating Poly(lactic- co-glycolic acid) Particles with Different Morphologies: A Comparative Study, *ACS Omega.* 6 (2021) 8322–8331. <https://doi.org/10.1021/acsomega.1c00031>.
- [256] P.Q. Ruhé, E.L. Hedberg-Dirk, N.T. Padron, P.H.M. Spauwen, J.A. Jansen, A.G. Mikos, Porous poly(DL-lactic-co-glycolic acid)/calcium phosphate cement composite for reconstruction of bone defects, *Tissue Eng.* 12 (2006) 789–800. <https://doi.org/10.1089/ten.2006.12.789>.

- [257] S. Baradaran, E. Moghaddam, B. Nasiri-Tabrizi, W.J. Basirun, M. Mehrali, M. Sookhakian, M. Hamdi, Y. Alias, Characterization of nickel-doped biphasic calcium phosphate/graphene nanoplatelet composites for biomedical application, *Mater. Sci. Eng. C*. 49 (2015) 656–668. <https://doi.org/10.1016/j.msec.2015.01.050>.
- [258] T. Elkhooly, Preparation and characterization of calcium phosphate ceramics containing some rare earth oxides for using as biomaterials., (2008). <https://doi.org/10.13140/RG.2.1.3902.5369>.
- [259] J.D. Masson, M. Thibaudon, L. Bélec, G. Crépeaux, Calcium phosphate: a substitute for aluminum adjuvants?, *Expert Rev. Vaccines*. 16 (2017) 289–299. <https://doi.org/10.1080/14760584.2017.1244484>.
- [260] A. Aminoroaya, R.E. Neisiany, S.N. Khorasani, P. Panahi, O. Das, H. Madry, M. Cucchiarini, S. Ramakrishna, A review of dental composites: Challenges, chemistry aspects, filler influences, and future insights, *Compos. Part B Eng.* 216 (2021) 108852. <https://doi.org/10.1016/j.compositesb.2021.108852>.
- [261] V. Lührs, S. Stöblein, K. Thiel, I. Grunwald, A. Hartwig, An in vitro bone-to-bone adhesion test method using the compression shear test, *Int. J. Adhes. Adhes.* 111 (2021). <https://doi.org/10.1016/j.ijadhadh.2021.102977>.
- [262] R. O’Neill, H.O. McCarthy, E.B. Montufar, M.P. Ginebra, D.I. Wilson, A. Lennon, N. Dunne, Critical review: Injectability of calcium phosphate pastes and cements, *Acta Biomater.* (2017). <https://doi.org/10.1016/j.actbio.2016.11.019>.
- [263] T. Nakamura, A. Matsumine, K. Asanuma, T. Matsubara, A. Sudo, Treatment of bone defect with calcium phosphate cement subsequent to tumor curettage in pediatric patients, *Oncol. Lett.* 11 (2016) 247–252. <https://doi.org/10.3892/ol.2015.3855>.
- [264] S. Ishiguro, Y. Kasai, A. Sudo, K. Iida, A. Uchida, Percutaneous vertebroplasty for osteoporotic compression fractures using calcium phosphate cement., *J. Orthop. Surg. (Hong Kong)*. 18 (2010) 346–351. <https://doi.org/10.1177/230949901001800318>.
- [265] I. Kunio, Effects of Spherical Tetracalcium Phosphate on Injectability and Basic Properties of Apatitic Cement, *Key Eng. Mater.* 240–242 (2003) 369–372. <https://doi.org/10.4028/www.scientific.net/kem.240-242.369>.
- [266] F. Buchanan, L. Gallagher, V. Jack, N. Dunne, Short-fibre reinforcement of calcium

- phosphate bone cement, *Proc. Inst. Mech. Eng. Part H J. Eng. Med.* 221 (2007) 203–211. <https://doi.org/10.1243/09544119JEIM235>.
- [267] M. Nakano, N. Hirano, M. Zukawa, K. Suzuki, J. Hirose, T. Kimura, Y. Kawaguchi, Vertebroplasty using calcium phosphate cement for osteoporotic vertebral fractures: Study of outcomes at a minimum follow-up of two years, *Asian Spine J.* 6 (2012) 34–42. <https://doi.org/10.4184/asj.2012.6.1.34>.
- [268] H. Ogata, M. Hayashi, H. Tsuda, N. Suzuki, M. Maeno, A. Sugawara, B. Ogiso, Effects of a calcium phosphate cement on mineralized nodule formation compared with endodontic cements, *Dent. Mater. J.* 31 (2012) 92–97. <https://doi.org/10.4012/dmj.2011-151>.
- [269] H.H.K. Xu, L.E. Carey, C.G. Simon, S. Takagi, L.C. Chow, Premixed calcium phosphate cements: Synthesis, physical properties, and cell cytotoxicity, *Dent. Mater.* 23 (2007) 433–441. <https://doi.org/10.1016/j.dental.2006.02.014>.
- [270] M. Habib, G. Baroud, F. Gitzhofer, M. Böhner, Mechanisms underlying the limited injectability of hydraulic calcium phosphate paste. Part II: Particle separation study, *Acta Biomater.* 6 (2010) 250–256. <https://doi.org/10.1016/j.actbio.2009.06.012>.
- [271] P. Spencer, Y. Wang, Adhesive phase separation at the dentin interface under wet bonding conditions, *J. Biomed. Mater. Res.* 62 (2002) 447–456. <https://doi.org/10.1002/jbm.10364>.
- [272] S. Takagi, L.C. Chow, S. Hirayama, A. Sugawara, Premixed Calcium-Phosphate Cement Pastes, *J. Biomed. Mater. Res. - Part B Appl. Biomater.* 67 (2003) 689–696. <https://doi.org/10.1002/jbm.b.10065>.
- [273] F. Chen, Y. Mao, C. Liu, Premixed injectable calcium phosphate cement with excellent suspension stability, *J. Mater. Sci. Mater. Med.* 24 (2013) 1627–1637. <https://doi.org/10.1007/s10856-013-4920-7>.
- [274] I. Rajzer, O. Castaño, E. Engel, J.A. Planell, Injectable and fast resorbable calcium phosphate cement for body-setting bone grafts, *J. Mater. Sci. Mater. Med.* 21 (2010) 2049–2056. <https://doi.org/10.1007/s10856-010-4078-5>.
- [275] U. Tariq, R. Hussain, K. Tufail, Z. Haider, R. Tariq, J. Ali, Injectable dicalcium phosphate bone cement prepared from biphasic calcium phosphate extracted from lamb

- bone, *Mater. Sci. Eng. C.* 103 (2019) 109863. <https://doi.org/10.1016/j.msec.2019.109863>.
- [276] S. Heinemann, S. Rössler, M. Lemm, M. Ruhnnow, B. Nies, Properties of injectable ready-to-use calcium phosphate cement based on water-immiscible liquid, *Acta Biomater.* 9 (2013) 6199–6207. <https://doi.org/10.1016/j.actbio.2012.12.017>.
- [277] M. Ricinoleate, Kolliphor® EL Poly oxyl 35 Cas tor Oil (USP-NF), (2019) 5–9.
- [278] F. Aloui, B. Maazoun, Y. Gargouri, N. Miled, Optimization of oil retention in sesame based halva using emulsifiers and fibers: an industrial assay, *J. Food Sci. Technol.* 53 (2016) 1540–1550. <https://doi.org/10.1007/s13197-015-2116-5>.
- [279] T.E. AU - Robinson, E.A.B. AU - Hughes, N.M. AU - Eisenstein, L.M. AU - Grover, S.C. AU - Cox, The Quantification of Injectability by Mechanical Testing, *JoVE.* (2020) e61417. <https://doi.org/doi:10.3791/61417>.
- [280] R. O’Neill, H.O. McCarthy, E. Cunningham, E. Montufar, M.P. Ginebra, D.I. Wilson, A. Lennon, N. Dunne, Extent and mechanism of phase separation during the extrusion of calcium phosphate pastes, *J. Mater. Sci. Mater. Med.* 27 (2016) 1–13. <https://doi.org/10.1007/s10856-015-5615-z>.
- [281] M.P. Ginebra, E.B. Montufar, *Injectable biomedical foams for bone regeneration*, Woodhead Publishing Limited, 2014. <https://doi.org/10.1533/9780857097033.2.281>.
- [282] R. O’Neill, H.O. McCarthy, E.B. Montufar, M.P. Ginebra, D.I. Wilson, A. Lennon, N. Dunne, Critical review: Injectability of calcium phosphate pastes and cements, *Acta Biomater.* 50 (2017) 1–19. <https://doi.org/10.1016/j.actbio.2016.11.019>.
- [283] P. Mondal, I. Chakraborty, K. Chatterjee, *Injectable Adhesive Hydrogels for Soft tissue Reconstruction: A Materials Chemistry Perspective*, *Chem. Rec.* 22 (2022). <https://doi.org/10.1002/tcr.202200155>.
- [284] P. Yaras, D.M. Kalyon, U. Yilmazer, Flow instabilities in capillary flow of concentrated suspensions, *Rheol. Acta.* 33 (1994) 48–59. <https://doi.org/10.1007/BF00453463>.
- [285] S. Khedmat, F. Momen-Heravi, M. Pishvaei, Rheological properties of endodontic sealers: The effect of time, temperature, and composition, *Iran. Polym. J. (English Ed.)* 21 (2012) 445–450. <https://doi.org/10.1007/s13726-012-0047-9>.

- [286] J. Liang, Q. Su, Y. Zhao, Y. Wang, Theoretical insights into three types of oxidized starch-based adhesives: Chemical stability, water resistance, and shearing viscosity from a molecular viewpoint, *J. Chem.* 2016 (2016). <https://doi.org/10.1155/2016/2369739>.
- [287] W. Liu, J. Zhang, G. Rethore, K. Khairoun, P. Pilet, F. Tancret, J.M. Bouler, P. Weiss, A novel injectable, cohesive and toughened Si-HPMC (silanized-hydroxypropyl methylcellulose) composite calcium phosphate cement for bone substitution, *Acta Biomater.* 10 (2014) 3335–3345. <https://doi.org/10.1016/j.actbio.2014.03.009>.
- [288] Y. Miyamoto, K. Ishikawa, M. Takechi, T. Taketomo, T. Yuasa, M. Nagayama, K. Suzuki, Histological and compositional evaluations of three types of calcium phosphate cements when implanted in subcutaneous tissue immediately after mixing, *J. Biomed. Mater. Res.* 48 (1999) 36–42. [https://doi.org/10.1002/\(SICI\)1097-4636\(1999\)48:1<36::AID-JBM8>3.0.CO;2-I](https://doi.org/10.1002/(SICI)1097-4636(1999)48:1<36::AID-JBM8>3.0.CO;2-I).
- [289] A.S. Lister, Validation of HPLC methods in pharmaceutical analysis, *Sep. Sci. Technol.* 6 (2005) 191–217. [https://doi.org/10.1016/S0149-6395\(05\)80051-0](https://doi.org/10.1016/S0149-6395(05)80051-0).
- [290] A.C. Olivieri, N.M. Faber, Validation and Error, *Compr. Chemom.* 3 (2009) 91–120. <https://doi.org/10.1016/B978-044452701-1.00073-9>.
- [291] F. Wu, J. Wei, H. Guo, F. Chen, H. Hong, C. Liu, Self-setting bioactive calcium-magnesium phosphate cement with high strength and degradability for bone regeneration, *Acta Biomater.* 4 (2008) 1873–1884. <https://doi.org/10.1016/j.actbio.2008.06.020>.
- [292] E. Bosch-Rué, L. Diez-Tercero, B. Giordano-Kelhoffer, L.M. Delgado, B.M. Bosch, M. Hoyos-Nogués, M.A. Mateos-Timoneda, P.A. Tran, F.J. Gil, R.A. Perez, Biological Roles and Delivery Strategies for Ions to Promote Osteogenic Induction, *Front. Cell Dev. Biol.* 8 (2021). <https://doi.org/10.3389/fcell.2020.614545>.
- [293] J. Konka, M. Espanol, B.M. Bosch, E. de Oliveira, M.P. Ginebra, Maturation of biomimetic hydroxyapatite in physiological fluids: a physicochemical and proteomic study, *Mater. Today Bio.* 12 (2021) 100137. <https://doi.org/10.1016/j.mtbio.2021.100137>.
- [294] I. Khairoun, F.C.M. Driessens, M.G. Boltong, J.A. Planell, R. Wenz, Addition of

- cohesion promoters to calcium phosphate cements, *Biomaterials*. (1999). [https://doi.org/10.1016/S0142-9612\(98\)00202-6](https://doi.org/10.1016/S0142-9612(98)00202-6).
- [295] J. Zhang, W. Liu, O. Gauthier, S. Sourice, P. Pilet, G. Rethore, K. Khairoun, J.M. Bouler, F. Tancret, P. Weiss, A simple and effective approach to prepare injectable macroporous calcium phosphate cement for bone repair: Syringe-foaming using a viscous hydrophilic polymeric solution, *Acta Biomater.* 31 (2016) 326–338. <https://doi.org/10.1016/j.actbio.2015.11.055>.
- [296] F. Tamimi, Z. Sheikh, J. Barralet, Dicalcium phosphate cements: Brushite and monetite, *Acta Biomater.* 8 (2012) 474–487. <https://doi.org/10.1016/j.actbio.2011.08.005>.
- [297] M. Böhner, Calcium orthophosphates in medicine: From ceramics to calcium phosphate cements, *Injury*. 31 (2000). [https://doi.org/10.1016/S0020-1383\(00\)80022-4](https://doi.org/10.1016/S0020-1383(00)80022-4).
- [298] J.M. Sadowska, J. Guillem-Marti, M. Espanol, C. Stähli, N. Döbelin, M.P. Ginebra, In vitro response of mesenchymal stem cells to biomimetic hydroxyapatite substrates: A new strategy to assess the effect of ion exchange, *Acta Biomater.* 76 (2018) 319–332. <https://doi.org/10.1016/j.actbio.2018.06.025>.
- [299] K. Klimek, A. Belcarz, R. Pazik, P. Sobierajska, T. Han, R.J. Wiglusz, G. Ginalska, “false” cytotoxicity of ions-adsorbing hydroxyapatite - Corrected method of cytotoxicity evaluation for ceramics of high specific surface area, *Mater. Sci. Eng. C*. 65 (2016) 70–79. <https://doi.org/10.1016/j.msec.2016.03.105>.
- [300] W. Schneiders, A. Reinstorf, W. Pompe, R. Grass, A. Biewener, M. Holch, H. Zwipp, S. Rammelt, Effect of modification of hydroxyapatite/collagen composites with sodium citrate, phosphoserine, phosphoserine/RGD-peptide and calcium carbonate on bone remodelling, *Bone*. 40 (2007) 1048–1059. <https://doi.org/10.1016/j.bone.2006.11.019>.
- [301] P. Procter, G. Hulsart-Billström, A. Alves, M. Pujari-Palmer, D. Wenner, G. Insley, H. Engqvist, S. Larsson, Gluing Living Bone Using a Biomimetic Bioadhesive: From Initial Cut to Final Healing, *Front. Bioeng. Biotechnol.* 9 (2021) 1–16. <https://doi.org/10.3389/fbioe.2021.728042>.

- [302] P. Murray, *Biocompatibility of Biomaterials for Dental Tissue Repair*, Elsevier Ltd, 2017. <https://doi.org/10.1016/B978-0-08-100884-3.00004-7>.
- [303] M.S. Zafar, R. Ullah, Z. Qamar, M.A. Fareed, F. Amin, Z. Khurshid, F. Sefat, *Properties of dental biomaterials*, Elsevier Ltd, 2019. <https://doi.org/10.1016/B978-0-08-102476-8.00002-5>.
- [304] P. Pinto, A. Carvalho, F.S. Silva, J.R. Gomes, O. Carvalho, S. Madeira, Comparative toothbrush abrasion resistance and surface analysis of different dental restorative materials, *Tribol. Int.* 175 (2022) 107799. <https://doi.org/10.1016/j.triboint.2022.107799>.
- [305] N.D. Ruse, Fracture mechanics characterization of dental biomaterials, *Dent. Biomater. Imaging, Test. Model.* (2008) 261–293. <https://doi.org/10.1533/9781845694241.261>.
- [306] E. Sajewicz, On evaluation of wear resistance of tooth enamel and dental materials, *Wear.* 260 (2006) 1256–1261. <https://doi.org/10.1016/j.wear.2005.08.010>.
- [307] M.A. Hussein, A.S. Mohammed, N. Al-Aqeeli, Wear characteristics of metallic biomaterials: A review, *Materials (Basel)*. 8 (2015) 2749–2768. <https://doi.org/10.3390/ma8052749>.
- [308] A. Lanza, A. Ruggiero, L. Sbordone, Tribology and dentistry: A commentary, *Lubricants*. 7 (2019) 1–15. <https://doi.org/10.3390/lubricants7060052>.
- [309] P. Thaitalay, N.L.O. Srakaew, S.T. Rattanachan, Comparison among alpha-tricalcium phosphate synthesized by solid state reaction and wet chemical reaction for calcium phosphate cements, *Chiang Mai J. Sci.* 45 (2018) 2123–2131.
- [310] S. Zhou, J. Ma, Y. Shen, M. Haapasalo, N.D. Ruse, Q. Yang, T. Troczynski, In vitro studies of calcium phosphate silicate bone cements, *J. Mater. Sci. Mater. Med.* 24 (2013) 355–364. <https://doi.org/10.1007/s10856-012-4794-0>.
- [311] ISO - ISO 10993-5:2009 - Biological evaluation of medical devices — Part 5: Tests for in vitro cytotoxicity, (n.d.).
- [312] L.L. Fernandes, C.X. Resende, D.S. Tavares, G.A. Soares, L.O. Castro, J.M. Granjeiro, Cytocompatibility of chitosan and collagen-chitosan scaffolds for tissue engineering, *Polimeros*. 21 (2011) 1–6. <https://doi.org/10.1590/S0104-14282011005000008>.

- [313] S.K. Swain, D. Sarkar, Fabrication, bioactivity, in vitro cytotoxicity and cell viability of cryo-treated nanohydroxyapatite-gelatin-polyvinyl alcohol macroporous scaffold, *J. Asian Ceram. Soc.* 2 (2014) 241–247. <https://doi.org/10.1016/j.jascer.2014.05.003>.
- [314] E. Song, S. Yeon Kim, T. Chun, H.J. Byun, Y.M. Lee, Collagen scaffolds derived from a marine source and their biocompatibility, *Biomaterials.* 27 (2006) 2951–2961. <https://doi.org/10.1016/j.biomaterials.2006.01.015>.
- [315] M.O. Wang, J.M. Etheridge, J.A. Thompson, C.E. Vorwald, D. Dean, J.P. Fisher, Evaluation of the in vitro cytotoxicity of cross-linked biomaterials, *Biomacromolecules.* 14 (2013) 1321–1329. <https://doi.org/10.1021/bm301962f>.
- [316] S.N. Rampersad, Multiple applications of alamar blue as an indicator of metabolic function and cellular health in cell viability bioassays, *Sensors (Switzerland).* 12 (2012) 12347–12360. <https://doi.org/10.3390/s120912347>.
- [317] J. Štembírek, M. Kyllar, I. Putnová, L. Stehlík, M. Buchtová, The pig as an experimental model for clinical craniofacial research, *Lab. Anim.* 46 (2012) 269–279. <https://doi.org/10.1258/la.2012.012062>.
- [318] T. Gotterbarm, S.J. Breusch, U. Schneider, M. Jung, The minipig model for experimental chondral and osteochondral defect repair in tissue engineering: Retrospective analysis of 180 defects, *Lab. Anim.* 42 (2008) 71–82. <https://doi.org/10.1258/la.2007.06029e>.
- [319] Q. Zhao, G. Li, T. Wang, Y. Jin, W. Lu, J. Ji, Human Periodontal Ligament Stem Cells Transplanted with Nanohydroxyapatite/Chitosan/Gelatin 3D Porous Scaffolds Promote Jaw Bone Regeneration in Swine, *Stem Cells Dev.* 30 (2021) 548–559. <https://doi.org/10.1089/scd.2020.0204>.
- [320] N. Mardas, X. Dereka, N. Donos, M. Dard, Experimental model for bone regeneration in oral and cranio-maxillo-facial surgery, *J. Investig. Surg.* 27 (2014) 32–49. <https://doi.org/10.3109/08941939.2013.817628>.
- [321] P. Felice, R. Pistilli, C. Barausse, A. Trullenque-Eriksson, M. Esposito, Immediate non-occlusal loading of immediate post-extractive versus delayed placement of single implants in preserved sockets of the anterior maxilla: 1-year post-loading outcome of a randomised controlled trial, *Eur. J. Oral Implantol.* 8 (2015) 361–372.

- [322] M. Shokri, F. Dalili, M. Kharaziha, M. Baghaban Eslaminejad, H. Ahmadi Tafti, Strong and bioactive bioinspired biomaterials, next generation of bone adhesives, *Adv. Colloid Interface Sci.* 305 (2022) 102706. <https://doi.org/10.1016/j.cis.2022.102706>.
- [323] T. Juvonen, J.P. Nuutinen, A.P. Koistinen, H. Kröger, R. Lappalainen, Biomechanical evaluation of bone screw fixation with a novel bone cement, *Biomed. Eng. Online.* 14 (2015) 3–12. <https://doi.org/10.1186/s12938-015-0069-6>.
- [324] L. Wang, Z. Gao, Y. Su, Q. Liu, Y. Ge, Z. Shan, Osseointegration of a novel dental implant in canine, *Sci. Rep.* 11 (2021) 1–11. <https://doi.org/10.1038/s41598-021-83700-4>.
- [325] R. Olkowski, P. Kaszczewski, J. Czechowska, D. Siek, D. Pijocha, A. Zima, A. Ślósarczyk, M. Lewandowska-Szumieł, Cytocompatibility of the selected calcium phosphate based bone cements: Comparative study in human cell culture, *J. Mater. Sci. Mater. Med.* 26 (2015) 1–12. <https://doi.org/10.1007/s10856-015-5589-x>.
- [326] L.A. Dos Santos, R.G. Carrodéguas, S.O. Rogero, O.Z. Higa, A.O. Boschi, A.C.F. De Arruda, α -Tricalcium phosphate cement: “In vitro” cytotoxicity, *Biomaterials.* 23 (2002) 2035–2042. [https://doi.org/10.1016/S0142-9612\(01\)00333-7](https://doi.org/10.1016/S0142-9612(01)00333-7).
- [327] D. Meng, L. Dong, Y. Yuan, Q. Jiang, In vitro and in vivo analysis of the biocompatibility of two novel and injectable calcium phosphate cements, *Regen. Biomater.* 6 (2019) 13–19. <https://doi.org/10.1093/rb/rby027>.
- [328] S. Jegou Saint-Jean, C.L. Camiré, P. Nevsten, S. Hansen, M.P. Ginebra, Study of the reactivity and in vitro bioactivity of Sr-substituted α -TCP cements, *J. Mater. Sci. Mater. Med.* 16 (2005) 993–1001. <https://doi.org/10.1007/s10856-005-4754-z>.
- [329] T. Konishi, M. Mizumoto, M. Honda, Y. Horiguchi, K. Oribe, H. Morisue, K. Ishii, Y. Toyama, M. Matsumoto, M. Aizawa, Fabrication of novel biodegradable α -tricalcium phosphate cement set by chelating capability of inositol phosphate and its biocompatibility, *J. Nanomater.* 2013 (2013). <https://doi.org/10.1155/2013/864374>.
- [330] K.C. da S. Modena, L.C. Casas-Apayco, M.T. Atta, C.A. de S. Costa, J. Hebling, C.R. Sipert, M.F. de L. Navarro, C.F. Santos, Cytotoxicity and biocompatibility of direct and indirect pulp capping materials, *J. Appl. Oral Sci.* 17 (2009) 544–554. <https://doi.org/10.1590/S1678-77572009000600002>.

- [331] B. Huzum, B. Puha, R. Necoara, S. Gheorghevici, G. Puha, A. Filip, P. Sirbu, O. Alexa, Biocompatibility assessment of biomaterials used in orthopedic devices: An overview (Review), *Exp. Ther. Med.* 22 (2021) 1–9. <https://doi.org/10.3892/etm.2021.10750>.
- [332] A. Kirillova, C. Kelly, N. von Windheim, K. Gall, Bioinspired Mineral-Organic Bioresorbable Bone Adhesive, *Adv. Healthc. Mater.* 7 (2018) e1800467. <https://doi.org/10.1002/adhm.201800467>.
- [333] J.W. Park, Y.J. Kim, J.H. Jang, C.H. An, MC3T3-E1 cell differentiation and in vivo bone formation induced by phosphoserine, *Biotechnol. Lett.* 33 (2011) 1473–1480. <https://doi.org/10.1007/s10529-011-0565-0>.
- [334] X. Ying, X. Chen, S. Cheng, X. Guo, H. Chen, H. Xu, Phosphoserine promotes osteogenic differentiation of human adipose stromal cells through bone morphogenetic protein signalling, *Cell Biol. Int.* 38 (2014) 309–317. <https://doi.org/10.1002/cbin.10203>.
- [335] G. Mestres, C. Le Van, M.P. Ginebra, Silicon-stabilized α -tricalcium phosphate and its use in a calcium phosphate cement: Characterization and cell response, *Acta Biomater.* 8 (2012) 1169–1179. <https://doi.org/10.1016/j.actbio.2011.11.021>.
- [336] A.M. Yousefi, A review of calcium phosphate cements and acrylic bone cements as injectable materials for bone repair and implant fixation, *J. Appl. Biomater. Funct. Mater.* (2019). <https://doi.org/10.1177/2280800019872594>.
- [337] R.A. Perez, H.W. Kim, M.P. Ginebra, Polymeric additives to enhance the functional properties of calcium phosphate cements, *J. Tissue Eng.* 3 (2012) 1–20. <https://doi.org/10.1177/2041731412439555>.
- [338] J.H. Jang, S. Shin, H.J. Kim, J. Jeong, H.E. Jin, M.S. Desai, S.W. Lee, S.Y. Kim, Improvement of physical properties of calcium phosphate cement by elastin-like polypeptide supplementation, *Sci. Rep.* 8 (2018) 1–11. <https://doi.org/10.1038/s41598-018-23577-y>.
- [339] X. Wang, J. Ma, Y. Wang, B. He, Structural characterization of phosphorylated chitosan and their applications as effective additives of calcium phosphate cements, *Biomaterials.* 22 (2001) 2247–2255. [https://doi.org/10.1016/S0142-9612\(00\)00413-0](https://doi.org/10.1016/S0142-9612(00)00413-0).
- [340] E. Fiume, G. Magnaterra, A. Rahdar, E. Verné, F. Baino, Hydroxyapatite for

- biomedical applications: A short overview, *Ceramics*. 4 (2021) 542–563. <https://doi.org/10.3390/ceramics4040039>.
- [341] K. Natesan, W. Shah, H.R. Le, C. Tredwin, A critical comparison on biocompatibility of different phases of sol–gel derived calcium phosphates as bone graft materials, *J. Biomater. Tissue Eng.* 5 (2015) 655–664. <https://doi.org/10.1166/jbt.2015.1364>.
- [342] Y. Hong, H. Fan, B. Li, B. Guo, M. Liu, X. Zhang, Fabrication, biological effects, and medical applications of calcium phosphate nanoceramics, *Mater. Sci. Eng. R Reports*. 70 (2010) 225–242. <https://doi.org/10.1016/j.mser.2010.06.010>.
- [343] S. Laasri, M. Taha, E.K. Hlil, A. Laghzizil, A. Hajjaji, Manufacturing and mechanical properties of calcium phosphate biomaterials, *Comptes Rendus - Mec.* 340 (2012) 715–720. <https://doi.org/10.1016/j.crme.2012.09.005>.
- [344] P.M.C. Torres, S. Gouveia, S. Olhero, A. Kaushal, J.M.F. Ferreira, Injectability of calcium phosphate pastes: Effects of particle size and state of aggregation of β -tricalcium phosphate powders, *Acta Biomater.* 21 (2015) 204–216. <https://doi.org/10.1016/j.actbio.2015.04.006>.
- [345] Z. Qiao, M. Lian, X. Liu, X. Zhang, Y. Han, B. Ni, R. Xu, B. Yu, Q. Xu, K. Dai, Electreted Sandwich Membranes with Persistent Electrical Stimulation for Enhanced Bone Regeneration, *ACS Appl. Mater. Interfaces*. 14 (2022) 31655–31666. <https://doi.org/10.1021/acscami.2c06665>.
- [346] A. Doostmohammadi, A. Monshi, R. Salehi, M.H. Fathi, Z. Golniya, A.U. Daniels, Bioactive glass nanoparticles with negative zeta potential, *Ceram. Int.* 37 (2011) 2311–2316. <https://doi.org/10.1016/j.ceramint.2011.03.026>.
- [347] R. Mathew, M. Pujari-Palmer, H. Guo, Y. Yu, B. Stevansson, H. Engqvist, M. Edén, Solid-State NMR Rationalizes the Bone-Adhesive Properties of Serine- And Phosphoserine-Bearing Calcium Phosphate Cements by Unveiling Their Organic/Inorganic Interface, *J. Phys. Chem. C*. 124 (2020) 21512–21531. <https://doi.org/10.1021/acs.jpcc.0c06224>.
- [348] T. Renner, P. Otto, A.C. Kübler, S. Hölscher-Doht, U. Gbureck, Novel adhesive mineral-organic bone cements based on phosphoserine and magnesium phosphates or oxides, *J. Mater. Sci. Mater. Med.* 34 (2023). [10.1007/s10856-023-06714-6](https://doi.org/10.1007/s10856-023-06714-6).

Appendices

Appendix 2.1: BBD design developed for the 1st DoE study for the analysis of α -TCP powder after 2 to 10 grinding cycles.

Factors			Responses			
LPR	Phosphoserine wt. %	Grinding Cycles	Adhesive Strength (MPa)	Compressive Strength (MPa)	Initial Time (s)	Final Time (s)
0.2	40	6	3.52	17.37	470	890
0.35	25	6	5.12	18.17	50	65
0.5	10	6	1.28	9.23	130	255
0.35	40	10	4.15	13.06	729	860
0.5	40	6	2.35	8.64	162	270
0.35	25	6	4.92	17.96	50	90
0.35	10	10	3.03	12.61	148	217
0.2	25	2	5.21	19.70	405	530
0.35	25	6	5.22	20.01	57	90
0.35	25	6	4.15	18.58	60	80
0.35	40	2	5.52	15.86	760	940
0.35	25	6	4.70	21.71	64	102
0.2	25	10	3.27	29.69	290	338
0.2	10	6	2.02	12.66	41	72
0.5	25	10	2.89	19.85	355	657
0.5	25	2	4.08	18.56	333	472
0.35	10	2	5.60	13.97	170	290

Appendix 2.2: BBD design developed for the 3rd DoE study for the analysis of α TCP powder after 9 to 13 grinding cycles.

Factors			Responses			
LPR	Phosphoserine wt. %	Grinding Cycles	Adhesive Strength (MPa)	Compressive Strength (MPa)	Initial Time (s)	Final Time (s)
0.35	25	11	5.65	14.89	57	80
0.35	40	9	5.03	5.452	860	920
0.35	40	13	4.46	24.79	40	80
0.2	10	11	1.55	14.33	40	45
0.35	10	9	3.38	8.10	170	375
0.2	40	11	5.66	11.05	627	840
0.35	25	11	5.02	21.39	64	85
0.35	10	13	1.86	4.02	54	60
0.2	25	9	3.97	29.69	290	338
0.5	25	13	5.38	12.01	90	120
0.35	25	11	5.32	21.41	62	154
0.5	40	11	2.53	1.769	180	330
0.5	10	11	4.71	8.22	180	230
0.35	25	11	5.33	13.57	60	82
0.35	25	11	5.17	17.81	57	75
0.2	25	13	4.51	33.01	20	50
0.5	25	9	3.89	19.86	355	657

Appendix 2.3: BBD design developed for the 3rd DoE study for the analysis of α -TCP powder after 13 to 17 grinding cycles.

Factors			Responses			
LPR	Phosphoserine wt. %	Grinding Cycles	Adhesive Strength (MPa)	Compressive Strength (MPa)	Initial Time (s)	Final Time (s)
0.35	35	17	3.16	7.25	25	40
0.35	10	17	7.35	9.12	40	75
0.5	22.5	17	5.74	10.58	90	140
0.35	22.5	15	0.84	16.24	20	35
0.35	22.5	15	3.38	18.02	30	55
0.35	22.5	15	5.11	16.36	40	55
0.35	22.5	15	7.49	20.04	67	78
0.2	22.5	17	4.29	37.22	7	10
0.35	35	13	4.29	25.31	40	80
0.35	10	13	3.07	4.05	54	60
0.5	35	15	4.73	8.26	60	75
0.2	35	15	7.94	5.01	20	30
0.5	10	15	2.07	5.64	89	150
0.2	10	15	6.04	7.80	30	40
0.2	22.5	13	7.03	33.30	20	50
0.5	22.5	13	2.12	12.17	90	120
0.35	22.5	15	6.96	15.64	30	60

Appendix 2.4: Coefficients in Terms of Coded Factors (Sum Contrasts) from the BBD design developed for the 1st DoE study for the analysis of α TCP powder after 2 to 10 grinding cycles.

	Factor	Coefficient Estimate	Standard Error	95% CI Low	95% CI High
	1st DoE study				
Initial Setting Time	Intercept	4.62	0.06	4.50	4.73
	A-L/P ratio	0.00	0.04	-0.09	0.10
	B-Phosphoserine	0.72	0.04	0.63	0.81
	C-Grinding cycles	-0.17	0.04	-0.26	-0.08
	D-Passivation	-0.59	0.06	-0.71	-0.48
	AB	-0.56	0.06	-0.69	-0.43
	AC	0.12	0.06	-0.01	0.25
	AD	0.01	0.04	-0.08	0.10
	BD	0.00	0.04	-0.10	0.09
	CD	0.11	0.04	0.02	0.20
Final Setting Time	Intercept	13.36	0.43	12.46	14.25
	A-L/P ratio	-0.18	0.34	-0.89	0.53
	B-Phosphoserine	6.12	0.34	5.41	6.83
	C-Grinding cycles	-1.62	0.34	-2.33	-0.91
	D-Passivation	-3.92	0.38	-4.72	-3.12
	AB	-5.44	0.48	-6.44	-4.43
	AC	2.27	0.48	1.27	3.28
	BD	0.13	0.34	-0.58	0.84
	CD	1.08	0.34	0.37	1.79
Compressive Strength	Intercept	3.09	0.04	3.00	3.18
	A-L/P ratio	-0.12	0.04	-0.19	-0.04
	B-Phosphoserine	0.00	0.04	-0.08	0.08
	C-Grinding cycles	-0.04	0.04	-0.12	0.04
	D-Passivation	-0.17	0.04	-0.24	-0.09
	AB	0.02	0.05	-0.09	0.13
	AD	-0.07	0.04	-0.15	0.01
	BC	-0.15	0.05	-0.26	-0.04
	BD	0.05	0.04	-0.03	0.13
	CD	0.06	0.04	-0.02	0.14
Adhesive Strength	Intercept	5.11	0.44	4.21	6.01
	A-L/P ratio	-0.41	0.34	-1.12	0.30
	B-Phosphoserine	0.05	0.34	-0.66	0.76
	C-Grinding cycles	0.07	0.34	-0.64	0.78
	D-Passivation	-0.43	0.24	-0.92	0.06
	CD	-0.95	0.34	-1.66	-0.24

Appendix 2.5: Coefficients in Terms of Coded Factors (Sum Contrasts) from the BBD design developed for the 2nd DoE study for the analysis of α TCP powder after 9 to 13 grinding cycles.

	Factor	Coefficient Estimate	Standard Error	95% CI Low	95% CI High
2nd DoE study					
Initial Setting Time	Intercept	89.20	20.91	45.43	132.97
	A-L/P ratio	0.13	16.53	-34.48	34.73
	B-Phosphoserine	158.31	16.53	123.71	192.92
	C-Grinding cycles	-127.31	16.53	-161.92	-92.71
	AB	-100.75	23.38	-149.69	-51.81
	BC	-118.62	23.38	-167.56	-69.69
Final Setting Time	Intercept	4.80	0.08	4.64	4.95
	A-L/P ratio	0.29	0.06	0.17	0.42
	B-Phosphoserine	0.54	0.06	0.41	0.66
	C-Grinding cycles	-0.57	0.06	-0.69	-0.44
	AB	-0.65	0.09	-0.82	-0.47
Compressive Strength	Intercept	20.04	1.69	16.59	23.48
	A-L/P ratio	-4.15	1.79	-7.80	-0.49
	B-Phosphoserine	-1.59	1.79	-5.24	2.07
Adhesive Strength	Intercept	4.72	0.21	4.27	5.17
	A-L/P ratio	0.14	0.19	-0.26	0.54
	B-Phosphoserine	0.76	0.19	0.36	1.15
	C-Grinding cycles	-0.40	0.19	-0.80	0.00
	AB	-1.06	0.27	-1.62	-0.49
	AC	-0.58	0.27	-1.14	-0.01
	BC	-0.21	0.27	-0.78	0.35

Appendix 2.6: Coefficients in Terms of Coded Factors (Sum Contrasts) from the BBD design developed for the 3rd DoE study for the analysis of α TCP powder after 13 to 17 grinding cycles.

	Factor	Coefficient Estimate	Standard Error	95% CI Low	95% CI High
3rd DoE study					
Initial Setting Time	Intercept	44.24	3.38	36.99	51.48
	A-Liquid to powder ratio	31.50	4.93	20.93	42.07
	B-Amount of Phosphoserine	-8.50	4.93	-19.07	2.07
Final Setting Time	Intercept	67.82	5.11	56.87	78.78
	A-Liquid to powder ratio	44.37	7.44	28.41	60.34
	B-Amount of Phosphoserine	-12.50	7.44	-28.46	3.46
Compressive Strength	Intercept	0.06	0.01	0.04	0.08
	A-Liquid to powder ratio	0.02	0.01	0.00	0.04
	B-Amount of Phosphoserine	-0.03	0.01	-0.05	-0.01
	C-Grinding cycles	0.00	0.01	-0.02	0.02
	AB	-0.03	0.01	-0.06	-0.01
	BC	0.06	0.01	0.03	0.09